DETERMINATION OF UNSATURATED SOIL PROPERTIES FROM SIMPLIFIED EXPERIMENTAL PROCEDURES

A THESIS SUBMITTED TO
THE GRADUATE SCHOOL OF NATURAL AND APPLIED SCIENCES
OF
MIDDLE EAST TECHNICAL UNIVERSITY

BY

MELİH BİRHAN KENANOĞLU

IN PARTIAL FULFILLMENT OF THE REQUIREMENTS
FOR
THE DEGREE OF DOCTOR OF PHILOSOPHY
IN
CIVIL ENGINEERING

JANUARY 2023

Approval of the thesis:

DETERMINATION OF UNSATURATED SOIL PROPERTIES FROM SIMPLIFIED EXPERIMENTAL PROCEDURES

submitted by **MELİH BİRHAN KENANOĞLU** in partial fulfillment of the requirements for the degree of **Doctor of Philosophy** i**n Civil Engineering, Middle East Technical University** by,

Prof. Dr. Halil Kalıpçılar
Dean, Graduate School of **Natural and Applied Sciences** _____

Prof. Dr. Erdem Canbay
Head of the Department, **Civil Engineering** _____

Assoc. Prof. Dr. Nabi Kartal Toker
Supervisor, **Civil Engineering, METU** _____

Examining Committee Members:

Prof. Dr. Erdal Çokça
Civil Engineering Dept., METU _____

Assoc. Prof. Dr. Nabi Kartal Toker
Civil Engineering Dept., METU _____

Assoc. Prof. Dr. Nejan Huvaj Sarıhan
Civil Engineering Dept., METU _____

Assoc. Prof. Dr. Mehmet Barış Can Ülker
Earthquake Engineering and Disaster Management Institute, ITU _____

Prof. Dr. Taha Taşkıran
Civil Engineering Dept., Yıldırım Beyazıt University _____

Date: 27.01.2023

I hereby declare that all information in this document has been obtained and presented in accordance with academic rules and ethical conduct. I also declare that, as required by these rules and conduct, I have fully cited and referenced all material and results that are not original to this work.

Kenanoğlu, Melih Birhan

Signature :

ABSTRACT

DETERMINATION OF UNSATURATED SOIL PROPERTIES FROM SIMPLIFIED EXPERIMENTAL PROCEDURES

Kenanoğlu, Melih Birhan
Doctor of Philosophy, Civil Engineering
Supervisor : Assoc. Prof. Dr. Nabi Kartal Toker

January 2023, 241 pages

Unsaturated soil mechanics provides theoretical basis to researchers and practitioners for the solution of various geotechnical engineering problems. The implementation of developed theories and experimental techniques into engineering practice is, however, questionable. The development of simple and rapid experimental procedures that are compatible with existing theoretical models could be beneficial in this regard. In this study, a complete framework of practical procedures for obtaining unsaturated soil properties was presented.

An experimental campaign consisting of saturated isotropic and K_0 consolidated drained triaxial tests and constant suction and constant water content unsaturated tests on a variety of soil types is accomplished in this study. Novel test setups were developed for soil water retention curve extraction and testing of unsaturated specimens. The experimental data is used to validate the effectiveness of developed practical procedures. The first recommended procedure concerns practical and rapid methods for adjusting the water content of test specimens. Another study presents a simple approach for the estimation of shear strength of unsaturated soils for which an experimental parameter that can be easily calibrated with the

evaporation test is employed. The hydraulic conductivity function of unsaturated soils is estimated from a straightforward numerical algorithm developed for the solution of the 1-D seepage problem during soil water retention curve measurement with axis translation technique. Finally, simple and rapid UU and oedometer tests are performed on unsaturated soil samples. The results from these tests, together with soil water retention curve measurements, are processed to determine the Barcelona Basic Model parameters.

Keywords: Unsaturated Soils, Triaxial Test, Soil Water Retention Curve, Shear Strength, Hydraulic Conductivity Function

ÖZ

BASİTLEŞTİRİLMİŞ DENEYSEL YÖNTEMLER ÜZERİNDEN SUYA DOYGUN OLMAYAN ZEMİN ÖZELLİKLERİNİN TAYİNİ

Kenanoğlu, Melih Birhan
Doktora, İnşaat Mühendisliği
Tez Yöneticisi: Doç. Dr. Nabi Kartal Toker

Ocak 2023, 241 sayfa

Suya doygun olmayan zemin mekaniği, birçok geoteknik mühendisliği probleminin çözümünde araştırmacılara ve uygulayıcılara teoriler sunmaktadır. Suya doygun olmayan zeminler üzerinde yapılan deneysel çalışmalar ve teorik araştırmalar, zemin davranışı hakkındaki anlayışımıza yeni ufuklar kazandırmaktadır. Ancak geliştirilen teorilerin ve deneysel tekniklerin mühendislik pratiğine geçişimi bir soru işareti olarak kalmıştır. Mevcut teorik modellerle uyumlu, basit ve hızlı deneysel yöntemlerin geliştirilmesi bu açıdan faydalı olabilir.

Bu araştırma kapsamında farklı türde birçok zemin üzerinde suya doygun ve doygun olmayan geniş bir deneysel çalışma yürütülmüştür. Elde edilen deneysel veri geliştirilen pratik yöntemlerin doğrulanabilmesi amacıyla kullanılmıştır. Geliştirilen yöntemlerden ilki, hızlı ve pratik bir şekilde deney numunelerinin su içeriğinin değiştirilmesine odaklanır. Başka bir çalışma, farklı araştırma disiplinlerinde sunulan çalışmalara atıfta bulunarak, suya doygun olmayan zeminlerin kayma dayanımının tahmini için basit bir yaklaşım sunmaktadır. Suya doygun olmayan zeminlerin kayma dayanımını tahmin etmek için buharlaşma testi ile kolayca kalibre edilebilen deneysel bir parametre kullanılır. Suya doygun

olmayan zeminlerin hidrolik iletkenlik fonksiyonu, eksen öteleme tekniği ile su tutma eğrisi ölçümü yapılırken gerçekleşen su akışını modellemek için geliştirilen basit bir sayısal algoritma üzerinden tahmin edilmektedir. Son olarak, suya doygun olmayan zemin numuneleri üzerinde basit ve hızlı UU ve ödometre deneyleri gerçekleştirilmiştir. Bu deneylerden kolayca elde edilebilen deney verisi, su tutma eğrisi ölçümleriyle birlikte, Barcelona Temel Modeli parametrelerini belirlemek için işlenir.

Anahtar Kelimeler: Suya Doygun Olmayan Zeminler, Üç Eksenli Deneyi, Su Tutma Eğrisi, Kayma Dayanımı, Hidrolik İletkenlik Fonksiyonu

To my beloved father

Ali Rıza Kenanoğlu

ACKNOWLEDGEMENTS

I would like to express my greatest gratitude to my dear advisor, Assoc. Prof. Dr. Nabi Kartal Toker for everything. It was a great privilege to have worked with him.

I would like to present very special thanks to Assoc. Prof. Dr. Nejan Huvaj Sarıhan. Everything made sense when I realized she is just an angel.

I would like to express my gratitude to Assoc. Prof. Dr. Mehmet Barış Can Ülker and Mert Eyüpgiller for our good times during the project that was funded by Scientific and Technological Research Council of Turkey under grant number TUBİTAK 117M330.

Thanks to my friends Ömercan, Melih, Melek, Nazım, Salih, Celal, Yavuz, Elife and Bilal for all our joyful memories. I used a random number generator to order their names.

Endless thanks to my sweet Özden who made me jump under the hard rocks.

I present my endless love to my beloved mother and my beloved sisters.

And I present my deepest appreciation to my dear father for giving me the kind of love I will never have again.

TABLE OF CONTENTS

LIST OF TABLES

TABLES

LIST OF FIGURES

FIGURES

CHAPTER 1

INTRODUCTION

1.1 Problem Statement

Unsaturated soil mechanics provides theoretical basis to researchers and practitioners for the solution of various geotechnical engineering problems. Experimental studies and theoretical investigations on unsaturated soils give new insights into our understanding of soil behaviour. The implementation of developed theories and experimental techniques into engineering practice is, however, questionable. The development of simple and rapid experimental procedures that are compatible with existing theoretical models could be beneficial in this regard.

1.2 Research Study Framework

The primary motivation of this research is to investigate laboratory procedures and constitutive relationships in a way that provides simple and consistent methods in the implementation of unsaturated soil mechanics into engineering practice. In this regard, the research items are summarized in the following paragraph.

Work items are identified as experimental (E), theoretical (T) and combination of both (ET). Experimental studies are classified into two groups as Experimental Study (A) and Experimental Study (B). Experimental Study (A) comprises extensive laboratory tests on saturated and unsaturated Ankara clay, Mersin silt and Elazığ silt soils, equipment development and modification. A detailed experimental study is carried out to reveal the behaviour of unsaturated soil specimens. The response of unsaturated specimens under controlled and monitored experimental variables is essential for devising and calibrating constitutive relationships. Experimental Study (B) aims to develop a testing program of simplified laboratory

procedures as an alternative to methods used in Experimental Study (A). Results obtained from Experimental Study (A) are used in developing constitutive relationships and validating numerical models. Theoretical studies comprise literature study and constitutive and numerical modelling studies. Constitutive modelling study is built on the experimental evidence and theoretical clarification.

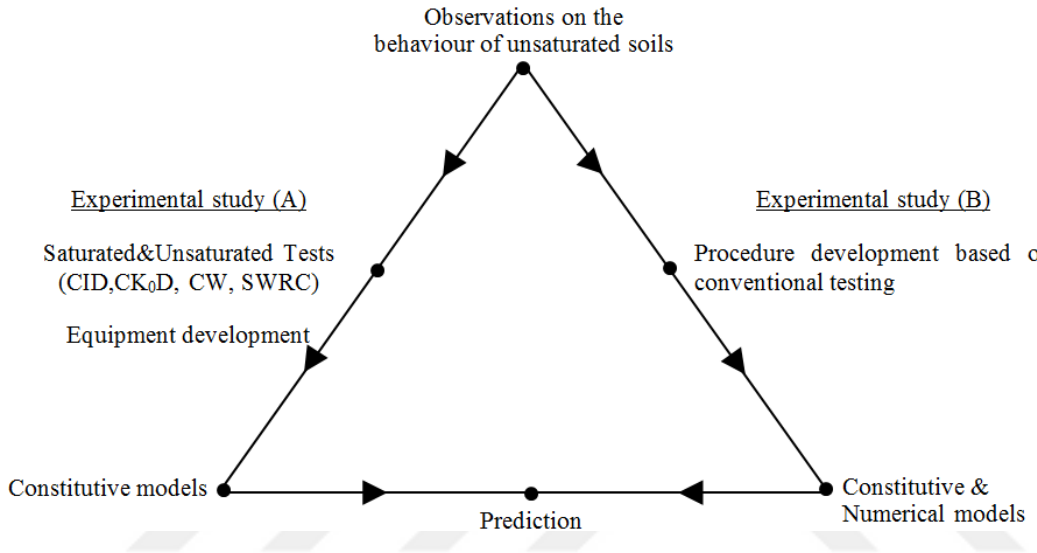

Figure 1.1 Designation of research items

1.3 Outline of the Thesis

Chapter 2 (Literature Review) summarizes experimental and theoretical aspects of unsaturated soil mechanics aiming to enlighten the current understanding on the behaviour of unsaturated soils and experimental procedures.

The experimental studies carried out during this study are covered in Chapter 3 (Experimental Studies). The methods, equipment and procedures together with the test results are given in this chapter. The results presented in Chapter 3 constitute the basis for the verification of findings and methods provided in Chapter 4.

Chapter 4 (Development of Practical Procedures) consist of four main sections. Each of these sections constitutes an independent but interrelated component for

the general framework of this thesis study. The proposed simplified procedures to determine unsaturated soil properties are presented in this chapter.

Chapter 5 (Conclusion) summarizes the main outcomes and elaborates future works.

CHAPTER 2

LITERATURE REVIEW

"Le hasard ne favorise que les esprits préparés
(Chance only favors the prepared minds) "

Louis Pasteur

The historical development of unsaturated soil mechanics can be traced back to the 1900s. Early studies were carried out by agricultural engineers and soil physicists, they mainly focused on soil water tension and capillary potential (Buckingham, 1907; Richards, 1931). Karl Terzaghi established modern geotechnical engineering by introducing the theory of effective stress. He emphasized capillary forces and capillary flow of water in his book (Theoretical Soil Mechanics, 1943) to explain drainage through earth dams, and he drew attention to capillary action in unsaturated soils. In between 50's-70's, researchers developed experimental techniques and proposed theories that link unsaturated and saturated soil mechanics (Bishop, 1959; Matyas and Radhakrishna, 1968). Starting from the 1970s, D.G. Fredlund became a prominent expert in unsaturated soil mechanics. From 1990s onward, the studies on modeling of unsaturated soil behaviour started to spread among many researchers. They established many experimental findings and advanced soil models to elucidate various features of unsaturated soils. Today, these studies allowed the accumulation of knowledge which is applied to many engineering problems such as instability induced by moisture changes in natural soils (swelling and collapsible soils), compacted soils and structures (fill, embankments, dams, rockfills), slope stability (rainfall effects, risk analysis), soil-atmosphere interactions (flow regimes in the ground, water table changes, weathering problem), isolation barriers (nuclear waste disposal), gas flow in

saturated/unsaturated soils (tunnel face stability under gas pressure, long term behaviour of isolation barriers), flow and mechanics of immiscible fluids (oil reservoirs) (Alonso, 2015).

2.1 Background Information

The soil as a porous medium is composed of solid particles and pores in between. The soil particles and pore spaces have various arrangements. The term fabric refers to arrangement of particles and pore spaces in soil (Mitchell and Soga, 2005). The pores provide the space for storage or retention and transport of soil water and gas. The retention of soil water stems from capillarity and adsorption mechanisms. The transport of soil water or flow is the product of conductivity of the porous medium and the change in the potential. Denoting the conductivity with k, and the change in potential with the potential gradient ∇h, the flux q can be expressed as follows:

$$q = -k\nabla h \tag{2-1}$$

The potential of soil water is the change of potential energy or work per unit weight (or volume or mass) of water transferred from the free, pure water state to the soil water state. Denoting the distance with z and required forces to transfer soil water mass to infinitesimal distance of dz with F, per definition, the potential difference dh becomes:

$$dh = -\frac{\sum F}{m} dz \Rightarrow h = -\int \frac{\sum F}{m} dz \tag{2-2}$$

The summation of forces is zero at static equilibrium (e.g. hydrostatic condition), therefore the integration term on the right hand side of (2-2) yields to constant total potential. The total potential of soil water at hydrostatic equilibrium consists of gravitational h_g and pressure h_p potentials. The gravitational and pressure potentials on mass basis can be derived using (2-2) (Koorevaar et al., 1983):

$$h_g = gz \tag{2-3}$$

$$h_p = \int \frac{1}{\rho} dp = \frac{p}{\rho} \tag{2-4}$$

where g gravitational acceralation, ρ density, p pressure. If density is constant, the integration in (2-4) results in pressure divided by density. The summation of gravitational and pressure potentials is termed as hydraulic potential.

There are several components of total potential of soil water in addition to gravitational and pressure potentials. These are generally reported as matric, osmotic (chemical) potentials in the literature (Campbell, 1985; Fredlund et al., 2012). The matric potential is associated with capillary phenomenon and osmotic potential is an effect of dissolved solutes in the soil water.

2.1.1 Matric and Osmotic Potentials

The water rise in a capillary tube inserted into water under atmospheric conditions has direct implication to capillary phenomenon (Fig. 2.1). A water molecule inside bulk water is attracted by neighboring water molecules in all directions under zero net force (Fig. 2.1b). In contrast, on the one hand a water molecule at the air-water interface is attracted towards interior due to the absence of water molecules at the air side, on the other hand its neighboring water molecules at the surface resist interior attraction generating tensile pull (Fig. 2.1c). The resultant force stretching the water's surface is called as surface tension T_s. The adhesive forces attract water molecules to the solid surface of capillary tube. The water molecules sticking on the solid surface decreases their potential energy by making bonds with hydrophilic solid molecules. Depending on the contact angle f, the adhesion forces are balanced by the surface tension and the radius of curvature of the air-water interface (Fig. 2.1d).

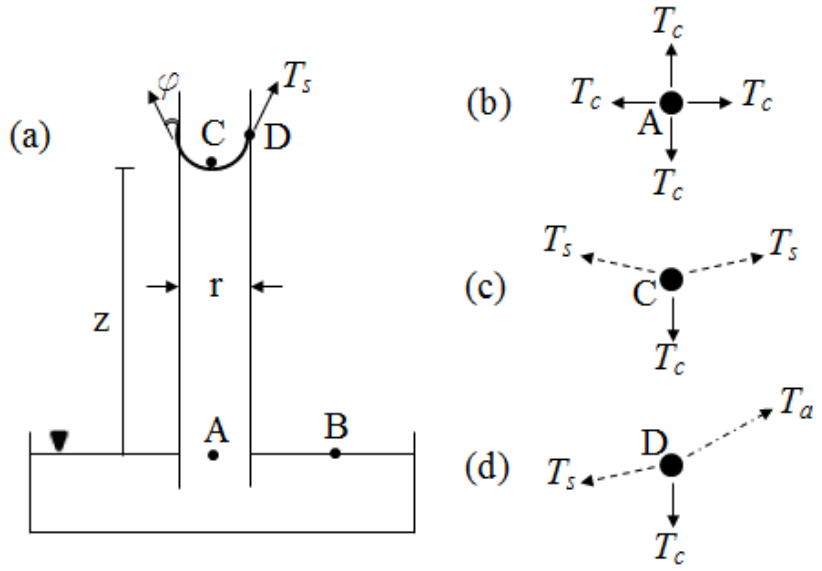

Figure 2.1. Sketch of capillary rise experiment (a), equilibrium of forces for a water molecule inside bulk water (b), a water molecule at the air-water interface (c), a water molecule at the air-water-solid intersection (d) (T_c: cohesive forces, T_s: surface tension,T_a: adhesive forces).

At hydrostatic equilibrium, capillary rise of the water generates gravitational potential that is compensated by the pressure potential. Using (2-3) together with (2-4) and assuming total potential is zero at point A in Fig. 2.1a, the pressure of water u_w inside capillary tube at point C in Fig. 2.1a can be expressed as:

$$h_t = h_g + h_p = gz + \frac{u_w}{\rho_w} = 0 \Rightarrow u_w = -\rho_w gz \tag{2-5}$$

where ρ_w is the density of water. According to (2-5), the water pressure is negative of the height of capillary rise multiplied by unit weight of water. Equating weight of the water column and force exerted per surface tension, vertical force equilibrium of the water column inside capillary tube can be expressed as:

$$\pi r^2 z \rho_w g = 2\pi r T_s \cos\varphi \tag{2-6}$$

Ignoring the elevation differences along the curved air-water interface, resulting curved interface becomes spherical. After rearranging (2-6) for zero contact angle, the height of capillary rise is :

$$z = \frac{2T_s}{\gamma_w r} \tag{2-7}$$

The net pressure on the air-water interface is the difference between the air pressure u_a and water pressure u_w and it is the capillary pressure or matric suction s. Air pressure is zero at atmospheric conditions. Thus matric suction at point C in Fig. 2.1a is positive since water pressure is negative as given in (2-5).

$$s = u_a - u_w = 0 - (-\rho_w g z) = \rho_w g z \tag{2-8}$$

Combining (2-7) with (2-8):

$$s = u_a - u_w = \frac{2T_s}{r} \tag{2-9}$$

Equation (2-9) is known as Young-Laplace equation for a spherical air-water interface.

The relationship between the vapor pressure of a point on the free water surface (point B) and point C in Fig. 2.1a can be established based on (2-4) and (2-8) (Alonso, 2015). The change in the vapor pressure du_v in a height differential dz can be described using (2-3) together with (2-4) as:

$$du_v = -\rho_v g dz \tag{2-10}$$

Air is compressible, therefore its density depends on its pressure according to ideal gas law:

$$\rho_v = u_v \frac{M_w}{RT} \tag{2-11}$$

where ρ_v density of water vapor, M_w molecular weight of water vapor, R universal gas constant, T temperature. Substituting (2-11) in (2-10)

$$dz = -\frac{du_v}{\rho_v g} = -\frac{du_v}{u_v}\frac{RT}{M_w g} \tag{2-12}$$

The integration between (0,z) and (u_{vB}, u_{vC}) and taking into account value of z in (2-8):

$$\frac{u_{vC}}{u_{vB}} = \exp\left(-\frac{sM_w}{RT\rho_w}\right) = \exp\left(-\frac{\psi M_w}{RT\rho_w}\right) \tag{2-13}$$

The quotient u_{vC}/u_{vB} is relative humidity (RH) above point C and expresses the relationship between relative humidity of air in equilibrium with a water with suction s. Equation (2-13) connects the suction change across a curved air-water interface to vapor pressure above the interface and it is known as Kelvin's equation. The suction change across a curved air-water interface is equal to the total suction (ψ) for zero osmotic suction.

2.1.2 Soil Water Retention Curve

Soil water retention curve (SWRC) defines the relation between amount of soil water and suction. Soil is fully saturated up to a threshold value of suction called as air-entry. Soil becomes partially saturated with increasing suction and curved air-water interfaces (capillary regime) emerge. Further increase of suction results in drainage by withdrawal of air-water interfaces and water is in the adsorbed film regime. Soil water retention behaviour is hysteretic, depending on the drying and wetting regime soil may have different suction values at the same amount of water (Fig. 2.2).

SWRCs can be determined from experimental measurements (ASTM 6836-02) or can be estimated with empirical or numerical approaches (Arya and Paris 1981, Sattari and Toker 2016). SWRC equations are used to characterize a complete branch of retention curve by fitting experimental data (Brooks and Corey, 1964; Van Genuchten, 1980; Fredlund and Xing, 1994).

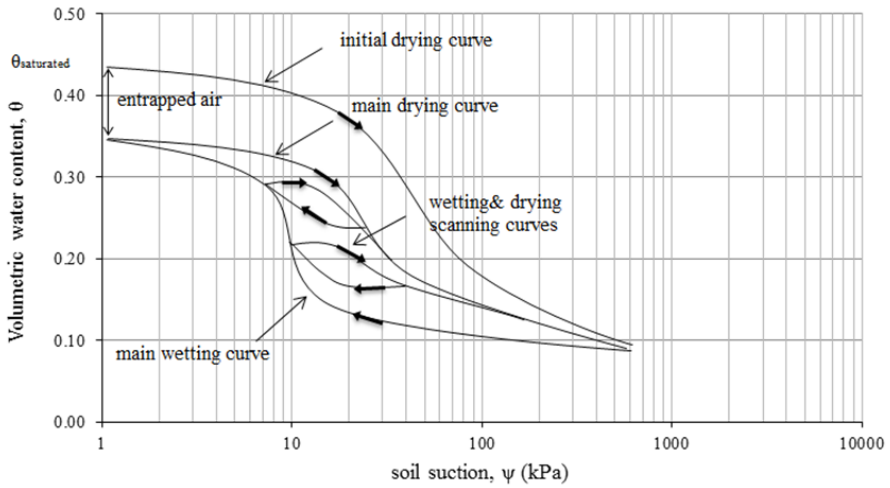

Figure 2.2 Schematic illustration of soil water retention curves.

Table 2.1 Mostly used closed form SWRC equations

Reference	Equation	Parameters
Brooks and Corey (1964)	$\theta = \theta_{res} + (\theta_{sat} - \theta_{res})\left(\frac{s}{s_{aev}}\right)^{-\lambda}$	s_{aev}: Air entry pressure λ: pore size distribution index
van Genuchten (1980)	$\theta = \theta_{res} + \frac{\theta_{sat} - \theta_{res}}{\left(1+\left(\frac{s}{a}\right)^{n}\right)^{m}}$	a, n, m: fitting parameters
Fredlund and Xing (1994)	$\frac{\theta}{\theta_{sat}} = C_s\left(\ln\left(e+\left(\frac{s}{a}\right)^{n}\right)\right)^{-m}$	Cs: correction function $C_s = 1 - \frac{\ln\left(1+\frac{s}{s_{res}}\right)}{\ln\left(1+\frac{(10^6\ kPa)}{s_{res}}\right)}$ a, n, m: fitting parameters

where, θ is the volumetric water content, θ_{sat} is the saturated volumetric water content (or porosity), θ_{res} is the residual volumetric water content, s is the suction corresponding to the residual water content.

2.1.3 Hydraulic Conductivity Function

Hydraulic conductivity of soils is dependent on grain size, specific surface area, void ratio, pore geometry and saturation (Ren and Santamarina 2017). Unsaturated hydraulic conductivity can be expressed as a function of suction or water content. Indirect methods use saturated hydraulic conductivity together with a relative coefficient of permeability to estimate hydraulic conductivity function (HCF). Brooks and Corey (1964) directly uses the pore size distribution parameter (λ), which is obtained from the soil water retention curve:

$$\begin{aligned} k(s) &= k_{sat} && \text{for } s \le s_{aev} \\ k(s) &= k_{sat}\left(\frac{s_{aev}}{s}\right)^{(2+3\lambda)} && \text{for } s > s_{aev} \end{aligned} \tag{2-14}$$

where k_{sat} is the hydraulic conductivity of the saturated soil.

The empirical equation proposed by Averjanov (1950) uses the effective degree of saturation or effective volumetric water content in a power function for determining the hydraulic conductivity function. The fitting parameter n is 3.5 for most soils.

$$\begin{aligned} k\left(S_r\right) &= k_{sat}\left(\frac{S_r - S_{res}}{1 - S_{res}}\right)^n \\ k\left(\theta\right) &= k_{sat}\left(\frac{\theta - \theta_{res}}{\theta_{sat} - \theta_{res}}\right)^n \end{aligned} \tag{2-15}$$

Fredlund et al. (1994) used the SWRC equation proposed by Fredlund and Xing (1994) to predict hydraulic conductivity function.

$$k(s) = \frac{\int_{\ln(s)}^{b} \frac{\theta\left(e^y\right) - \theta(\psi)}{e^y}\theta'\left(e^y\right)dy}{\int_{\ln(s_{aev})}^{b} \frac{\theta\left(e^y\right) - \theta_{sat}}{e^y}\theta'\left(e^y\right)dy} \tag{2-16}$$

where $k(s)$ is the hydraulic conductivity as a function of suction, b is equal to $\ln(10^6)$, s_{aev} is the air-entry pressure (kPa), e is the natural number 2.71828, y is a dummy variable of integration representing the logarithm of suction, θ_{sat} is the saturated volumetric water content, θ' denotes the first derivative of equation proposed by Fredlund and Xing (1994) with respect to suction s.

2.2 Experimental Tecchniques in Unsaturated Soil Testing

2.2.1 Suction Control Techniques

2.2.1.1 Axis Translation

The most used techniques for controlling suction can be summarized in three different approaches (Delage et al., 2008). The first and most common technique is axis translation technique (Hilf, 1956). The water pressure in the unsaturated soil is negative and the air pressure is atmospheric or zero gage pressure (if air phase is continuous, not in the form of bubbles). The simulation of this natural condition for the laboratory specimen requires negative pressure application to the water phase and this causes cavitation in the water pressure system during testing. To eliminate this problem, both pressures are shifted to higher levels at which the water pressure is always kept positive. Matric suction can be controlled by elevating air and water pressure, and it becomes equal to the difference of these two pressures. High air entry (HAE) porous ceramics are used to prevent intrusion of air into the water pressure system which has lower pressure. The air entry value of these materials can be as high as 1500 kPa. A disadvantage in this method is pressurized air diffuses through ceramic disc and forms air bubbles inside low pressure water compartment. Accumulated air affects water volume measurement in a drained test or suction measurement in an undrained test and readings become erroneous. An auxiliary device is implemented to flush air bubbles regularly (Fredlund 1975).

The effect of axis translation technique on the retention behaviour of soil is questionable. Baker and Frydman (2009) presented experimental data that shows inconsistency between axis translation and dew point (vapor pressure) retention curve measurements. On the other hand, Ng et al., (2015) reported an experimental study that presents comparison of retention curve measurements for various techniques (i.e. axis translation, osmotic and vapor equilibrium) and showed consistent results. Drainage of porous soil matrix results from either suction increase beyond air-entry pressure or cavitation of pore water under negative water pressures; latter is not permitted in axis translation technique (Or and Tuller, 2002; Toker et al., 2003). Lu (2019) stated that the use of axis translation technique might be problematic for fine grained soils.

2.2.1.2 Osmotic Control

Another technique used for controlling matric suction is osmotic technique (Kassif and Ben Shalom, 1971; Komornik et al., 1980; Cui and Delage, 1996; Delage et al., 1998; Ng et al., 2007). In this technique matric suction is controlled by means of a semi-permeable membrane and an osmotic solution (commonly polyethylene glycol-PEG). Different types of PEG depending on the molecular weight cut-off (MWCO) could be found in the market. Delage et al. (1998) reported that calibration curve (suction vs. PEG concentration) becomes unique that is independent of the type of PEG. Delage et al. (1998) reported values of suction up to 10 MPa could be obtained in this technique. The calibration for PEG concentration vs. suction relationship can be carried out with a psychrometer (Williams and Shaykewich, 1969), an osmotic tensiometer (Peck and Rabbidge, 1969), a high-suction probe (Dineen and Burland, 1995) or an osmotic pressure cell (Slatter et al., 2000). Natural processes could be simulated more realistically in the osmotic method compared to axis translation since cavitation of pore water is permitted (Ng et al. 2007).

2.2.1.3 Vapor Equilibrium Technique

The third technique is vapor equilibrium (Blatz et al., 2008). In this technique, a chemical solution inside of the sealed container is used to create total suction. Suction controlling is achieved by controlling the relative humidity of environment in the container based on thermodynamic principles. Very high suction values ranging from 4 MPa to 600 MPa can be created in this technique (Murray and Sivakumar, 2010). However, strict temperature control is required during testing since relative humidity is very sensitive to temperature changes.

All of aforementioned methods have their advantages and disadvantages (Ng and Menzies, 2007; Delage et al., 2008). Independent of which method is used to control suction, suction equalization is essential in unsaturated soil testing (Ng and Zhou, 2005). Too much time is needed to achieve suction equilibrium in the unsaturated specimen. This can be in several days or months depending on the controlling method and soil type (Kunze and Kirkham, 1962; Oliveira and Marinho, 2003; Tang et al., 1998; Tang and Cui, 2005; Cui et al., 2002; Lloret et al., 2003).

2.2.2 Suction Measurement Techniques

2.2.2.1 Measurement of Matric Suction

Tensiometers are used to directly monitor soil matric suction. Tensiometers consist of a water reservoir with a porous tip (generally high air-entry ceramic) and a pressure measurement device. Tensiometer porous tip is inserted into soil to equilibrate soil water matric suction with the pressure of water inside tensiometer reservoir. The main limitation in the measurement matric suction is the interruption of continuity of the water in the measurement system (water reservoir of tensiometer) due to the cavitation. The water inside tensiometer cavitates beyond a certain value of suction, and invalid readings are taken from the pressure sensor.

This limit is about 90 kPa for early tensiometer while water cavitates at absolute negative pressure. The measurement range of tensiometers has been increased up to 2.4 MPa with the development of high capacity tensiometers (Ridley and Burland 1993, Tarantino and Mongiovi 2001, Toker 2002, Delage et al. 2008). Mendes et al. (2019) has used a special nanoporous glass instead of porous ceramic and have measured matric suction up to 7.3 MPa.

Matric suction can be measured directly with the suction plates (Suits et al. 2010). Matric suction is measured implementing axis translation technique. Ceramic disc is placed between soil and pressure measurement device. Air pressure is applied on the soil specimen that generates the tendency to exchange water between soil and reservoir water beneath ceramic disc. Pressure of reservoir water equilibrates with soil matric suction such that the difference between applied air pressure and measured reservoir water pressure becomes equal to soil's matric suction. For long term measurements, diffused air bubble flushing process is required.

Contact filter paper method is an indirect method to measure matric suction (ASTM D5298, Bulut et al. 2001, Bicalho et al. 2007, Suits et al. 2008). In this method, filter paper is placed in contact with the soil, and it comes equilibrium with the soil matric suction. The gravimetric water content of the filter paper is measured, and matric suction is indirectly determined using the calibration curve of the filter paper.

2.2.2.2 Measurement of Osmotic Suction

Osmotic suction is indirectly determined from the electrical conductivity of extracted pore water, this method called as squeezing technique (Krahn and Fredlund 1972, Romero 1999, Peroni and Tarantino 2005). Electrical conductivity measurement is converted to osmotic suction using a calibration curve.

2.2.2.3 Measurement of Total Suction

Total suction of soil is indirectly determined from pore air relative humidity measurements. Psychrometers are used to measure humidity. The simplest form of psychrometer comprises thermometers that measure temperature during evaporation or condensation of a dew. Measured temperatures are related to relative humidity and can be calibrated with salt solutions to determine total suction (Wexler and Hasegawa 1954). Different types of electrical devices have been developed to measure relative humidity. Thermocouple psychrometers utilizes temperature measurement at junctions of two different kind of wires (Richards 1965, Abuel-Naga and Bouazza 2011). Krahn and Fredlund (1972) have stated that the upper limit of total suction is about 8 MPa and the lowest limit is 100 kPa with thermocouple psychrometer. Measurement range can be extended up to 300 MPa using wet-loop-type psychrometers (Fredlund et al., 2012).

The dewpoint can be accurately detected with chilled mirror hygrometers (Leong et al., 2003). The measurement accuracy of relative humidity is ±0.1%. Measurement range is from 3 MPa to 300 MPa.

Filter paper method can be used to measure total suction by equilibrating soil and non-contact filter paper in the sealed environment.

2.2.3 Measurement of Soil Water Retention Curve

Soil water retention curve measurements are commonly carried out by extracting suction vs water content data pairs. Intermittent experimental data is then used to calibrate the preferred retention curve equation (e.g. Van Genucten, 1980; Fredlund and Xing, 1994). Continuous measurements comprising real-time monitoring of the variation of suction and water content have indeed been performed (Toker, 2002; Schindler and Mueller, 2006).

Hanging column method is suitable for low range suction (up to 40 kPa) implementation. In hanging column method, suction is controlled by elevating water-filled containers to generate vacuum inside the closed system (Vanapalli et al., 2008). Soil matric suction equilibrates with the applied vacuum and water content is measured.

Hanging column technique could be used for coarse grain soils with small air-entry value. The soil inside the test column reaches equilibrium under hydrostatic conditions such that soil imbibes (wetting test) or drains (drying test) through the column base while top is covered. Matric suction is calculated from the height measurements from the supply water level at the base. The soil inside column is separated into pieces to measure water contents.

Most common method for retention curve measurement is use of pressure plate extractors. This method is based on axis translation technique to control suction. Pressure plates consisting of high air-entry ceramic are placed in an air-tight chamber. Air pressure is applied upon soil specimens and water pressure is kept atmospheric. Specimen's water content is measured when equilibrium is reached. The range of suction can be extended up to 1500 kPa with pressure plate extractors. Tempe cell is a particular type of pressure plate extractor, where measurement of retention curve is carried out on single specimen (Reginato and van Bavel, 1962). Total mass of specimen and cell is measured at the end of each suction step and water contents are back calculated from final water content measurement together with mass measurements.

Small scale centrifuge test is an alternative method for rapid measurement of soil water retention curve at suctions up to 250 kPa. In this method, different angular velocities are applied to the specimens to generate suction and water mass variation is monitored by weighing specimen (Rahardjo et al., 2019).

High suction data pairs could be obtained with filter paper technique, chilled mirror hygrometers or vapor equilibrium technique (equilibrating specimens with salt solution in a desiccator). Chilled mirror hygrometers (such as WP4C) are suitable

for rapid measurement of soil water retention curve at suctions higher than 500 kPa.

Experimental variables in retention curve measurements could be extended implementing sophisticated techniques when particular constitutive variables are necessary. Suction controlled oedometers are designed for controlling and/or monitoring of vertical and horizontal stresses, suction, volume change and water content variation (Romero et al., 1995; Tarantino and Mongiovi, 2000; Ng and Pang, 2000; Cuisinier and Masrouri, 2004; Hoffman et al., 2005; Burton et al., 2016; Ajdari et al., 2016). Modified triaxial test setups are another elaborate option that allows following various stress paths to measure retention behaviour.

2.2.4 Measurement of Hydraulic Conductivity Function

Direct and indirect methods can be used in the measurement of unsaturated hydraulic conductivity (ASTM D7664). Direct measurement methods could be performed in the laboratory or in the field. Direct measurements can be carried out in steady state or transient conditions. Constant head steady state measurement is carried out by keeping unsaturated specimen under constant hydraulic gradient (generating constant flow rate and constant suction) (Olsen et al. 1994, Huang et al. 1998). A modified triaxial cell based on axis translation could be used as flexible wall permeameter (Fig. 2.3a). Unsaturated hydraulic conductivity is calculated from measured water flux or headloss assuming Darcy's law is valid. Transient measurements of unsaturated hydraulic conductivity are based on back calculation from the flow equations with unsteady condition measurements. Horizontal infiltration testing is carried out by commencing wetting front propagation through specimen under constant head boundary for a given time span. Water contents of individual segments are determined at the end of test duration (Klute and Dirksen 1986). Instantaneous profile method uses water content (e.g. using time-domain-reflectrometry) and suction (using tensiometer or psychrometer) measurements on several points along soil specimen during transient flow process (Su et al., 2018).

Water volume change and hydraulic gradient between two points are respectively calculated using time dependent change in water content and suction profiles (Fig. 2.3b). Steady state measurement methods require longer testing time than transient methods; but measurements are considered more reliable (Benson ve Gribb, 1997).

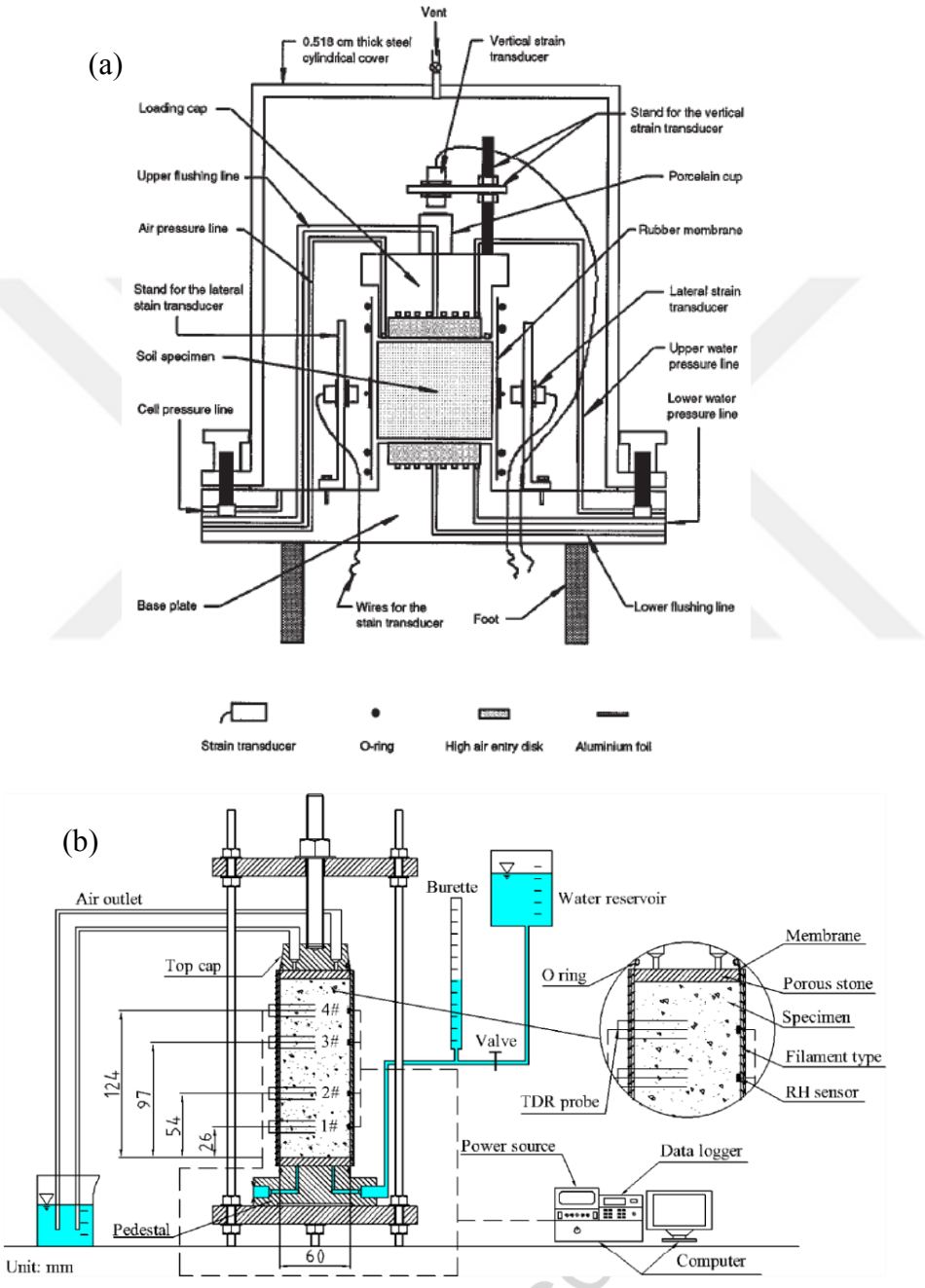

Figure 2.3 (a) Flexible wall permeameter for determination of HCF (Huang et al., 1998), (b) Instantaneous profile method (Su et al., 2018).

The experimental methods described above in determining hydraulic conductivity function (HCF) of the unsaturated soil are time-consuming and require specialized equipment. Alternatively, analysis of inflow/outflow experiments provides the hydraulic conductivity curve parameters. The inflow/outflow experiments can be done either by applying large suction increment in the one-step outflow test or applying smaller suction steps in the multi-step outflow test. Kool et al. (1985) evaluated the parameters of soil hydraulic functions by nonlinear least square fitting of predicted to observed cumulative outflow with time. They concluded that the inverse simulation of one-step outflow test may provide accurate solution of parameter identification problem if final outflow corresponds to large fraction of soil water between saturated and residual water contents during testing. The non-uniqueness in inverse analysis is caused by a lack of sensitivity of outflow data to certain parameter combinations (van Dam et al. 1992). Selecting a correct parametric form for retention and hydraulic conductivity functions is important to overcome the non-uniqueness (Zachmann et al. 1982). The inverse solution technique can be improved by combining cumulative transient outflow data with the tensiometric measurements inside the sample (Enching and Hopmans 1993). Crescimanno and Iovino (1995) investigated the effect of volume change due to shrinkage in outflow experiments on fine soils. They reported that shrinkage barely occured in the suction range explored in their study and does not affect the outflow experiment. The ceramic impedance was not a concern in the aforementioned studies. The advancements in the numerical algorithms have prompted the inverse simulation of one-step outflow from two-layered specimen composed of soil and ceramic disk (Schelle et al. 2011, Nasta et al. 2011, Wayllace and Lu 2011). However, the stochastic errors inhere in the optimization process and the reliability of the results should always be examined for different initial parameters in repeated runs.

The experimental methods in determining hydraulic conductivity function (HCF) of the unsaturated soil are too time-consuming, and not preferable in geotechnical engineering practice. Indirect methods are quite common in the estimation of

unsaturated hydraulic conductivity. Indirect measurement methods are based on relating particular soil properties (mostly retention curve) with hydraulic conductivity. Water retention curve experiments are much more prevalent and HCF is generally estimated by utilizing soil water retention curve in practice (Brooks and Corey, 1964; Van Genuchten, 1980; Fredlund et al., 1994).

2.2.5 Triaxial Testing on Unsaturated Soils

2.2.5.1 Suction Control in Unsaturated Triaxial Testing

Suction control in triaxial tests requires modification on conventional test equipment. Axis translation technique is the most popular option in suction control. High-air entry ceramics are placed in the pedestal and/or top cap to control pore water pressure. A water compartment (generally spiral shaped groove) that starts and ends at two outlets (one for pressure supply and other for flushing process) beneath the ceramic disc is manufactured inside pedestal and top cap. Ceramic is fixed along its perimeter with epoxy. Porous stone or metal either surrounding ceramic disc or on the ooposite end of the specimen is placed on pedestal and/or top cap to apply air pressure inside specimen. An auxiliary device (i.e. diffused air volume indicator) for flushing and volume measurement of diffused air is connected to pore water pressure outlet.

Alternatively, suction control could be achieved using osmotic technique (Cui and Delage, 1996; Ng and Menzies, 2007) or vapor equilibrium technique (Blatz et al., 2005). In both methods, suction is induced to specimen by circulating liquid (PEG solution) or vapor (vapor of salt solution) through pedestal and top cap.

Suction measurement instead of suction control is preferred in case of undrained or constant water content test procedures. Various sensors (e.g. miniature high capacity tensiometer, electrical resistivity probe) are implemented in the triaxial

cell for measurement of suction or water content during testing (Mendes et al., 2012; Munoz-Castelblanco et al., 2014; Li and Zhang, 2015).

2.2.5.2 Volume Change Measurement

The pore water volume change measurement cannot be used to evaluate overall volume change of the unsaturated specimen since pore air is compressible. Several volume change measurement methods such as i) using cell fluid volume change ii) separate measurement of air and water volume iii) direct measurement of the specimen geometry have been developed.

Cell fluid volume change measurement cannot be directly used for the specimen volume change, correction is required due to expansion of cell and pipes, piston extrusion/intrusion or possible existence of occluded air bubbles in cell fluid. Inner cell method has been developed and improved by several researchers to avoid corrections on cell fluid measurements (Bishop and Donald, 1961; Cui and Delage, 1996; Ng et al., 2002). In this method, the inner cell is filled with different types of liquid exposed to the same pressure as the outer cell liquid; so that, it is excluded from the correction factors. The volume change of sample is measured by precise monitoring of inner cell fluid level. Another version of the inner cell method is double cell method (Wheeler, 1988). In this case, the inner cell is sealed from the outer cell and specimen volume change is taken equal to the inner cell liquid volume change. Ahmadi-Naghadeh and Toker (2017) have developed a laboratory protocol to measure specimen volume change directly from liquid volume change measurement from a single cell. They have modeled viscoelastic behaviour of triaxial cell and tubing system. Once model parameters have been calibrated, cell liquid volume change measurement can be corrected through the model calculations. The good thing about this method is it does not require any modification on a conventional triaxial cell.

The separate measurement of pore air and pore water volumes is carried out by implementing pressure-volume controller for air phase as in same case for pore water pressure control. The total volume change of the specimen is the summation of both volume change of pore air and water. However, undetectable air leakage, as well as high sensitivity of air volume change to temperature variation could become problematic (Fredlund and Rahardjo, 2012).

Volume change measurement based on direct measurements could be performed by monitoring axial and radial deformations with special type sensors (LVDT, hall effect transducer, strain gage etc.). Such local deformation measurements become meaningless in case of shear plane formation. Romero et al., 1997 proposed a sophisticated laser scanner technique for deformation measurements that non-homogeneous distribution of deformations can be detected. Finally, image processing technique could be used analyzing photographs that are taken during testing (Gachet et al., 2003).

2.2.5.3 Test Procedures

Desired suction (difference between air pressure and water pressure) and net stress (difference between cell pressure and air pressure) is applied into specimen in the suction equalization step. Air pressure and cell pressure are gradually increased while keeping water pressure constant. Suction is measured if specimen's suction/water content is adjusted in a separate procedure before testing (e.g. equilibrating with salt solution).

The loading stage follows suction equalization stage. There are several alternatives to test procedures depending on the drainage conditions. In drained loading, suction is kept constant and net stress (difference between cell pressure and air pressure) is gradually adjusted preventing excess pore pressure development inside specimen (Sivakumar, 1993; Cui and Delage, 1996). In constant water content loading, pore air drainage is permitted; but that of pore water is not. In this case, pore water

pressure is measured to monitor suction. The loading rate should be slow enough to ensure homogeneous distribution of suction within the specimen. In undrained loading, drainage of both pore air and pore water is not permitted. A suitable rate of loading could be estimated from the trial measurements.

The shear stage following loading stage is carried out under preferred drainage condition. Suitable strain rate could be estimated according to Fredlund et al. (2012).

2.3 Constitutive Modelling

2.3.1 Incorporation Soil Water Retention Behaviour

Soil water retention curve (SWRC) is a fundamental soil property in unsaturated soil mechanics. SWRCs are dependent on various factor such as the pore size distribution (Cheng et al. 2019), soil type, stress state (Lee et al., 2005), void ratio (Salager et al., 2013; Ma et al., 2015; Zou et al., 2018), initial water content (Ng and Pang, 2000), plasticity index etc. Sheng and Zhou (2011) stated that the effect from most of these factors are incorporated into parameters of retention curve function. But they have specifically separated effect of void ratio and have considered samples with same particle size distribution, but different initial void ratio should be treated as different soils. Zhou and Ng (2014) have stated that the effect of stress state should be included in addition to void ratio. They have argued that a small increase in stress can exceed the elastic shear range of soil and alter pore structure (therefore, the water retention behaviour) due to induced plastic deformations; void ratio itself is not a sensitive parameter to incorporate the effect of these small changes.

The state-dependent nature of soil water retention behaviour reveals that soil water retention curve is actually a surface in suction-water content-void ratio space. Soil water retention behaviour varies when soil's void ratio is changed with external

mechanical loading and cannot be predicted using single branch (Tarantino, 2009; Gallipoli et al., 2015). For example, degree of saturation can decrease under constant suction compression in the space of degree of saturation-suction-void ratio, that is, such behaviour cannot be observed on the two-dimensional surface of degree of saturation vs suction (Pasha et al., 2019).

Soil water retention behaviour is hysteretic, depending on the drying and wetting regime soil may have different suction values at the same amount of water. Experimental studies have shown that closed loops called scanning curves emerge inside boundary retention curves (Lins et al., 2007; Miller et al. 2008; Lu and Khorshidi, 2015).

2.3.2 State Variables

Constitutive relations are established using state variables that could be defined independently from the physical properties of the materials (Fredlund, 2016). A great diversity of the choice of state variables exists in the literature; but there is a general agreement that at least two variables are required to represent various features of unsaturated soil behaviour (Gens, 2010). State variables could be chosen for suitability to experimental operations, or their theoretical soundness based on the physical interpretation of behaviour or thermodynamic analysis (Gallipoli et al., 2018).

Gens (2010) classified state variables used in unsaturated soil constitutive models into three categories. Each category was generalized with two constitutive variables. In the first category, net stress and suction or degree of saturation are respectively used as first and second constitutive variables. This approach is known as independent stress state variables theory (Fredlund and Morgenstern, 1977; Alonso et al., 1990; Sheng et al., 2008). In the second approach suction is included in the first constitutive variable together with the net stress and suction or degree of saturation is used as second constitutive variable (Kohgo et al., 1993; Loret and

Khalili, 2000-2002). Constitutive models developed based on the first two categories are not convenient to include hysteresis and hydraulic effects. In the third category, both suction and degree of saturation are combined with net stress as first constitutive variable and suction or degree of saturation is used as second constitutive variable (Wheeler et al., 2003; Gallipoli et al., 2003). Constitutive models based on this category are suitable for coupled formulation. The second and third categories are known as an effective stress approach in literature.

2.3.3 Barcelona Basic Model (BBM) (Alonso et al., 1990)

Alonso et al. (1990) developed the earliest elasto-plastic constitutive model for unsaturated soils (Barcelona Basic Model, BBM) using net stress (p) and suction (s) as independent stress state variables. The formulation in the isotropic stress state was developed by defining loading-collapse (LC) and suction increase (SI) yield curves. LC yield curve emerges from the fact that soil can attain higher void ratio under the same stress level after yielding due to the stabilizing effect of suction (Fig. 2.2). In other words, apparent preconsolidation stress or yield stress increases with suction.

The volume change behaviour of soil under isotropic stress condition is described by linear compression lines on the v-ln$p$ plane:

$$v = N(s) - \lambda_s \ln(p/p_c) \tag{2-17}$$

$$dv = -\kappa\, dp/p \tag{2-18}$$

$$dv = -\kappa_s\, ds/(s + p_{atm}) \tag{2-19}$$

where v is specific volume, $\lambda(s)$ is slope of virgin compression line under constant suction s, p_c is reference stress, $N(s)$ is value of specific volume corresponding to extension of virgin compression line with slope of $\lambda(s)$ to reference net stress, κ is slope of elastic compression line, κ_s is slope of elastic compression line due to

suction change, p_{atm} is atmospheric pressure. The value of $N(s)$ is expressed using (2-19).

$$N(s) = N(0) - \kappa_s \ln\left(\frac{s + p_{atm}}{p_{atm}}\right) \tag{2-20}$$

$N(0)$ is specific volume at reference stress for virgin saturated compression line. The geometrical relationship between post-yield slopes of different compression curves at constant suctions are used to derive an equation for the shape of the LC curve using (2-17) to (2-20):

$$p_0 = p_c \left(p_0^* / p_c\right)^{\frac{\lambda(s)-\kappa}{\lambda(0)-\kappa}} \tag{2-21}$$

where $\lambda(0)$ is the slope of saturated virgin compression line and p_0^* is preconsolidation stress for saturated condition. $\lambda(s)$ is defined as a function of suction in the following form:

$$\lambda(s) = \lambda(0)\left[(1-r)\exp(-\beta s) + r\right] \tag{2-22}$$

where β controls the rate of increase of soil stiffness with suction and r is a ratio of asymptotic value of compression index as suction tends to infinity to saturated compression index $\lambda(0)$. Compression lines could be modelled as divergent or convergent with increasing net stress depending on the value r. r less than 1 results in divergent compression lines ($\lambda(s)$ decreases with increasing suction) whereas r higher than 1 results in convergent compression lines ($\lambda(s)$ increases with decreasing suction) (Wheeler et al., 2002).

Isotropic loading at constant suction on an unsaturated specimen located on the yield curve shifts LC curve with increasing p (path denoted with L in Fig. 2.2). The decreasing suction (wetting) at constant mean stress can also result in same movement of LC curve (path denoted with C in Fig. 2.2). Therefore, compression due to loading or collapse due to wetting can result in same plastic volumetric strains that can be expressed using Cam-clay type hardening law:

$$d\varepsilon_v^p = \frac{\lambda(0)-\kappa}{v}\frac{dp_0^*}{p_0^*} \tag{2-23}$$

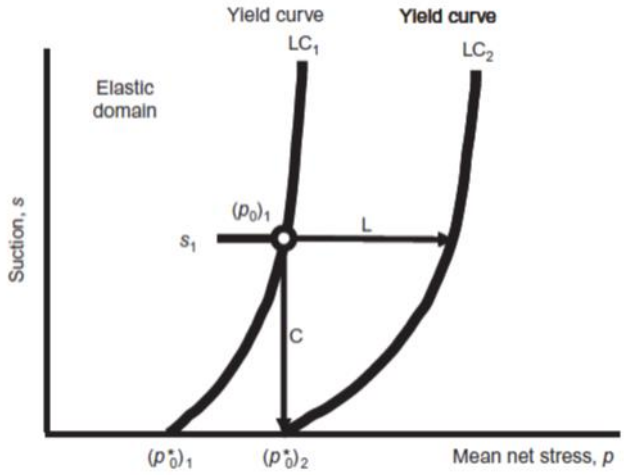

Figure 2.4 LC yield curve shifting due to loading at constant suction and wetting at constant mean stress (Gens, 2010).

Other yielding curve termed as suction increase (SI) yield curve is included to predict plastic volumetric strains caused by suction increase (drying) beyond the maximum past suction ever experienced by the soil (s_0) with the following hardening law:

$$d\varepsilon_v^p = \frac{\lambda(s)-\kappa_s}{v}\frac{ds_0}{s_0 + p_{atm}} \tag{2-24}$$

The formulation in the deviatoric stress state implements elliptic yield surface defined in the Modified-Cam Clay (MCC) model. MCC ellipse expands with increasing preconsolidation stress due to increasing net stress and increasing shear strength due to suction; the effect of suction on the shear strength is included with a linear approximation such as multiplying suction by a contant *k*:

$$f = q^2 - M^2(p+ks)(p_0 - p) \tag{2-25}$$

The flow rule defines the ratio of plastic shear strains to plastic volumetric strains:

$$\frac{d\varepsilon_s^p}{d\varepsilon_v^p} = \frac{2q\alpha}{M^2\left(2p+ks-p_0\right)} \tag{2-26}$$

where α is a parameter used to define associated or non-associated flow rule.

Table 2.2 BBM Formulations

<table>
<tr><td colspan="2">Isotropic formulation</td></tr>
<tr><td>Elastic</td><td>plastic</td></tr>
<tr><td>$d\varepsilon_v^e = \frac{\kappa_s}{v}\frac{ds}{s+p_{atm}} + \frac{\kappa}{v}\frac{dp}{p}$</td><td>Yield surface:
$p_0 = p_c\left(p_0^*/p_c\right)^{\frac{\lambda(s)-\kappa}{\lambda(0)-\kappa}}$
$\lambda(s) = \lambda(0)\left((1-r)\exp(-\beta s)+r\right)$
Hardening law:
$d\varepsilon_{vp}^p = \frac{\lambda(0)-\kappa}{v}\frac{dp_0^*}{p_0^*}$
$d\varepsilon_{vs}^p = \frac{\lambda(s)-\kappa_s}{v}\frac{ds_0}{s_0+p_{atm}}$
$d\varepsilon_v^p = d\varepsilon_{vp}^p + d\varepsilon_{vs}^p$</td></tr>
<tr><td colspan="2">Deviatoric formulation</td></tr>
<tr><td>Elastic</td><td>Plastic</td></tr>
<tr><td>$d\varepsilon_v^e = \frac{\kappa_s}{v}\frac{ds}{s+p_{atm}} + \frac{\kappa}{v}\frac{dp}{p}$
$d\varepsilon_q^e = \frac{1}{3G}dq$</td><td>Yield surface:
$q^2 = M^2\left(p+ks\right)\left(p_0-p\right)$
$p_0 = p_c\left(p_0^*/p_c\right)^{\frac{\lambda(s)-\kappa}{\lambda(0)-\kappa}}$
Hardening law:
$d\varepsilon_{vp}^p = \frac{\lambda(0)-\kappa}{v}\frac{dp_0^*}{p_0^*}$
Flow rule:
$\frac{d\varepsilon_s^p}{d\varepsilon_v^p} = \frac{2q\alpha}{M^2\left(2p+ks-p_0\right)}$
$\alpha = \frac{M\left(M-9\right)\left(M-3\right)}{9\left(6-M\right)}\frac{1}{1-\kappa/\lambda(0)}$</td></tr>
</table>

2.3.4 Gallipoli Model

Bruno and Gallipoli (2019) proposed bounding surface model to predict hydromechanical behaviour of unsaturated soil specimens under isotropic stress state. This model is the combination of hydraulic model proposed by Gallipoli et al., (2015) and mechanical model proposed by Gallipoli and Bruno (2017).

In the hydraulic model, degree of saturation is related with a parameter termed as scaled suction that consist of the effect of both suction and void ratio. The water retention behaviour is consequently described on the plane of degree of saturation and scaled suction rather than within the space of degree of saturation-suction-void ratio. The scaled suction is defined with relating suction and void ratio in a power equation (Tarantino, 2009; Gallipoli et al., 2015).

$$\overline{s} = se^{1/\lambda_s} \tag{2-27}$$

λ_s is material parameter.

Hysteretic water retention behaviour is bounded by main wetting and main drying retention curves. Gallipoli et al. (2015) defined main retention curves using the equation type proposed by Van Genuchten (1980):

$$S_r = \left(1 + \left(\frac{\overline{s}}{\omega_i} \right)^{\frac{\lambda_S}{m_i}} \right)^{-m_i} \tag{2-28}$$

ω_i is scaled air-entry suction, m_i is material parameter, index i denotes wetting (w) or drying (d). Scaled suction increases in drying regime and decreases in wetting regime. The derivative of (2-28) with respect to suction is:

$$\frac{dS_r}{d\overline{s}} = -\frac{\lambda_s}{\overline{s}} S_r^{-(1/m_i)} \left(S_r^{-(1/m_i)} - 1 \right) \tag{2-29}$$

The gradient of a drying curve for a given degree of saturation on the degree of saturation-scaled suction plane is related with the gradient of main drying curve

(M_d) at that specific point and could be expressed in the following power function (Zhou et al., 2012):

$$\left(\frac{dS_r}{d\bar{s}}\right)_d = \left(\frac{\bar{s}}{\bar{s}_d}\right)^{\beta_d} \left(\frac{dS_r}{d\bar{s}}\right)_{Md} \tag{2-30}$$

where $\bar{s}_d$ is scaled suction on the main drying curve for a given degree of saturation. The derivative main drying curve on the right-hand side of (2-30) and $\bar{s}_d$ are respectively obtained using (2-29) and (2-28). The derivative of any drying curve can be expressed after arranging (2-30):

$$\frac{dS_r}{d\bar{s}} = -\frac{\lambda_s}{\omega_d^{\beta_d}} \bar{s}^{\beta_d - 1} S_r^{1+(1/m_d)} \left(S_r^{-(1/m_d)} - 1\right)^{\left(1-\beta_d m_d/\lambda_s\right)} \tag{2-31}$$

Integration of (2-31) results in a closed form expression for drying curves bounding between main wetting and main drying curves:

$$\left(S_r\right)_d = \left(1 + \left(\frac{\bar{s}^{\beta_d} + C_d}{\omega_d^{\beta_d}}\right)^{\lambda_s/\beta_d m_d}\right)^{-m_d} \tag{2-32}$$

C_d is integration constant and defined as an initial boundary condition after extracting from (2-32) for a known degree of saturation and scaled suction pair.

The gradient of a wetting curve is related with the gradient main wetting curve (M_w), similar to (2-30):

$$\left(\frac{dS_r}{d\bar{s}}\right)_w = \left(\frac{\bar{s}_w}{\bar{s}}\right)^{\beta_w} \left(\frac{dS_r}{d\bar{s}}\right)_{Mw} \tag{2-33}$$

The derivative of a wetting curve becomes:

$$\frac{dS_r}{d\bar{s}} = -\frac{\lambda_s \omega_w^{\beta_w}}{\bar{s}^{\beta_w + 1}} S_r^{1+(1/m_w)} \left(S_r^{-(1/m_w)} - 1\right)^{\left(1-\beta_w m_w/\lambda_s\right)} \tag{2-34}$$

Integration of (2-34) results in a closed form expression for drying curves bounding between main wetting and main drying curves:

$$\left(S_r\right)_w = \left(1+\left(\frac{\overline{s}^{\beta_w}}{\omega_w^{\beta_w}\left(1+C_w\overline{s}^{\beta_w}\right)}\right)^{\lambda_s/\beta_w m_w}\right)^{-m_w} \tag{2-35}$$

C_w is integration constant and defined as an initial boundary condition after extracting from (2-35) for a known degree of saturation and scaled suction pair.

Seven parameters λ_s, m_d, ω_d, β_d, m_w, ω_w and β_d should be determined to predict a hysteretic loop. Model parameters could be calibrated with S_r, e and s experimental data obtained from either varying suction under constant net stress test (i.e. retention curve mesurements) or varying net stress under constant suction test (drained loading-unloading test).

In mechanical model proposed by Gallipoli and Bruno (2017), average skeleton stress, $p' = p - u_a + Sr$ x s and degree of saturation are used to describe hysteretic variation of void ratio. The term used for the definition of average skeleton stress recovers Terzaghi's effective stress in saturated state. The interparticle stresses are increased due to capilarity strengthtening the bond between soil grains. This results in unsaturated soils remaining stable at higher void ratios compared to saturated state under the same average skeleton stress. Gallipoli and Bruno (2017) stated that the variations in the degree of saturation become more effective in generating capillary effects than the variations in the suction since capillary effect mainly depends on the number of water meniscuses within a unit volume rather than the level of forces within the meniscus that attract particles to each other. In this approach, capilary effect is described using the inverse of degree of saturation $1/S_r$. There is no capilary effect at the saturated state since degree of saturation and so the proposed description equals to 1; capillary effect increases with decreasing degree of saturation that is less than 1 and description becomes greater than 1. The following expression for capillary effect is proposed using this description:

$$\frac{e}{e_s} = \left(\frac{1}{S_r}\right)^{\lambda_r} \tag{2-36}$$

λ_r is slope of virgin compression line, e is void ratio for unsaturated specimen and e_s is void ratio corresponds to same average skeleton stress at saturated state. The description of inverse of degree of saturation converges to infinity with increasing suction; but, number of menisci decreases and so does capillary effects at very large suctions. Therefore, proposed description might be problematic for very dry soils.

(2-36) is expressed on the log(e/e_s)-log(S_r) plane and following equation can be written:

$$\log\left(e/e_s\right) = -\lambda_r \log S_r \tag{2-37}$$

The equation of virgin compression line is expressed using loge_s:

$$\log e_s = -\lambda_p \log\left(p'/p'_{ref}\right) \tag{2-38}$$

λ_p and p'_{ref} are respectively the slope of virgin compression line and reference average skeleton stress for virgin compression line at void ratio is equal to 1. The combination of (2-36), (2-37), (2-38) results in following expression:

$$\log e = -\lambda_p \log\left(p' S_r^{\frac{\lambda_r}{\lambda_p}} \Big/ p'_{ref}\right) \tag{2-39}$$

Gallipoli and Bruno (2017) defined a new parameter termed as scaled stress based on (2-39).

$$\bar{p} = p' S_r^{\frac{\lambda_r}{\lambda_p}} \tag{2-40}$$

A unique compression line for both unsaturated and saturate states can be defined using scaled stress:

$$\log e = -\lambda_p \log\left(\bar{p}/\bar{p}_{ref}\right) \tag{2-41}$$

Gallipoli and Bruno (2017) assumed that the gradient of any compression line would converge to gradient of unique compression line on the plane of $\log e - \log \bar{p}$ and proposed a closed form equation for all isotropic loading paths:

$$e = \left(\left(\bar{p}/\bar{p}_{ref}\right)^{\gamma} + C_l\right)^{-\frac{\lambda_p}{\gamma}} \tag{2-42}$$

C_l is integration constant and γ is material parameter.

In the unloading path, the gradient of unloading line would be equal to slope of unloading line κ on the $\log e - \log \bar{p}$ plane. The integration of this constant results in following expression:

$$e = C_u / \bar{p}^{\kappa} \tag{2-43}$$

C_u is integration constant.

Five model parameters λ_p, λ_s, $\bar{p}_{ref}$, γ, k are required to predict isotropic loading-unloading behaviour of soil.

Bruno and Gallipoli (2019) combined hydraulic and mechanical model to obtain coupled solution under isotropic stress state. Hydraulic and mechanical equations are iteratively solved by commencing iteration with an initial degree of saturation (can be taken as the result from previous solution step). The scaled stress is calculated based on initial degree of saturation using (2-40) and then, (2-32) or (2-43) depending on the loading-unloading stress path that is used to calculate void ratio. This calculated value of void ratio is introduced into (2-32) or (2-35) depending on the hydraulic regime to determine new degree of saturation. New scaled stress, void ratio and scaled suction are calculated based on the new degree of saturation. Old and new scaled stresses are compared to check if loading or unloading condition is valid.

2.4 Shear Strength of Unsaturated Soils

In most of geotechnical engineering problems, the ultimate loads are restricted by the shear strength of the soil rather than the compression and tensile strength and therefore its evalution is quite significant. The Mohr-Coulomb relationship is the most accepted approach for describing shear strength of saturated soils.

$$\tau = c' + \sigma' \tan(\varphi') \tag{2-44}$$

where τ is the shear strength (or shear stress acting on the failure plane), c' is the effective cohesion, σ' is the effective stress normal to the failure plane and f' is the angle of internal friction. In this equation, the component of shear strength due to friction forces along the shear surface is captured by the second term on the right hand side and the cohesion term captures the contribution of attraction forces between soil particles (Van der Walls forces, cementation, capillary forces, etc.).

In unsaturated soils, the tension in the water draws the soil particles to each other and causes increase in the normal stresses at the particle contacts, thus effective stress also increases. Bishop (1959) extended the expression of Terzaghi's effective stress for unsaturated soils:

$$\sigma' = \sigma - u_a + \chi(u_a - u_w) \tag{2-45}$$

where χ is the effective stress parameter. χ is constrained between 0 when soil is completely dry and 1 when soil is saturated. For simplicity, effective stress parameter can be generally equated to degree of saturation (Öberg and Sällfors, 1995).

Karube et al. (1996) used effective degree of saturation in order to describe parameter:

$$\chi = \frac{S_r - S_{res}}{1 - S_{res}} \tag{2-46}$$

where S_r is the degree of saturation and S_{res} is the degree of saturation at residual condition.

Khalili and Khabbaz (1998) proposed an empirical equation:

$$\chi = \left(\frac{s}{s_{aev}} \right)^{-0.55} \tag{2-47}$$

where s is the suction and s_{aev} is the air-entry pressure of the soil.

The general definition of matric suction is reduced to capillary pressure (u_a-u_w) and adsorption mechanism is not recovered (Lu and Zhang, 2019). Bishop's effective stress is not capable of capturing adsorption (Lu, 2020). Lu and Likos (2006) defined a term called as suction stress to account for both capillarity and adsorption effects on effective stress and proposed following expression of effective stress in a form similar to Terzaghi's effective stress:

$$\sigma' = (\sigma - u_a) - \sigma_s \tag{2-48}$$

σ_s is suction stress and it is defined by suction stress characteristic curve (SSCC). A closed form equation for SSCC could be defined using the form of Bishop's effective stress (Lu et al., 2010); but, the effect of adsorption on effective stress remains missing.

CHAPTER 3

EXPERIMENTAL STUDIES TO CAPTURE UNSATURATED SOIL BEHAVIOUR

The methods, equipment and procedures together with the test results are given in this chapter. The results presented here aim to reveal the saturated and unsaturated behaviour of the soils used in this study. Results from the proposed practical procedures are compared with the findings provided in this chapter for validation.

3.1 Materials

The saturated and unsaturated engineering properties of several types of soils were revealed during the experimental campaign in this study. Soil types studied during experiments cover wide range on the gradation spectrum from fine sands to highly plastic clays. However; three different soil samples were mostly used during the experimental studies.

A silt sample taken from the city of Mersin in Turkey during Ahmadi-Naghadeh (2016)'s previous research study was already available in the laboratory and further experiments were carried out on the same soil sample. This soil is termed as Mersin silt in this study. The index properties of Mersin silt were provided by Ahmadi-Naghadeh (2016). The specific gravity, liquid limit and plasticity index were respectively given as 2.725, 25% and 5%. The USCS classification of Mersin silt is ML. The air-dry water content of Mersin silt sample in the laboratory environment was measured as 0.7%.

Another silt sample was provided by Dr. Mehmet Barış Can Ülker who visited the city of Elazığ in Turkey after Elazığ (Sivrice) earthquake in 2020 and recovered soil sample in the vicinity of the disaster area. This soil is termed as Elazığ silt in

this study. The materials passing from 2 mm sieve (No:10) was separated and used in the experimental studies. The specific gravity of Elazığ silt is determined as 2.809. The USCS classification of this soil is ML. The air-dry water content of Elazığ silt sample in the laboratory environment was measured as 1.7%.

Finally, Ankara clay soil sample was taken from the construction site of 100. Yıl market place in 2017. Ankara clay is a highly plastic expansive type soil. Mineralogical composition of Ankara clay is kaolinite-illite-montmorillonit and the exchangable ion seems calcium (Çokça, 1991). Soil sample at in-situ water content was mixed with water and coarse gravels and cobbles were separated on 9.5 mm sieve. The slurry passing 9.5 mm sieve was left in open-air. Air-dry sample was crushed into smaller portions by hitting with a plastic hammer and pulverized by rolling a wooden cylinder on it. Dust material was sieved through No:10 (2 mm) and passing portion collected in a container to use in experimental studies. Air-dry water content of this material was measured as 6.5%. The specific gravity is 2.704, liquid limit and plastic limit are 57% and 35%, respectively. The gradation curve was obtained by performing wet sieve analysis and hydrometer tests (Fig. 3.1). Harvard miniature compaction test was performed to obtain compaction curve (Fig. 3.2) showing optimum water content of 25%. The USCS classification of soil was determined as CH type.

Table 3.1 Index properties of the soil samples used in this study

	Mersin silt	Ankara clay	Elazığ silt
Specific gravity	2.725	2.704	2.809
Liquid limit (%)	25	57	21
Plasticity index (%)	5	35	3
USCS classification	ML	CH	ML
Saturated conductivity* (m/sec)	2.71×10^{-8}	1.69×10^{-10}	3.55×10^{-4}

*Saturated hydraulic conductivity of Mersin silt specimen with initial void ratio of 0.72 was measured by performing flexible wall permeability test, saturated hydraulic conductivity of Ankara clay specimen consolidated under 50 kPa vertical

stress was measured by falling head test, the saturated hydraulic conductivity of Elazığ silt was back calculated from consolidation data of saturated triaxial test.

The gradation curves of these soils are given in Fig. 3.1 and their index properties are tabulated in Table 3.1.

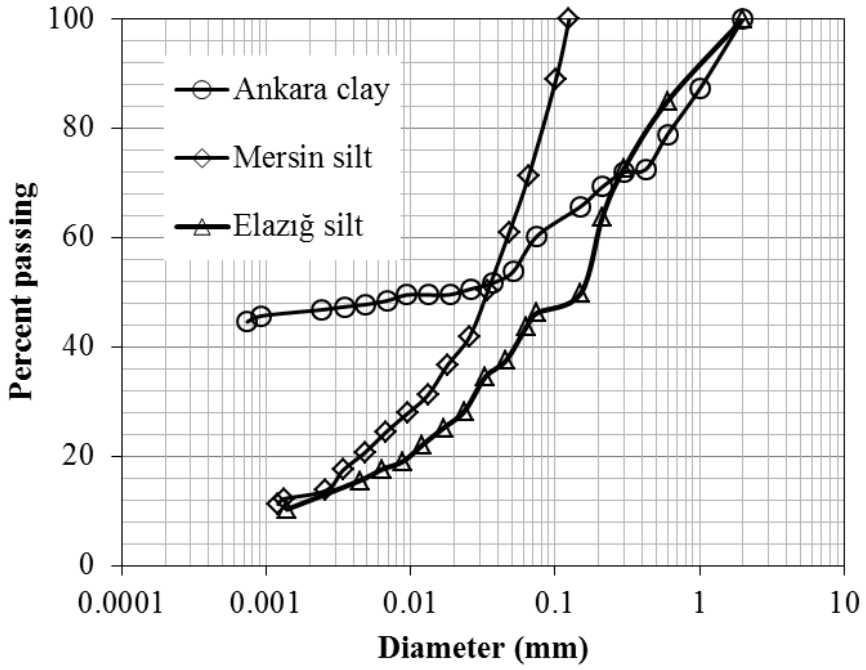

Figure 3.1 The gradation curves of soil samples used in this study

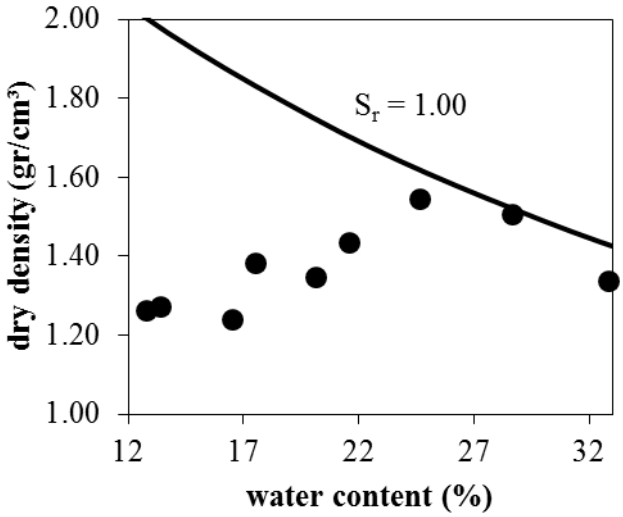

Figure 3.2 Harvard miniature compaction curve of Ankara clay sample

3.2 Specimen Preparation

3.2.1 Preparation of Mersin Silt and Elazığ Silt Specimens

Test specimens were formed from soil samples through several specimen preparation procedures. Mersin silt and Elazığ silt specimens were created implementing static compaction method at desired gravimetric water content and dry density. The undercompaction method (Ladd, 1978) was preferred in case of triaxial test specimens to achieve homogeneity along specimen's vertical axis. Mersin silt specimens were prepared by the procedure given in Ahmadi-Naghadeh (2016): Mersin silt sample at initial gravimetric water content of 0.104 was compacted in ten layers to initial void ratio of 0.72 with the undercompaction ratio of 0.06. In this study, several tests were carried out for Mersin silt specimens having different initial void ratio such as 0.83 and 0.92 in addition to initial void ratio of 0.72.

In case of Elazığ silt, the initial gravimetric water content of soil sample was selected as 0.221 and initial void ratio was set at 0.845. The soil sample was compacted in seven layers with undercompaction ratio of 0.06.

The procedure that is elaborated below is implemented for both Mersin and Elazığ silt. Air-dry soil sample is taken from the soil batch. The air-dry soil is poured into a bowl that is placed on the balance until the specific amount is read from the balance. This amount is arranged such that approximately 30 grams of bulk soil remains after finalizing specimen preparation and used in determination of initial gravimetric water content of soil sample. Water is added to air-dry soil sample inside a bowl that is placed on the balance using a syringe with needle. The balance is carefully monitored during pouring water through syringe to assure that the certain amount of water is added to achieve desired initial gravimetric water content. Then, bowl is taken from the balance and placed into a nylon bag in order to minimize the water loss during the mixing operation. The soil-water mixture is

kneaded with the fingers approximately 15 minutes while giving special attention for crushing soil lumps. The nylon bag is nicely tied after kneading and sealed in a second nylon bag. A sprayer is used to moisten the sealed volume between first and the second nylon bags to achieve utmost sealing of the soil sample by eliminating mass loss due to evaporation. The mixture is equilibrated inside the bowl for at least 1 day.

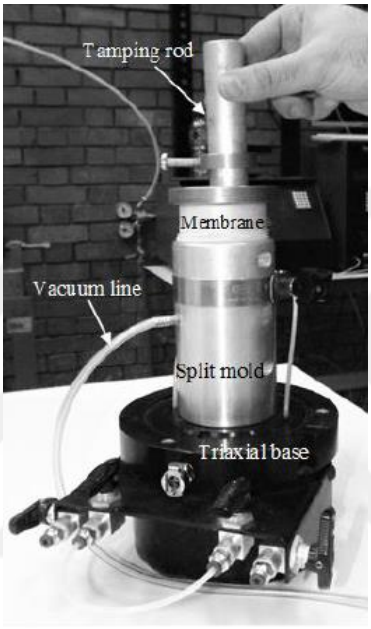

Figure 3.3 General arrangement for mosit tamping compaction (Ahmadi-Naghadeh, 2016)

The equilibrated soil sample is taken and separated into equal mass of soil portions inside plastic cups. The plastic cups are kept closed with lids during weighing process. A split mold is set up around a smooth cylinder platform. A latex membrane is fixed around this cylinder with an o-ring. The upper edge of the membrane is wrapped around outer side of the split mold at the top. A vacuum pump is connected to the split mold and used to stretch the mebrane to the inner surface of the split mold. First soil portion is poured into split mold. A thin spatula is used to mix and flatten the soil portion resulting a loose soil layer. The upper surface of the loose soil layer is further flattened by gently twisting the short edge of a ruler at the top of loose soil layer. A tamping rod is taken and its free height is

arranged by fixing it to a collar at a certain height. The required free heights to constitute each layer are previously calculated based on the formulations given in Ladd (1978). The loose soil layer is compacted by pressing with the tamping rod inside split mold. A few milimeters of the resulting flat surface is scratched by means of the thin spatula before starting the next layer operations.

3.2.2 Preparation of Ankara Clay Specimens

Ankara clay specimens were prepared by consolidating a slurry in 1D. A conventional oedometer test apparatus was used for oedometer test specimens. In case of preparation of triaxial test specimens, slurry is consolidated inside a large consolidation box (Fig. 3.4a). Air-dry Ankara clay sample was mixed with water to obtain slurry at water content of 4% higher than the liquid limit. The inner lateral surfaces of 30x30x17 cm size square shape aluminium container were lubricated by means of silicone oil. Slurry was poured into the box by taking attention to avoid air occlusion. A geotextile and filter paper was laid at the top and bottom of sample to prevent material loss through drainage holes. Square topcap is carefully placed upon the geotextile. Vertical force was applied on the sample by means of a pneumatic piston. A calibration curve that relates the air-pressure applied to the pneumatic piston and force exerted by the piston rod was extracted to accurately control the vertical stress acting on the consolidation box's topcap. A proving ring was placed on the loading frame and pneumatic piston was calibrated against the proving ring to obtain relationship between applied air pressure with resulting force (the relationship was obtained as $0.333u_a+10=\sigma_v$ -all pressures in kPa- for piston labeled as 4 in the laboratory, where u_a is air pressure applied to pneumatic piston and σ_v is resulting vertical stress which acts on the slurry). Slurry was anisotropically consolidated under 50 kPa vertical stress. 1 month duration was required to accomplish the consolidation of slurry according to the displacement measurements taken from the box's topcap. Three boxes of sample were required during the whole experimental campaign on Ankara clay.

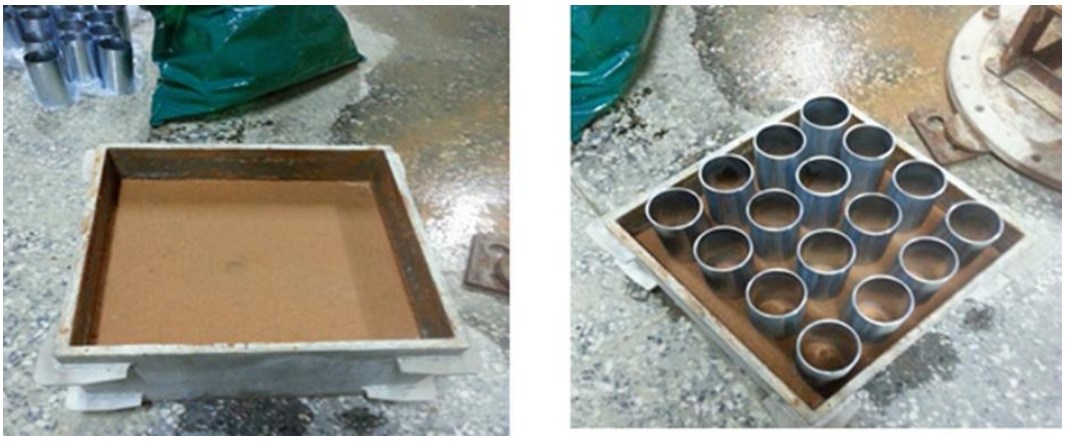

Figure 3.4 a) Ankara clay sample consolidated under 50 kPa vertical stress, b) Specimen samplers

Sixteen samplers that are 5 cm in diameter and 11 cm in height were placed upon the consolidated soil batch after removing topcap. The inner surface of each sampler was lubricated with silicone oil. Each sampler was slightly pressed into the soil and topcap was placed upon samplers. Consolidation box was placed on the loading frame and topcap was gently loaded. All samplers simultaneously inserted into soil under the applied load (Fig. 3.4b). The soil around the samplers was dug out using a spatula and some of discarded material was used for water content measurements. The standard deviations of the gravimetric water content measurements taken from various locations within the samples were 0.003, 0.005 and 0.006. Specimens were extruded from the samplers by pushing an extrusion rod, which is a solid cylinder at approximately same diameter with sampler's inner diamter. The extrusion should be performed in the exact opposite direction of insertion, otherwise extrusion process generally causes specimen disturbance. Specimens were placed on the base plates after extrusion and sealed with nylon bags. Sealed specimens were handled through their base plates and placed in a desiccator which is filled with water at its compartment.

In the begining of the study, some specimens were kept inside the samplers, sealed inside a water filled container. Any possible swelling of specimens inside samplers were prohibited by placing weights at the top of the samplers. In such a case, there

is no loss of specimen's water. However, keeping specimens inside water tank for several weeks or months resulted in bacterial attack inside specimen and corrosion of samplers. Therefore, this procedure was never implemented for the later operations.

3.3 Saturated Tests

3.3.1 Saturated Tests on Mersin Silt

Saturated triaxial and oedometer tests were performed on Mersin silt specimens. The saturated test program on Mersin silt is given in Table 3.2. CID triaxial tests on Mersin silt (MCID01, MCID02, MCID03) had already been carried out by Ahmadi-Naghadeh (2016), two CK_0 tests and one CK_0D were performed in this study.

Table 3.2 Saturated test program on Mersin silt

Test type	ID	e_0	σ_{net} (kPa)	s (kPa)
CK_0	$MCK_0$01	0.74	400	0
CK_0D	MCK_0D02	0.78	400	0
CK_0	$MCK_0$03	0.81	400	0

In the CK_0D test, specimen was saturated under 500 kPa back pressure. In the following stage, specimen was anisotropically consolidated by applying vertical effective stress with the loading steps of 25-50-100-400 kPa. At the end of the consolidation, triaxial cell was dismantled and specimen's water content and dry density were measured at four locations for $MCK_0$01 and $MCK_0$03 tests. Water displacement method was used for determination of dry density (ASTM D7263-09). In case of MCK_0D02 test, specimen was sheared under drained condition with the shear rate of 0.004 mm/min.

Four standard oedometer tests were performed on Mersin silt (Moed01, Moed02, Moed03, Moed04). First three of them are repeatibility tests on compacted specimens and in the forth one (Moed04), slurry soil was consolidated.

Anisotropic compression curves from aforementioned tests are plotted in Fig. 3.5. The results of oedometer tests seem repeatible. The slopes of recompression (C_r) and virgin compression lines (C_c) are respectively determined as 0.007 and 0.183 in average. In case of oedometer test on slurry (Moed04), virgin compression line slope is 0.097. For $MCK_0$01, MCK_0D02 and $MCK_0$03 tests virgin compression line slopes are respectively 0.156, 0.21 and 0.209. The preconsolidation pressures are determined according to strain energy method for both oedometric and K_0 consolidated curves (Germaine and Germaine, 2009), for $MCK_0$01, MCK_0D02 and $MCK_0$03 triaxial tests, preconsolidation pressures are respectively 149 kPa, 160 kPa and 154 kPa; and for Moed01, Moed02 and Moed03 tests preconsolidation pressures are 44 kPa, 58 kPa and 38 kPa, respectively. It is expected that compression characteristics should be similar between oedometric compression curves and K_0 consolidated curves which are extracted using triaxial system since specimens are tested under the same loading path in both cases; however, there is an inconsistency especially for preconsolidation stresses. A possible explanation of such inconsistency could be the difference between layer numbers during static compaction since triaxial specimen is compacted in 10 layers whereas oedometer specimen is compacted in a single layer and the preconsolidation stress better manifests itself in the former case. For example, the compression curves obtained from K_0 triaxial tests were compared with the isotropic compression curve (MCID03) which is a test carried out in Ahmadi-Naghadeh (2016) on the mean effective stress $(\sigma'_1+2\sigma'_3)/3$ axis in Fig. 3.6. Specimens for both types of test were compacted in 10 layers and their compression curves are much more compatible.

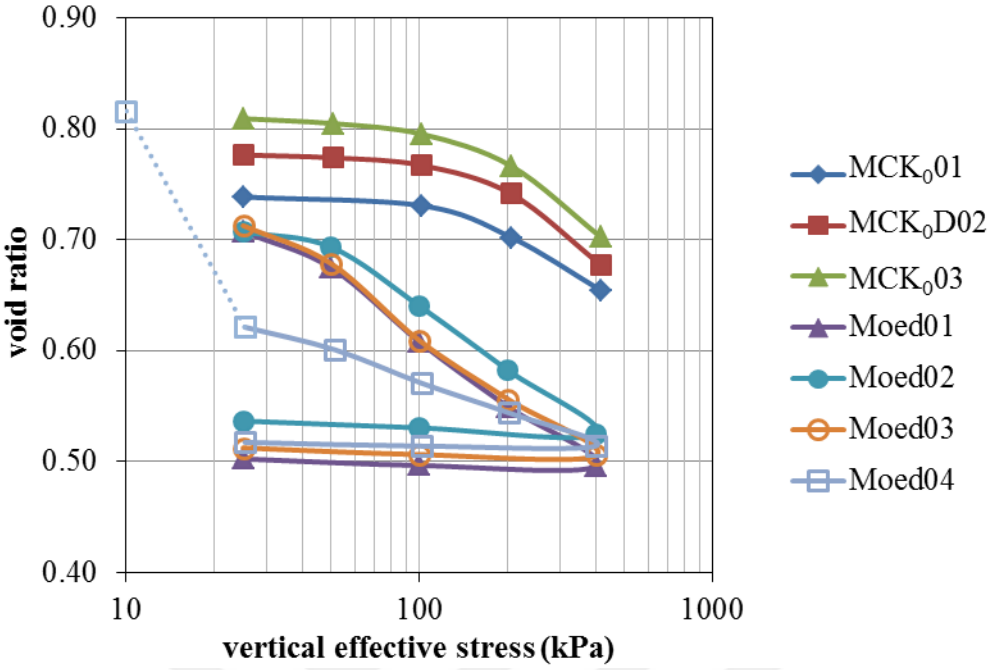

Figure 3.5 Anisotropic (K_0) compression curves of saturated Mersin silt

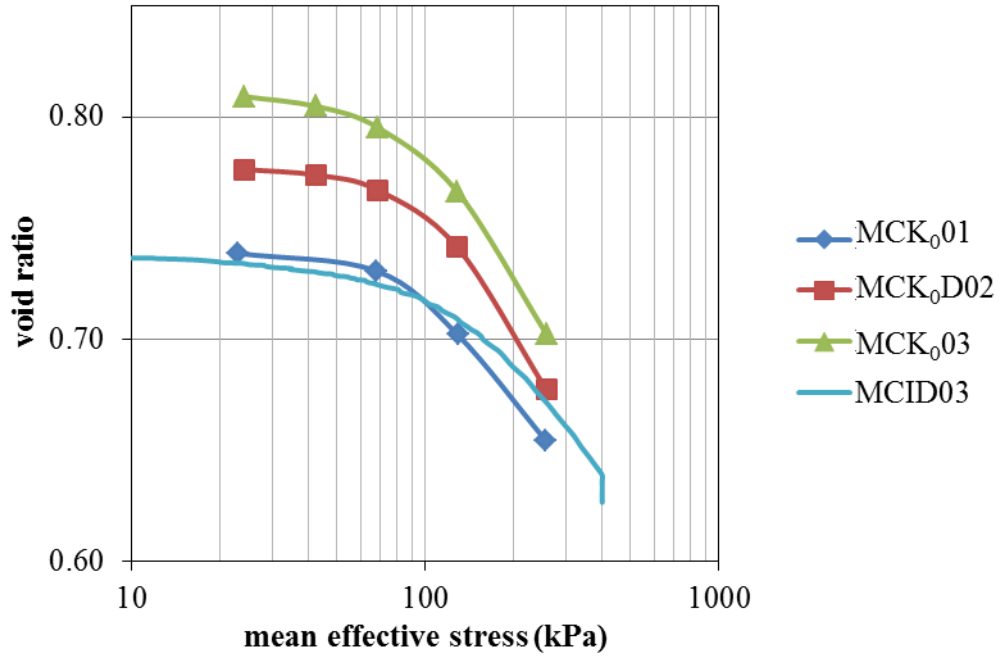

Figure 3.6 Comparison of K_0 compression curves and isotropic compression curves of Mersin silt

The variation of coefficient of lateral earth pressure at rest (K_0) is demonstrated in Fig. 3.7. K_0 of Mersin silt specimen compacted at initial void ratio of 0.72 is measured as 0.43. In case of overconsolidated stress state, variation of K_0 can be captured using a power type equation (in 3-1) which its power parameter is calibrated as 0.4.

$$K_{0,oc} = K_{0,nc}(OCR)^{p} \tag{3-1}$$

where $K_{0,oc}$ is the coefficient of earth pressure at rest under overconsolidated stress state, $K_{0,nc}$ is coefficient of earth pressure at rest under normally consolidated stress state and p is the power parameter.

Stress paths during K_0 consolidation are plotted in Fig. 3.8. These stress paths are not a straight line, a bilinear trend is observed between elastic and plastic states instead. The slope of K_0-line for normally consolidated stress state (or plastic stage) on deviatoric stress vs mean effective stress axes is determined as 0.674 which corresponds to Poisson's ratio of 0.35 ($\sigma_{dev}/\sigma_{mean}=0.674$, $\sigma_{dev}=\sigma_v-\sigma_h$, $\sigma_{mean}=(\sigma_v-2\sigma_h)/3$ and $K_0=\sigma_h/\sigma_h=\upsilon/(1-\upsilon)$). In the elastic stage, slope of K_0 line is higher and it is determined as 0.798 which corresponds to Poisson's ratio of 0.32.

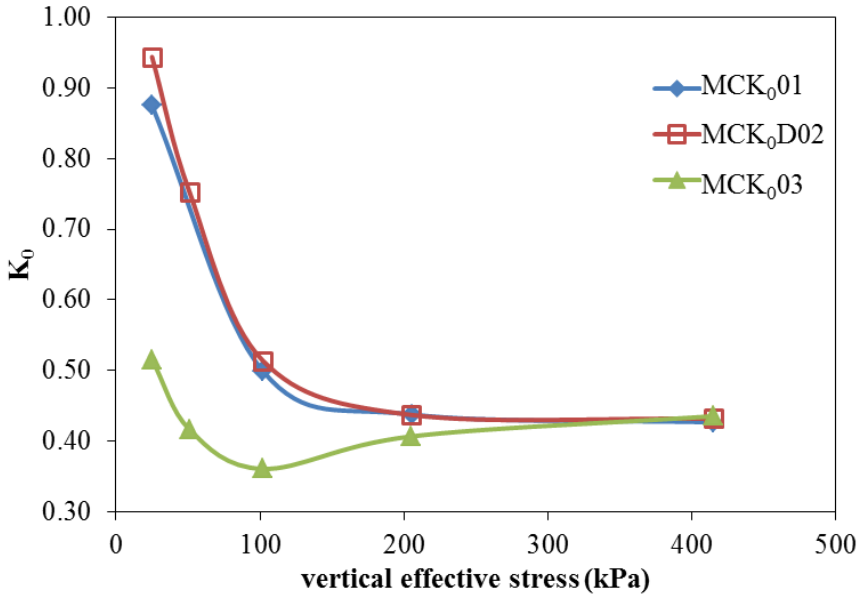

Figure 3.7 Variation of at rest earth pressure coefficient for Mersin silt tests

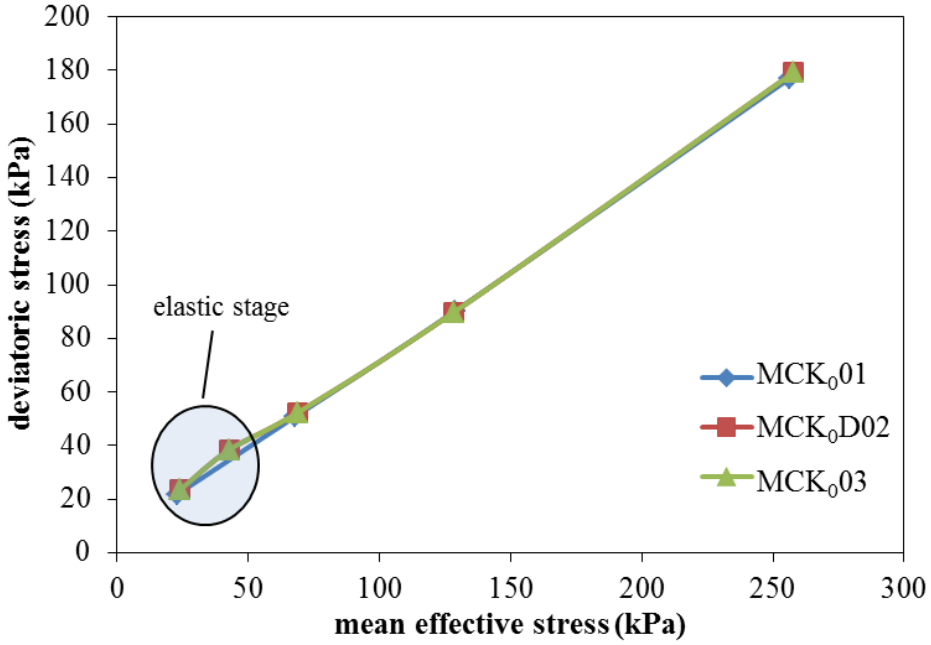

Figure 3.8 Stress paths during K_0 consolidation for Mersin silt

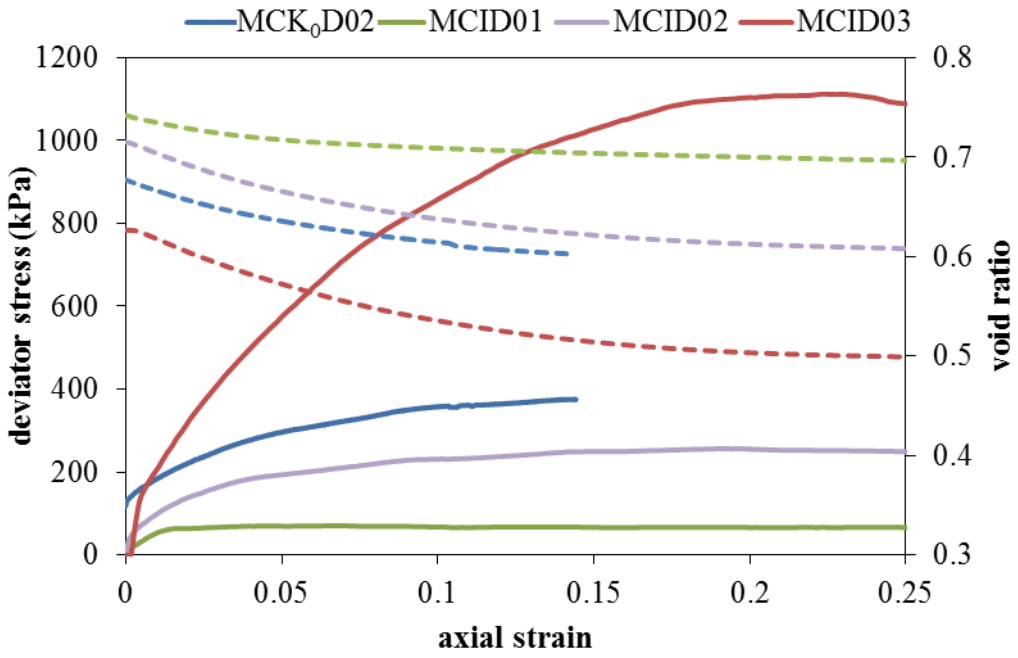

Figure 3.9 Deviatoric behavior of K_0 consolidated Mersin silt specimen in comparison with isotropically consolidated specimens, dashed lines denote void ratio variation on the secondary axis

The deviatoric behaviour monitored during MCK_0D02 is given together with previous isotropic tests results from Ahmadi-Naghadeh (2016) in Fig. 3.9. The effective confining stresses for MCID01, MCID02, MCID03 tests are 100 kPa, 200 kPa and 400 kPa. Ahmadi-Naghadeh (2016) was determined the internal friction angle f' and effective cohesion c' as 35.5° and 0 kPa and the slope of critical state line *M* was determined as 1.44.

3.3.2 Saturated Tests on Ankara Clay

Saturated triaxial and oedometer tests were performed on Ankara clay specimens. The saturated test program on Ankara clay is given in Table 3.3.

In the triaxial testing of Ankara clay specimens, saturation stage is only necessary to dissolve air entrapped between membrane and specimen during setup assembly procedure since specimens were produced from a saturated slurry. 200 kPa backpressure was applied during saturation stage. Specimens were consolidated under both K_0 and isotropic conditions at 25-50-100-400 kPa vertical efective stresses and isotropic stresses, respectively. Ankara clay slurry at liquid limit water content was tested in addition and consolidated under K_0 condition ($ACK_0 05$) to capture the virgin compression line. Specimens were covered with strip filter paper to reduce consolidation time and this is essential to finish experiments in a reasonable time period. After the consolidation stage, specimens were shear under drained condition. Strain rate at shear stage was determined as 0.0012%/min using method proposed by Bishop and Henkel (1964) based on coefficient of consolidation c_v value of 3.66×10^{-9} m^2/sec, which was determined using t_{100} value obtained from the consolidation stage results, and assuming strain at the failure is 8%:

$$c_v = \frac{\pi h^2}{100 t_{100}} \; and \; t_f = \frac{20 h^2}{\eta c_v} \tag{3-2}$$

where *h* is the drainage lentgh (half of specimen's height) and η is taken as 35.

Table 3.3 Saturated test program on Ankara clay

Test type	ID	σ_{net} (kPa)	s (kPa)
CK_0D	ACK_0D01	25	0
CK_0D	ACK_0D02	50	0
CK_0D	ACK_0D03	100	0
CK_0D	ACK_0D04	400	0
CK_0	ACK_005	400	0
CID	ACID01	25	0
CID	ACID02	50	0
CID	ACID03	100	0
CID	ACID04	400	0

Three standard oedometer tests (Aoed01, Aoed02, Aoed03) were performed on specimens trimmed from the reconstituted triaxial specimens.

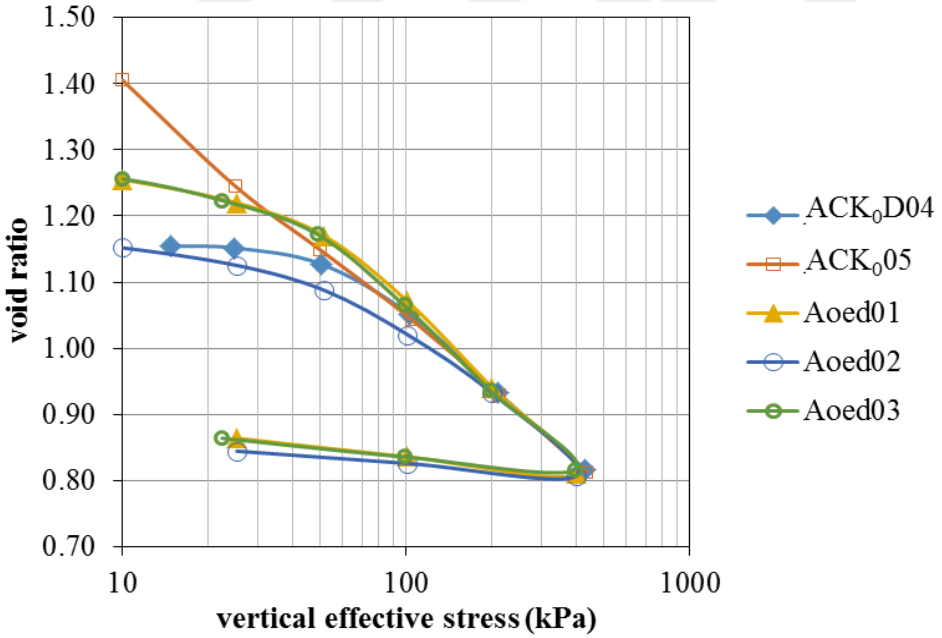

Figure 3.10 Comparison of K_0 and oedometric compression curves of Ankara clay

K_0 compression and oedometric compression curves are given in Fig. 3.9. Both type of curves show consistent behaviour. The preconsolidation pressures are nearly 50 kPa in all cases, which is vertical stress applied in consolidation box,

except for specimen tested at its liquid limit. The slopes of recompression (C_r) and virgin compression lines (C_c) are respectively determined as nearly 0.12 and 0.41 for all tests. On the mean effective stress axis, both isotropic and K_0 compression curves coincide with each other (Fig. 3.11) and virgin (λ)and recompression (κ) compression line slopes are respectively determined as 0.35 and 0.022.

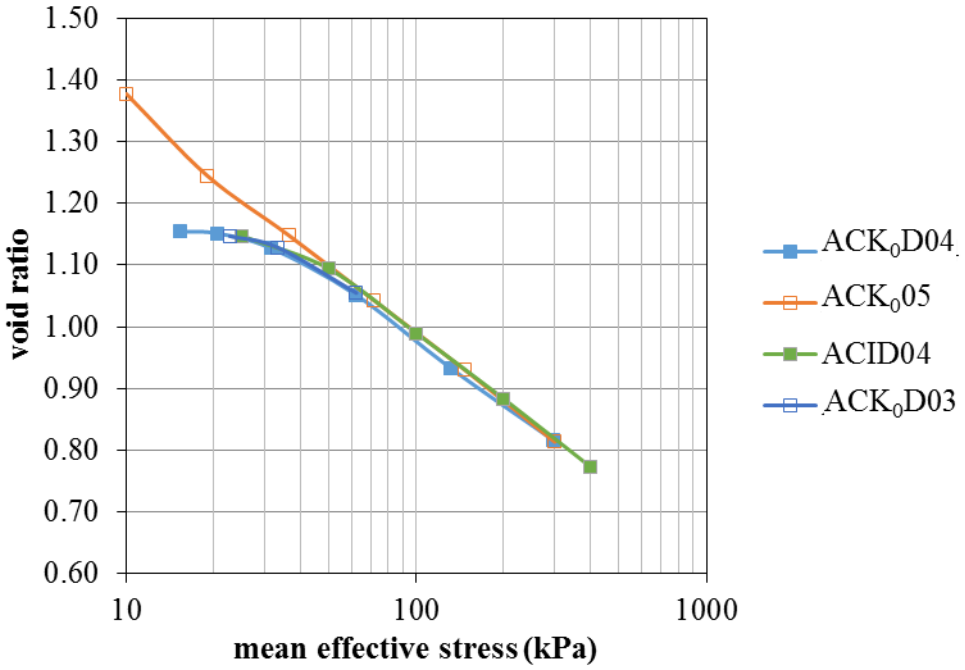

Figure 3.11 Comparison of isotropic and K_0 compression curves of Ankara clay

The variation of coefficient of lateral earth pressure at rest 'K_0' is demonstrated in Fig. 3.12. K_0 of normally consolidated Ankara clay is measured as 0.46. In case of overconsolidated stress state, the power parameter in 3-1 is calibrated as 0.71.

Stress paths from the K_0 consolidation stage of experiments are plotted in Fig. 3.13 and initially overconsolidated specimens show transition between elastic and plastic states. In case of ACK_005 test (specimen starts at its liquid limit) straight curve was obtained. The slope of K_0-line for normally consolidated stress state (or plastic stage) on deviatoric stress vs mean effective stress axes is determined as 0.633 which corresponds to Poisson ratio of 0.36 ($\sigma_{dev}/\sigma_{mean}=0.633$, $\sigma_{dev}=\sigma_v-\sigma_h$, $\sigma_{mean}=(\sigma_v-2\sigma_h)/3$ and $K_0=\sigma_h/\sigma_h=\upsilon/(1-\upsilon)$). In the overconsolidated (elastic)

state, slope of K_0 line is higher and it is determined as 0.981 which corresponds to Poisson ratio of 0.29.

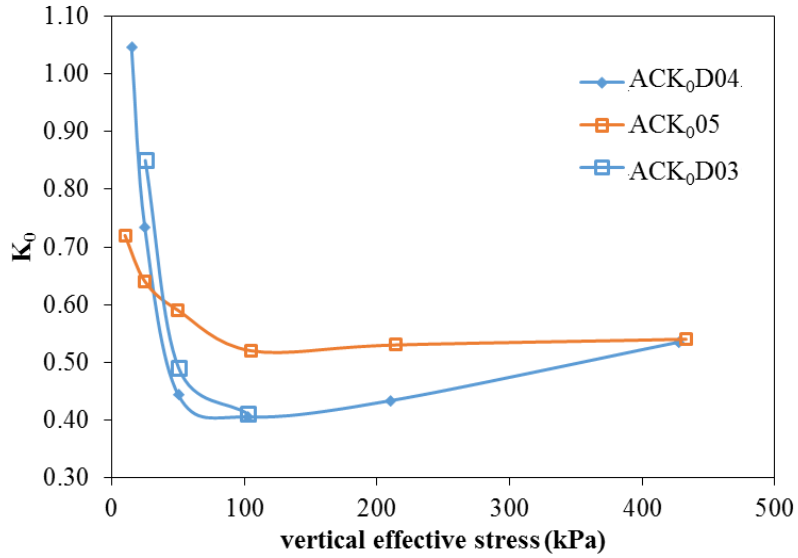

Figure 3.12 Variation of K_0 for Ankara clay tests

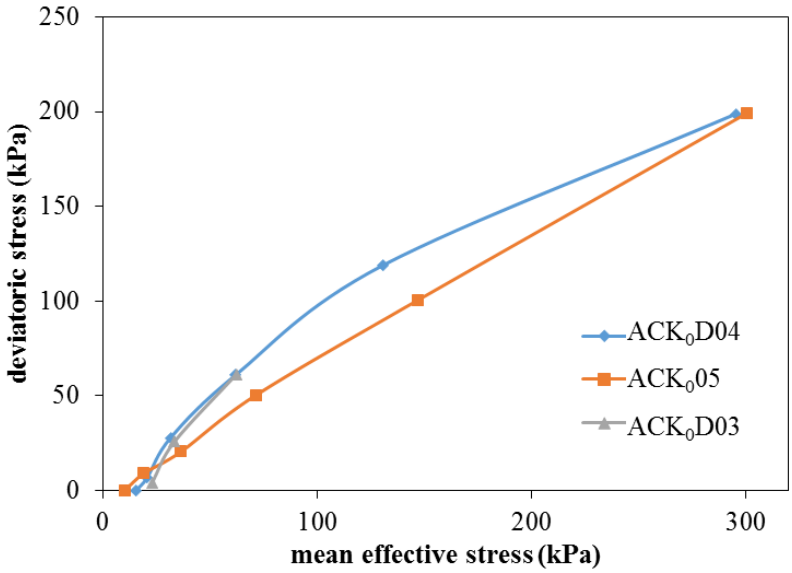

Figure 3.13 Stress paths for Ankara clay experiments

The deviatoric behaviour of both K_0 consolidated and isotropically consolidated Ankara clay specimens are shown in Fig 3.14 and 3.15. For low-confining stress

test (25 and 50 kPa), deviatoric stress fluctuates during plastic stage like stick and slip mechanism observed in case of granular soils.

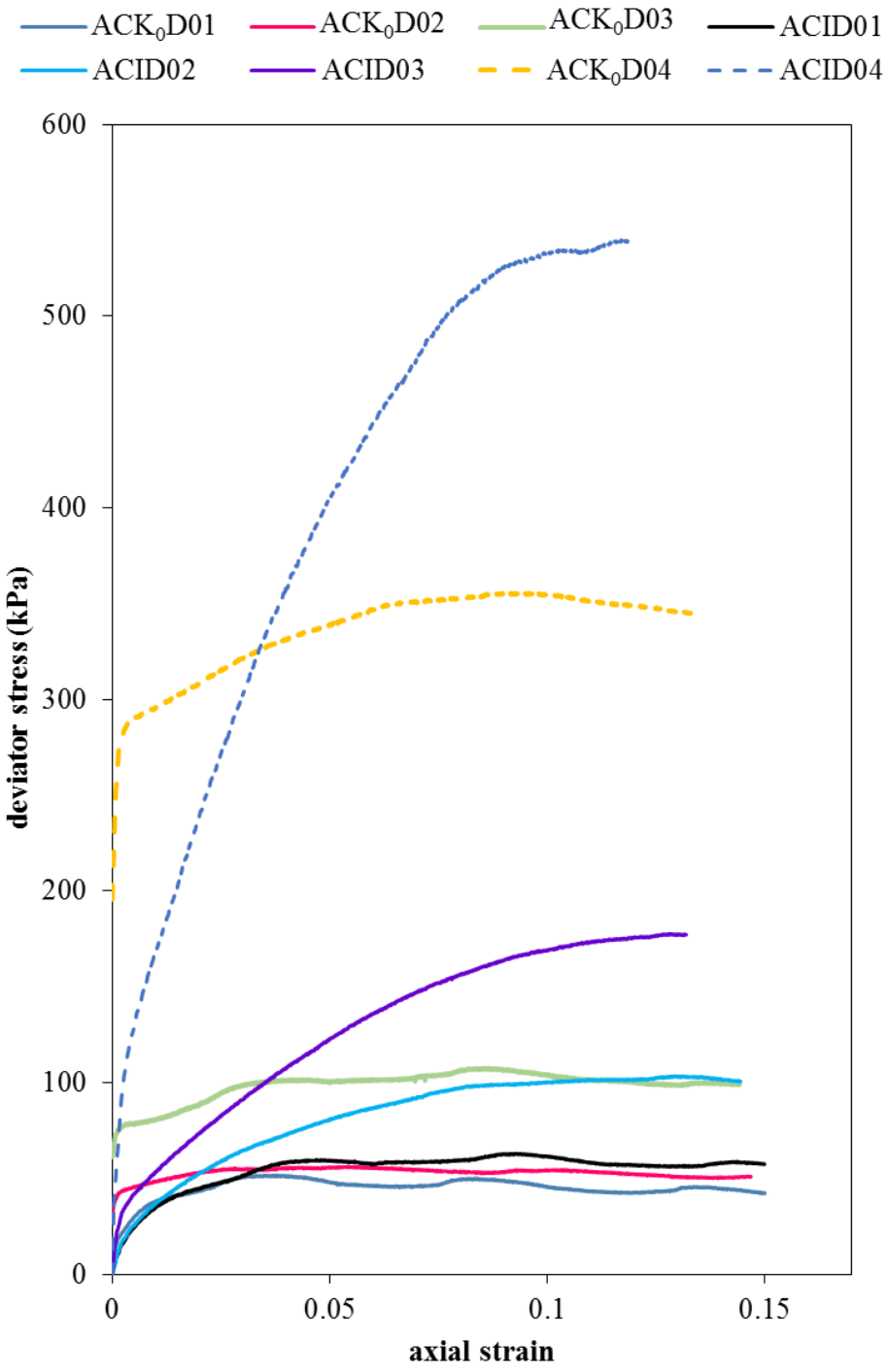

Figure 3.14 Deviatoric behaviour of Ankara clay specimens

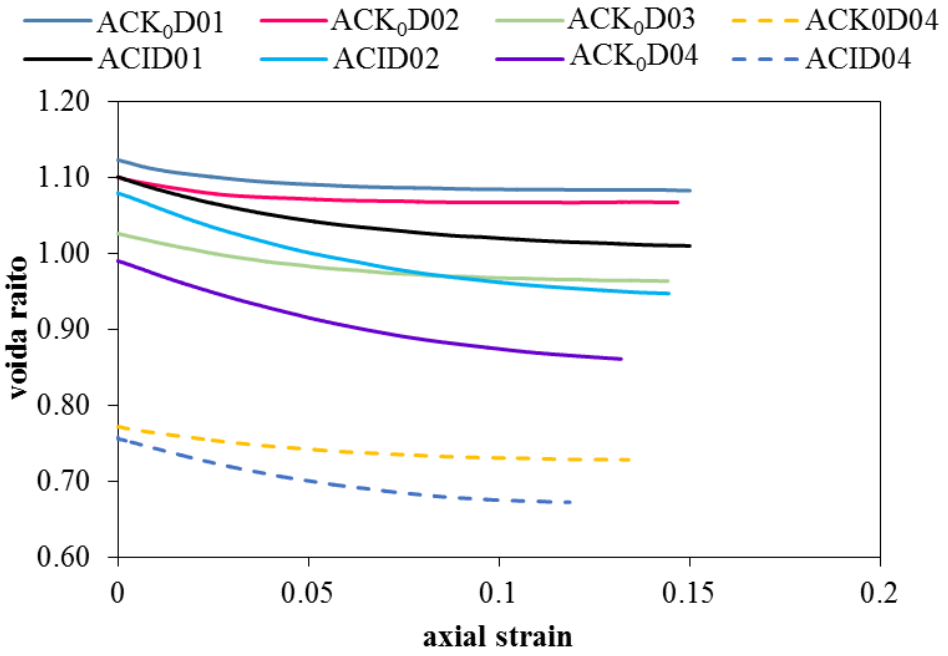

Figure 3.15 Variation of void ratio during drained shearing of Ankara clay

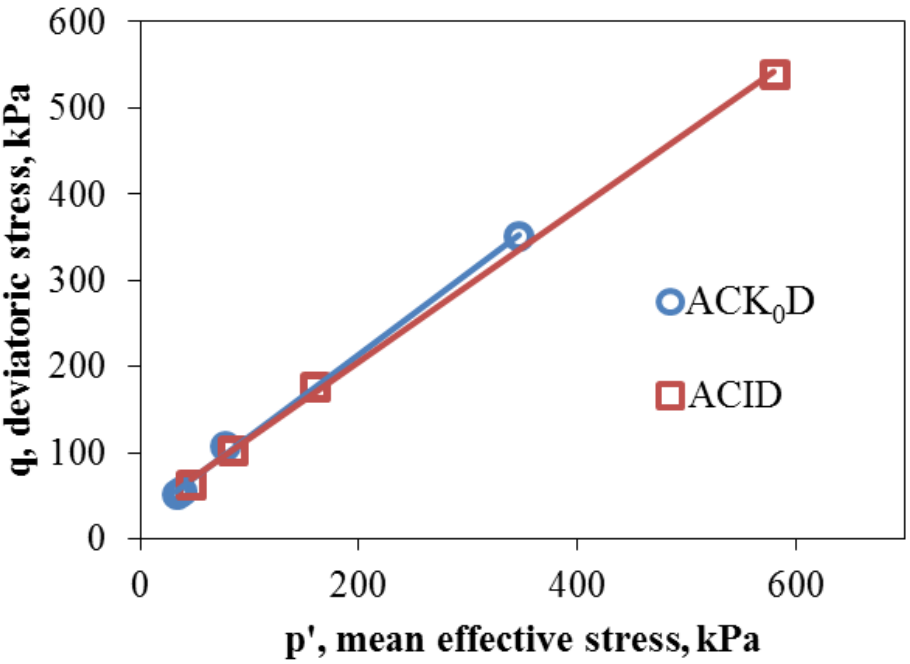

Figure 3.16 Critical state failure envelopes of Ankara clay

The failure envelopes obtained from both K_0 and isotropically consolidated shear test are depicted in Fig. 3.16. For isotropically consolidated Ankara clay specimens

(this is during the triaxial consolidation stage, not in the specimen preparation procedure) the internal friction angle f' and effective cohesion c' are determined as 22.6° and 13.7 kPa whereas for anisotropically (K_0) consolidated Ankara clay specimens these are 22.9° and 11.6 kPa. The slope of critical state line *M* is determined as 0.95.

3.3.3 Saturated Tests on Elazığ Silt

Saturated isotropically consolidated drained triaxial shear tests were performed at 50 kPa, 200 kPa and 400 kPa on compacted Elazığ silt specimens. In addition to these tests, isotropic and deviatoric loading-unloading tests were carried out on saturated Elazığ silt specimens. The complete saturated test program on Elazığ silt is given in Table 3.4.

Table 3.4 Saturated test program on Elazığ silt

Test type	ID	e_0	σ_{net} (kPa)	s (kPa)
CID	ECD01	0.845	50	0
CID	ECD02	0.845	200	0
CID	ECD03	0.845	400	0
CID	ECD08	0.845	200-10	0
CID	ECD10	0.845	200	0

The internal friction angle f' and effective cohesion c' were determined as 35.0° and 1 kPa. The slope of critical state line *M* was determined as 1.397. The deviatoric behaviour of Elazığ silt is shown in Fig. 3.17.

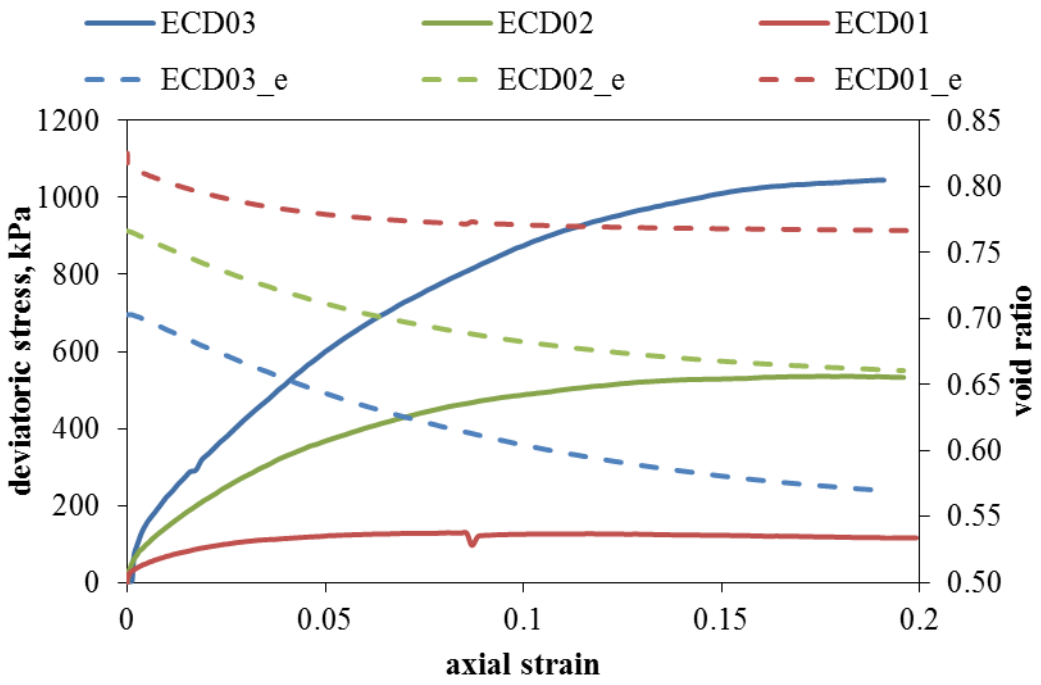

Figure 3.17 Deviatoric behaviour of saturated Elazığ silt

Isotropic loading-unloading behaviour of Elazığ silt was investigated in ECD08 test. The effective mean stress was traced 15-200-10-200-10-200 kPa by ramping the cell pressure with the rate of 0.4 kPa/min under drained condition. The ramped load rate is determined according to equation 7.1 in Bishop and Henkel (1964). In case of ECD10, specimen was isotropically consolidated to 200 kPa effective stress, then specimen was sheared up to 200 kPa deviatoric stress. Next, the deviatoric stress was reduced to 150 kPa to investigate response to shear cycles. In the cycle that followed, deviatoric stress was increased and decreased with 200 kPa increments and sheared up to 20% axial strain. The strain rate was selected as 0.05 %/min to ensure drained condition. The behaviour measured during ECD08 and ECD10 are shown in Fig. 3.18 and 3.19.

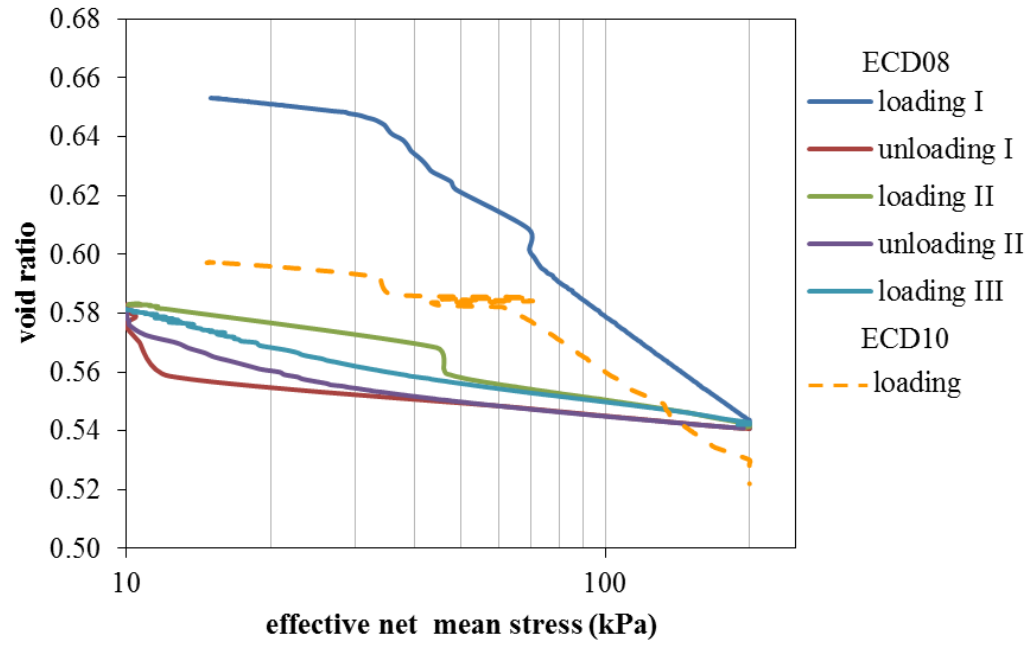

Figure 3.18 Isotropic loading-unloading test (ECD08) on Elazığ silt together with isotropic compression curve from ECD10 test

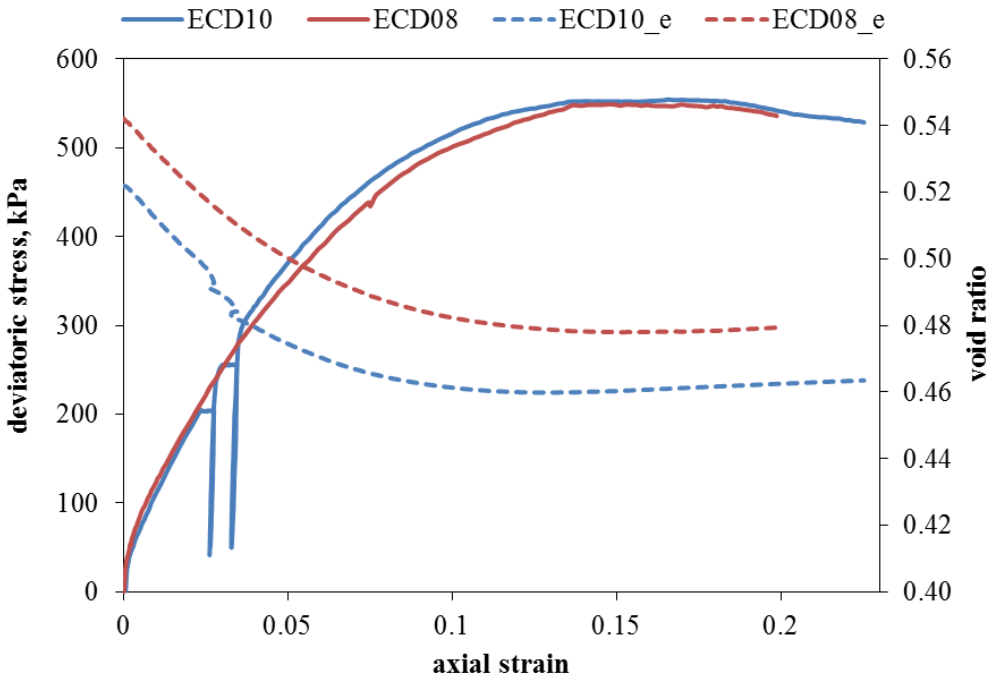

Figure 3.19 Deviatoric loading-unloading test (ECD10) together with ECD08 results

3.4 Soil Water Retention Curve Measurements

3.4.1 Measurements with Hanging Column

Soil water retention curve meaurements were performed with hanging column equipment up to suctions of 40 kPa. A cell was produced to control or monitor void ratio during testing. A polyvinyl chloride (PVC) pipe in 5 cm inner diameter was cut by means of a hand hacksaw blade to use as an oedometer ring. A PVC lid was grooved to form a drainage path and an exit was drilled to make a connection to vacuum generated by hanging columns. 15 bar high air-entry (HAE) ceramic disc, which was the only type present in the laboratory during laboratory work, was placed on the lid; but, lower capacity ceramics are much more suitable for the test setup in order to reduce test duration. A flat o-ring in specific size was manufactured in the laboratory to prevent air-leakage between ceramic and lid. A liquid gasket was poured between two latex membranes (disused membranes for triaxial specimens could be preferred) and squeezed. A flat o-ring in desired size and shape could be obtained by snipping the hardened liquid gasket. A cylindrical specimen extruder 5 cm in diameter was used to control vertical stress with a pneumatic piston and monitor change in specimen's height with a dial gage. A membrane was placed on both extruder and PVC cell to prevent loss of water mass due to evaporation. But, exposing membrane to open-air in long-term testing causes breakage of membrane. Therefore, latex glove was weared on PVC cell and extruder instead of using membrane; fingers of the glove was filled with water to increase humidity above specimen and cease mass loss due to evaporation. A detailed sketch of the hanging column equipment is shown in Fig. 3.20 and 3.21.

Soil water retention curve measurement on a single specimen can be carried out weighing PVC cell and specimen together in similar to tempe cell method or several specimens are used for each experimental data point. The extraction of one data point took at least 3 weeks in the hanging column setup.

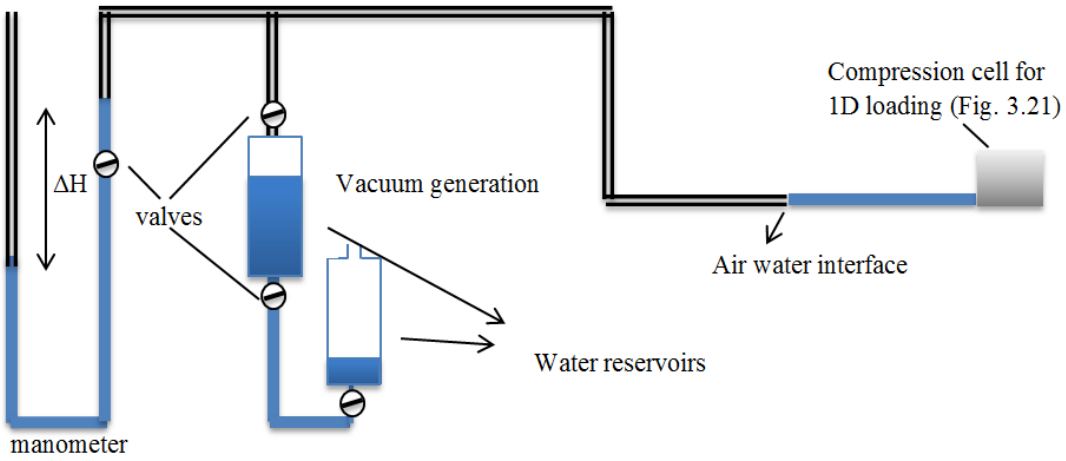

Figure 3.20 Hanging column equipment (single blue line show water filled parts, double black lines show air filled part)

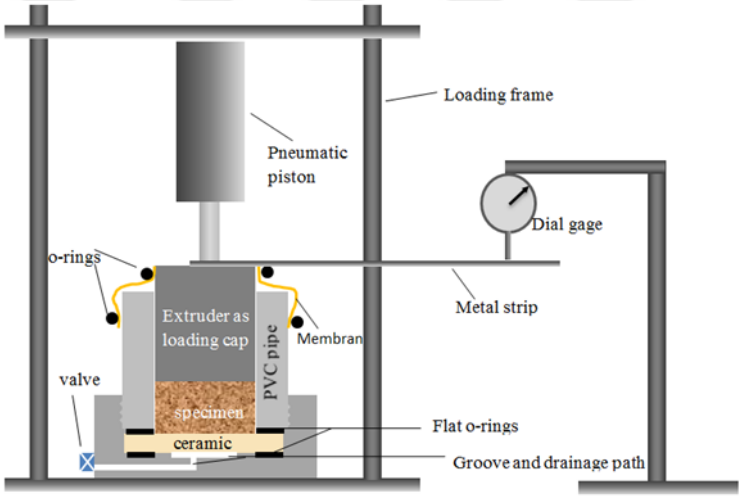

Figure 3.21 Compression cell for one-dimensional loading used in hanging column setup

3.4.2 Measurements with Suction Controlled Oedometer

A suction controlled oedometer was developed using axis translation technique. 15 bar HAE ceramic was used at the base of oedometer ring inside air-tight chamber. Vertical stress was applied onto specimen by means of a loading rod and a pneumatic piston. The specimen drainage lines are connected to a beaker placed upon a mass balance. The change of soil water mass is monitored from the outflow

water mass measurements. Top of the water inside the beaker is covered with an oil layer to minimize evaporation that cause erroneous measurements of water mass. Placing oil layer considerably reduces the mass loss due to evaporation, but it does not completely eliminate the effect as oil also evaporates. The variation of mass of a separate identical beaker filled with water and oil layer is monitored to calibrate effect of evaporation on the mass measurements. The rate of evaporation from the beaker in our laboratory conditions (24±2 °C) is determined as 0.0034 gr/day and used as correction to time-series water mass data. The sketch of test setup is shown in Fig. 3.22 and the details of suction controlled oedometer cell is illustrated in Fig. 3.23.

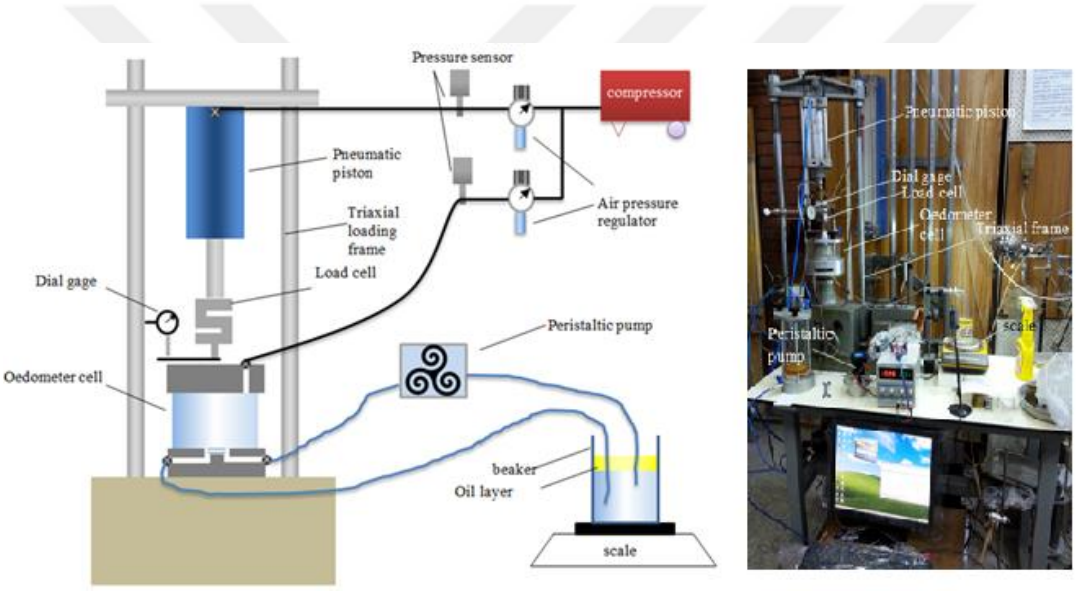

Figure 3.22 Sketch of the suction controlled oedometer test setup (on the left), picture of the suction controlled oedometer test setup (on the right)

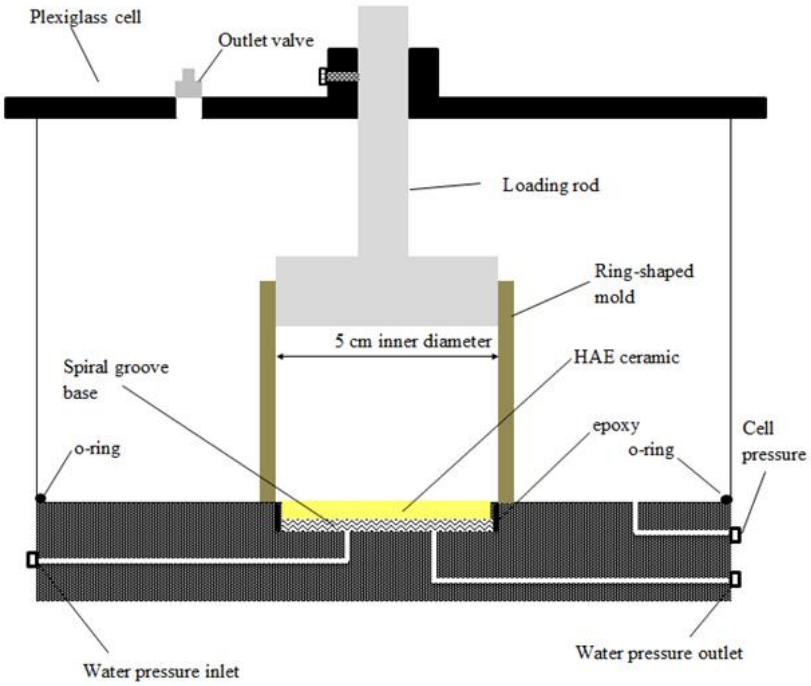

Figure 3.23 Details of suction controlled oedometer cell

Main drawback in testing with axis translation technique is that high pressure air diffuses in the water and forms air bubbles in the low pressure compartment beneath the ceramic. Regular flushing process using an auxilary device is necessary to be able to fulfill suction control during testing, otherwise accumulated air volume drains off water within the ceramic resulting in decrease of pressure difference and so the applied suction (Fredlund, 1975). A novel procedure for flushing diffused air bubbles was developed in this study. A peristaltic pump was employed to circulate water beneath ceramic disc and water mass variation was monitored using a reservoir container placed on the scale. Low priced Grothen G028 and Kaomer NKP-DC-B08D peristaltic pumps can be found in the market; these consist of only a peristaltic pump rotary in connection with a DC motor. Hovewer, there are several disadvantages in the usage of these low price products. Peristaltic pumps with a DC motor are not suitable for the long term usage, the poor quality peristaltic pump rotary malfunctions after prolonged usage. Goso 42 stepping motor has better quality designs for rotary component. On the other hand, tearing of pipe around peristaltic pump rotary is almost inevitable in continuous

operation. After some trials stepper motor driven peristaltic pump (Goso 42) was deemed usable for long term operation if it is periodically activated for brief durations (30 seconds every 30 minutes). Arduino board was used for this automation. Flushing diffused air bubbles beneath the ceramic disc with a peristaltic pump can thus be automated and weighing the circulated water is much more practical than using diffused air volume indicators.

3.4.3 Measurements with Vapor Equilibrium Method

Vapor equilibrium method was implemented to measure soil water retention behaviour at suctions higher than 1 MPa. Five different saturated chemical salt solutions have been prepared in glass jars (Fig. 3.24). The type of chemical salts and generated total suctions by their saturated solutions are given in Table 3.5. During testing, presence of salt-saturated solution is ensured during water mass exchange process between specimen and solution since solutions contain undissolved or precipitated salt material that remains in solid state. Equilibrium is achieved in about 2 weeks for specimens having the volume to surface area ratio of approximately 0.3 cm (i.e. half-cylindrical shaped specimens are used to shorten the equlibration duration).

Table 3.5 Suctions generated by different saturated chemical salt solutions (ASTM E104.02)

Chemical salts	Relative Humidity	Generated total suction (kPa)
K_2SO_4	97.3	3697
KNO_3	93.6	8932
KCl	84.2	23226
NaCl	75.3	38313
NaBr	57.6	74502

Figure 3.24 Implementation of vapor equilibrium technique for Ankara clay specimens

3.4.4 Studies on Osmotic Suction Control

Polyethylene glycol 20000 (PEG 20000) and a Spectra/Por 7 semipermeable membrane with molecular weight cut off (MWCO) of 14000 were purchased for osmotic suction control. A calibration curve for PEG concentration vs suction relationship is required to control suction with osmotic method. Several methods were tried to obtain calibration curve.

Calibration with Tensiometer:

In the first attempt, tensiometer developed by Köksalan (2013) was used to perform direct measurement. PEG solution was prepared in a beaker. Tensiometer's tip was covered with a plastic hose and inserted into PEG solution without touching tensiometer's tip to the surface of the solution. In this way, a closed environment is generated between tensiometer and PEG solution. The relative humidity of closed enviroment depends on the PEG concentration and suction of the humid air could be measured with tensiometer. However, water inside tensiometer's reservoir cavitates prior to humidity equilibrium, resulting in failure of this method. In order

to increase humidity inside plastic hose at initial state, air inside closed environment is mixed with saturated air in order to prevent cavitation prior to equilibrium. A connection from plastic hose at the tensiometer's tip to another closed environment consisting saturated air was established. Saturated air was obtained by filling half of a container with water and waiting a period of time to reach equilibrium between water and air phases. This saturated air was opened to closed environment between tensiometer and solution just after inserting the plastic hose; however, this method did not stop the cavitation. The sketch of the devised method is illustrated in Fig. 3.25.

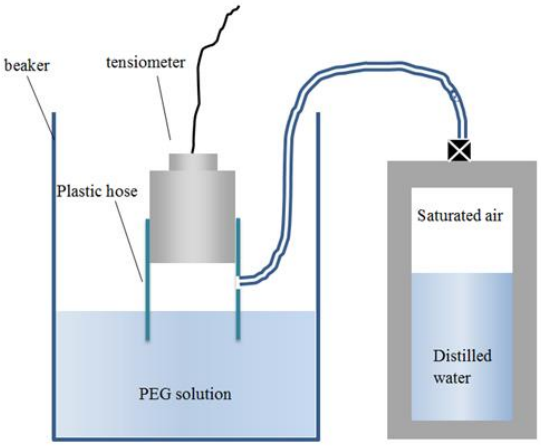

Figure 3.25 The sketch of the method for calibration of PEG concentration and suction relationship with direct tensiometer measurement

Calibration with Air Back Pressure:

This method aims to measure osmotic suction via air pressure. PEG solution was put into a container with a semipermeable membrane placed at its base. The part beneath the semipermeable membrane was filled with distilled water and connected to a burette. Air pressure was applied to container filled with PEG solution. In this setup (Fig. 3.26), semipermeable membrane separates distilled water and PEG solution resulting in water flow from burette to PEG solution due to osmotic suction difference. Air pressure was carefully adjusted to keep the water level inside burette constant. The air pressure at the equilibrium condition is equal to the osmotic suction. It is possible to obtain calibration data at low suctions with this

method; however, increasing air pressure results in precipitation of PEG molecules. The calibrated data points were compared with the parabolic calibration curve proposed by Delage et al., (1997) in Fig. 3.27.

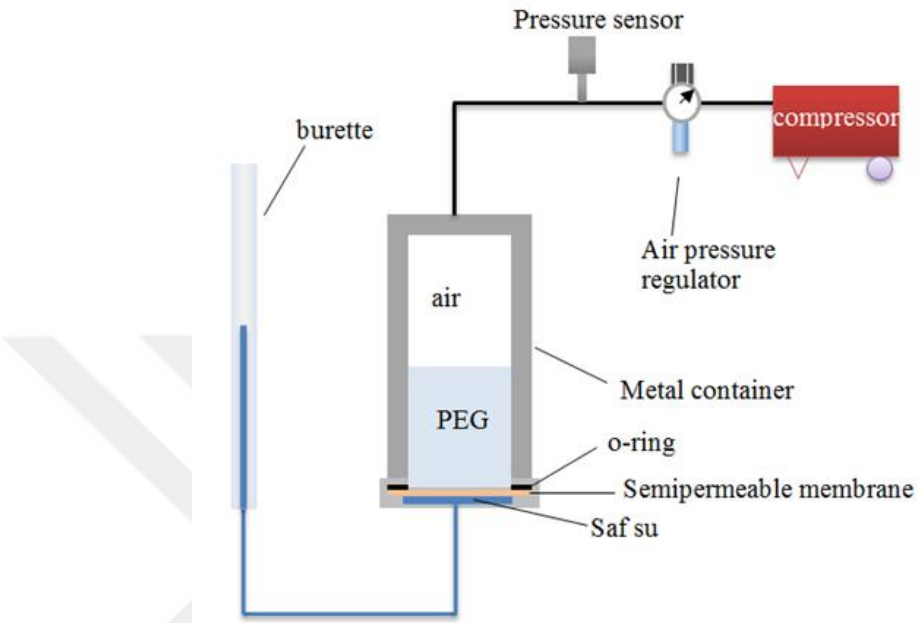

Figure 3.26 The sketch of the air pressure method

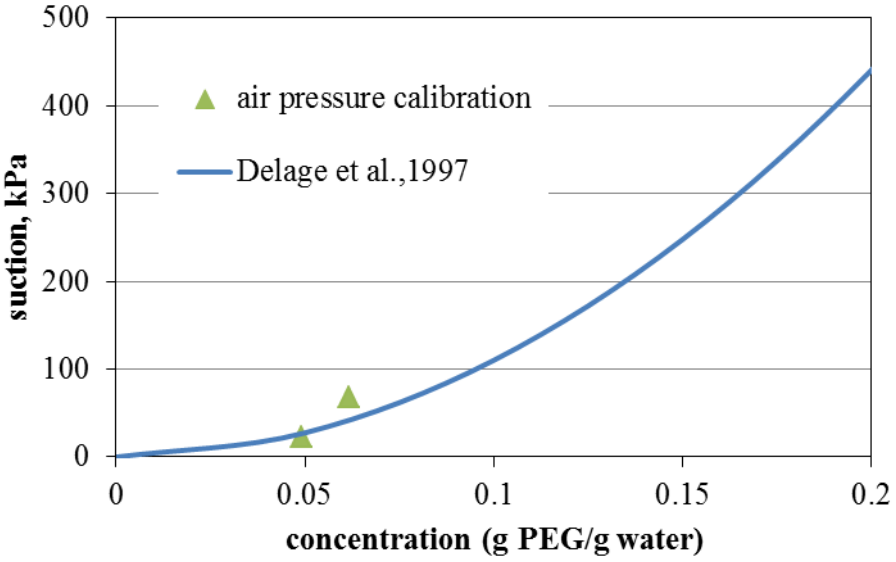

Figure 3.27 Measured calibration curve data points and relationship proposed by Delage et al., (1997)

Calibration with measurement on specimen:

In another attempt, tensiometer was used to measure suction of the specimen whose suction is adjusted by osmotic solution. An osmotic suction controlled oedometer cell was manufactured and used in this method (Fig. 3.28). Specimen was placed inside oedometer cell that its base is covered with semipermeable membrane sitting on a metal mesh. PEG solution was circulated beneath the semipermeable membrane to generate osmotic suction. Tensiometer was inserted into specimen at the top to monitor suction. A latex membrane was placed around tensiometer and oedometer ring to prevent evaporation from the specimen. Peristaltic pump circulated PEG solution to avoid ponding of outflow pore water beneath semipermeable membrane. However, this method did not work since the monitored pore water pressure remained constant. It is suspected that poor quality peristaltic pump is not capable of sensitive control for the flow rate and causes pressure development beneath the semipermeable membrane.

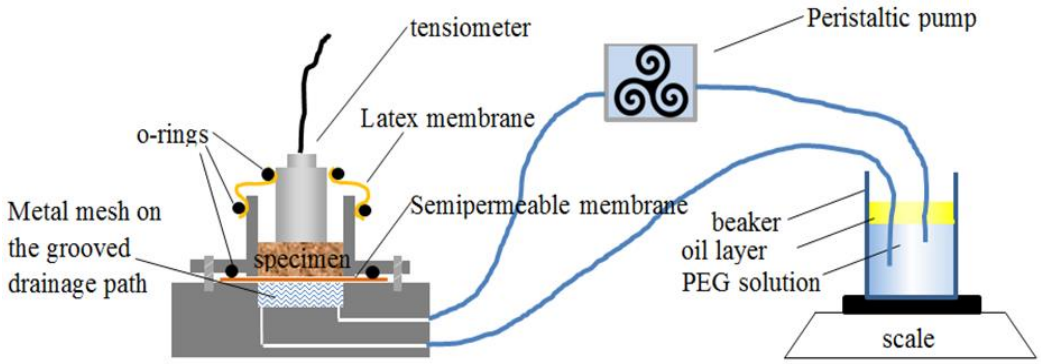

Figure 3.28 The sketch of the method of measurement of osmotic suction within specimen

Calibration with chemical solutions:

In another method, vapor equilibrium technique was used to obtain calibration curve. Five different chemical salts were purchased to prepare saturated salt solutions (K_2SO_4, KNO_3, KCl, NaCl and NaBr). Saturated salt solution together with PEG solution inside a beaker were put into an air-tight container. The

concentration of PEG solution varies with the total suction generated by saturated salt solution until the equilibrium state is reached. Glass jars were used as containers and saturated salt solution was prepared inside. PEG solution at known concentration was prepared within a beaker and placed inside the container. A rubber stopper was plunged into salt solution inside container to place PEG filled beaker in non-contact with the salt solution, otherwise beaker should be cleaned before mass measurements. Top of the jar was covered with three layer paraffin film. Metal jar lid was heated inside a boiled water prior to sealing to enhance the tightness. Periodic measurements for the variation of concentration of PEG solution revealed that too much testing time would be required to reach equilibrium state. Preliminary measurements were plotted in Fig. 3.29. Precipitation was observed for the PEG solutions equilibrated with saturated NaCl and NaBr solutions. This method could be enhanced by implementing procedures for increasing rate of evaporation such as decreasing height of the container instead of using glass jars and increasing the area of beaker that the PEG solution is placed and decreasing the volume of the PEG solution. But, equilibrium is not achieved in a reasonable duration in this study. In conclusion, the difficulties in the implementation make osmotic technique impractical for this study.

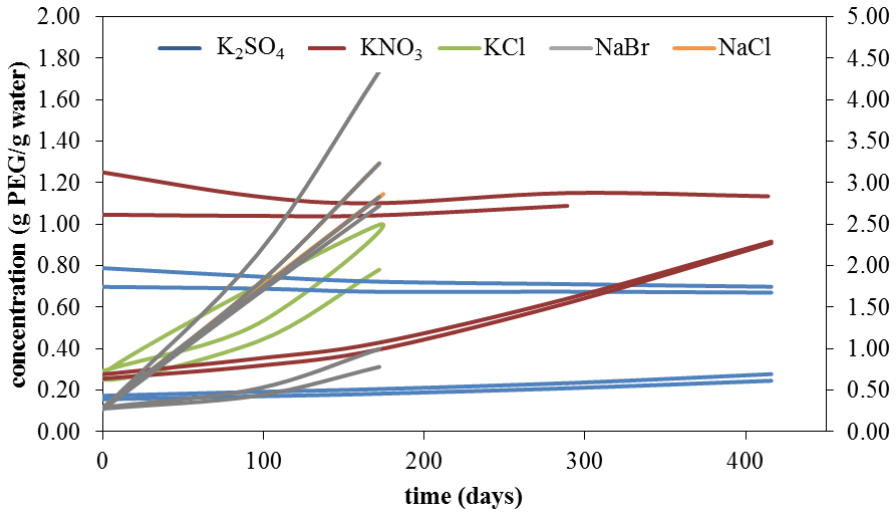

Figure 3.29 Variation of concentration of PEG solutions equilibrated with saturated salt solutions

3.4.5 Soil Water Retention Curve of Mersin Silt

Mersin silt samples at initial water content of 10.2% were compacted to two different initial void ratios 0.72 and 1.184. The initial diameter and height of the compacted specimens are 5 cm and 1 cm, respectively. No vertical stress was applied during testing. In the extraction of main drying branch of retention curve, first, specimens were saturated within the pressure plate extractor, which is another axis translation based test setup, at zero suction. At least 1 month duration was required to achieve the saturation of specimens inside pressure plate extractor. A saturated specimen was taken from the pressure plate extractor to apply suction to it in either hanging column test setup or suction controlled oedometer. This procedure was repeated on remaining saturated specimens for each suction level. Hanging column equipment was used for extracting data points at suctions less than 40 kPa and suction controlled odeometer setup was used for suctions up to 1000 kPa.

In the extraction of wetting path, specimens were prepared inside suction controlled oedometer ring at initial water content of 10.2% and desired initial void ratio. Specimens were first dried to 1000 kPa suction then suction was reduced to desired level to extract main wetting soil water retention curves of Mersin silt.

Vapor equilibrium method was implemented for suctions higher than 1 Mpa. Mersin silt specimens compacted at initial water content of 10.2% were equilibrated with saturated chemical salt solutions' vapor.

The dry density of all specimens were measured according to ASTM D7263 at the end of suction equilibrium in order to evaluate retention behavior in terms of degree of saturation and volumetric water content.

The soil water retention curves of Mersin silt are shown in Fig. 3.30 to Fig. 3.32.

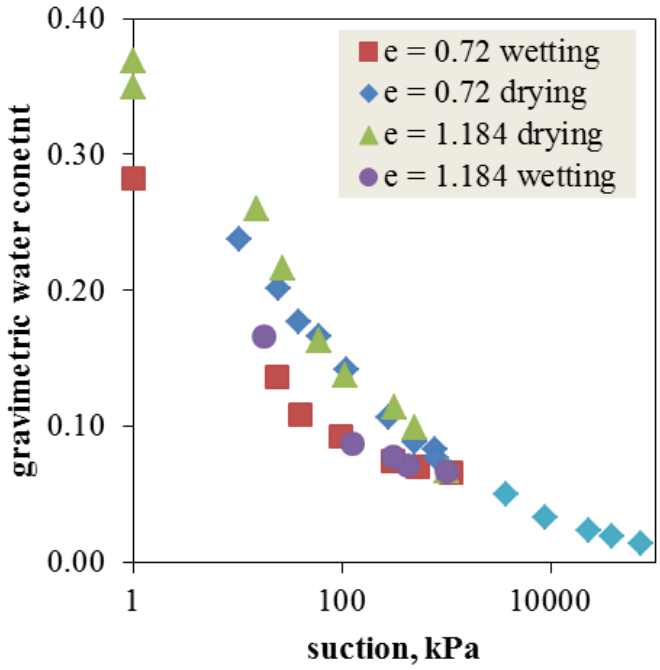

Figure 3.30 Soil water retention curves (in terms of gravimetric water cotent) for Mersin silt specimens at initial void ratio of 0.72 and 1.184

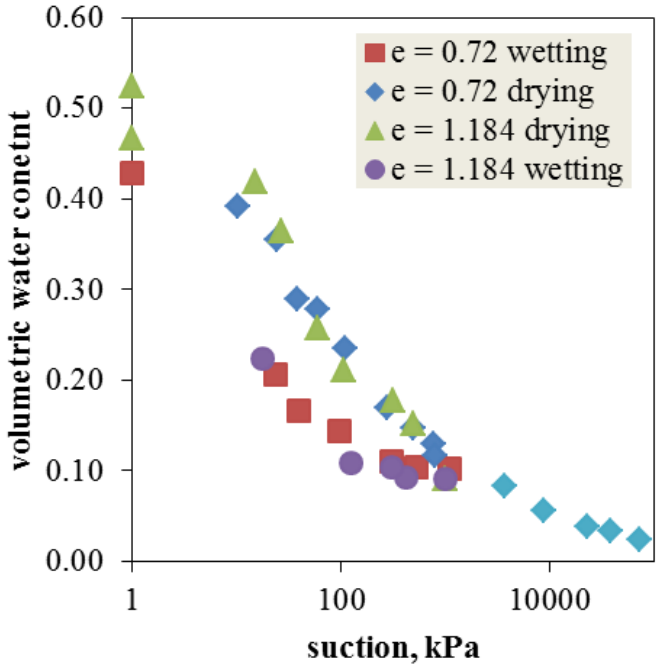

Figure 3.31 Soil water retention curves (in terms of volumetric water cotent) for Mersin silt specimens at initial void ratio of 0.72 and 1.184

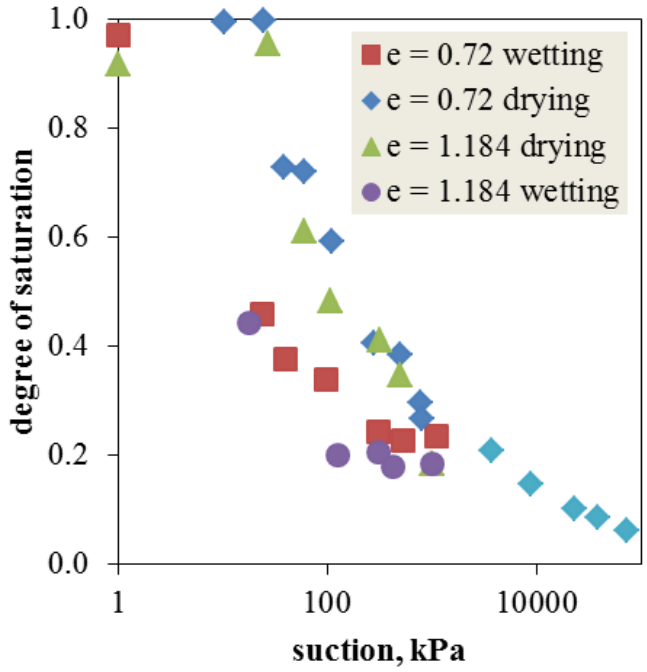

Figure 3.32 Soil water retention curves (in terms of degree of saturation) for Mersin silt specimens at initial void ratio of 0.72 and 1.184

3.4.6 Soil Water Retention Curve of Ankara Clay

Ankara clay specimens were prepared by consolidating slurry sample in the conventional oedometer cell. Slurry was consolidated under 50 kPa and 200 kPa vertical stresses to obtain two different initial void ratios. Trial measurements was revealed that to obtain identical specimens from Ankara clay slurry is quite difficult. It is suspected that the fine contents of slurry portions spooned into oedometer ring might be different for each preparation. This results in non-monotonic water retention curves. Therefore, using a single specimen for soil water retention curve measurement was preferred. Ankara clay is a highly plastic expansive soil. Specimen shrinks due to increasing suction, loses contact with the oedometer ring wall and violates K_0 condition; vertical displacement measurements become useless in determining specimen volume. But, volume measurement is essential in order to plot water retention curve at different types of water content

measures (e.g. volumetric water content, degree of saturation). For this reason, specimen was extruded from oedometer cell at the end of each suction step and its size was measured by means of a caliper to calculate volume. Alternatively, shrinkage curve for Ankara clay was determined in order to relate void ratio with gravimetric water content (Fig. 3.33). Saturated specimens were air-dried for various durations and then their gravimetric water content and dry densities were measured. The equation proposed by Fredlund et al. (2002) was fitted to measurements:

$$e(w) = a\left(\left(\frac{w}{b}\right)^{c} + 1\right)^{1/c} \tag{3-3}$$

where $e(w)$ is void ratio as a function of gravimetric water content 'w', and a, b, c are constants. 'a, b, c' constants in (3-3) were resepctively determined as 0.349, 0.132 and 3.319 for Ankara clay.

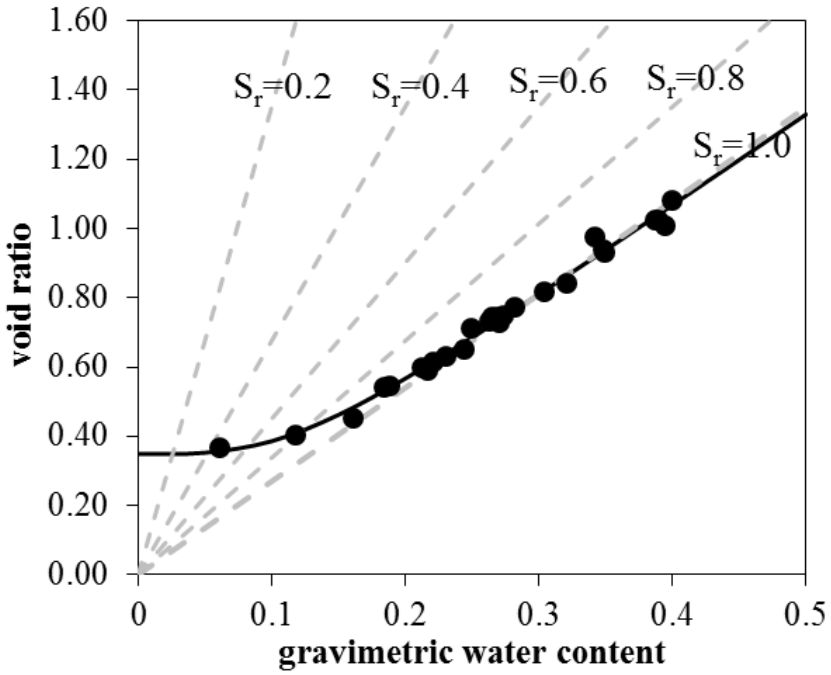

Figure 3.33 Shrinkage curve of Ankara clay

Fig. 3.34, 3.35 and 3.36 illustrate the soil water retention curves of Ankara clay specimens in terms of gravmetric water cotent, volumetric water content and

degree of saturation, respectively. The serie labels denote initial void ratio of Ankara clay specimens. The correct estimation of air entry suction could be carried out on the degree of saturation type soil water retention curve since the shape of gravimetric or volumetric water content type soil water retention curves are influenced by specimen's volume change behaviour (Pasha et al. 2015). Overconsolidated specimens cause erronous interpretation of air entry suction. Fig. 3.35 reveals that desaturation in Ankara clay specimens starts around 2 MPa suction.

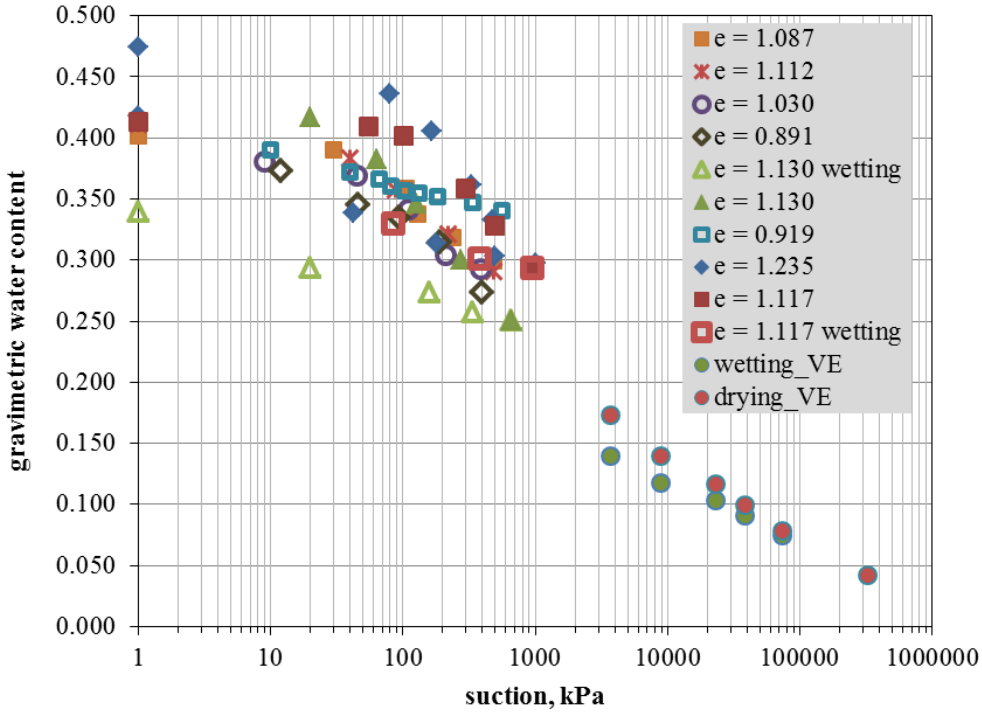

Figure 3.34 Soil water retention curve of Ankara clay (gravimetric water content) (VE: vapor equilibrium method)

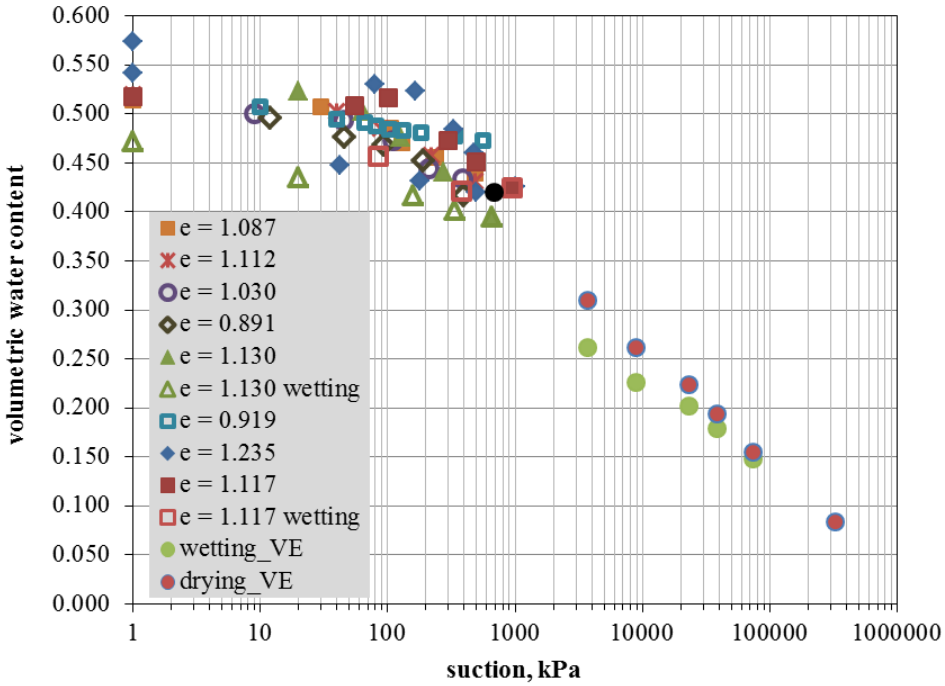

Figure 3.35 Soil water retention curve of Ankara clay (volumetric water content) (VE: vapor equilibrium method)

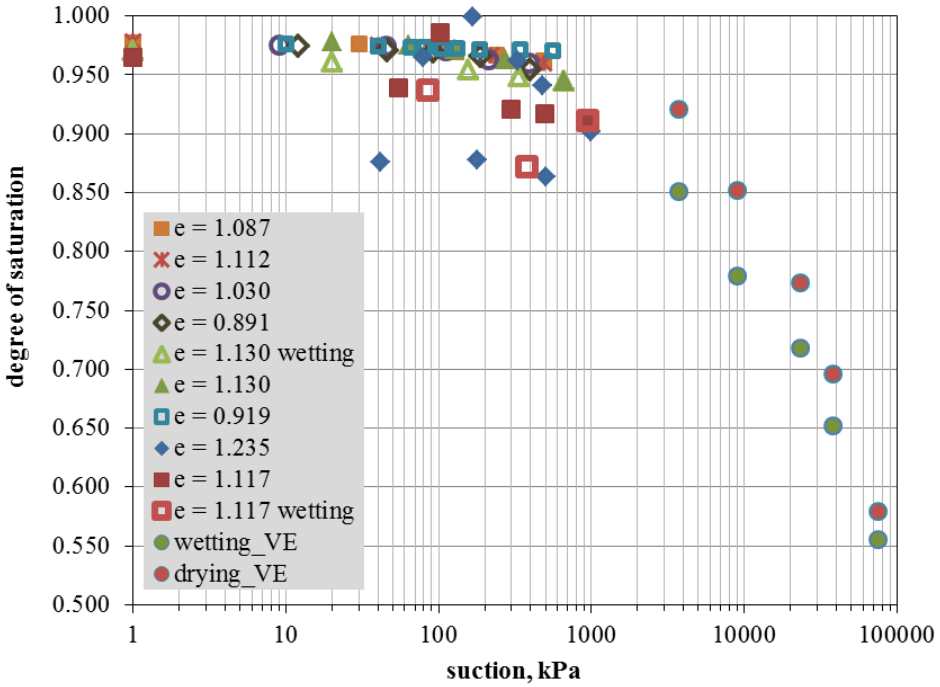

Figure 3.36 Soil water retention curve of Ankara clay (degree of saturation) (VE:vapor equilibrium method)

3.4.7 Soil Water Retention Curve of Elazığ Silt

Elazığ silt specimens were compacted to initial void ratio of 0.845 at initial water content of 22.1% within PVC mold with 3.6 cm inside diameter. The initial height of the compacted specimens is 1 cm. PVC mold was placed into suction controlled oedometer ring. No vertical stress was applied during testing. The gap between the oedometer ring and PVC mold was filled with distilled, deaired water to saturate specimen inside PVC mold. Specimen and PVC mold were taken out from the suction controlled oedometer apparatus at the end of each suction step and weighed together. After tracing all suction steps, specimen water content was measured and previous water contents were back calculated from the latest measurement using mass measurements. Negligible volume change was observed during retention curve extraction. The vapor equilibrium method was implemented to extract high suction data points. The soil water retention curves of Elazığ silt are shown in Fig. 3.37.

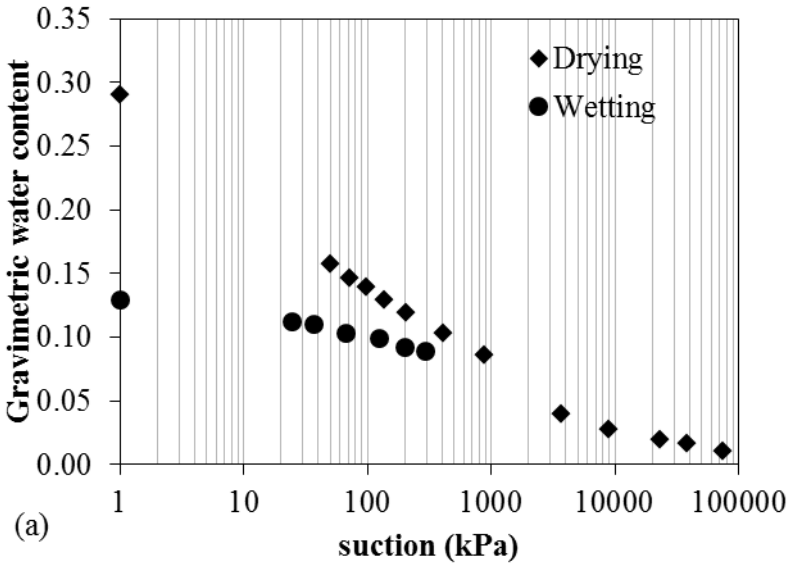

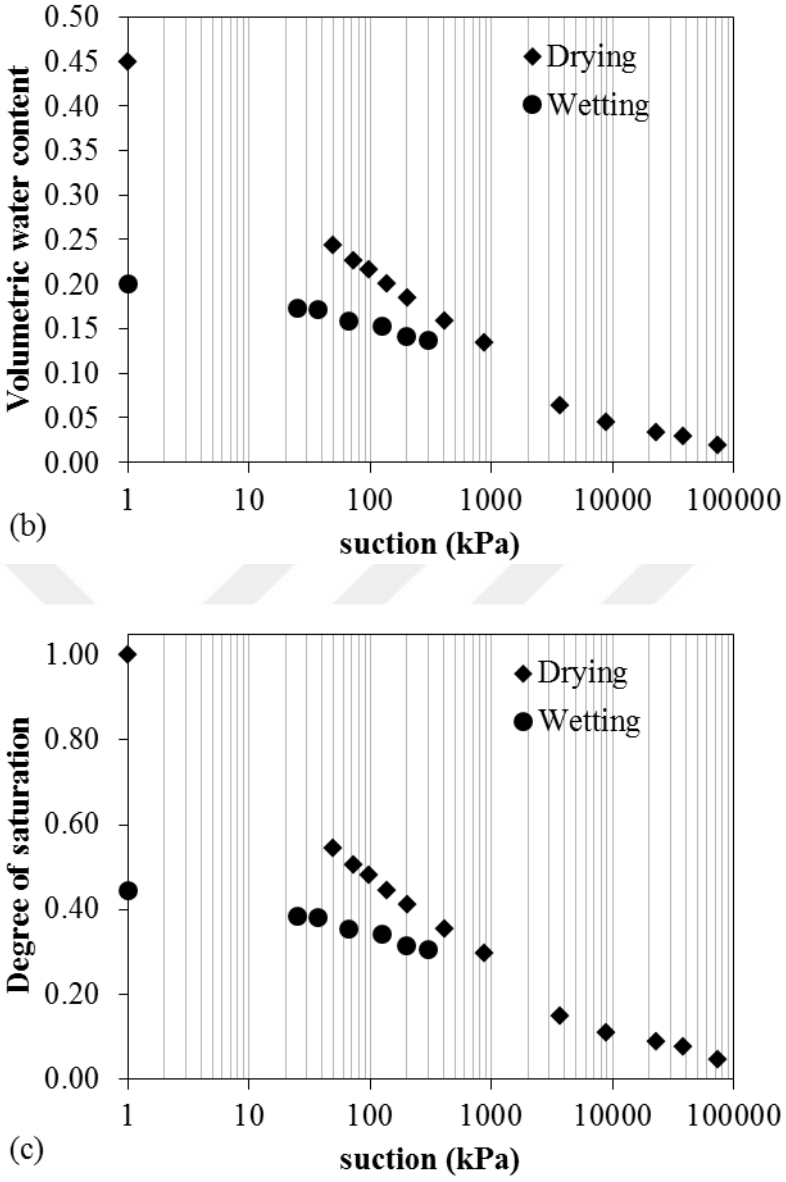

Figure 3.37 Soil water retention curve of Elazığ silt

3.5 Unsaturated Tests

3.5.1 Unsaturated Triaxial Tests on Mersin Silt

The constant water content triaxial tests on Mersin silt cover three different initial degrees of saturation (30%, 50% and 70%) and there different initial void ratios

(0.72, 0.83 and 0.92). The initial degree of saturation values were kept to prescribed values using methods explained in section 4.1. Rate of loading and strain rate were determined from trial experiments as 0.02 kPa/min and 0.002%/min, respectively. This value is slow enough to ensure homogenisation of suction within the specimen while measuring suction only from the top and the bottom of the specimen. The constant suction triaxial tests (9 experiments in total) were already carried out by Ahmadi-Naghadeh (2016). In addition to his study two constant suction triaxial tests on Mersin silt specimens prepared at 0.83 initial void ratio were completed at 50 kPa and 100 kPa suctions. The completed unsaturated triaxial test programme for Mersin silt is given in Table 3.5.

Table 3.5 The test programme completed on Mersin silt

type	label	e_0	σ_{net} (kPa)	s (kPa)	S_{r0} (%)
CW	MCW01	0.72	25	-	30
CW	MCW02_1	0.72	25	-	50
CW	MCW02_2	0.72	25	-	50
CW	MCW03	0.72	100	-	50
CW	MCW04	0.72	400	-	50
CW	MCW05	0.72	25	-	70
CW	MCW06	0.83	25	-	50
CW	MCW07	0.92	25	-	50
CD	MCD10	0.83	400	50	-
CD	MCD11	0.83	400	100	-

3.5.2 Unsaturated Tests on Ankara Clay

The constant water content triaxial test on Ankara clay specimens were carried out. Ankara clay specimens' initial gravimetric water contents were adjusted prior to testing using methods explained in section 4.1.

The loading rate for testing on Ankara clay specimens was determined as 0.009 kPa/min from trial experiments.

The procedure proposed by Fredlund et al. (2012) was used to determine suitable strain rate for Ankara clay specimens. Bishop and Gibson (1963) stated that the required time to failure is related with admissible amount of excess pore water pressure during shearing:

$$t_f = \frac{L^2}{\eta c_v^w \left(1-\overline{U}_f\right)} \tag{3-4}$$

where L is the specimen height (10 cm), $\overline{U}_f$ shows the percentage of excess pore water pressure dissipation for the whole test duration (suggested as 95% by Bishop and Henkel, 1964). η parameter depends on the drainage condition and it is given for the double drainage condition as:

$$\eta = 3/\left(1+3/\lambda\right) \tag{3-5}$$

where λ parameter is impedance factor and given as:

$$\lambda = \frac{k_d d}{k_w L_d} \tag{3-6}$$

k_d is the permeability of high-air entry ceramic that is measured as $5.9\text{x}10^{-10}$ m/sec. L_d is ceramic thickness and measured as 7 mm; d is length of drainage path and it becomes the half of specimen height in double drainage condition. k_w is permeability of unsaturated specimen and taken as $5\text{x}10^{-12}$ m/sec for Ankara clay.

c_v^w given in (3-4) is average coefficient of consolidation with respect to liquid phase:

$$c_v^w = k_w/\left(\rho_w g m_w\right) \tag{3-7}$$

ρ_w density of water, g is gravitational acceleration and m_w is the slope of volumetric water content vs suction plot in the arithmetic scale. This value was taken as $5.6x10^{-5}$ m^2/kN using retention curve experimental data.

Strain rate for Ankara clay specimens was estimated as 0.00065%/min (approximately 1%/day) using aforementioned procedure.

The completed unsaturated triaxial test programme for Ankara clay is given in Table 3.6.

Table 3.6 The test programme completed on Ankara clay

type	label	σ_{net} (kPa)	s (kPa)	S_{r0} (%)
CW	ACW01	88	110	97
CW	ACW02	99	385	95
CW	ACW03	49	425	94
CW	ACW04	109	653	94
CW	ACW05	183	150	98

3.5.2.1 Unsaturated Constant Water Content Isotropic Compression Test on Ankara Clay

Soil water retention curve measurements on Ankara clay specimens reveal that suction level where desaturation starts can not be reached with axis translation technique. Alternatively, vapor equilibrium method was implemented in a different testing setup using in-house equipment (Bernier et al., 1997; Delage et al., 2008). Any saturated chemical salt solution is in equilibrium with the ambient air at the certain value of relative humidity (and so at the certain suction). Test setup was designed to perform constant suction isotropic compression tests and drying-wetting cycles under constant net stress. Thus, it would be possible to control net stress, suction and to measure volume change and specimen's water volume change. Volume measurement was conducted based on inner cell method (Bishop and Donald, 1961). An inner cell that has a mounted burette on the top to monitor

volume change of the specimen. Suction was controlled by circulating vapor of saturated chemical salt solution which is kept inside a sealed container. An air pump was used to enchance vapor transfer process between specimen and the air above salt solution. The variation of specimen's water volume was monitored by measuring the mass variation inside the salt solution container.

It was initially planned to fill inner cell with mercury during the equipment design stage. However, it was observed that to use mercury is not suitable with the existing equipment since mercury leakage from the inner cell could not be prevented. In this case, water inside inner cell and transparent silicone oil in the outer cell was used. Different coloring agents were mixed with water in order to highlight the interface between oil and water (food dye, methylene blue). It was observed that food dyes might not be suitable option for the long term testing due to bacterial attack problem. Methylene blue was available in the laboratory and used to encolour the water inside the inner cell. However, it was observed that standard latex membranes used in the triaxial testing are not able to prevent passing of methylene blue molecules from cell fluid into the specimen. It was decided to place a solid object to the oil-water interface inside burette instead of encolouring the inner cell water. A piece of sponge was covered with aluminium tape to obtain specific density for composite material that is able to hang at the oil-water interface.

Another problem was related to monitoring the water mass change during the preliminary tests. The stiffness of pipes that connects the test cell and chemical salt solution filled container causes noise in the mass balance measurements. A special pipe connection was designed to diminish the cable stiffness. The pipe connecting the container and test cell was cut off and the finger portion of a latex glove was used to join open ends of the pipe. It was devised that latex portion along the connection diminish the effect of pipe stiffness on the mass measurement. Although, adding latex portion on the pipe connection can modulate the noise on the mass measurement data, this method can not completely solve the pipe stiffnes problem. Different approach was implemented; a special lid covered with rubber at

the top surface was manufactured.The lid has pipe connections at the top and is placed on top of the wind barrier of the mass balance.

The previous testing programme for Ankara clay specimen traces specific stress path covering constant suction isotropic loading and unloading and wetting-drying cycles. It was planned to carry out the given test programme on a single test specimen. However; preliminary tests was revealed that required duration for such a test programme is excessively long. Therefore, a new test programme was planned as to carry out five constant suction loading and unloading tests on separate specimens. Specimens's suction were initially equilibrated with various saturated chemical salt solutions as a separate stage and tested for isotropic loading-unloading stress path under constant suction. The sketch of the final version of the developed test setup together with its picture are given in Fig. 3.38.

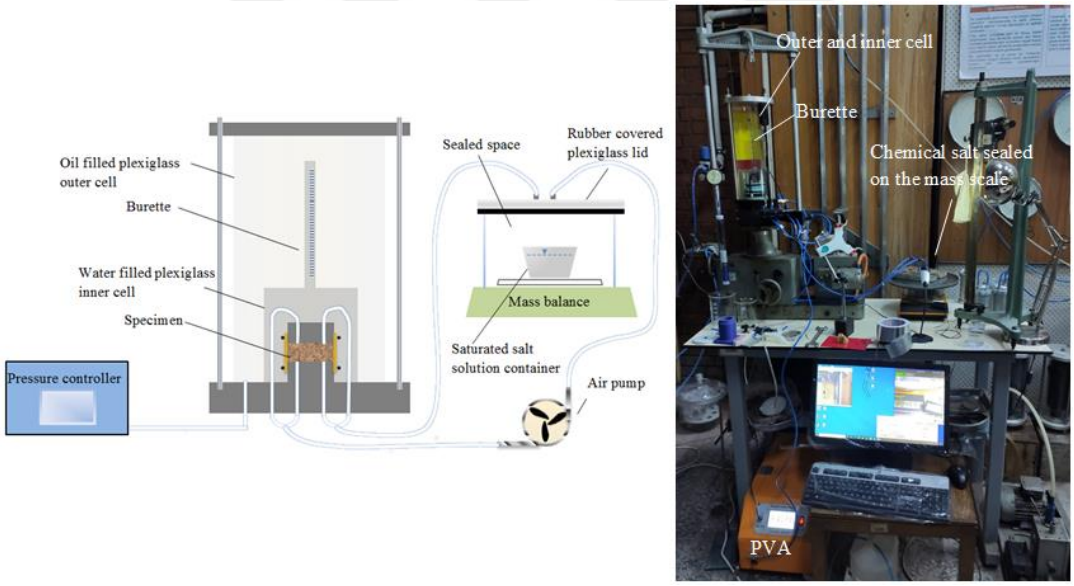

Figure 3.38 The developed test setup based on vapor equilibrium method.

3.5.2.2 Constant Water Content Triaxial Shear Test on Ankara Clay at High Suctions

The constant water content triaxial tests on unsaturated Ankara clay specimens at high suction (9 to 75 MPa) was carried out based on testing method proposed by

Chen et al. (2021). The soil water retention behavior is independent of the dry density or void ratio over a high suction range, they argue that, if the water content of a soil specimen is kept constant, the suction remains constant and independent of the void ratio (deformation) at high suctions. In their study, a simple testing method for measuring the stress-strain relations of unsaturated triaxial specimens at high suctions is proposed by combining the vapor equilibrium technique with saturated salt solutions and the triaxial shear tests at constant water contents. First, a known initial high suction is imposed on the specimen by using the vapor equilibrium method with a saturated salt solution. Then, the specimen is triaxially sheared under a constant water content, thereby resulting in a constant high suction during triaxial shearing. As a contribution to their study, further simplification to testing procedure is proposed in our work. The volume change of unsaturated specimen during triaxial testing required rigorous methods. Alternatively, the triaxial shearing of the unsaturated specimens could be performed under zero net stress such as unconfined compression test inside ordinary triaxial testing equipment. In such a way, the volume change of cell liquid becomes directly equal to the specimen's volume change minus loading ram since the expansion of the cell, pipes etc. under applied pressure is eliminated. Four different chemical salt solutions (KNO_3, KCl, NaCl, NaBr) were used to equilibrate Ankara clay triaxial specimens. Two specimens, one initially saturated and another one initially air dry, are equilibrated under the same suction for each salt solution.

3.5.3 Unsaturated Triaxial Tests on Elazığ Silt

Constant water content and constant suction triaxial tests were performed on Elazığ silt specimens at different initial void ratios and degrees of saturation.

The ramped loading rate for testing on Elazığ silt specimens was determined as 0.012 kPa/min from trial experiments. In the trial measurements, the variation of specimen's suction is monitored under undrained condition after the net stress is increased to certain level under drained condition at prescribed ramped loading

rate. The suitable strain rate was determined as 0.0039 %/min. The completed unsaturated triaxial test programme for Elazığ silt is given in Table 3.7.

Table 3.7 The test programme completed on Elazığ silt

type	label	e_0	σ_{net} (kPa)	s (kPa)	S_{r0} (%)
CID	ECD04	0.845	50	40	-
CID	ECD05	0.845	50	80	-
CID	ECD06	0.845	200	40	-
CID	ECD07	0.845	200	80	-
CW	ECW01	0.845	100	-	30
CW	ECW02	0.845	100	-	50
CW	ECW03	0.845	200	-	50
CW	ECW04	0.845	300	-	50
CW	ECW05	0.845	100	-	70
CW	ECW06	0.78	100	-	50
CW	ECW07	0.72	100	-	50
CID	ECD08	0.845	200	0	-
CID	ECD09	0.845	200	40	-
CID	ECD10	0.845	200	0	-
CID	ECD11	0.845	200	40	-

3.5.4 Equipment and Procedures in Unsaturated Triaxial Testing

Axis translation technique was implemented in Geocomp triaxial testing system by Ahmadi-Naghadeh (2016). High air-entry ceramics of 5 bar capacity were fixed on the topcap and pedestal of the triaxial cell. Porous metal rings were inserted around ceramics for the application of air pressure inside specimen. Cell pressure and pore water pressure were controlled by means of two pressure volume actuators (PVA). The volume change of specimen was monitored using cell fluid volume change measurements which are corrected through the calibration procedure described in Ahmadi-Naghadeh and Toker (2017). Diffused air bubbles were flushed during

testing by means of diffused air volume indicator device. The picture of the test setup is given in Fig. 3.38.

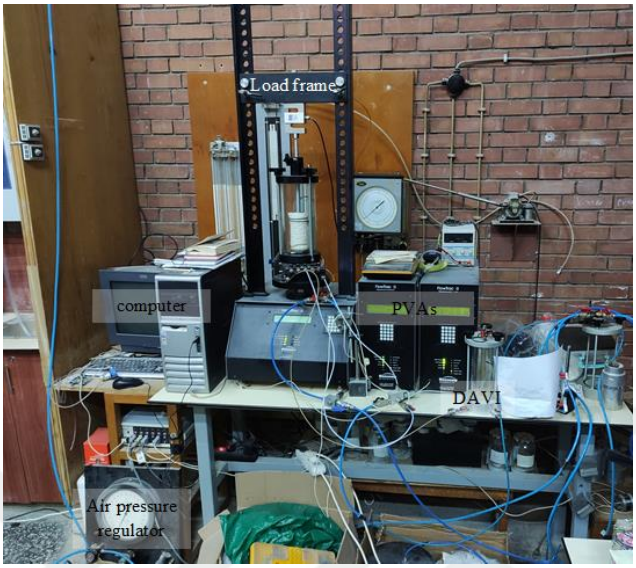

Figure 3.38 The picture of the unsaturated triaxial test setup

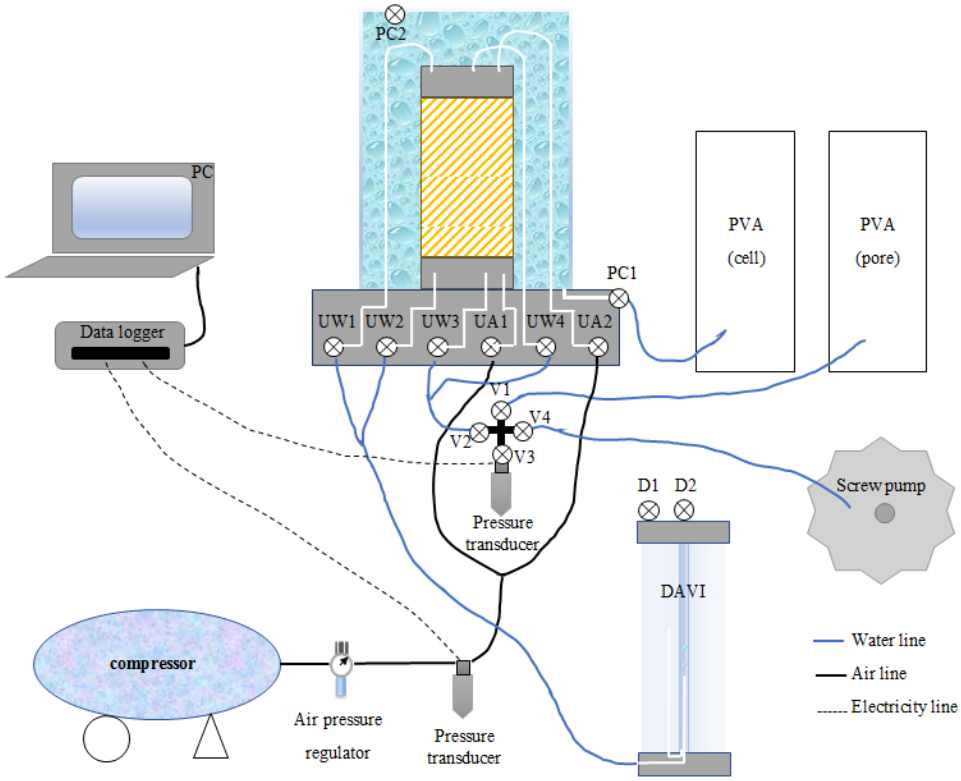

Figure 3.39 The sketch of the unsaturated triaxial test setup

The sketch and the connections in the test setup is shown in Fig. 39. The procedure followed during unsaturated triaxial testing of soil specimens in the METU soil mechanics laboratory is given in the following sections. Italicized commands are specific for Geocomp Loadtrac-Flowtrac and its control software.

3.5.4.1 Saturation of HAE Ceramics

- Distilled and deaired water should be used to fill triaxial cell and PVA pistons. Distilled water is deaired by applying vacuum. Separate the connection between vacuum pump and water container in first then shut down the vacuum pump motor.
- Clean the triaxial cell's o-ring using a piece of paper towel, there should be no sticked particles on its surface. Grease the triaxial cell's o-ring after cleaning.
- Place a hollow cylinder that fits outside the pedestal.
- Place the top cap onto the hollow cylinder.
- Remove the loading piston after releasing the piston lock. Clean the loading piston's o-ring using a thin spatula then insert the loading piston and lock the piston.
- Place the triaxial cell on the triaxial base. Check if the mark is aligned with the bolt on the base.
- Unlock the piston lock and let the loading piston touch to the top cap
- Fix the triaxial cell's bolts to their places. Gradually tighten the bolts by twisting the screw nuts applying small forces, don't fully tighten a bolt in a single step by applying a huge force.
- Close the outlet valve at the top of the triaxial cell 'PC2'. Fill the triaxial cell with CO_2 a couple of seconds (e.g. 10 seconds) after connecting CO_2 tank to the cell's inlet valve at the bottom of the triaxial cell 'PC1'. Remove the CO_2 connection and close PC1 immediately. Wait a couple of minutes. Open PC2.

- Place one end of the pipe inside distilled deaired water. Apply small vacuum to the other end to fill thepipe and connect it to PC1. Open PC1 and fill the cell.
- When the water level exceeds the topcap level, open the air pressure connections (UA1 and UA2). Observe the water coming out from the air pressure connections on the triaxial base. If there is no water, apply a small vacuum to that connection until the water is dribbling. When air pressure connections are filled with water close UA1 and UA2.
- After completely filling the cell, close the PC1 and then PC2. Remove the pipe from PC1.
- Place the triaxial cell to its place on the triaxial loading frame. Move the loading plate upward by clicking on the manual control screen until a small gap is obtained between loading piston and loadcell (*2:position, 1:raise, press:enter* to start, *press:esc* to stop the motor movement).
- Start the Triaxial software on the computer.
- Open pore water pressure volume actuator 'PPVA' supply valve and close PPVA output valve (*control, valves, sample pressure, supply valve-open, output valve-close*). Open cell pressure volume actuator 'CPVA' supply valve and close CPVA output valve (*control, valves, cell pressure, supply valve-open, output valve-close*)
- Empty the PVA pistons by clicking manual control screen (*2:position,1:empty*)
- Place deaired and distilled water filled container at the top of one of the PVAs. Insert supply valves connection pipe inside water filled container. Fill the PVA pistons by clicking manual control screen (*2:position,2:fill*).
- Close PPVA supply valve and open PPVA output valve (*control, valves, sample pressure, supply valve-close, output valve-open*). Close CPVA supply valve and open CPVA output valve (*control, valves, cell pressure, supply valve-close, output valve-open*)
- Open pore PVA, V1, UW1,UW4 close UW2, UW3.

- Flush water from the compartment beneath the topcap HAE ceramic (*2:position, 4:jog, press: up arrow* to accelerate, *press:esc to stop piston motion*). Be sure that there is no air bubble coming out from the connections.
- Close UW1, UW4 and open UW2, UW3.
- Flush water from the compartment beneath the pedestal HAE ceramic (*2:position,4:jog, press: up arrow* to accelerate, *press:esc to stop piston motion*). Be sure that there is no air bubble coming out from the connections.
- Close UW2 and open UW4.
- Make wet connection between PC1 and CPVA pipe. To do this, jog the water from CPVA (*2:position, 4:jog, press:up arrow* to accelerate, *press:esc to stop piston motion*) until there is no air bubble coming from the CPVA pipe. Insert CPVA pipe tip on to the PC1 while water is dribbling. Tighten the CPVA connection.
- Open PC1.
- Make arrangements on Triaxial software (*Initialization, horizontal stress: 800 kPa, vertical stress: 800 kPa, sample pressure: 80 kPa, stress rate: 50 kPa/min, duration: 10000 min*). This results in application of 800 kPa of cell pressure and 80 kPa pore water pressure.
- Start test (*Run, initialize platen:wait until a slight force is read by the load cell*)
- After sample pressure reaches its target pressure close UW3, UW4.
- Sequential allow the water flow from CPVA to PPVA by opening UW3, UW4 for a while (e.g. 10 minutes). During this period calculate the permability of ceramic discs. The change of water volume can be monitored on the sample volume change bar in the Triaxial software (*View, test monitor, sample volume change*). Record initial value before opening UW3, UW4 and take final value after closing them to measure the water volume change. Use timer to record the duration of water flow. Calculate the

permeability of ceramics from Darcy's law. Compare this value with saturated permeability of the HAE ceramics reported in the product spesification.

- 1 day period is generally sufficient to achieve full saturation of HAE ceramics.
- After full saturation is achieved stop the test (*Run, abort*)
- Reduce pressures gradually (*control, cell pressure, enter the quantity for pressure decrement; control, sample pressure, enter the quantity for pressure decrement; "repeat the cycle to decrease cell pressure and then sample pressure*)
- Empty the triaxial cell.
- Remove the triaxial cell from the base. Do not dry the remaining water from the base.
- Suck the water inside air pressure pipes by connecting the vacuum pump together with a water trap to UA1 and UA2
- Remove the water on the ceramics using a wet towel.

3.5.4.2 Unsaturated Triaxial Testing

- Prepare two ring-shaped filter papers to cover the surface of annular porous metal around ceramics.
- Place soil specimen on the pedestal.
- Cover the specimen with the elastic membrane and place two o-rings around the pedestal.
- Place the top cap and seal the membrane around it by placing two o-rings around topcap.
- Assemble and fill the triaxial cell with the same procedure described in 3.5.4.1 and place it on the loading frame. Take care to avoid air bubbles trapped inside the triaxial cell during the filling procedure.

- Adjust pressure transducers' zero readings to the same referance state. The mid-height of the specimen can be choosen as the reference state. Fill the PVA outlet pipes (*2:position, 4:jog,press:Up arrow, press:esc to stop piston motion*) and fix the ends of the outlet pipes at the referance height. Read the raw value on the system monitor screen (*View, system*). Update the transducers'zero readings in the Triaxial software (*Calibrate,Summary, Channel:select either load, cell, sample or displacement, Offset:enter the raw value read, Apply, Download*). For the air pressure transducer, bring the end of the water filled pipe of air pressure connection to the reference height then take zero in the Testbox software.
- Connect the CPVA pipe to the triaxial cell by taking care to avoid trapped air bubbles during the connection. To continiously jog the water from the CPVA outlet at a slow speed helps make a good wet connection.
- Connect the diffused air volume indicator inlet pipe to the pore water pressure outlet valves. Close V3, V4, open V1, V2, UW1, UW2, UW3, UW4, D1, D2. Flush all connections with water without trapping any air bubbles in the connections (*2:position, 4:jog, press: Up arrow, press: esc to stop piston motion)*. Maintain jogging the water until the diffused air volume indicator's burette is filled with water. Close UW1, UW2, D2.
- Connect air pressure pipes to UA1 and UA2.
- Make necessary arrangements in the Triaxial software. Unsaturated triaxial tests consist of three separate stages. In the first stage, suction is applied to the specimen and this stage is called suction equalization stage. The arrangement of test parameters are specified in the *initialization* tab of the Triaxial software. Specimen should be kept under a small net stress, which is the difference between the cell pressure and air pressure, during this stage (e.g. 10 kPa). Therefore set the *horizontal stress,* which is the cell pressure value acting on the specimen, as the target air pressure plus 10 kPa. The *vertical stress* is set to a value slightly higher than *horizontal stress* (e.g. 3 kPa) to ensure to keep loading piston always in contact with the topcap. Set

sample pressure to a small pressure value (e.g. 10 kPa). Target air pressure is determined based on the target suction and applied pore water pressure since matric suction is equal to the difference between pore air pressure and pore water pressure. For example, to apply target suction of 80 kPa to specimen take *sample pressure:* 10 kPa, target air pressure: 90 kPa, *horizontal stress:* 100 kPa, *vertical stress:* 103 kPa. During the test, air pressure is manually controlled and monitored by a separate system. Set a suitable *stress rate* that the operator can keep up (e.g. 10 kPa/min). The second stage is isotropic loading-unloading and the test parameters are specified in *consolidation/A Table* in the Triaxial software. The target net stress is set under *effective horizontal stress* column. For example, to apply 100 kPa net stress to the specimen in the example given above, operator enters 180 kPa, that is the target air pressure of 90 kPa minus 10 kPa of pore water pressure plus target net stress value of 100 kPa. Triaxial software uses effective stress in its algorithm to calculate cell pressure, therefore pore water pressure is subtracted from the summation. Predetermined stress rate is specified as the rate of loading. The final stage is shearing of specimen and parameters are defined in *Shear Table*.

- Once all test parameters are defined and all connections are checked, the test can be commenced (*Run, start*). The air pressure is adjusted manually at the same rate of loading with the prescribed stress rate in the *initialization* tab by means of a air pressure regulator.
- Each stage of the test can be carried out either drained or undrained for pore water, whereas pore air is kept under drained condition. In the suction equalization stage, specimen's suction is either controlled or measured. To control the suction, the water volume change is allowed by arranging UW3, UW4, V1 and V2 in open position during testing. If the operator aims to measure specimen's suction instead of controlling it, V1 should be closed and V2, V3 are kept open. The water pressure change is monitored by means of a separate pressure transducer. Wait for the equilibrium of pore

water pressure variation; the difference between the applied air pressure and the measured pore water pressure is equal to the specimen's suction. It should be noted that for this type of test, operator should not permit the negative pore water pressure values and air pressure should be set to a value higher than the expected suction. This stage ends when the water pressure variation/water volume change becomes asymptotic to the time axis. Press *Run, Next Step* in the Triaxial software to start the following stage.

- The isotropic loading-unloading stage can be carried out under either constant suction or constant water content condition. In the constant suction test, pore water and pore air are kept under drained condition during loading. To do this, UW1, UW2, V2 and V1 are kept open. The stress rate should be slow enough to ensure no excess suction development inside specimen during loading. The suitable stress rate can be determined in a separate trial run. Specimen is loaded under drained condition for a certain net stress interval (e.g. 40 kPa) at the prescribed loading rate then it is turned into the undrained condition. There should be negligible variation of pore water pressure under undrained condition if the loading rate is slow enough. In the constant water content test, pore water is kept under undrained condition and pore air is kept under drained condition. The pore water pressure is measured instead of controlling it. UW1, UW2, V2, V3 are kept open and V1 is closed in order to perform constant water content test. This stage ends when the water pressure variation/water volume change becomes asymptotic to the time axis. Press *Run, Next Step* in the Triaxial software to start the following stage.
- The final stage is shear stage. It can be carried out as either constant suction or constant water content type, similar to the isotropic loading-unloading stage with the same operations described in the previous step.
- To finish the test, *Run, Abort* in the Triaxial software. Reduce pressures gradually (*control, cell pressure, enter the quantity for pressure decrement; control, sample pressure, enter the quantity for pressure decrement;*

"repeat the same cycles decrease cell pressure and then sample pressure). The air pressure is simultaneously reduced by means of air pressure regulator. The expansion/shrinkage of membrane can be observed during this operation. If the air pressure within the specimen does not dissipate at the anticipated rate, it causes expansion of membrane during dismantling process at the end of test. This means that annular porous metals around the high air entry ceramic discs are clogged.

- Specimen is removed from the triaxial base. Specimen's gravimetric water content and unit weight are measured at four different locations along the height.
- The raw test data is taken from the Triaxial software (*File, Load, select the related test file, File, Dump, Engineering*).

3.5.4.3 Measurement of Diffused Air Volume

- Record the water level inside the diffused air volume indicator (DAVI) as the initial reading.
- Close V1, V3 open V4, V2, UW1, UW2, UW3, UW4, D1. Make sure D2 is closed. Slowly move the water beneath the ceramics by means of screw pump until there are no air bubbles coming out. Top cap and pedestal should be flushed separately by closing UW1 and UW2 in sequence.
- Record the water level inside the DAVI as the final reading.
- Close UW1, UW2. Open V3.
- Make the pore water pressure same as with the value just prior to the operation using the screw pump.
- Close V4, V3. Open V1 (if the test stage is carried out under constant water content condition, V1 must always be closed in the aformentioned test procedure descriptions).

- Refer to Fredlund (1975) to calculate the volume of diffused air. The absolute pressure in the indicator is taken as atmospheric since D1 remains open during the whole test period.

3.5.4.4 Replacement of High Air Entry Ceramics

Existing 5-bar HAE ceramics were replaced by those with 15 bar capacity to perform tests at higher suction in early periods of this study. The ceramics were glued in their place using commercial Bison metal epoxy. The removal of old ceramics from the test setup can be achieved by hammering a screwdriver on it. Crumbs of ceramic are removed with caution to avoid getting any material to the drainage lines. Hammering operation should be carried out after the drainage lines are dried by flushing pressurized air, since removal of material from the wet drainage lines is much more difficult. After removal of old ceramics and cleaning the compartments, new ones can be glued in place.

Ceramics can be cut almost in any shape by water jet, but a cheaper procedure can be followed to obtain a disc shape ceramic. In this study, 15 bar ceramics at desired size were obtained from a large pressure plate ceramic which was broken. Ceramics pieces were taken from the pressure plate by means of a pincer. Before cutting off the ceramic piece, pressure plate surface was scratched in a rough circular shape at the size slighly larger than the desired one to avoid the breaking off a small pieces from the extracted ceramic portion. The ceramic portion was then wetted by water and rubbed with the hand on a rasp to give it a disc shape.

After drying the ceramic disc, it is ready for gluing process. A 2 mm gap between the compartment's lateral surface and the ceramic is suitable for gluing process, a thinner gap make gluing process difficult whereas a wider gap is prone to leakage in long term usage. Ceramic disc is centered inside the compartment and pressed by finger to fix it during entire gluing process. A needle is used to fill the epoxy in

small amounts into the gap. A great care should be given not to form air voids within the gap.

3.5.5 Mersin Silt Test Results

Two constant suction triaxial test on Mersin silt specimens which are prepared at initial void ratio of 0.83 were carried out. For completeness, the results of these tests are given together with the previous constant suction test results performed and reported by Ahmadi-Naghadeh (2016).

The variation of void ratios during constant suction isotropic compression are given in Fig. 3.40. The specimens' stiffness and preconsolidation stress increase with increasing suction. MCD10 and MCD11 tests that correspond to initial void ratio of 0.83 have less preconsolidation pressure than that of 0.72. MCD10 test at 50 kPa constant suction results in a single virgin compression line which has the slope of 0.156. MCD11 test at 100 kPa constant suction consists and both elastic and plastic parts.

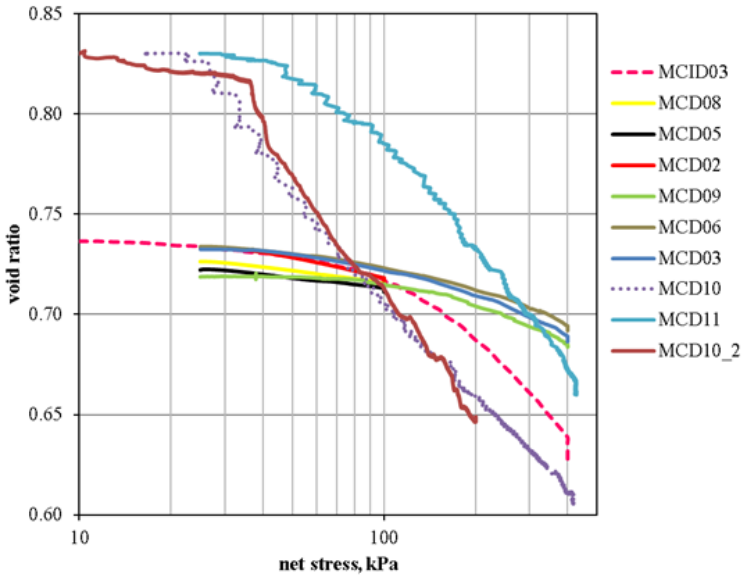

Figure 3.40 Variation of void ratio during constant suction isotropic compression for Mersin silt specimens.

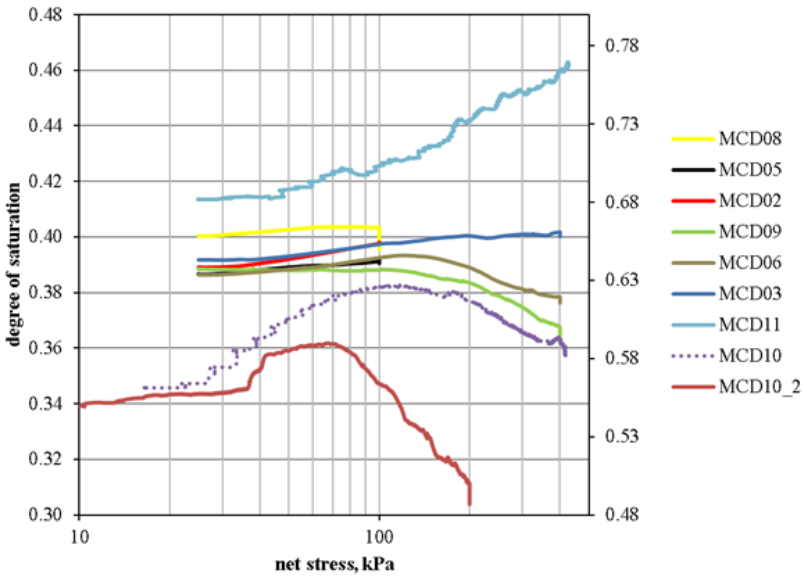

Figure 3.41 Variation degree of saturation during constant suction isotropic compression for Mersin silt specimens (MCD10 is plotted on the secondary axis at the right).

The variation of degree of saturation at constant suction isotropic compression is plotted in Fig. 3.40, the result for MCD10 test is plotted on the secondary axis at the right to highlight it better. The behaviour observed in MCD10 test is an interesting result since the degree of saturation initially tends to increase from 0.561 to 0.627 with increasing net stress at constant suction of 50 kPa. The degree of saturation starts to decrease under constant suction once the net stress exceeds 100 kPa. This stage of the test was repeated in a different test which was planned to trace loading-unloading and drying wetting paths and almost same behaviour was observed. Unfortunately, this test was not accomplished due to several setbacks that might be encountered during every laboratory works. In the intended test, the isotropic compression at 50 kPa constant suction started at initial degree of saturation at 0.55 and the net stress acting on the specimen was increased to 200 kPa. The degree of saturation showed increasing trend up to 70 kPa and then started to decrease. This experimental data is labeled as MCD10_2 and shown in Fig. 3.40 and 3.42. Furthermore, somewhat slight version of the same behaviour is observed in MCD6 test which was the 200 kPa constant suction isotropic compression test performed by Ahmadi-Nahgadeh (2016).

In these tests, it was observed that the pore water always comes out from the specimen during the isotropic compression. The volume change of specimen initially follows a steep path up to the remarked net stress (100 kPa and 70 kPa) and then it changes in a trend similara to the pore water volume change. Therefore, the decrease in void ratio is much higher than the decrease of water content during the increasing trend of degree of saturation. In the second part, the decrease in void ratio becomes less than that of the water content and degree of saturation starts to decrease. This behaviour can be interpreted in the space of degree of saturation, suction and void ratio. If several retention curve branches corresponding to the each decreasing void ratio during isotropic compression are considered, it can not be generalized that the water retention curves make translations on the projection of degree of saturation and suction plane. This is a general point of view when the aim is to incorporate the effect of void ratio in the soil water retention models. For example, e_0, e_1 and e_2 respectively correspond to void ratios at the initial condition, during increasing degree of saturation in first part and during decreasing degree of saturation in the second part. During isotropic compression $e_0>e_1>e_2$ is valid. The water retention curves '$SWRC_0$', '$SWRC_1$', '$SWRC_2$' can be specified for each of e_0, e_1 and e_2. The observed behaviour during constant suction isotropic compression can only happen if the data point on the $SWRC_0$ is in between $SWRC_1$ and $SWRC_2$.

The deviatoric behaviour during constant suction shearing are illustrated in Fig. 3.42 to 3.44. The results of the tests performed at high confining pressure are plotted on the secondary axis on the right in Fig. 3.42.

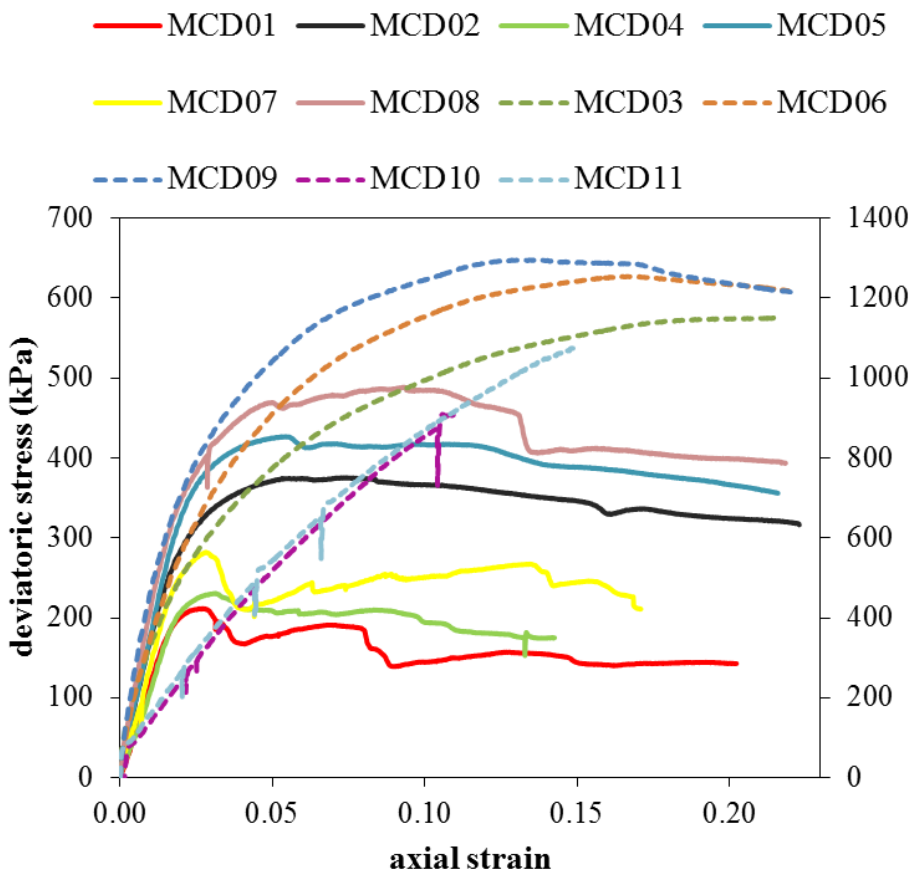

Figure 3.42 Deviatoric stress curves for constant suction shearing of Mersin silt (dashlined data series are plotted on the secondary axis on the right).

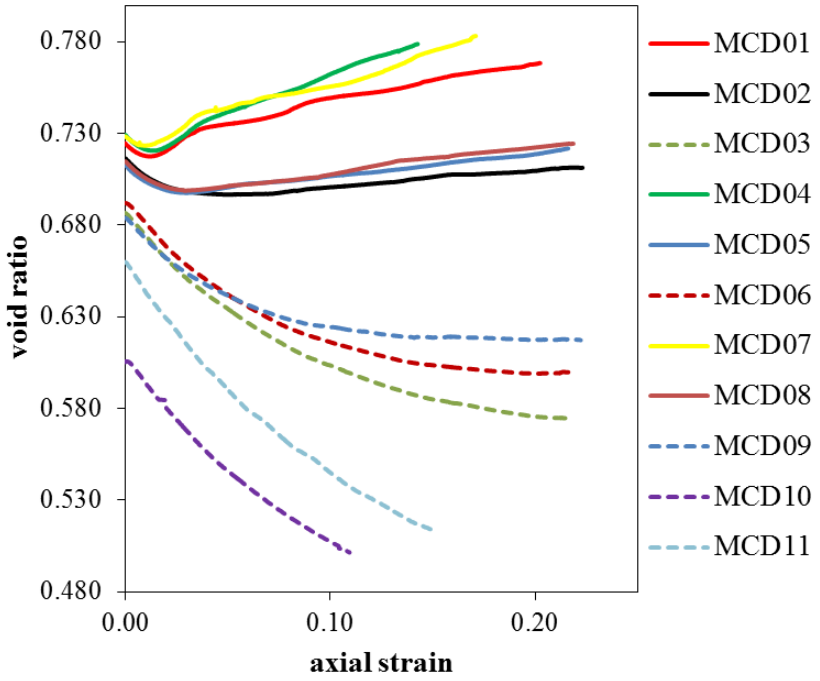

Figure 3.43 Variation void ratio during constant suction shearing of Mersin silt.

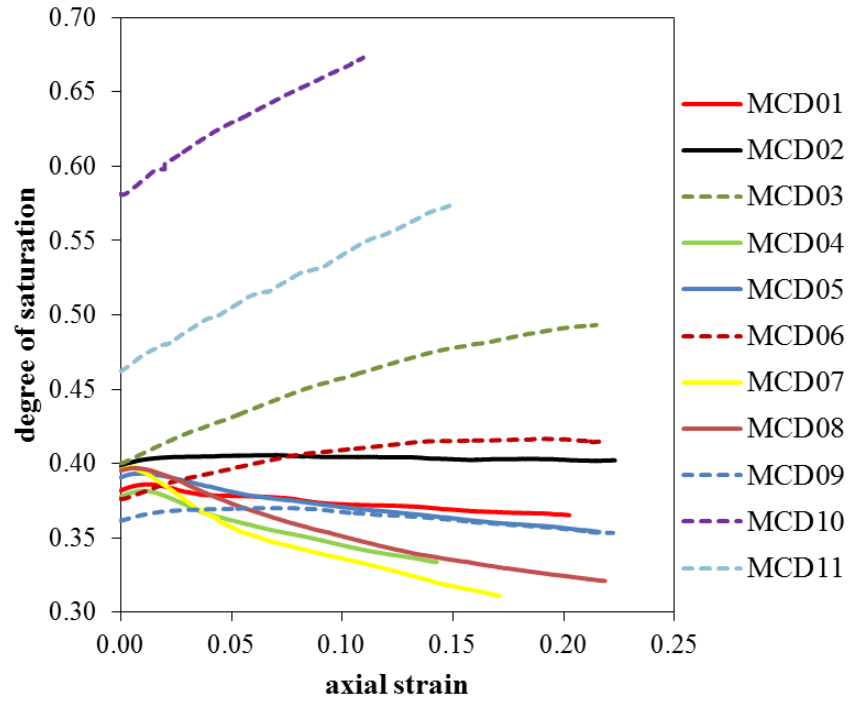

Figure 3.44 Variation of degree of saturation at constant shearing of Mersin silt.

The results of the constant water content tests are given in Fig. 3.45 to 3.50. In Fig. 3.46, suction did not vary much during isotropic compression at constant water content except for MCW04 test. In the MCW04, suction drastically changes after yielding of the specimen with increasing net stress.

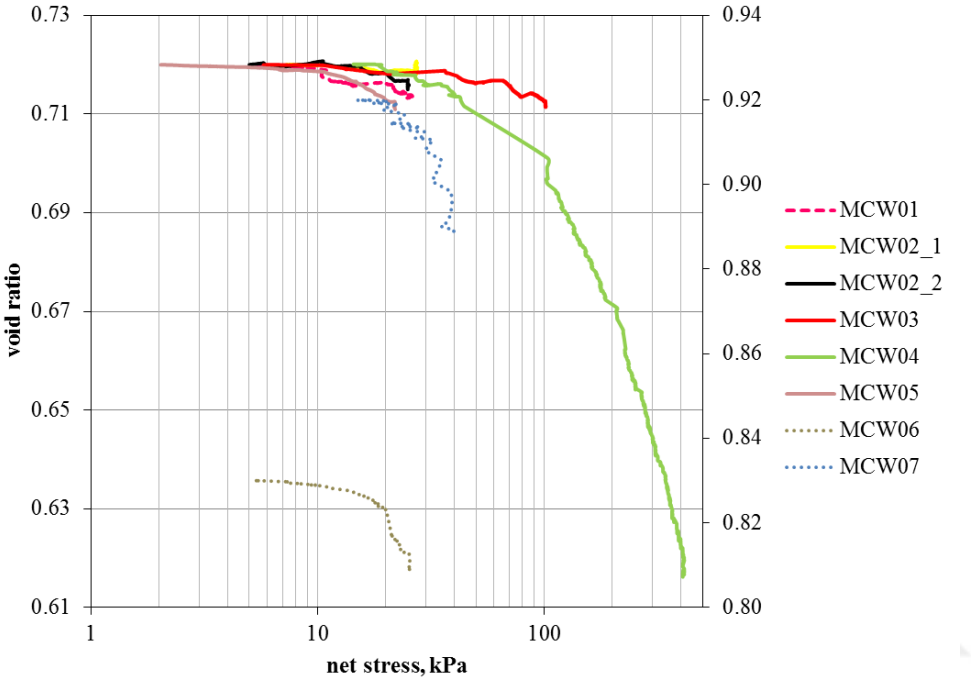

Figure 3.45 Variation of void ratio at constant water content isotropic compression of Mersin silt (MCW06 and MCW07 are plotted on the secondary axis at the right).

Fig. 3.47 shows deviatoric behaviour of Mersin silt specimens at constant water content shearing. MCW02 experiments on Mersin silt specimens having almost same initial suction and confining stress but different initial degree of saturation. The maximum deviatoric stress reached by these two specimens are different in Fig. 3.47; MCW01 specimen that has lower initial degree of saturation and reaches higher deviatoric stress than MCW02_1 specimen. In Fig. 3.48, the suction reduction in MCW01 having lower initial degree of saturation is consistenly less than that in MCW02_1. As it was discussed in Gallipoli and Bruno (2017) stabilising effect of water menisci increases with number of menisci per unit volume of solids and the intensity of the pull of the menisci. The intensity of the

pulling by menisci are quite similar for MCW01and MCW02_1 specimens having same initial suction. MCW02_1 specimen has higher initial degree of saturation and so the higher number of meniscuses. Theoretically, higher deviatoric stresses would be reached in drained or constant suction shearing of MCW02_1 specimen. But, to shear specimens under constant water content condition has provided the opposite outcome since the higher the initial degree of saturation, the higher the suction reduction and thus the less the pulling effect of the meniscuses.

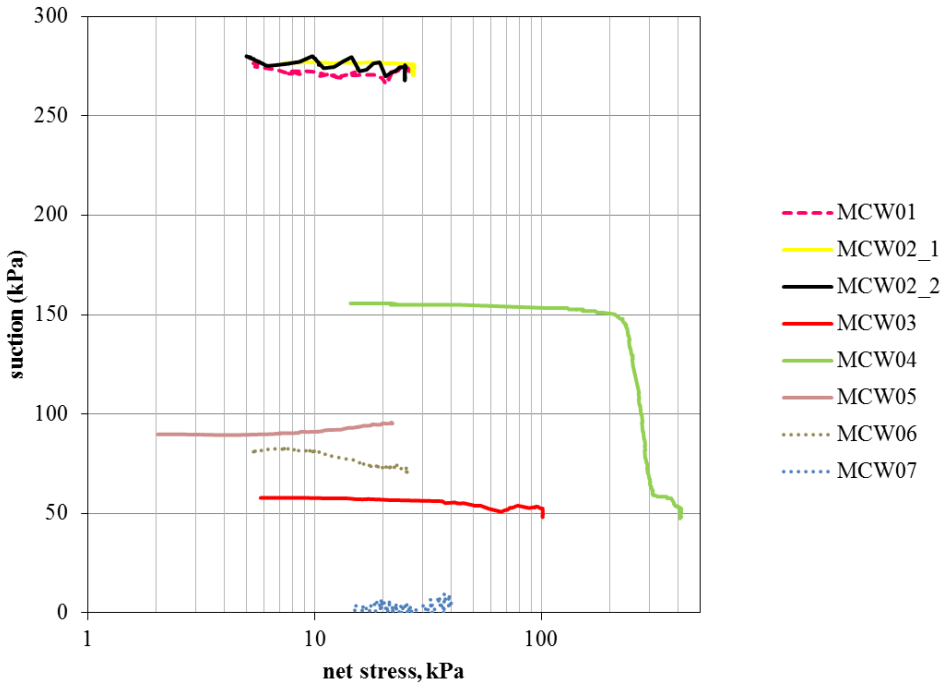

Figure 3.46 Variation of suction at constant water content isotropic compression of Mersin silt.

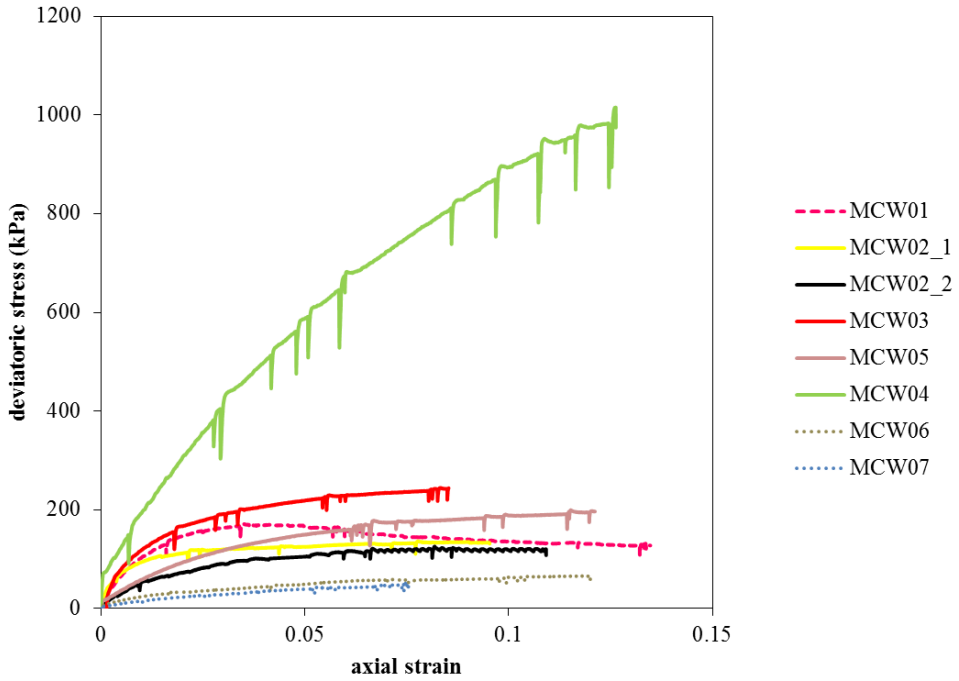

Figure 3.47 Deviatoric stress curves for constant water content shearing of Mersin silt.

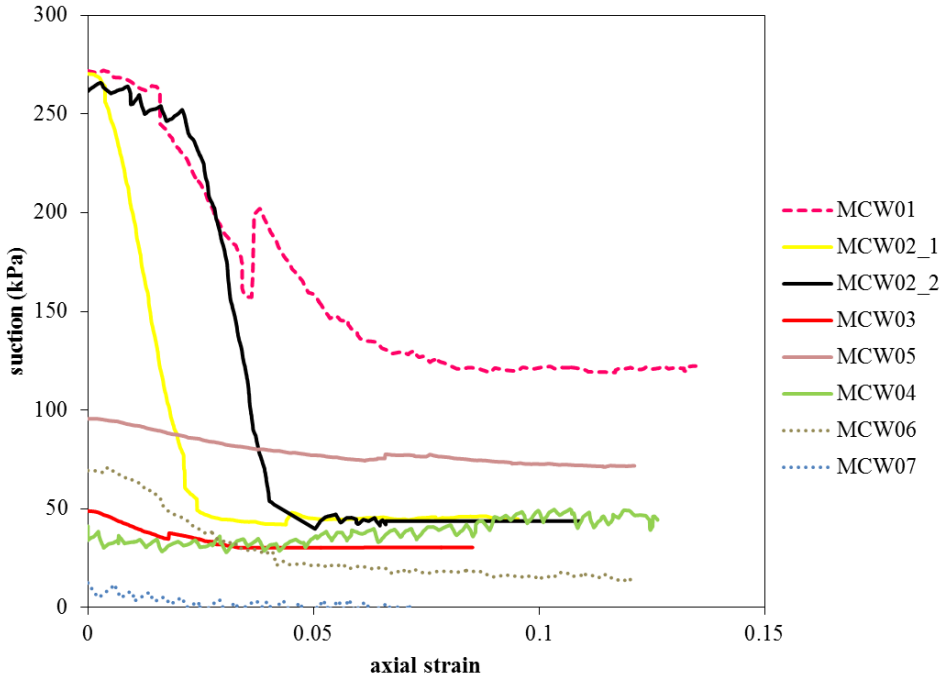

Figure 3.48 Variation of suction during constant water content shearing of Mersin silt.

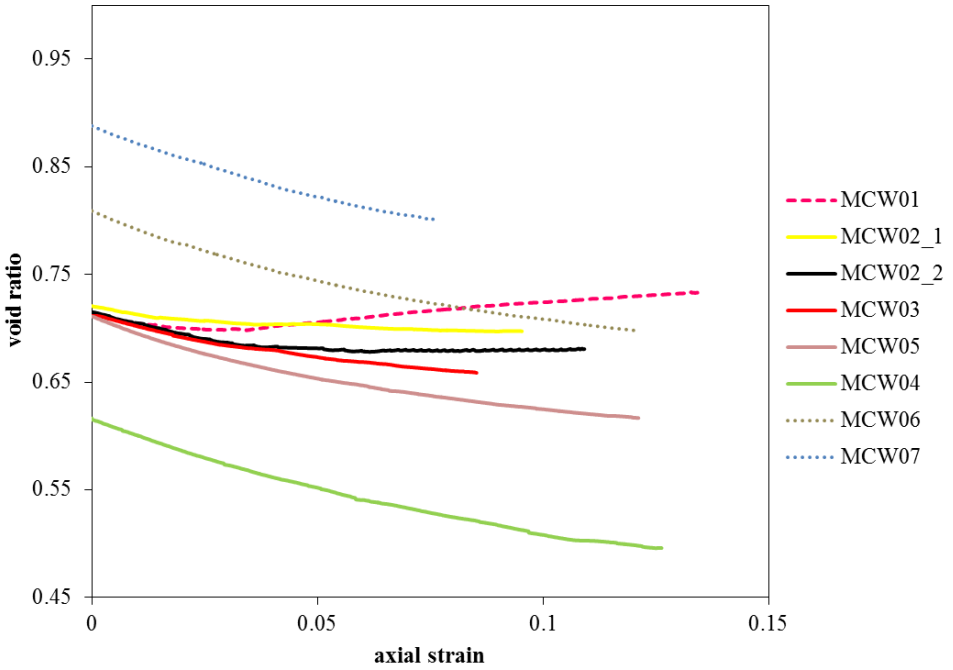

Figure 3.49 Variation of void ratio during constant water content shearing of Mersin silt.

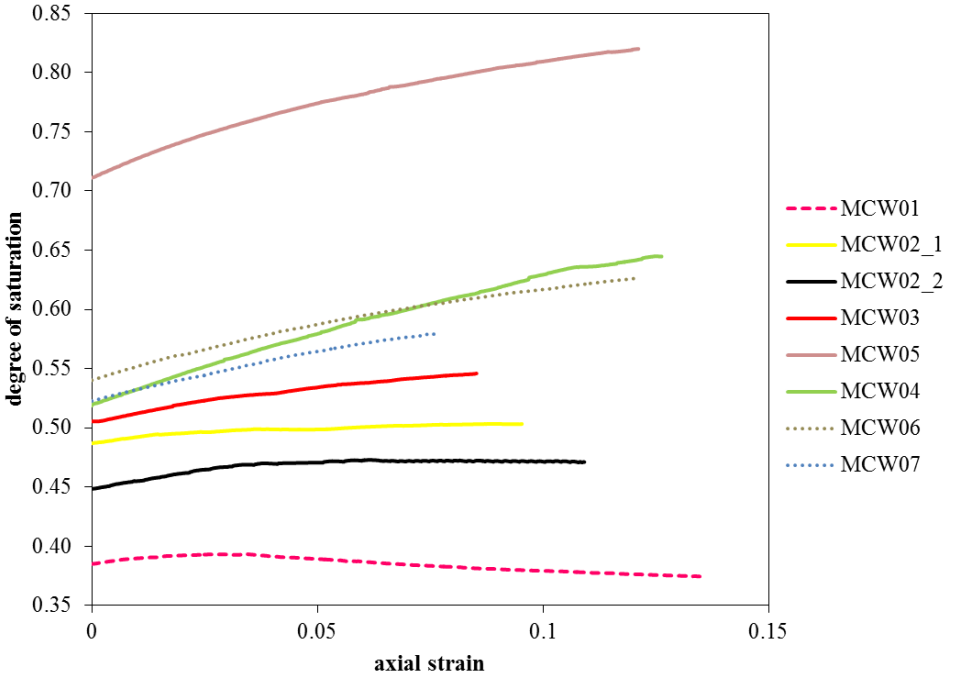

Figure 3.50 Variation of degree of saturation during constant water content shearing of Mersin silt.

3.5.6 Ankara Clay Test Results

Five constant water content triaxial tests were carried out on Ankara clay specimens. However, the isotropic compression stages are carried out under constant suction condition for these tests. In fig. 3.50 and 3.51, the varation of void ratio and degree of saturation of Ankara clay specimens under constant suction isotropic compression are illustrated, respectively.

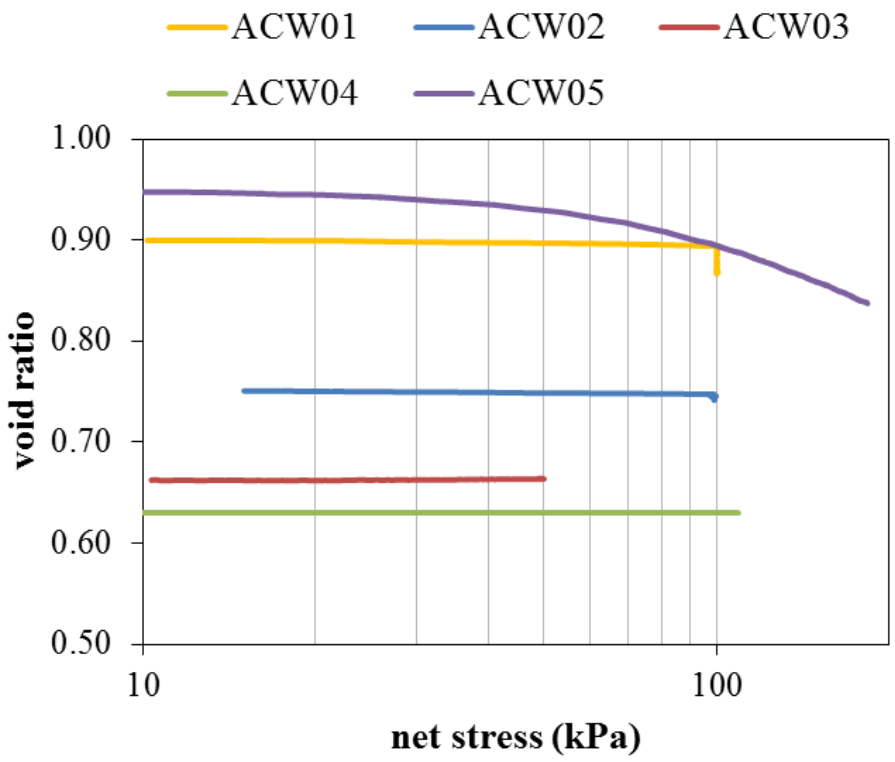

Figure 3.51 Variation of void ratio during constant suction isotropic compression of Ankara clay.

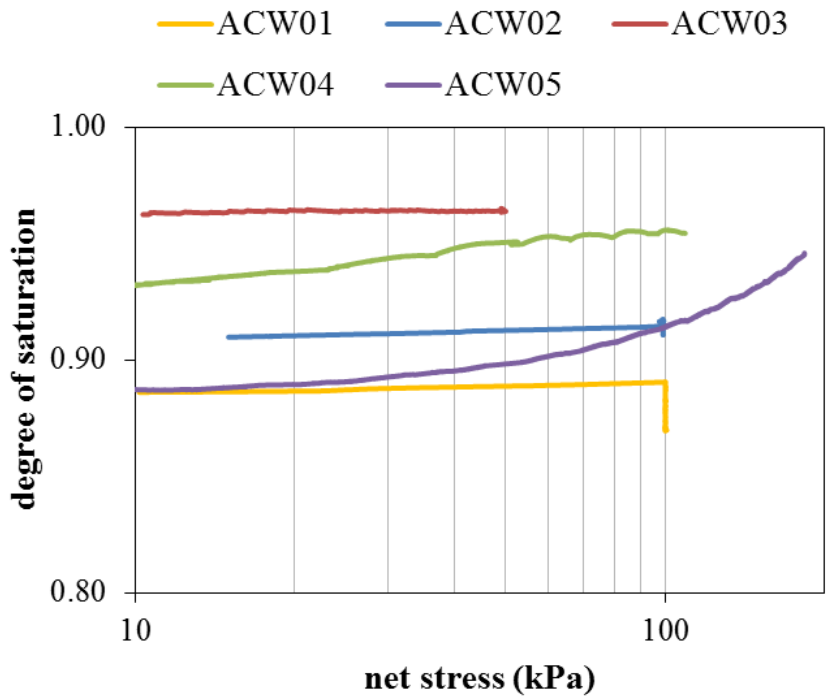

Figure 3.52 Variation of degree of saturation during constant suction isotropic compression of Ankara clay.

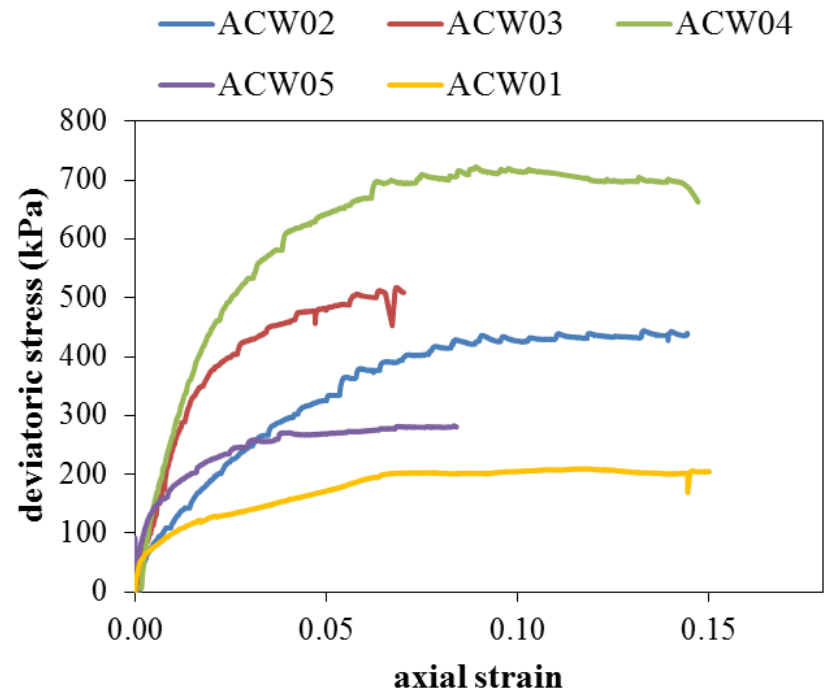

Figure 3.53 Deviatoric behaviour of Ankara clay specimens during constant water content shearing.

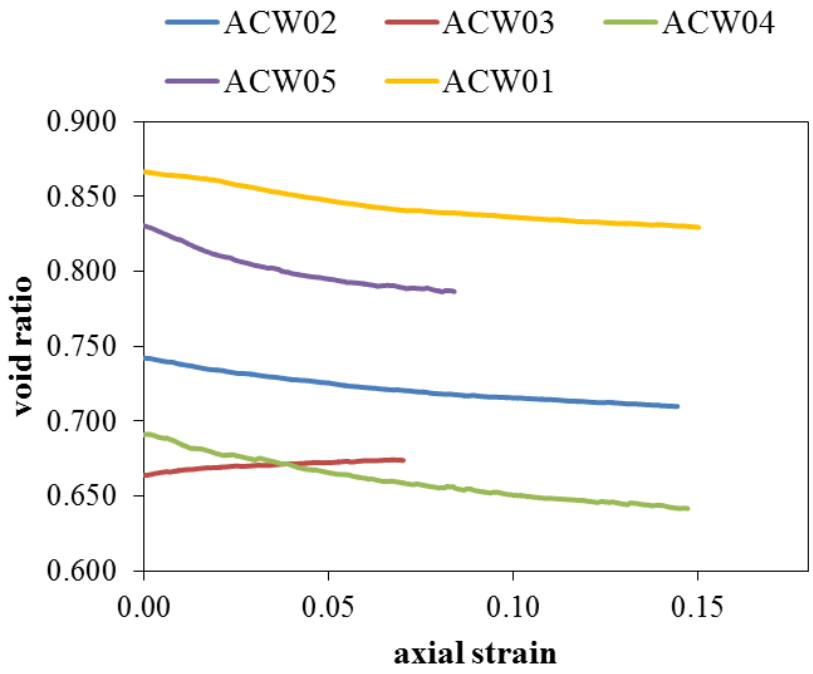

Figure 3.54 Variation of void ratio of Ankara clay specimens during constant water content shearing.

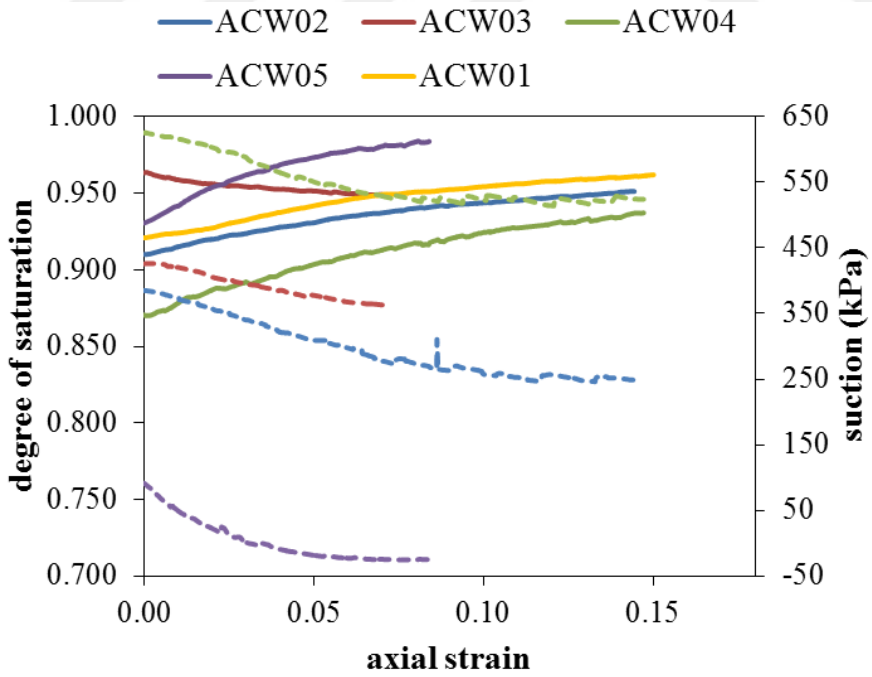

Figure 3.55 Variation of suction and degree of saturation of Ankara clay specimens during constant water content shearing (dashed lines with the same color correspond to suction and plotted on the secondary axis at the right).

The isotropic loading-unloading curves of Ankara clay specimens at high suctions were extracted based on procedure explained in Section 3.5.2.1. Four different chemical salt solutions such as KNO_3 (RH=92.8%, corresponding total suction is 10 MPa), KCl (RH=83%, corresponding total suction is 24 MPa), NaCl (RH=75.2%, corresponding total suction is 34 MPa) and NaBr (RH=56.6%, corresponding total suction is 77 MPa) were used to generate high suctions on the Ankara clay specimens. The aforementioned relative humidity of the chemical salts were determined based on the temperature of the laboratory environment. The results are shown in Fig. 3.56 including the variation of both void ratio and degree of saturation. The specimens did not show any yielding with increasing net stress up to 1000 kPa, exerting high suctions results in overconsolidated specimens.

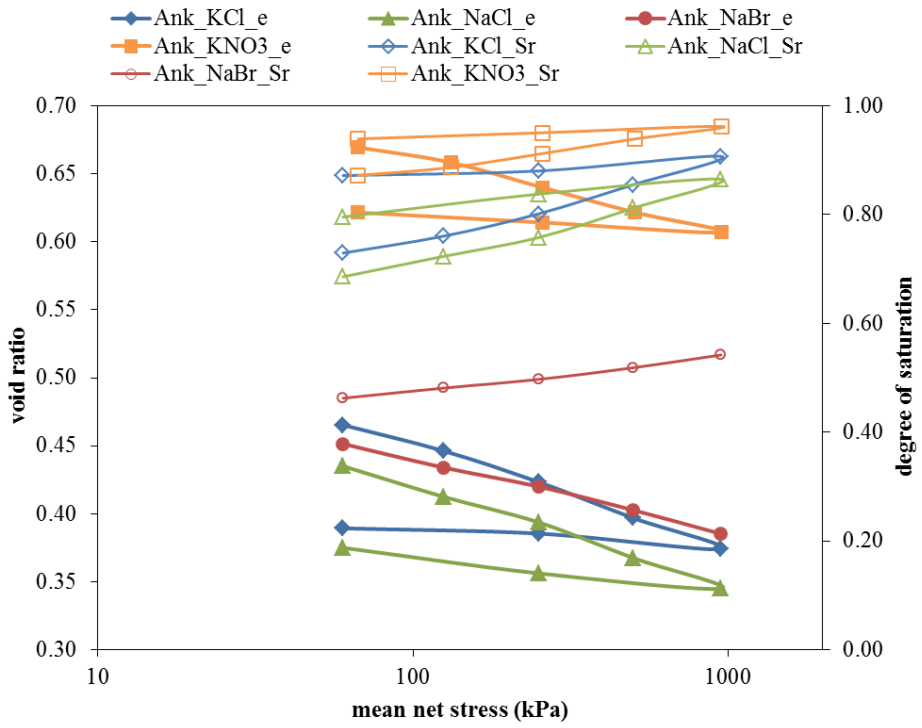

Figure 3.56 Isotropic loading-unloading curves of Ankara clay specimens at high suctions under constant water condition.

The variation of deviatoric stress under zero confining stress for Ankara clay specimens at high suctions is shown in Fig. 3.57. In addition to the aforementioned chemical salts, K_2SO_4 (RH=96.5%, corresponding to 4.8 Mpa total suction) was

used. In these tests, Ankara clay specimens were equilibrated to the same suction in both drying and wetting direction. The initially saturated Ankara clay specimens were directly placed into the jars for the equilibrium in the direction of drying whereas air-dried specimens were obtained from saturated specimens and placed into the jars in the direction of wetting. The extension 'w'at the end of labels in Fig. 3.57 is used to address the specimens equilibrated in the direction of wetting. Those specimens have less degree of saturation than specimens equilibrated in the direction of drying and reach much more higher deviatoric stresses at the same suction. Ankara clay specimens at high suction show rock-type behaviour during deviatoric loading such that the deviatoric deformations result in combined and cataclasis failure. There are two tests for specimens equilibrated with NaBr chemical salt, which generates the highest suction, in the direction of drying. But, the resulting shear strength differ too much in these tests due to random generation of weak zones during deviatoric loading.

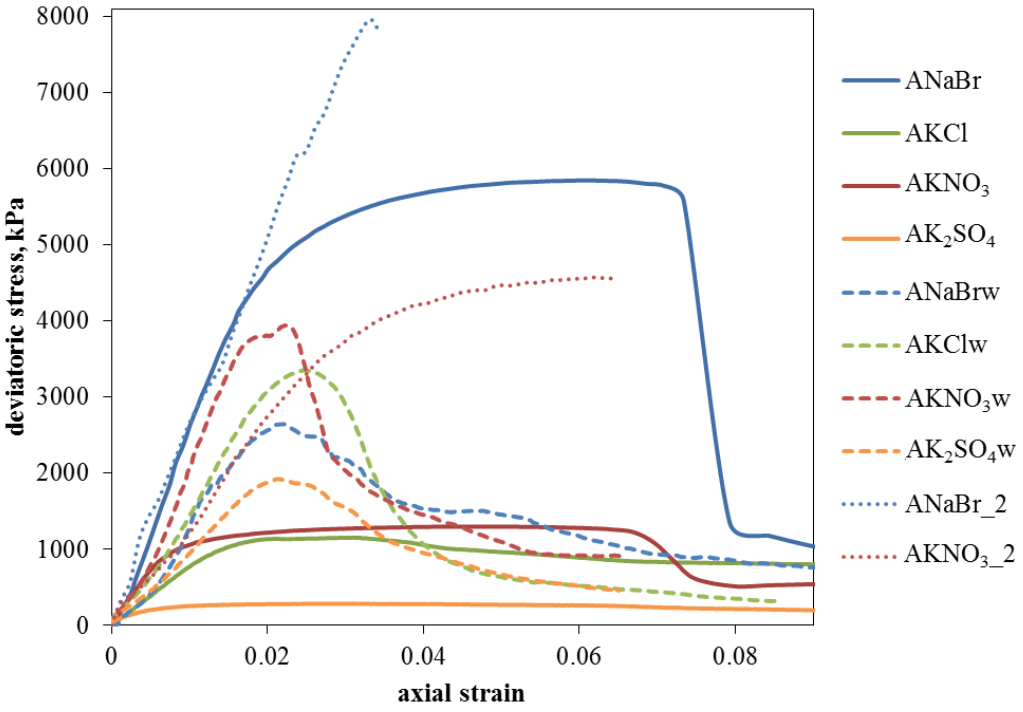

Figure 3.57 Deviatoric stress curves of Ankara clay specimens at high suctions under constant water content condition.

3.5.7 Elazığ Silt Test Results

Four constant suction triaxial tests and seven constant water content triaxial tests, one isotropic loading-unlouding cycle test at constant suction and one deviatoric loading-unloading cycle test at constant suction were carried out on Elazığ silt specimens.

The results from isotropic loading at constant suction and constant water content condition are illustrated in Fig. 3.58 to 3.60.

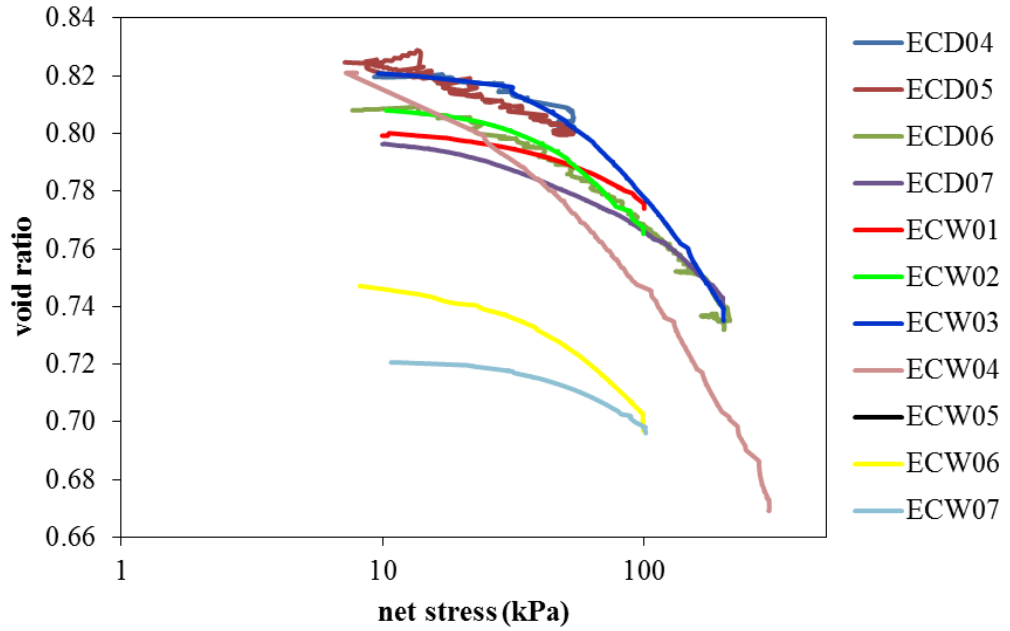

Figure 3.58 The variation of void ratio during isotropic loading at constant suction and constant water content condition for Elazığ silt.

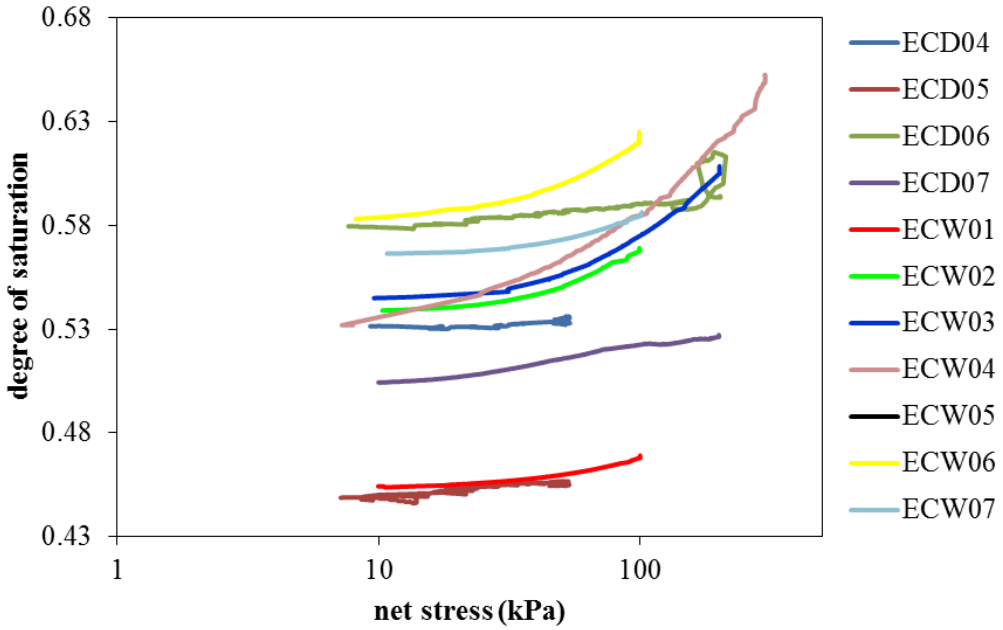

Figure 3.59 The variation of degree of saturation during isotropic loading at constant suction and constant water content condition for Elazığ silt.

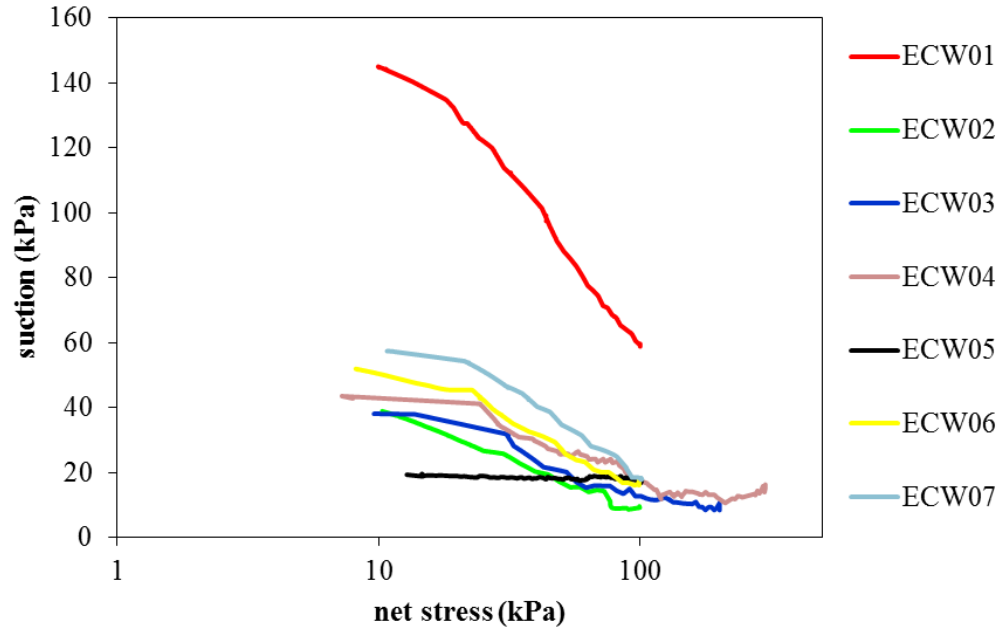

Figure 3.60 The variation of suction during isotropic loading at constant water content condition for Elazığ silt.

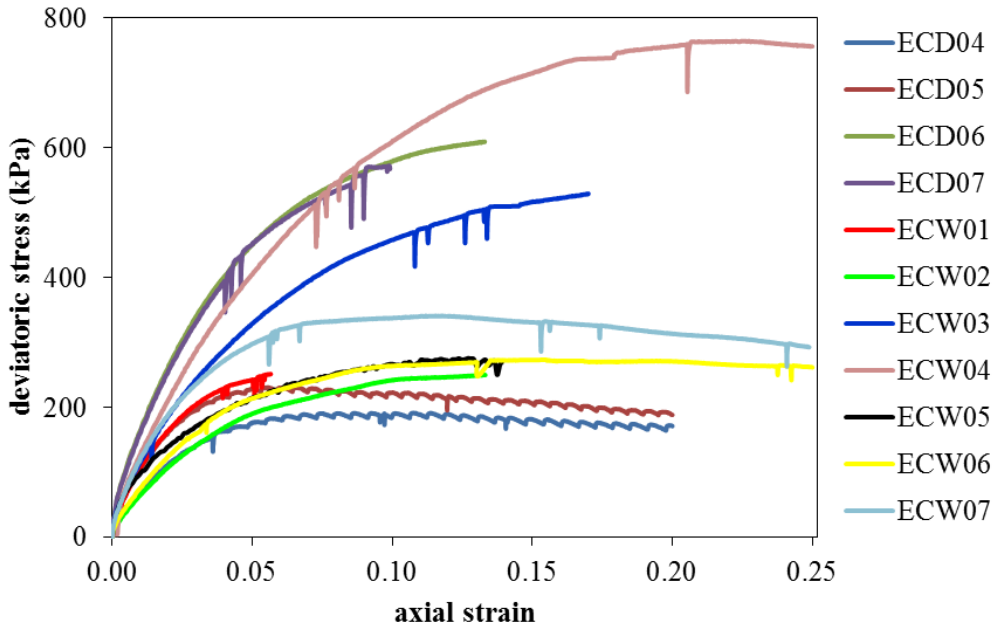

Figure 3.61 Deviatoric loading curves under constant suction and constant water content condition for Elazığ silt.

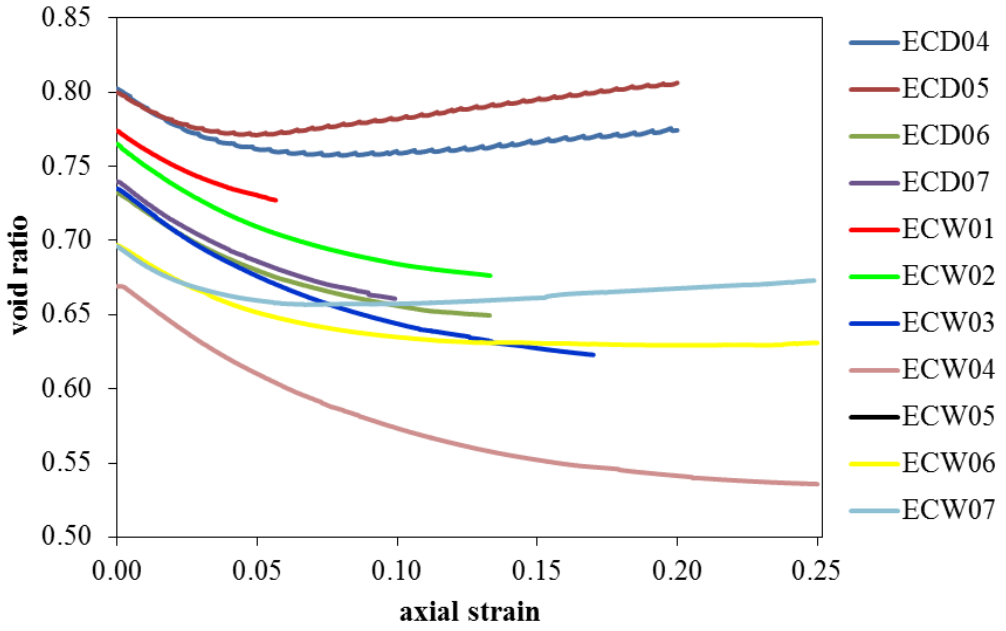

Figure 3.62 The variation of void ratio under constant suction and constant water content condition for Elazığ silt during deviatoric loading.

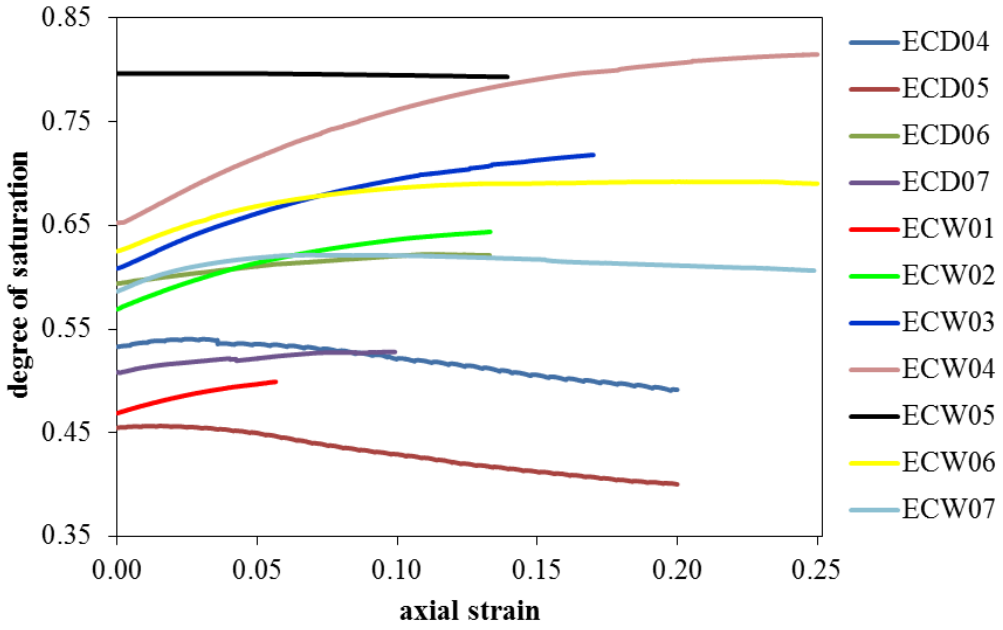

Figure 3.63 The variation of degree of saturation under constant suction and constant water content condition for Elazığ silt during deviatoric loading.

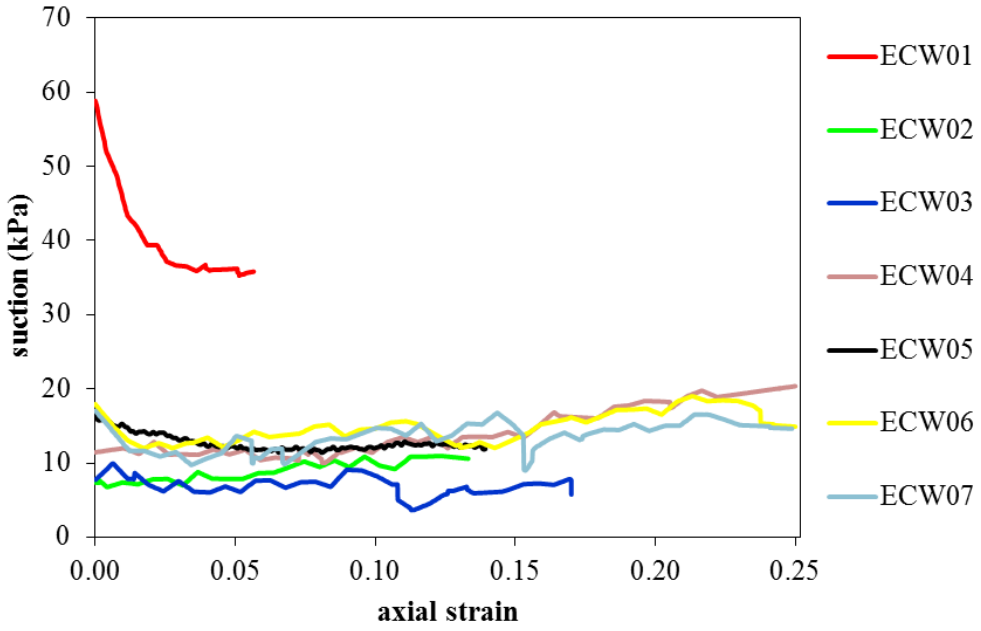

Figure 3.64 The variation of suction under constant water content condition for Elazığ silt during deviatoric loading.

Isotropic and deviatoric loading-unloading cycles were carried out on Elazığ silt specimens under 40 kPa constant suction. During isotropic loading net stress was followed the path of 10 kPa, 200 kPa, 50 kPa, 200 kPa, 50 kPa and 200 kPa. At the end of isotropic loading-unloading cycles specimen was monotonically sheared (ECD09). In another test, specimen was isotropically loaded up to 200 kPa under constant suction and then the deviatoric stress cycles were applied. The results of these tests are given in together in Fig. 3.65 to 3.68.

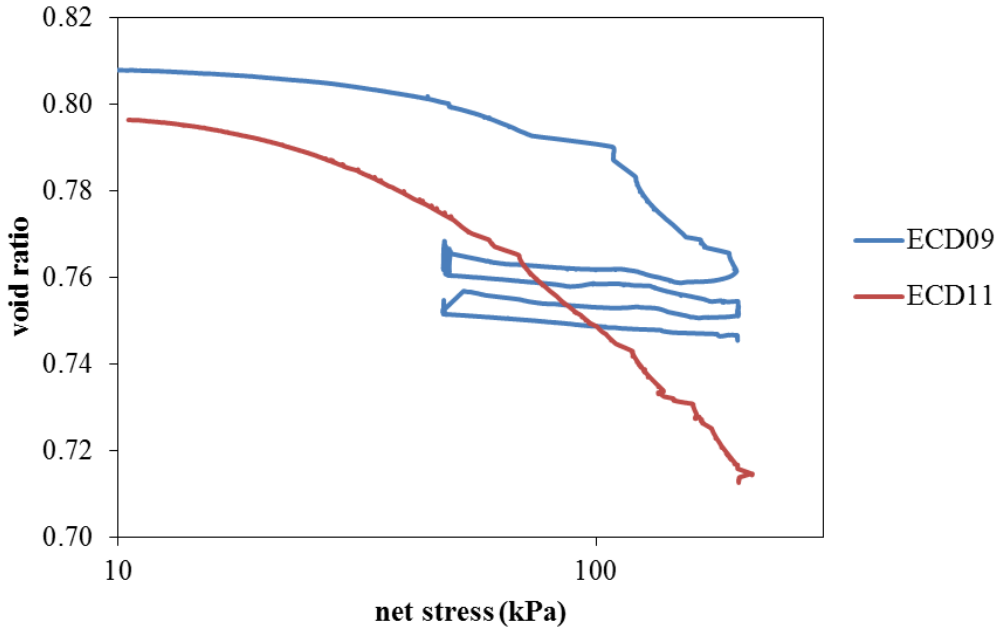

Figure 3.65 The variation of void ratio during isotropic loading-unloading cycle at 40 kPa constant suction on Elazığ silt (ECD09) together with monotonic isotropic loading data from ECD11.

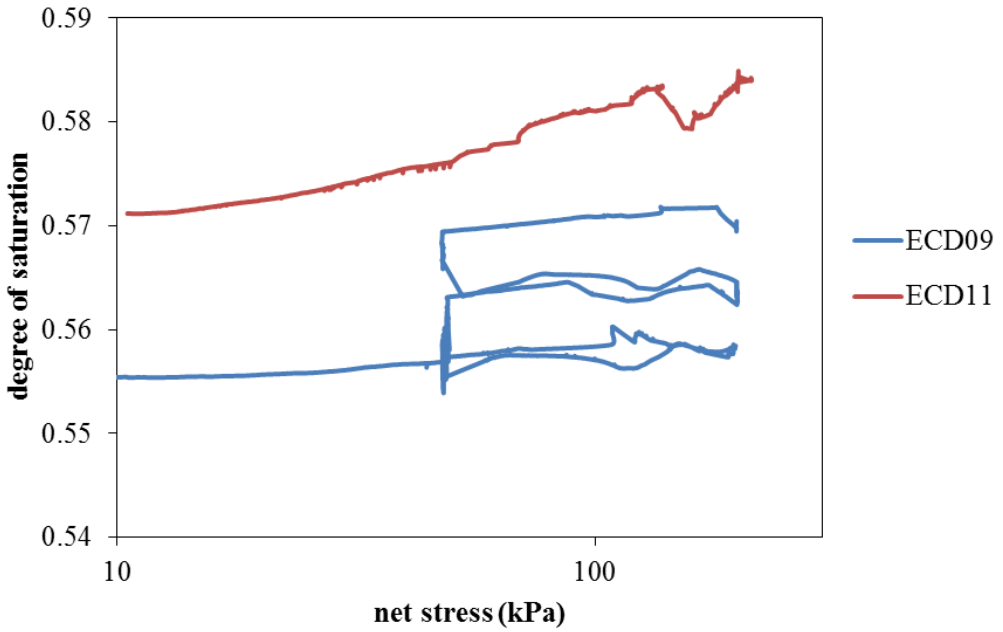

Figure 3.66 The variation of degree of saturation during isotropic loading-unloading cycle at 40 kPa constant suction for both ECD09 and ECD11 tests.

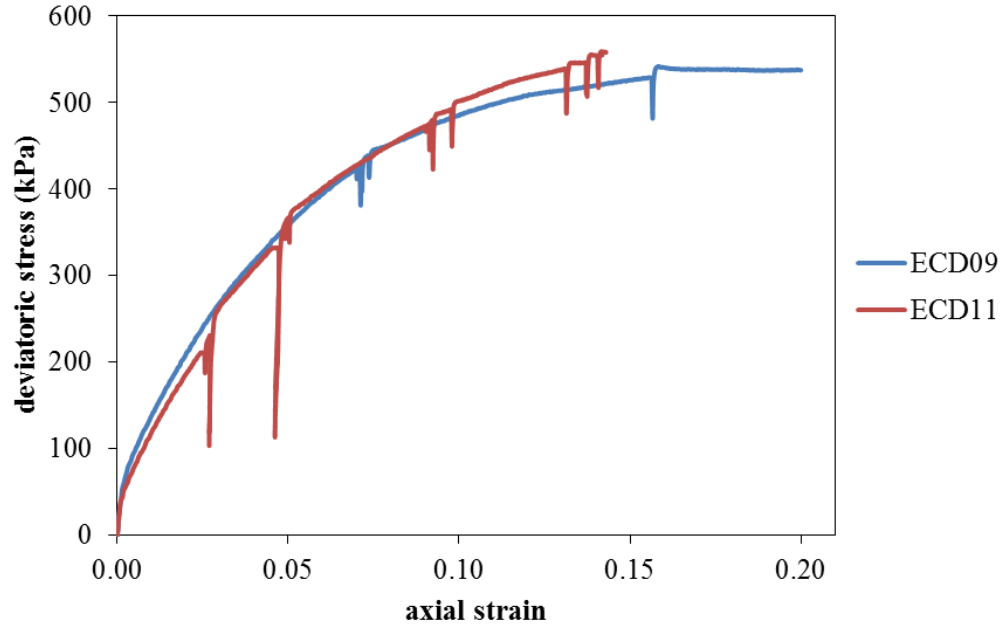

Figure 3.67 Deviatoric loading-unloading cycles at 40 kPa constant suction on Elazığ silt (ECD11) together with monotonic shearing data from ECD09.

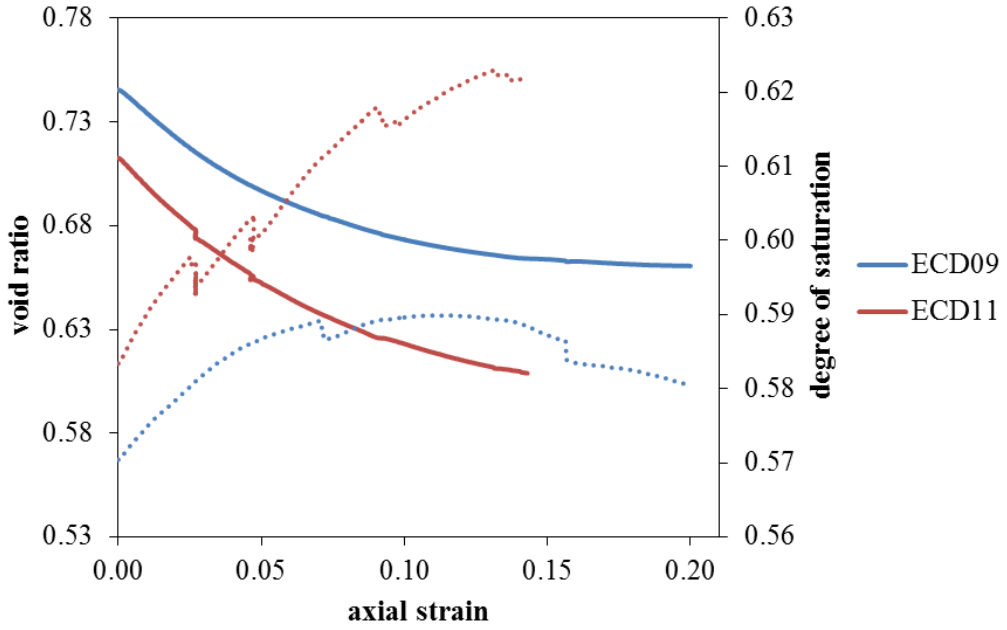

Figure 3.68 The variation of void ratio and degree of saturation at 40 kPa constant suction during deviatoric loading for both ECD09 and ECD11 tests.

3.5.8 Implementation of Gallipoli's Model on Experimental Results

The hydromechanical coupled model developed by Bruno and Gallipoli (2019) is implemented on experimental results. The closed-form equations proposed in this model are given in 2.3.3.2.

The results from soil water retention curve measurements on Mersin silt specimens prepared at two different void ratios were used to calibrate hydraulic model parameters. The closed-form equations given for the hydraulic component of the model were separately best-fitted to experimental data for drying and wetting soil water retention curves extracted at two different void ratios. The drying branches were best-fitted in the first place to determine m_d, λ_{sd}, ω_d and β_d. Then, the data for wetting branches were best-fitted by taking λ_{sw} and λ_{sd} as equal in order to determine m_w, λ_{sw}, ω_w and β_w. The hydraulic model calibrated for Mersin silt were given in Table 3.8. The calibration result for Mersin silt is given in Fig. 3.69a.

The parameters of mechanical component were calibrated using drained triaxial test results reported by Ahmadi-Naghadeh (2016). λ_p parameter was obtained as 0.163 by taking the slope of the virgin part of the saturated isotropic compression curve. $\bar{p}_{ref}$ was taken as the stress value of the point corresponding to the void ratio of 1 on the saturated isotropic compression curve. The slope of the unique compression 'λ_r' and parameter 'γ' which describes the overconsolidation degree were calibrated by best-fitting the mechanical model's closed-form equations to experimental data from MCD06 in which suction was constant as 200 kPa, and net stress was increased up to 400 kPa during constant suction isotropic compression. These parameters were respectively determined as 0.61 and 1.418. The parameter κ was not calibrated due to lack of unloading data. The best-fitted experimental data together with the model's result are given in Fig. 3.69b.

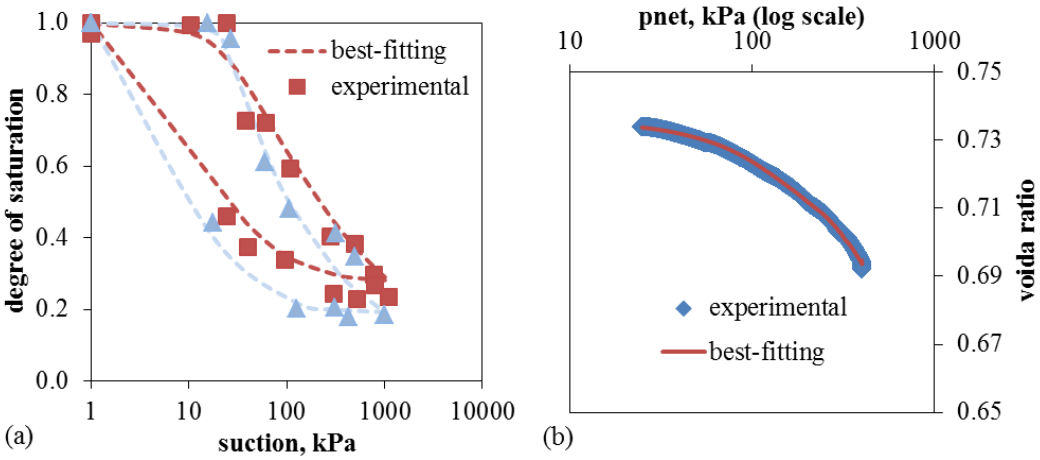

Figure 3.69 Calibration of Gallipoli model's parameters for Mersin silt.

In the simulations, net stress and suction path followed during tests are prescribed as input variables and the variation of void ratio and degree of saturation are predicted. Two constant suction tests, MCD03 (Mersin silt specimen at 0.72 initial void ratio was isotropically loaded at 100 kPa constant suction up to 400 kPa net stress) and MCD11 (Mersin silt specimen at 0.83 initial void ratio was isotropically loaded at 100 kPa constant suction up to 400 kPa net stress) are simulated in Fig 3.70a and 3.70b, respectively. Additionally, two constant water content tests,

MCW04 and MCW03 are simulated in Fig. 3.70c and 3.70d. In Fig. 3.70, bold lines denote degree of saturation.

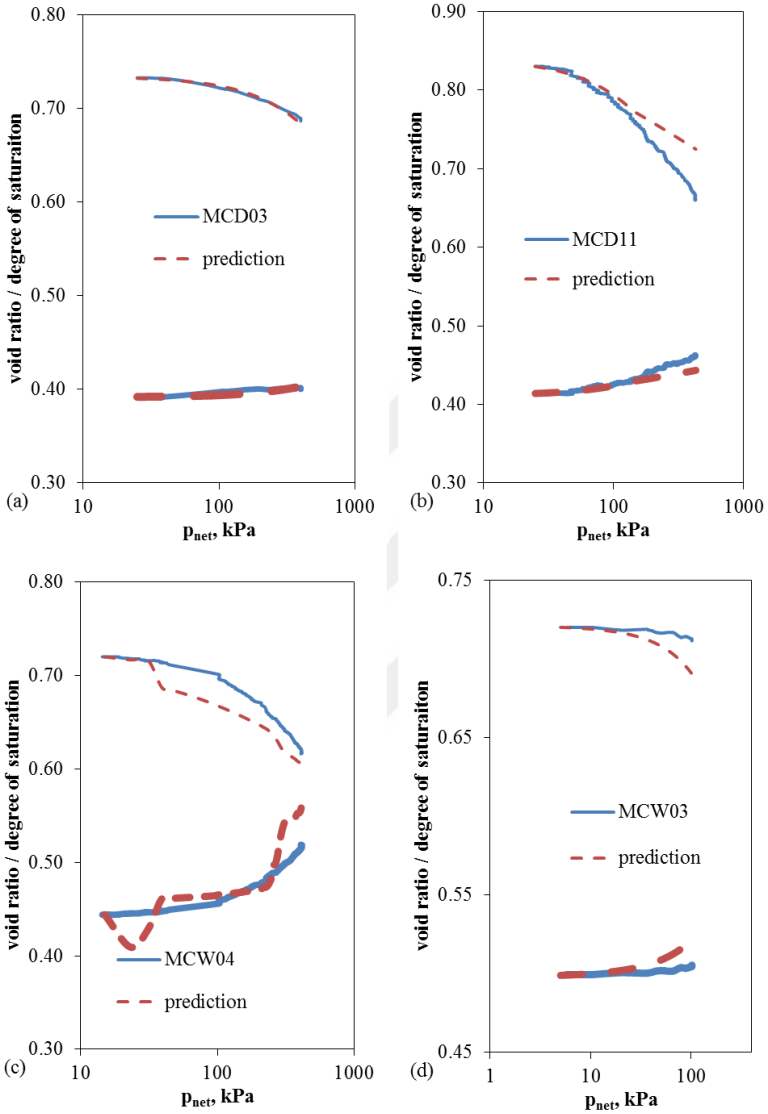

Figure 3.70 Simulation of Mersin silt test results implementing Gallipoli's model (bold lines denote degree of saturation).

The drying soil water retention curve measurements on Elazığ silt specimens was used to calibrate hydraulic model's drying parameters. The drying branch of the soil water retention curve was best-fitted in order to determine m_d, λ_{sd}, ω_d and β_d. The wetting parameters of the hydraulic model were calibrated using the degree of saturation versus void ratio data from 80 kPa constant suction isotropic

compression test 'ECD07'. The parameter λ_{sw} was taken as equal to λ_{sd}, then m_w, ω_w and β_w were best-fitted to experimental data. The calibration result is given in Fig. 3.70a and 3.70b. In Fig. 3.70b, the degree of saturation data is plotted on the secondary axis at the left side and pale colors are preferred to indicate.

The parameters of mechanical component were calibrated using drained triaxial test results from ECD07 in the same way as described for Mersin silt. λ_p parameter was obtained as 0.211 by taking the slope of the virgin part of the saturated isotropic compression curve. $\bar{p}_{ref}$ was taken as the stress value of the point corresponding to the void ratio of 1 on the saturated isotropic compression curve and it was determined as 15.3 kPa. The slope of the unique compression 'λ_r' and parameter 'γ' which describes the overconsolidation degree were calibrated by best-fitting the mechanical model's closed-form equations to experimental data from ECD07 in which suction was constant as 80 kPa, and net stress was increased up to 200 kPa during constant suction isotropic compression. These parameters were respectively determined as 0.983 and 0.736. In addition, the parameter κ was taken as the slope of unloading curve obtained in ECD09 as 0.009. The best-fitted experimental data together with the model's results are given in Fig. 3.71.

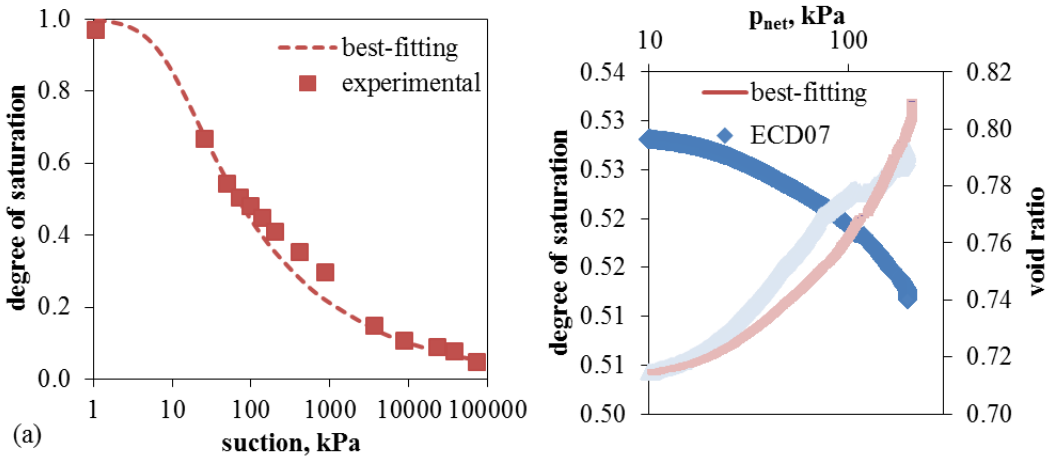

Figure 3.71 Simulation of Elazığ silt test results implementing Gallipoli's model (pale colored series on the graph at the right side denote degree of saturation and plotted on the left axis).

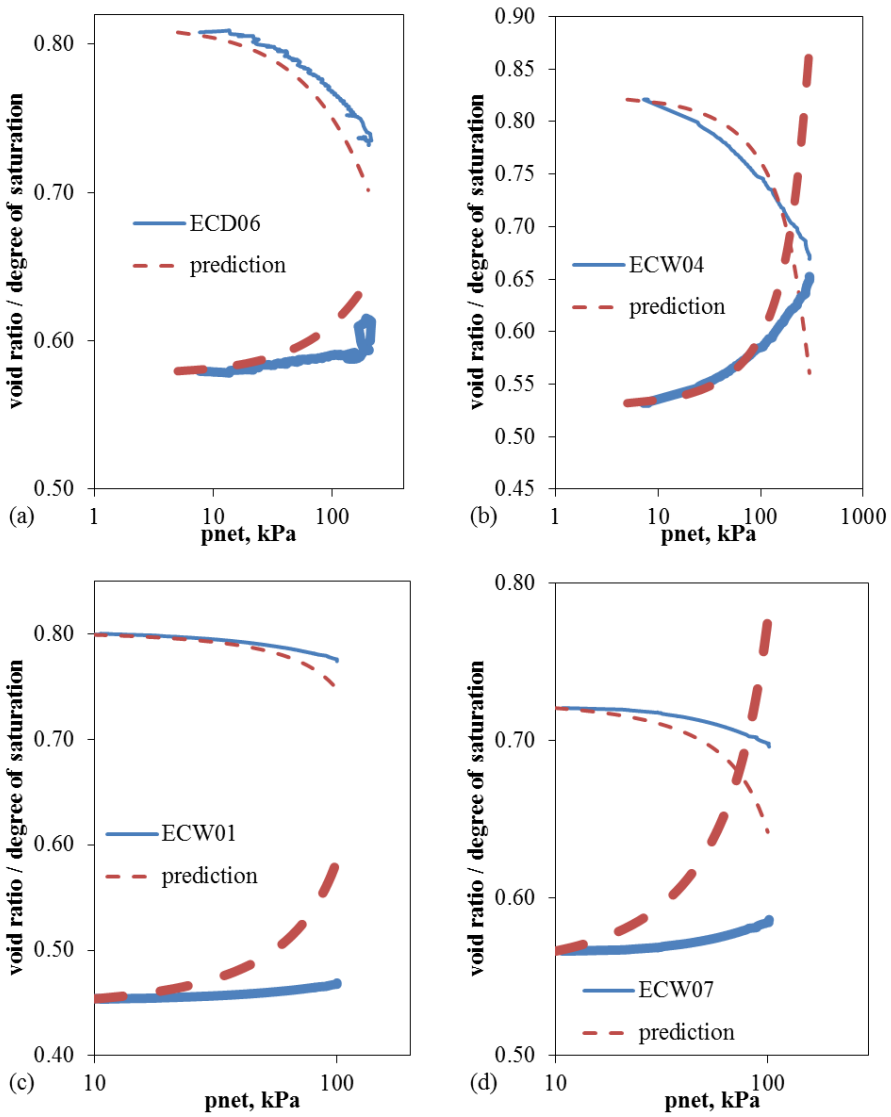

Figure 3.72 Simulation of Elazığ silt test results implementing Gallipoli's model (bold lines denote degree of saturation).

In the simulations, net stress and suction path followed during tests are prescribed as input variables and the variation of void ratio and degree of saturation are predicted. The constant suction test, ECD06 (Elazığ silt specimen at 0.845 initial void ratio was isotropically loaded at 40 kPa constant suction up to 200 kPa net stress) is simulated in Fig 3.72a. Additionally, the constant water content tests, ECW04 (Elazığ silt specimen at 0.845 initial void ratio and initial degree of saturation around 0.5 was isotropically loaded at constant water content), ECW01(Elazığ silt specimen at 0.845 initial void ratio and initial degree of

saturation around 0.3 was isotropically loaded at constant water content) and ECW07 (Elazığ silt specimen at 0.72 initial void ratio and initial degree of saturation around 0.5 was isotropically loaded at constant water content) are simulated in Fig. 3.72b, 3.72c and 3.72d, respectively. In Fig. 3.72, bold lines denote degree of saturation.

Table 3.8 Calibrated Gallipoli Model Parameters

Parameter	Mersin silt	Elazığ silt
m_d	0.123	0.171
λ_{sd}	0.403	0.322
ω_d	24.1	4.2
β_d	0.52	0.56
m_w	0.01	0.15
λ_{sw}	0.403	0.322
ω_w	1.8	0.01
β_w	1.18	0.05
λ_p	0.163	0.211
λ_r	0.61	0.983
γ	1.418	0.736
κ	-	0.009
$\overline{p}_{ref}$	2.4	15.3

CHAPTER 4

DEVELOPMENT OF SIMPLE PROCEDURES

The proposed simplified procedures to determine unsaturated soil properties are presented in this chapter.

4.1 Changing and equilibrating water content of triaxial test specimens without suction control (Kenanoğlu and Toker, 2018a)

All of the suction control methods described in section 2.2.1 have their advantages and disadvantages (Ng and Menzies, 2007). Independent of which method is used to control suction, suction equalization is essential in unsaturated soil testing (Ng and Zhou, 2005). Usually a long period of time is needed to achieve suction equilibrium in an unsaturated specimen. This can be several days to months, depending on the controlling method and soil type (Lloret et al., 2003). Such a long equalization time of suction in the specimen is one of the main difficulties in unsaturated soil testing, limiting the quantity of tests that can be performed in a single test setup.

Separating the suction equalization stage from the test and doing it in a separate setup (or multiple parallel setups if needed) could greatly reduce total time of a test program. This idea may appear to be more suitable for water content controlled tests (Thu et al., 2006), but is equally viable in preparation to suction controlled tests. Before deformation, bringing suction in a homogeneous specimen to a single constant value is almost identical to bringing its water content to a single constant value. In this study, the authors aim to adjust water content of specimens using simple procedures and equipment in a relatively short period of time, to be followed by suction (or water content) controlled test. Such an approach can be beneficial to increase test result output of unsaturated soil mechanics researchers,

and perhaps make their theories more accessible for geotechnical engi-neering practice since it provides a way to perform constant water content tests without employing suction control techniques for extended periods and occupying costly equipment.

4.1.1 Test Procedures and Results

Specimens were statically compacted in three layers inside a cylindrical hollow plastic mold by means of a hydraulic jack. A variaety of procedures are devised and tried in stages for wetting and drying of triaxial test specimens (10 cm in height and 5 cm in diameter). The attempts at increasing water content of specimens are based on the capillary absorption phenomenon. In case of decreasing water content, specimens were dried by exposing them to open air. Resulting distribution of water content within specimens is not homogeneous after such procedures. Therefore, for both cases, process of equilibrating water content in the specimen as a subsequent stage is required to diminish the differences in the water content distribution within the specimen. Any specimen would come to equilibrium after a sufficiently long period of equilibration process. The main concern in these trials is the time that is required for achieving homogeneous distribution of water content within specimen after proposed operations. Specimens were separated into pieces and water content of each piece was determined in order to evaluate the distribution of water content values within the specimen. First, specimens were divided into four or more disc-shaped slices by using a spatula to determine the distribution of water content along the vertical direction. Then each disc was divided into eight portions as shown in Fig. 4.1. Into each soil disc, two thin metal rings (diameters are approximately 10 mm and 35 mm) are inserted to prevent mixture of different parts in radial direction. Then each soil ring is separated into pieces in the hoop direction by using a 5 mm spatula. Water content measurements are recorded to nearest 0.1%. The difference of water contents between each piece and mean value being less than 0.1% was considered as acceptable error margin in this study.

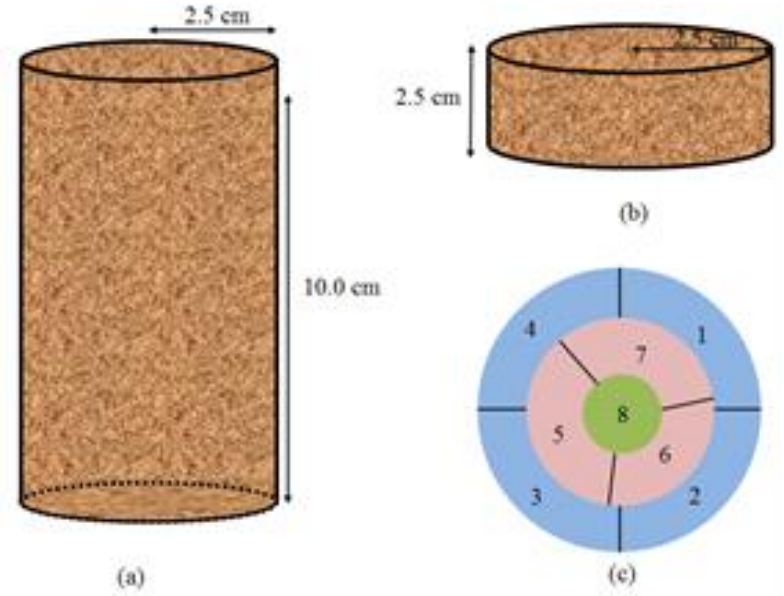

Figure 4.1 Dimensions of triaxial specimens (a), dimensions of disc-shaped slices after dividing specimen (b), plan view of the pattern which is followed during partition of one of disc-shaped slice, colors denote distance of radial groups from center (c) and match graph colors in Fig. 4.2 through 4.9.

4.1.1.1 Wetting by Capillary Soaking

Three different procedures were tried for increasing water content of specimens. First attempt is placing triaxial test specimen into a basin filled with water. In this case, specimen is not extruded from its mold after compaction. The bottom of the mold is covered with filter paper to prevent loss of material in water. The basin is filled with water up to a level slightly less than the mold's height. Specimen takes water in only through the bottom of the mold; creating a wetting front that rises inside the specimen. After a certain time, depending on the soil type and difference between initial and desired values of water content, the mold is removed from the basin and sealed in a nylon bag for water content equilibration. At the end of this procedure, water content values within the specimen vary along the specimen's height, (higher at the bottom and less at the top). During water content equilibration, water moves to dryer parts of the specimen due to difference in capillary potential.

Gravimetric water content of Ankara clay sample in air-dry condition was %7. The initial dry densities for all prepared specimens were in the range of 1.46 to 1.52 g/cm^3. The swelling of specimen caused by increase in water content was permitted. Specimen was kept in this condition until wetting front reached the specimen's mid-height. It was found by trial and error, that the duration of two hours is adequate for this soil. To determine water content variation at the end of wetting, one of the specimens was extruded from its mold and divided into ten disc-shaped slices immediately. Other specimens were sealed in nylon bags for water content equilibration for various times. Specimens were not turned over during water content equilibration; thus, mass transfer was only caused by capillary absorption against the direction of gravity.

This procedure did not yield useful results because too much time was required for water content equilibration stage (see Fig. 4.2-a). The error margin of water content values within specimen became acceptable (<1%) after 55 days in water content equilibration.

An attempt to accelerate the upward flow during water content equilibrium was by application of a thermal gradient in the direction in the first 3-21 hours of the water content equilibration stage. By placing the sealed specimen on a warm plate, an almost constant gradient of approximately 1.8°C/cm was generated (calculated value based on continuous temperature measurements at three points along the height). However, this modification did not improve the procedure sufficiently (Fig. 4.2-b), as it created too much flow, and added a second location with large gradient of water content to the system.

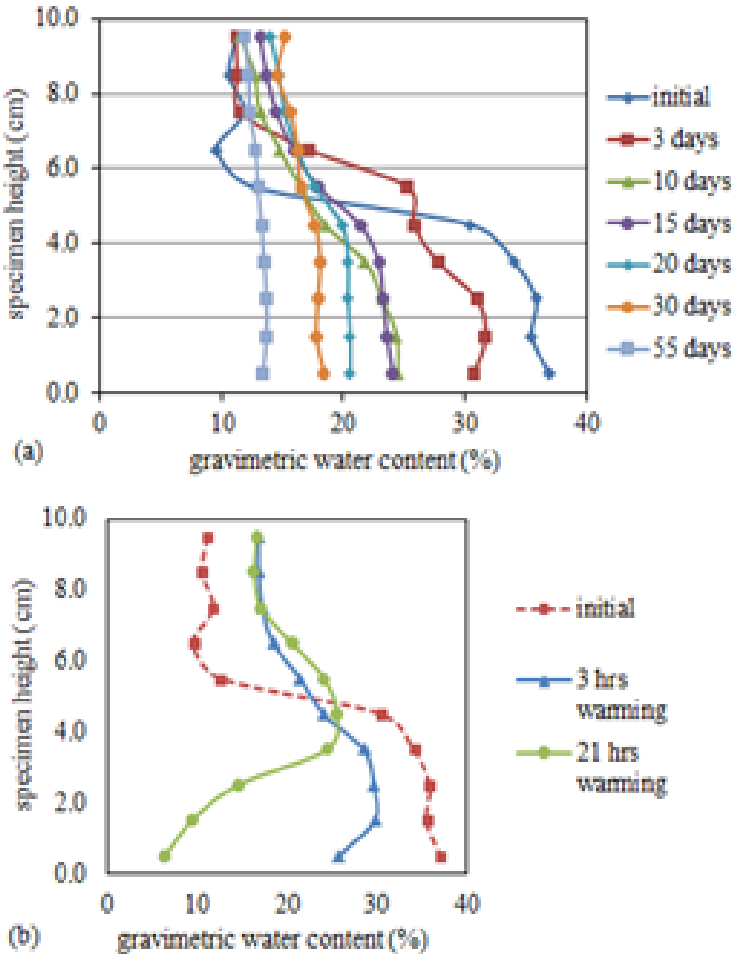

Figure 4.2 The distribution of water content within the Ankara clay specimens for different equilibration durations (a), results for equilibration with thermal gradient (b)

As a result, the time required to obtain a homogeneous distribution of water content is impractical. Thus, this method is not tried with another soil type.

4.1.1.2 Wetting by Lateral Spraying

The second procedure involves reducing the distance covered by the water during water content equilibration stage. To do this, specimen was wetted throughout the specimen's lateral surface by means of a a sprayer, by the following procedure:

- The required amount of water to achieve desired water content is calculated by using (4-1),

$$\Delta m_w = m_{T_0} / (1 + w_0) \times (w_f - w_0) \qquad (4\text{-}1)$$

where, Δm_w is the required mass of water that should be added to the specimen to achieve the desired water content, m_{T0} is the initial total mass of the specimen, w_0 is the initial water content of the specimen and w_f is the desired water content after spraying.

- The specimen is placed on a plate. The plate helps avoiding unfavorable stress concentration and pre-vent damage to the specimen when carrying or changing position. Another plate is also placed upon the top of the specimen in order to moisten the specimen through only its lateral surface; otherwise, the upper part of the specimen would be excessively moistened and water content would differ in the axi-al direction. In this study, transparent plexiglass discs are used for this purpose (Fig. 4.3).

- Before starting spraying, initial weight of specimen and plates are recorded.

- The sprayer nozzle is aligned horizontally at the mid-level of the specimen. The flow coming out of sprayer should be in the form of mist; stream flow erodes specimen surface. Also, sprayer nozzle should be at a distance of about 0.50 m away from the specimen, to create a uniform mist.

- Specimen should be moisturized uniformly from all horizontal directions. The transparent top cap may allow the operator to observe moistened parts of the specimen, if wetting front is visible.

- Droplets of water accumulate on the base plate and create a water pond around the base of the specimen. This water should be regularly removed by means of a paper towel to prevent loss of material from specimen and localized excessive wetting.

- Total weight of the specimen and plates is frequently measured to check whether the required amount of water has been added or not. Note that water on the surface of the plates should be dried with paper towel before measuring the weight.

- When the specimen reaches the desired water content, it is sealed in a nylon bag. It is more reliable to use multiple nylon bags. Then, the sealed specimen is left for water content equilibration.

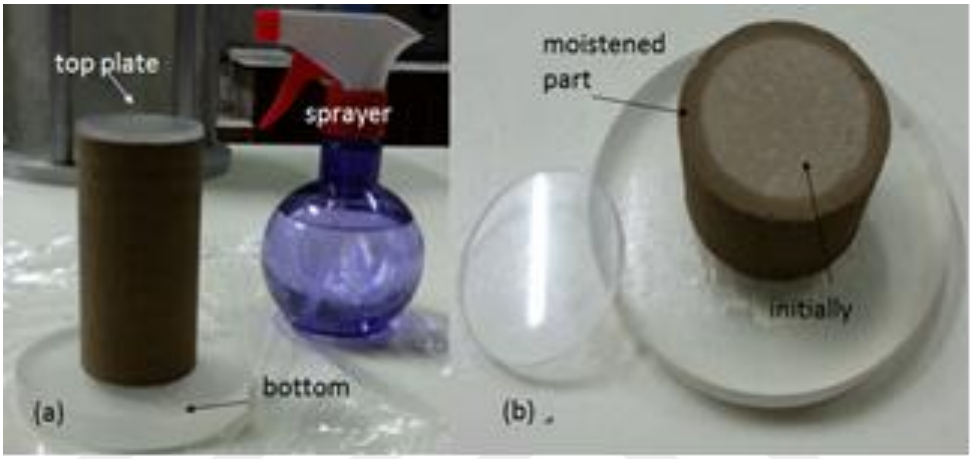

Figure 4.3 Equipment (a), the top view of specimen immediately after spraying (b)

Mersin silt was used and dry densities of specimens prepared by compaction were in the range of 1.50 to 1.58 g/cm^3. The water content was increased from an initial value of 5% during compaction to about 13% at the end of water content equilibration (Fig. 4.4). The maximum error for the water content became 0.9% (Fig. 4.4-a) and 0.8% (Fig. 4.4-b) after 1 day and 2 days water content equilibration, respectively.

When Ankara Clay specimens are sprayed, their expansive nature resulted in deformation and cracks propagating radially with the moisture.

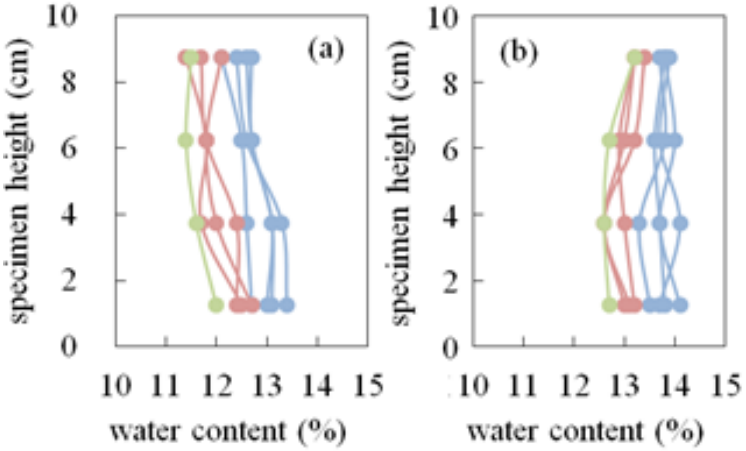

Figure 4.4 Water content distribution of Mersin silt specimen, that was moistened with a sprayer, followed by 1 day of equilibration in nylon bag (a), or by 2 days for equilibration (b)

4.1.1.3 Wetting by Radial Soaking

This procedure is developed to counter swelling of Ankara clay that was observed in lateral spraying. The specimen was wetted throughout the specimen's lateral surface by means of a perforated mold (holes that are approximately 2 mm in diameter were drilled at four different elevations in vertical direction, with 60° intervals around perimeter) made of relatively rigid (1 cm thick) poly-vinyl chloride (PVC). Thus, distribution of water content values differs in radial direction, not in vertical direction. In this method, the bottom surface of the mold is closed by means of a lid to permit water entry to the specimen only through its lateral surface. A filter paper was placed throughout the mold's inner lateral surface to provide uniform water flow to the specimen and to prevent intrusion of swelling soil in holes of the mold. The filter paper also helps specimen extrusion. It is important to note that the water level in the basin should be close to the specimen's height during wetting; otherwise, distribution of water content also differs in vertical direction, prolonging water content equilibrium stage duration. The volume change in the vertical direction can be prevented by covering top surface of the specimen with a rigid plate that lightly touches the specimen. Then, this plate is

loaded more than the expected swelling pressure load, and this load is transferred to a support frame to avoid excessive load application upon specimen or mold (Fig. 4.5). Separate Ankara clay specimens were submerged for 30 and 50 minutes and Mersin silt specimen was submerged for 3 minutes.

The results show that wetting the specimen through its lateral surface reduces the required water content equilibration stage duration remarkably. Overall water content of the specimen that remained in basin for 30 minutes increased from 7% (water content of air-dry soil) to 17%. The maximum variation of water content from the mean value within the specimen was 11.9% initially (Fig. 4.6-a) and decreased to 1.9% after 2 days (Fig. 6-b). The variation was still 2.5% (Fig. 4.6-c) after 5 days of water content equilibration. Another specimen was soaked for 50 minutes and its water content increased to 19%. The maximum variation of water content from the mean value became 3.4% after 3 days of equilibration (Fig. 4.7-b), down from the initial variation of 10.4% at the end of soaking (Fig. 4.7-a). The water content of Mersin silt specimen increased to 16.4% from 1% and the maximum variation from the mean water content was 0.5% after 5 days of equilibration (Fig. 4.6-c).

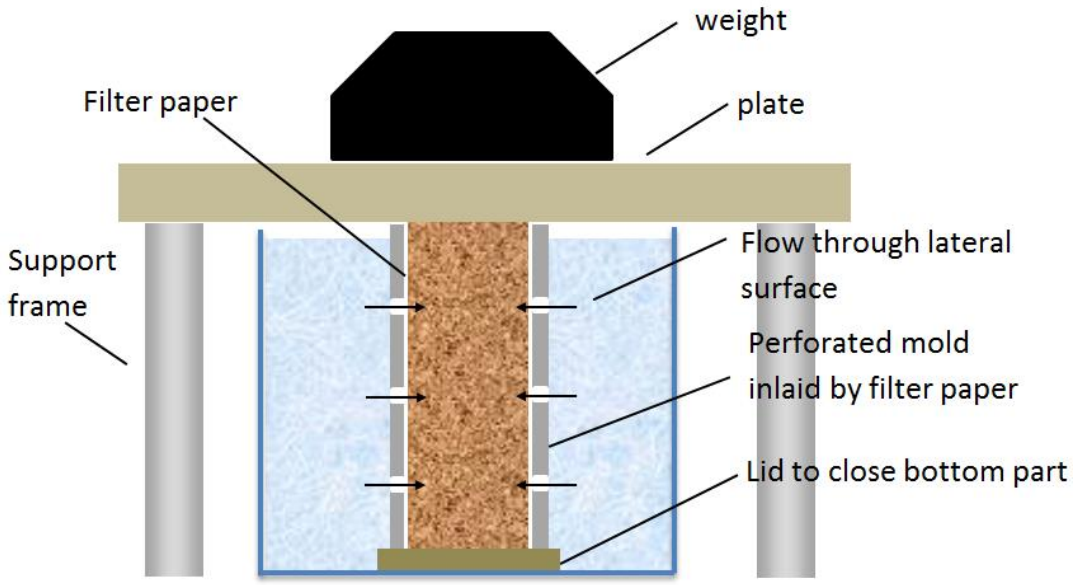

Figure 4.5 Sketch of radial soaking method

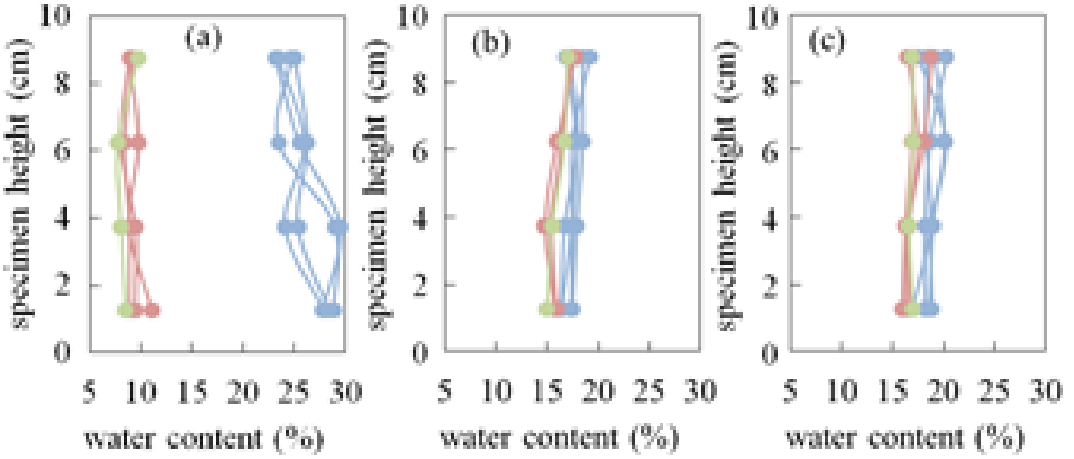

Figure 4.6 Water content distribution of Ankara clay specimen that remained in basin for 30 min. (a), followed by 2 days of sealed equilibration (b), 5 days of sealed equilibration (c)

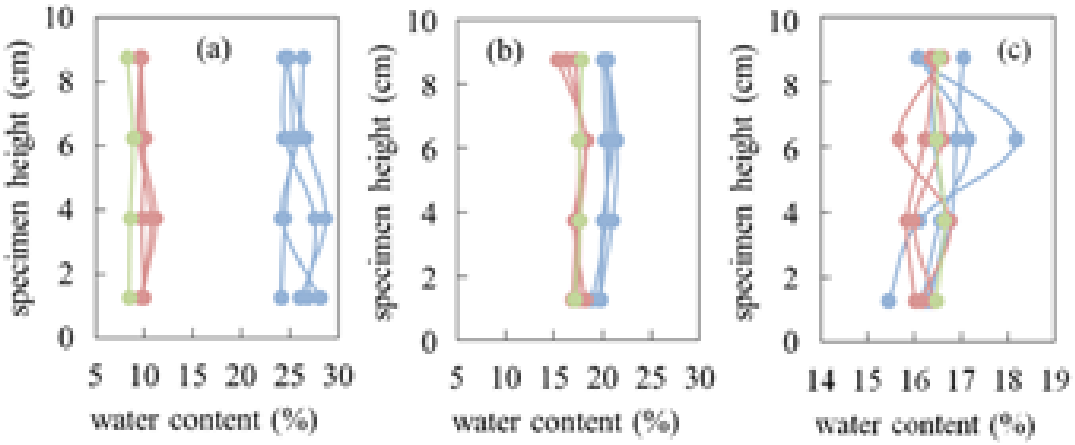

Figure 4.7 Water content distribution of Ankara clay specimen that remained in basin for 50 minutes (a), followed by 3 days of water content equilibration sealed in nylon bag (b), (c) Water content distribution of Mersin silt specimen that remained in basin for 3 minutes followed by 4 days of equilibration

The maximum variation values for water content within Ankara clay specimens are higher than the acceptable error of 1% and it did not significantly decrease even if the water content equilibration duration was extended, water contents of inner parts are consistently less than outer parts. For this method, outer parts that are wetted by soaking experience drying whereas inner parts experience wetting during equilibration. The hysteretic nature of soil water characteristic curve results in larger water content in case of drying (of outer parts) compared to the wetting of

inner parts, at the equilibrium suction. This effect can be minimized by keeping the specimen in water for a short period (e.g. in seconds) then waiting for equilibration (e.g. in hours) to prevent excessive saturation of outer parts.

4.1.1.4 Drying by Evaporation

Water content of the specimen decreases due to evaporation when it remains in open air. Water content inside the specimen is higher than that of the outer parts just after drying. Therefore, the specimen is sealed in nylon bags for water content equilibration.

It was noticed that the rate of evaporation is higher at the upper parts of specimen although the top surface of specimen is covered with plexiglass cap. The elevation head difference can not cause this variation; otherwise, it would have appeared in the previous Figures 4.4, Fig. 4.6 and Fig. 4.7 as well. At first, the reason of this variation was considered to be evaporation through the little gap between specimen's top surface and the top plate. When the specimen was placed on a perforated, elevated platform to expose bottom surface of specimen directly to atmosphere; however, the same variation was again observed. The authors speculate that this variation emerge due to endothermic nature of evaporation, which cools the moist air around the specimen. This cool moist air travels down due to convection resulting in higher relative humidity at the bottom part, decreasing the rate of evaporation at that location. To overcome this problem, a step of turning the specimen upside down for half of the drying duration was incorporated into the procedure.

Ankara clay sample was mixed with water and compacted in the mold to prepare specimens at high water content (28.2%). The dry densities of these specimens were in the range of 1.51 to 1.52 gr/cm^3. The specimen was placed in open air for two days and another two days in nylon bags for water content equilibration (Fig. 4.8). All but one of the specimens were turned over after the first day of drying to

avoid water content difference along vertical direction. There is significant variation of water content along vertical direction (Fig. 4.8-a) unless specimen is overturned (Fig. 4.8-b). Overall water content of specimen decreased to 14%. The maximum variation for not-turned-over specimen and turned-over specimens were 5.4% and 2.4%, respectively. This variation decreased to 1.5% after water content equilibration (Fig. 4.8-c).

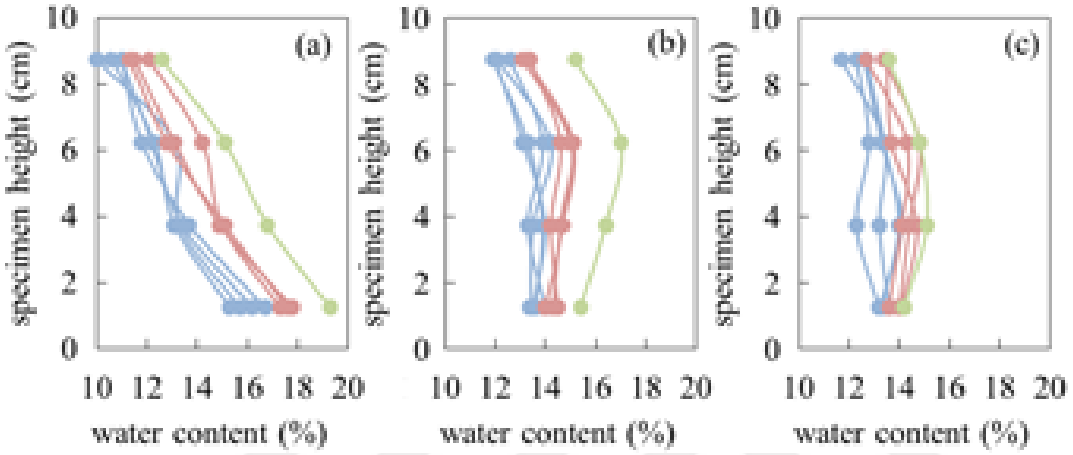

Figure 4.8 Water contents within Ankara clay specimen, that remained in open-air for 2 days without turning over (a), that remained in open-air for 2 days with turning over (b), followed by 2 days for equilibration for turned over specimen (c)

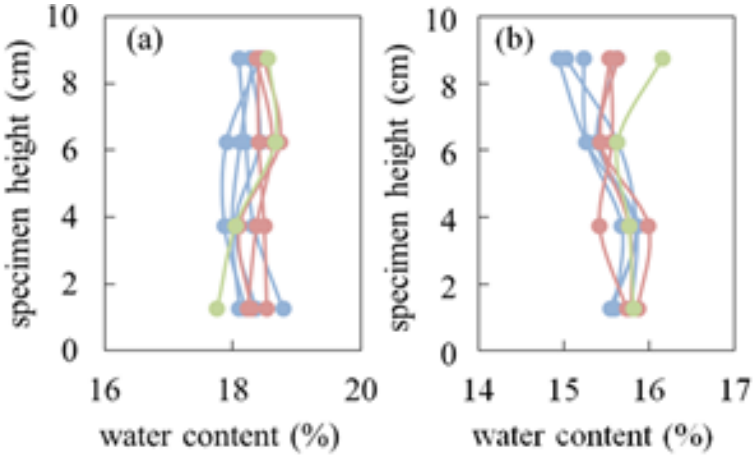

Figure 4.9 Water contents within Mersin silt specimen, that remained in open-air for 8 hours with turning over (a), that remained in open-air for 14 hours days with turning over (b)

Mersin silt specimens were prepared at initial water content of 22.3% and initial dry density of 1.50 g/cm^3. They are placed in open air for eight hours and fourteen hours and overturned at the half-time of drying. Overall water content of specimens were decreased to 18.3% and 15.6%, respectively after one day water content equilibration stage and maximum variation of water content became 0.3% in both cases (Fig 4.9).

4.2 Separation of Macrostructural and Microstructural Components of Soil Water based on Simple Evaporation Test to Evaluate Shear Strength of Unsaturated Soils

The influence of soil structure, defined as the combined effects of fabric, compositon and interparticle bonding (Mitchell, 1993), on the hydromechanical behaviour of soils becomes the prominent issue for researchers in the light of a remarkable number of experimental investigations (Sridharan et al., 1971; Delage and Lefebvre, 1984; Romero et al., 1999; Cuisinier and Laloui, 2004; Delage et al., 2006; Koliji et al., 2010). Various particle associations in soils are characterized by two different classes corresponding to micro (intra-aggregate) and macro (inter-aggregate) pores. The soil water that is held in macropores due to capillarity phenomenon is sensible to mechanical actions; whereas, micropores contain quasi-immobile water fraction resulting from the adsorptive processes that is unaffected by mechanical action (Romero et al., 1999). As it is discussed in literature (Burton et al., 2015; Yuan et al., 2020), distinguishing micropores and macropores is not straightforward and different selection criteria result in different answers. More importantly, Yuan et al. (2020) have stated that the separation of micro and macro pores should be considered from behavioral features related to the water adsorption or volume change rather than solely in terms of pore sizes. As an example for this, Alonso et al. (2013) have plotted contours of equal saturated permeability of a silty clay compacted at various preparation water content on the compaction plane and a strong variation of permeability emerges when compaction water content increases.

Alonso et al. (2013) have stated that permeability is better indicator for microstructural effects than the mechanical tests since it is mainly controlled by the pore structure.

Evaporative drying of porous media is studied by various research fields including agriculture, soil science, hydrology and chemical engineering. Huge amount of literature describing evaporation is available in these disciplines. However; theoretical and experimental findings in previous works currently stand outside of the area of geotechnics.

The variation of drying rate during evaporation of soil water follows two distinct stages: i) constant rate period, ii) falling rate period. The rate of evaporation is governed by ambient conditions during constant rate period. The air-water interface at the surface starts to recede when capillary pressure of water exceeds the air entry pressure. However; continuous liquid network can be still present under funicular state. Surface evaporative demand can be supplied by the capillary flow network between receding air-water interface and the external surface (van Brakel, 1980; Shokri et al., 2010; Or et al. 2013). Further increase of capillary pressure results in the interruption of capillary flow network; last water film at the top moves beneath surface and this results in the end of constant rate period (Kumar and Arakeri, 2018). Therefore, constant rate period is constrained by two capillary pressures characteristic to drying specimen such that air entry pressure and the capillary pressure that coincides with the interruption of liquid phase continuity (Or et al. 2013). In the falling rate period, the interruption of hydraulic connections result in the immobile water regime presence at pendular and adsorptive state (Scherer, 1990; Moyne et al. 1991, Knight et al., 1996). Drying rate starts to decrease since water mass transport is controlled by vapor diffusion to the external surface. The rate of drying depends on the soil moisture conditions and soil hydraulic properties during falling rate period (Brutsaert, 1982; Lockington, 1994; Shokri and Or, 2011, Thiery et al., 2017). The point at which transition from the constant rate period to the falling rate period is defined as the critical moisture content in drying literature (Sherwood, 1929).

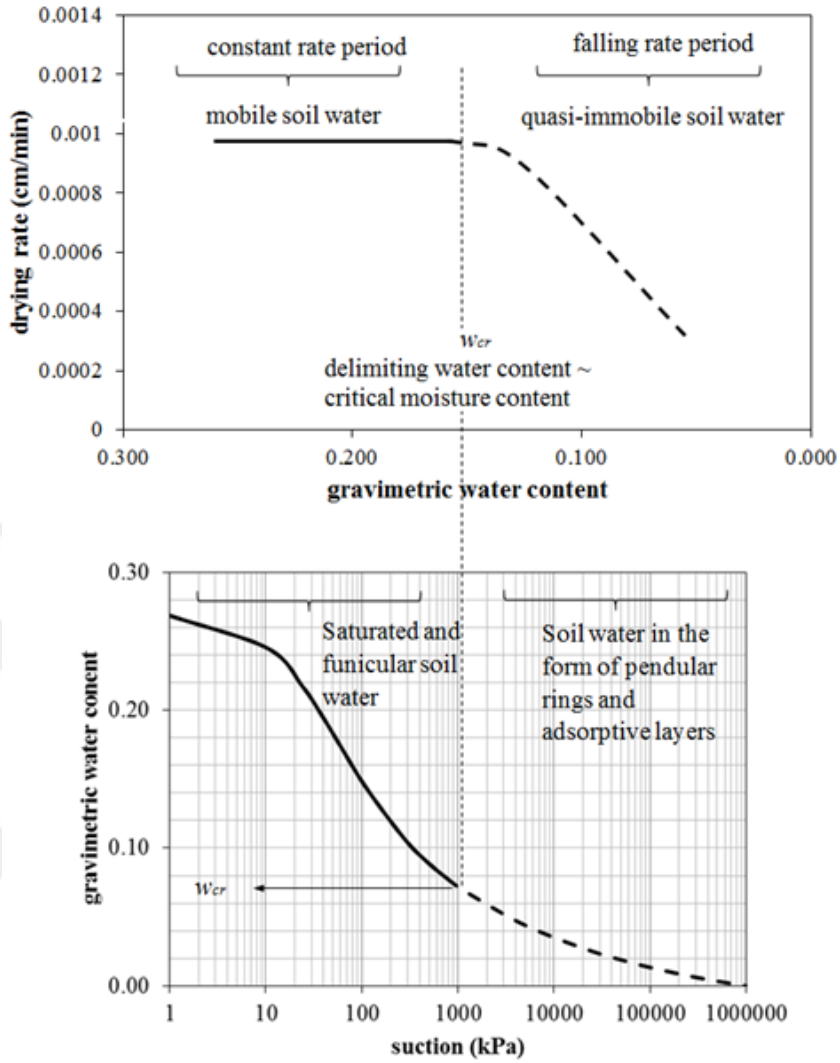

Figure 4.10 Schematic illustration of interconnection between drying rate curve and soil water retention curve providing separation of macro and micro pores

Aformentioned studies on evaporation phenomenon in soils reveal that initially bulk and funicular soil water contained in macropores leave the soil during the constant rate period and, in the following, soil water held in the micropores in the form of pendular rings and adsorptive layers diminish during falling rate period. In another study, Ma et al. (2020) investigated the evolution of microstructure during drying and wetting of an expansive clay. They have showed that macropores dominate the behavior in the low suction range whereas micropores dominate the high suction range. The suction boundary between these two domains is close to

the suction value separating the adsorption and capillary regimes on the retention curve. In this regard, drying rate curve of evaporated soil specimen becomes a suitable indicator to reveal the microstructural effects. The term critical moisture content provided by soil sciencists serves actually as a boundary between macroscopic and microscopic soil water (Fig. 4.10).

This study aims to provide a simple test process in which soil microstructure effect is intrinsically prominent in the experiment rather than investigation of true microstructural behaviour of evaporated soil specimen. Therefore, the experimental parameter determined through the evaporation test is investigated as an indicator for the microstructural effect to further evalution of the macroscopic soil behaviour. In the consequent part, this parameter is introduced into shear strength model proposed by Alonso et al. (2010) for the purpose of this study.

Bishop's (1959) extended the expression of Terzaghi's effective stress for unsaturated soils by introducing an effective stress parameter χ. χ is constrained between 0 when soil is completely dry and 1 when soil is saturated. Different forms for χ have been proposed in the literature (Karube et al., 1996; Vanapalli et al., 1996; Khalili and Khabbaz, 1998). For simplicity, effective stress parameter is generally equated with degree of saturation. This assumption seems to be valid for granular soils. But, Bishop's effective stress is not capable of capturing adsorption mechanism and its application on the shear strength prediction becomes problematic for fine soils (Alonso et al., 2010; Lu, 2020). Alonso et al. (2010) provided a novel expression for effective degree of saturation by separating degree of saturation into macrostructural and microstructural components. They showed that such an interpretation of effective degree of saturation is capable to predict shear strength of unsaturated soils. However; identification of microscopic component is not straightforward and additional information on the soil-water retention or pore size distribution is necessary to determine the transition from macropores to micropores. Their interpretation for effective degree of saturation (

S_r^e) depends on the fraction of water that is more strongly attached to the solid skeleton, as:

$$S_r^e = \left\langle \frac{S_r - S_r^m}{1 - S_r^m} \right\rangle \tag{4-2}$$

where S_r^m is defined as microstructural degree of saturation that coincides with the fraction of immobile soil water. The shear strength of the unsaturated soil is defined in terms of Bishop effective stress together with the classical Mohr-Coulomb equation:

$$\tau = c' + \sigma_{net} \tan\phi + S_r^e s \tan\phi \tag{4-3}$$

where σ_{net} is the net stress (difference of total stress and air pressure) and s is the suction (difference of air pressure and water pressure).

Alonso et al. (2013) transformed the microstructural degree of saturation parameter in (4-2) by introducing a new parameter termed as microstructural state variable (ξ_m) as the ratio of microstructural void ratio (e_m) to total void ratio (e):

$$S_r^m = \xi_m = \frac{e_m}{e} \tag{4-4}$$

where microstructural void ratio e_m is defined as the ratio of volume of micro voids to volume of solids. In this study, the microstructural parameter depending on the critical moisture content is defined from the soil index properties assuming critical moisture content (w_{cr}) corresponds to the soil water occupying the micro pores:

$$\xi_m = \frac{w_{cr}}{w_{sat}} \tag{4-5}$$

4.2.1 Experimental Procedure for Evaporation Test

Two silts (Mersin silt and Elazığ silt) and a highly plastic clay (Ankara clay) were chosen in this study. Specimens were prepared in the same way as the corresponding triaxial test specimens aiming to obtain same characteristics. Thin specimen discs (i.e. 1 to 2 cm in height and 3.6 and 5 cm in diameter) is used in the evaporation test (Knight et al. 1996, Derdour et al. 2000, Belhamri 2003). Mersin silt sample was compacted at initial water content of 10.2% in a single layer to initial void ratio of 0.72 inside a plastic tube. Same procedure is used to obtain Elazığ silt specimens at initial water content of 22.1% and initial void ratio of 0.845. Specimen was saturated based on capillary soaking (Fig. 4.11a). The plastic tube is placed on a small basin. The basin is filled with deaired water up to a level slightly less than the specimen's height. The top of the plastic tube is covered to minimize the evaporation from the specimen. After one day of saturation, water is poured out of the basin and a paper towel is used to remove water droplets that remain on the solid surfaces (Fig. 4.11b, c). Thus, evaporative water only exist as soil water and slight ponding water layer on the surface of the specimen. Ankara clay specimens were prepared by consolidating slurry sample under 50 kPa vertical stress in conventional oedometer cell. At the end of consolidation, saturated Ankara clay specimen is removed from the oedometer and directly used for the testing.

Saturated specimen is placed on the mass balance to monitor decrease of specimen mass due to evaporation under ambient conditions. Lateral surface of the specimen is covered and only the top surface is exposed to open-air during drying. For soils that are not susceptible to drying induced shrinkage (e.g. Mersin silt and Elazığ silt), specimen could be kept inside its mold/extruder and both are placed on the mass balance. For soils that show volume change due to suction variation (e.g. Ankara clay), specimen could be surrounded by latex membrane that maintains contact on the specimen's lateral surface during shrinkage (Fig. 4.11e). If the mass balance is not capable of computer connection, a webcam could be placed on the desk to capture the display unit of mass balance via any free software for

automatically taking screenshoots to monitor specimen's mass variation with time. The data of specimen's mass variation is then processed to obtain time-series drying rate data. The rate of drying in the evaporation test is calculated as follows and plotted as a function of moisture content.

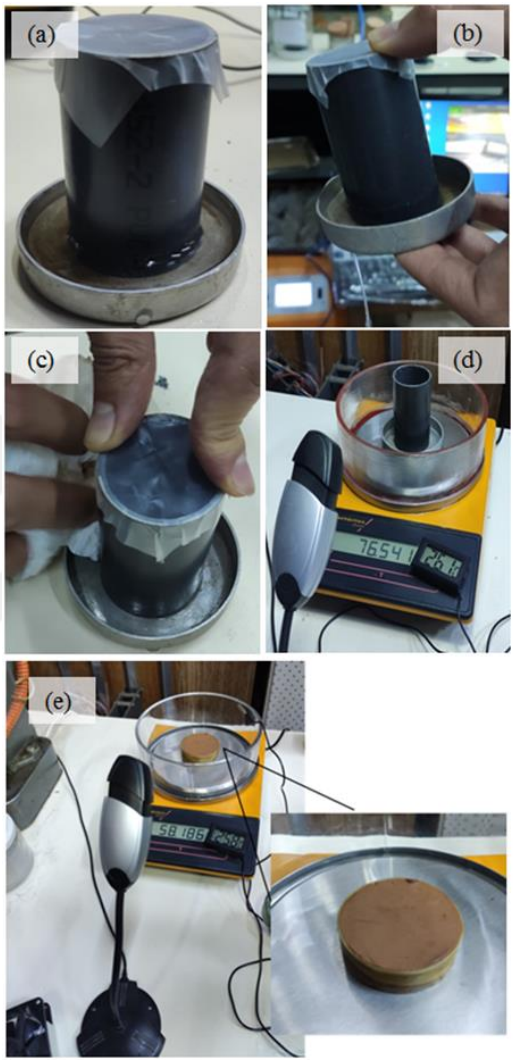

Figure 4.11 Specimen saturation for evaporation test (a), excess water is removed prior to testing (b and c), specimen is placed on balance and a camera monitors the mass variation (d), latex membrane surrounds the Ankara clay specimen (e)

$$q = \frac{dm}{dt}\frac{1}{A(w_c)n(w_c)} \tag{4-6}$$

where, q is the surface flux, dm is the difference between successive mass readings, dt is the time interval during recording, $A(w_c)$ is the surface area of specimen as a function of gravimetric moisture content, $n(w_c)$ is the porosity as a function of gravimetric moisture content. For soils that are not showing shrinkage, latter two variables are constant. For soils that are prone to suction induced volume change, additional measurements are necessary to accurately calculate surface flux. Either, the diameter and height of the specimen are measured by means of calipers at each data point while drying, or volumes of separate identically prepared specimens can be determined at different points along the drying process to determine shrinkage curve that gives the volume change characteristics as a function of gravimetric moisture content. Latter method might be useful to avoid possible noise on the time-series mass data caused by handling operations. In this study, the equation (3-3) proposed by Fredlund et al. (2002) was preferred to obtain shrinkage curve of Ankara clay from separate specimens. The variation of diameter of the drying specimen with respect to gravimetric moisture content change is assumed linear such that initial and final diameter measurements are related with corresponding gravimetric moisture contents as a linear function. However, the correct calculation of surface flux will not be important for the estimation of critical moisture content; since, as explained in the following part, this parameter will be determined from the gravimetric moisture content versus time plot.

4.2.2 Results of Evaporation Tests

Experimental drying rate curves of Mersin silt, Elazığ silt and Ankara clay specimens are determined from evaporation tests. The initial portion of drying rate curve has a sharp decrease from relatively higher values into the constant rate period in most of the experiments. This is the result of water ponding on the surface which is apart from the soil water; therefore, the value of the gravimetric moisture content just at the beginning does not coincide with the true initial gravimetric moisture content of the specimen. The initial value is taken as the data

point at the end of initial falling portion and it is considered as the saturated gravimetric moisture content of the specimen. In the subsequent part, the drying rate remains almost constant, albeit with some data noise and mild fluctuations. For the Ankara clay specimens, the constant rate period for the corrected drying rate curve ascends monotically until the falling rate period. The Mersin silt specimen prepared at 0.72 initial void ratio and 5 cm height (Fig. 4.13e) and Elazığ silt specimen at 0.845 initial void ratio and 2 cm height (Fig. 4.14b) show clear transition between constant rate and falling rate periods. This transition is often slow and smooth, necessitating a systematic method for precise and repeatable determination of the critical moisture content. There are several methods proposed in the literature for the determination of critical moisture content (Derdour et al., 1998). It should be noted that identification method influences the numerical value of critical moisture content and therefore the microstructural parameter.

In this study, the method proposed by Knight et al. (1996) is preferred to determine the critical moisture content. Measurements and calculations are carried out in terms of gravimetric moisture content; thus, it becomes unnecessary to evaluate the volume change of the specimen during drying. A line is fitted to the constant rate period of the experimental gravimetric moisture content versus time data (Fig. 4.12). The evaporation tests on Mersin silt and Elazığ silt specimens usually have noise and periods of mild ascent/descent of drying rate. Therefore, the selection of the entire data series within the constant rate period for line fitting might not ensure a suitable geometric interpretation. A linear segment prior to the bend on the gravimetric water content versus time plot is selected, excluding previous ascents or descents within the constant rate period to fit a line to the variation of gravimetric moisture content over time. The gravimetric moisture content corresponding to 0.01 relative deviation of the experimental data from the linear relationship is taken as critical moisture content. In other words, data points that deviate from the defined linear relationship by less than 0.01 relative error are considered to fall within the constant rate period:

- $(w_i(t) - w(t))/w(t) < 0.01 \rightarrow$ constant rate period

- $((w_i(t) - w(t))/w(t) = 0.01 \rightarrow$ critical moisture content
- $(w_i(t) - w(t))/w(t) > 0.01 \rightarrow$ falling rate period

where $w_i(t)$ is gravimetric moisture content calculated from fitted linear relationship as a function of time, $w(t)$ is the experimental data.

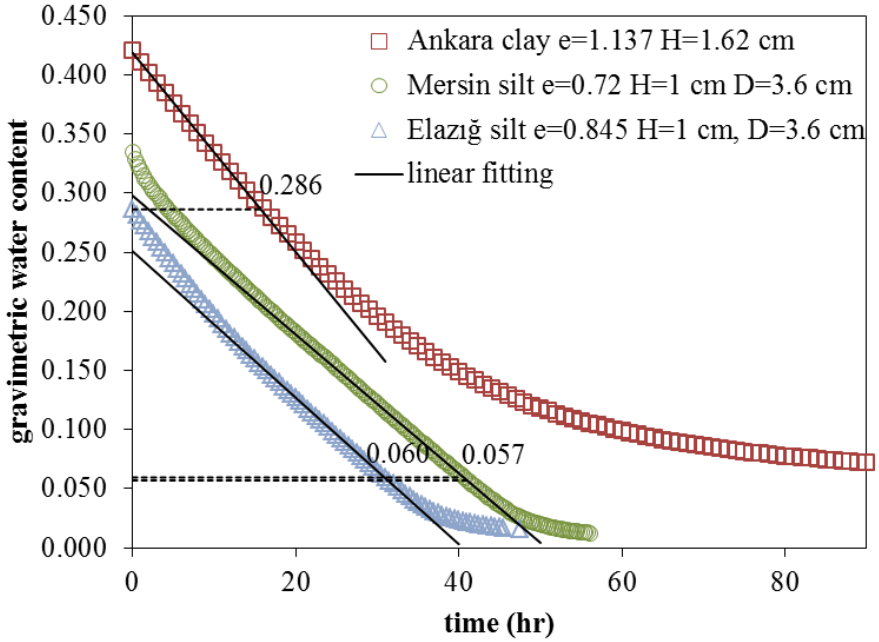

Figure 4.12 Gravimetric moisture content versus time plots for specimens of different types of soils and fitted lines to determine critical moisture content

The effect of specimen height is investigated by carrying out several tests on specimens with the same initial void ratio but different heights. Critical moisture contents for Mersin silt specimens at initial void of 0.72 with varying height of 1 cm to 5 cm are around 0.055 with the exception of 0.075 which is the result for the test on specimen at 3 cm height (Fig. 4.13a,b,c,d,e). The drying rate curve for Mersin silt specimen at 3 cm height did not provide suitable data for the geometric interpretation of critical moisture content since ascending/descending progress of drying rate is predominant. For the specimen tested at 5 cm height transition point is quite distinct and critical moisture content determined as 0.055 (Fig. 4.13e). Therefore, the height of the drying specimen seems to have marginal effect on the critical moisture content for the test range. In the soil science literature, novel term

of characteristic length has been substituted for critical moisture content in order to delineate the extent of hydraulically connected region between receding drying front and external evaporating surface (Lehmann et al. 2008). Drying front within the specimen is connected with the external evaporative surface due to the existence of capilary flow network while depth of the drying front is less than the characterictic length. Pore size distribution, hence the soil type to some degree, essentially control the characteristic length. Lehmann et al. 2008 have illustrated that characteristic length is a function of soil type. For various types of soils such as sand, silt loam, clay loam characteristic length is higher than 10 cm. Specimens at short heights (i.e. the heigths preferred in this study) reach air-dried condition in which the overall moisture content of the specimen particularly represents either bulk and funicular state (constant rate period) or soil water in the pendular ring and adsorptive form (falling rate period). Therefore, measured time-series moisture content data within the evaporation tests inherently belong to each of constant and falling rate periods. The microstructural parameter for Mersin silt specimens at 0.72 initial void ratio (excluding test result for 3 cm tall specimen) is determined by dividing critical moisture contents with the saturated moisture contents, resulting in the average value of 0.212 with a standard deviation of 0.011. Furthermore, evaporation tests on Mersin silt specimen at initial void ratios of 0.52, 0.83 and 0.92 provide microstructural parameters of 0.344, 0.189 and 0.178, respectively (Fig. 4.13f,g,h). Critical moisture contents are very close to that determined for initial void ratio at 0.72 and microstructural parameter is essentially influenced by the difference in saturated moisture contents. This is an expected result since the amount of micropores and so the microstructural parameter itself increase with decreasing void ratio (Alonso et al., 2013).

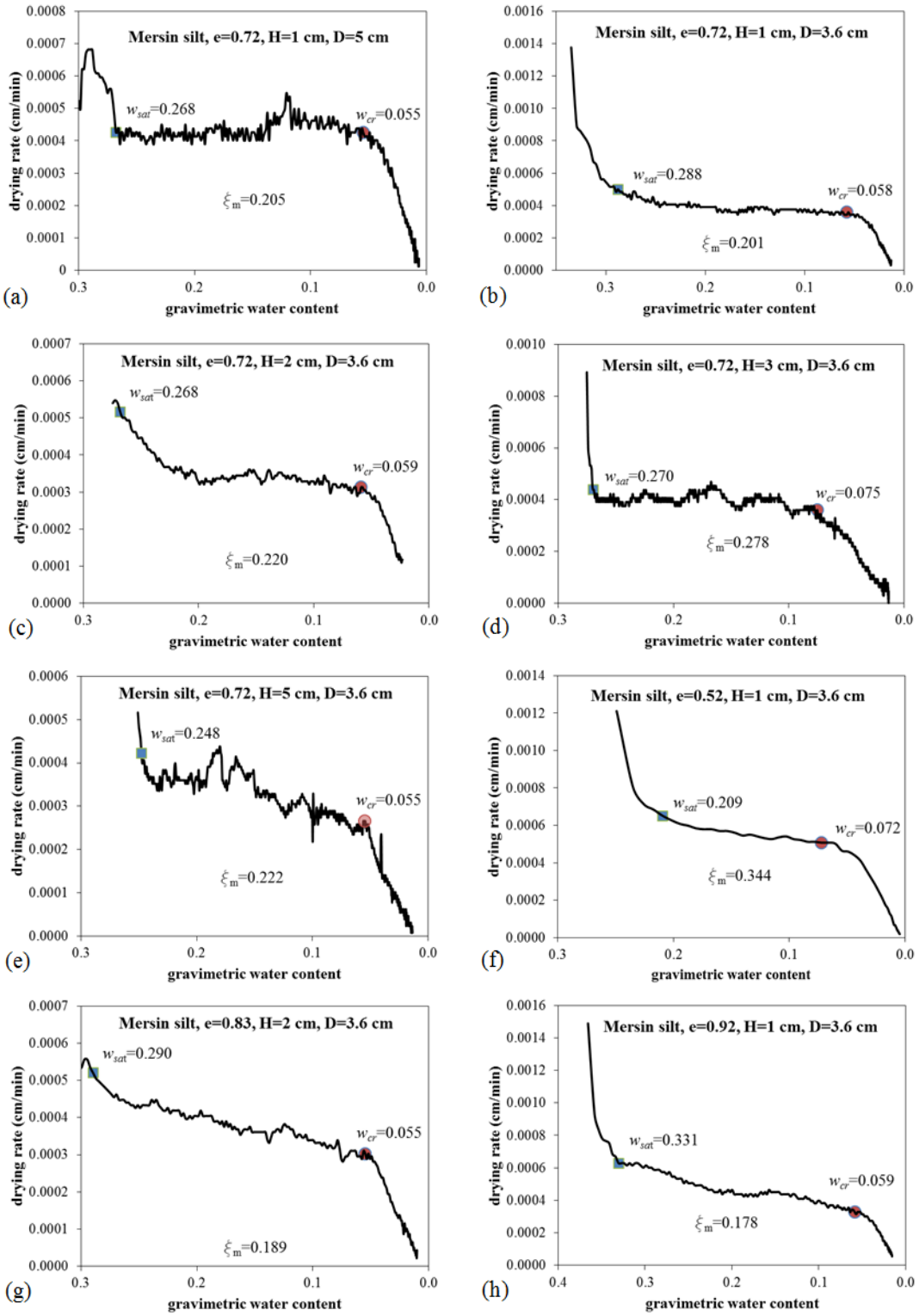

Figure 4.13 Experimental drying rate curves for Mersin silt, highlighted blue and red data points respectively correspond to saturated and critical moisture contents

Elazığ silt specimens are tested at initial void ratio of 0.845 and varying height between 1 cm to 2 cm (Fig. 4.14a,b,c,d). The test on 1.5 cm height specimen is duplicated (Fig. 4.14a,b). There is difference between both the saturated moisture content and critical moisture content of the duplicated tests. Elazığ silt specimens contain particle agglomeration that can be visually inspected. Duplicated specimens can undergo somewhat different wetting process during capillary soaking that is attributed to features of the soil texture. However, the microstructural parameters determined from these tests are 0.214 and 0.220 which are very close to each other. The microstructural parameter for Elazığ silt specimen at initial void ratio of 0.845 is determined as the average value of 0.216 from four evaporation tests, with the standard deviation of 0.003.

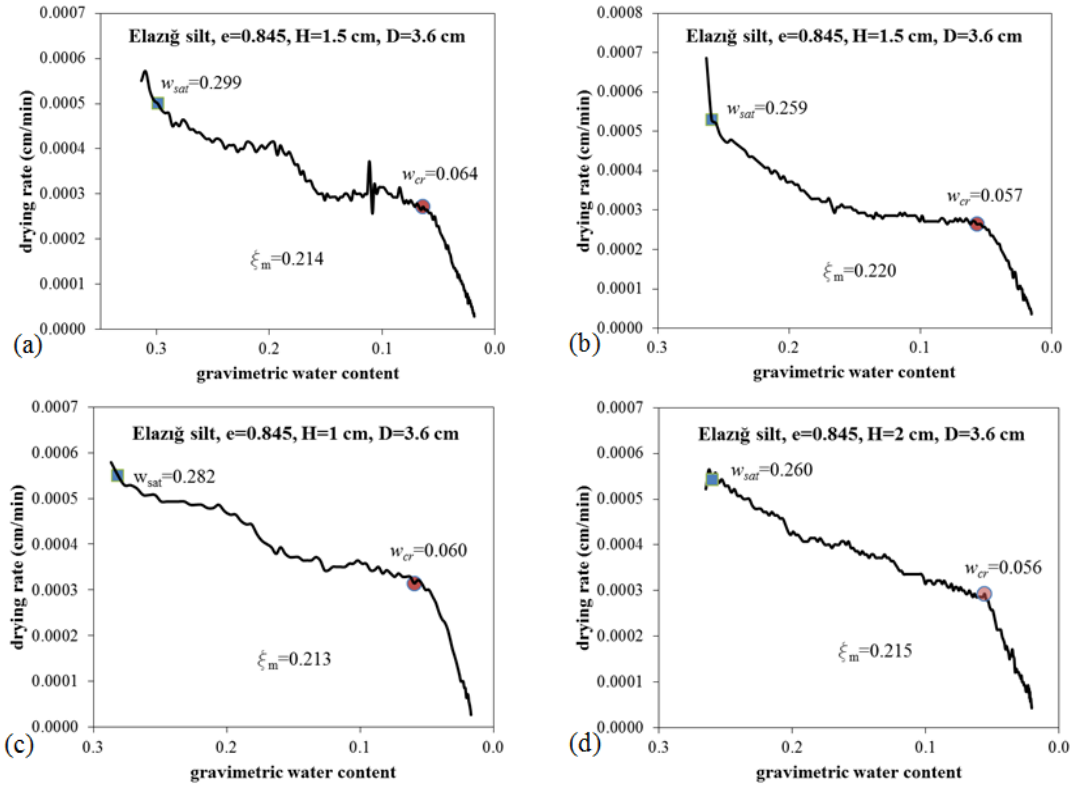

Figure 4.14 Experimental drying rate curves for Elazığ silt, highlighted blue and red data points respectively correspond to saturated and critical moisture contents

Ankara clay specimens at initial void ratio of 1.137 and 1.252 are used in the evaporation tests (Fig. 4.15a,b). Microstructural parameters are determined as 0.683 and 0.600, respectively. Ankara clay is highly plastic soil and the

characterization of this soil with relatively higher value of microstructural parameter is consistent with Alonso et al. (2010) who have studied highly plastic Boom clay resulting in higher value for the microstructural parameter.

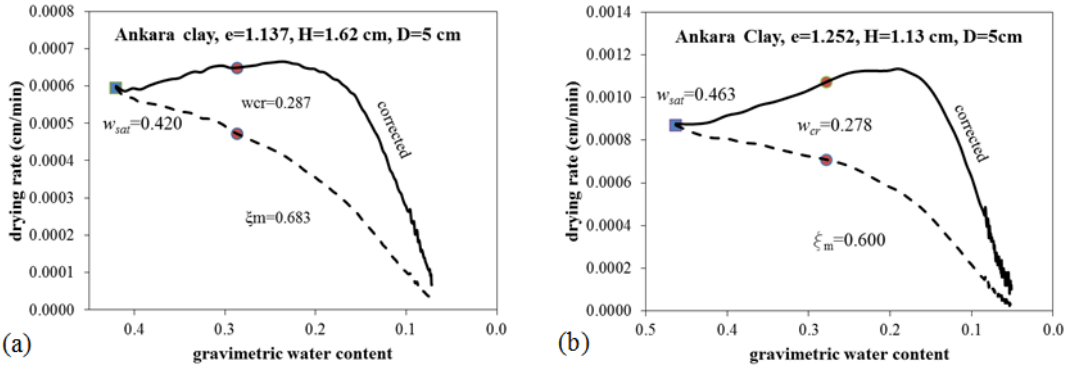

Figure 4.15 Experimental drying rate curves for Ankara clay, highlighted blue and red data points respectively correspond to saturated and critical moisture contents

4.2.3 Validation

Saturated strength parameters such as effective friction angle f′ and effective cohesion c′ of studied soils are given in Table 4.1. The test results on unsaturated specimens were illustrated in Chapter 3 in detail. Test program together with the experimental results that are used in the shear strength model are presented in Table 4.2.

Table 4.1 Saturated strength parameters of studied soils

Soil	f′ (°)	c′ (kPa)
Mersin silt	35.5	0
Elazığ silt	34.5	1
Ankara clay	22.6	13.9

Table 4.2 Test program on unsaturated specimens (e_0: initial void ratio of the specimen before testing, σ_3:confining net stress in kPa, s: suction in kPa at the time of failure, S_r: degree of saturation at the time of failure, σ_d: deviator stress reached at the time of failure in kPa)

soil	ID	e_0	σ_3	s	S_r	σ_d
Mersin silt	MCD01	0.72	25	100	0.382	212
Mersin silt	MCD02	0.72	100	100	0.406	376
Mersin silt	MCD03	0.72	400	100	0.493	1151
Mersin silt	MCD04	0.72	25	200	0.371	231
Mersin silt	MCD05	0.72	100	200	0.380	427
Mersin silt	MCD06	0.72	400	200	0.416	1255
Mersin silt	MCD07	0.72	25	400	0.377	282
Mersin silt	MCD08	0.72	100	400	0.354	489
Mersin silt	MCD09	0.72	400	400	0.364	1296
Mersin silt	MCW02_1	0.72	27	45	0.503	136
Mersin silt	MCW05	0.72	22	72	0.820	199
Mersin silt	MCW01	0.72	25	122	0.375	172
Mersin silt	MCW02_2	0.72	25	44	0.472	126
Mersin silt	MCW03	0.72	98	24	0.545	245
Ankara clay	ACW02	1.133	99	249	0.946	444
Ankara clay	ACW03	1.133	49	363	0.940	520
Ankara clay	ACW04	1.133	109	524	0.938	663
Ankara clay	ACW05	1.133	183	-25	0.984	283
Elazığ silt	ECD04	0.845	54	40	0.520	191
Elazığ silt	ECD05	0.845	52	80	0.448	231
Elazığ silt	ECD06	0.845	202	40	0.621	610
Elazığ silt	ECD07	0.845	200	80	0.528	573
Elazığ silt	ECW01	0.845	96	36	0.499	251
Elazığ silt	ECW02	0.845	100	11	0.643	250
Elazığ silt	ECW03	0.845	200	8	0.718	529

Experimental value of shear stress on failure planes at the time of the failure of the specimen is calculated from the following relationship based on Mohr circle representation of stress state:

$$\tau_{f,exp} = \frac{\sigma_{dev}}{2}\cos\phi \qquad (4\text{-}7)$$

The prediction of shear strength is calculated inserting the normal stresses acting on failure planes at the time of failure in (4-3)

$$\tau_{f,m} = \tan\phi\left(\sigma_3 + \frac{\sigma_{dev}}{2}(1-\sin\phi) + sS_r^e\right) + c' \qquad (4\text{-}8)$$

Shear strength equation given by Alonso et al. (2010) (4-8) is fitted to experimental shear strength data (4-7) from unsaturated triaxial tests. Microstructural parameter ξ_m for Mersin silt, Elazığ silt and Ankara clay are respectively determined as 0.213, 0.238 and 0.681 through least square fitting.

The microstructural parameter ξ_m values that were determined solely from the evaporation tests on the specimens that are prepared at the same initial void ratio and gravimetric moisture content with the triaxial test specimens are presented in Table 4.6. For the Mersin silt ξ_m was taken as the average of evaporation tests on Mersin silt specimens prepared at 0.72 initial void ratio which is 0.212 with the standard deviation of 0.011. In case of Elazığ silt, ξ_m was determined as 0.216 with the standard deviation of 0.003. ξ_m was determined as 0.683 for Ankara clay specimen having initial void ratio of 1.137 which is quite close to average of that of triaxial test specimens.

Table 4.3 Comparison of microstructural state parameters calibrated from the best fitting of (4-1) to experimental shear stress data and determined from the evaporation test results

	Mersin silt	Elazığ silt	Ankara clay
Best fitting of ξ_m	0.213	0.238	0.681
ξ_m from evaporation test	0.212	0.216	0.683

The performance of the shear strength equation when the microstructural parameter is calibrated based on only evaporation test results is illustrated in Fig. 4.16. Microstructural parameter was taken as 0.201 and 0.223 for Mersin silt whereas it was taken as 0.213 and 0.219 for Elazığ silt. In case of Ankara clay, predictions corresponding to the single value of 0.683 was added. The predictions based on evaluation of microstructural parameter from evaporation tests almost completely

match experimental data. The difference on the shear strength predictions using the result from best fitting of microstructural parameter and the results of the evaporation test can only be noticed for Mersin silt specimens which have highest standard deviation of 0.011 for microstructural parameter. The sensitivity of the model predictions have been marginally affected by the error margin of the microstructural parameter determined from the evaporation tests. The absolute error in terms of shear stress for microstructural state parameter calibrated from best fitting of (4-3) to experimental shear stresses are plotted against the absolute error corresponding to microstructural state parameter determined from evaporation tests in Fig 4.17. The strong compatibility between both procedures is revealed in Fig. 4.17 since absolute errors from both procedures fall on the 1:1 line.

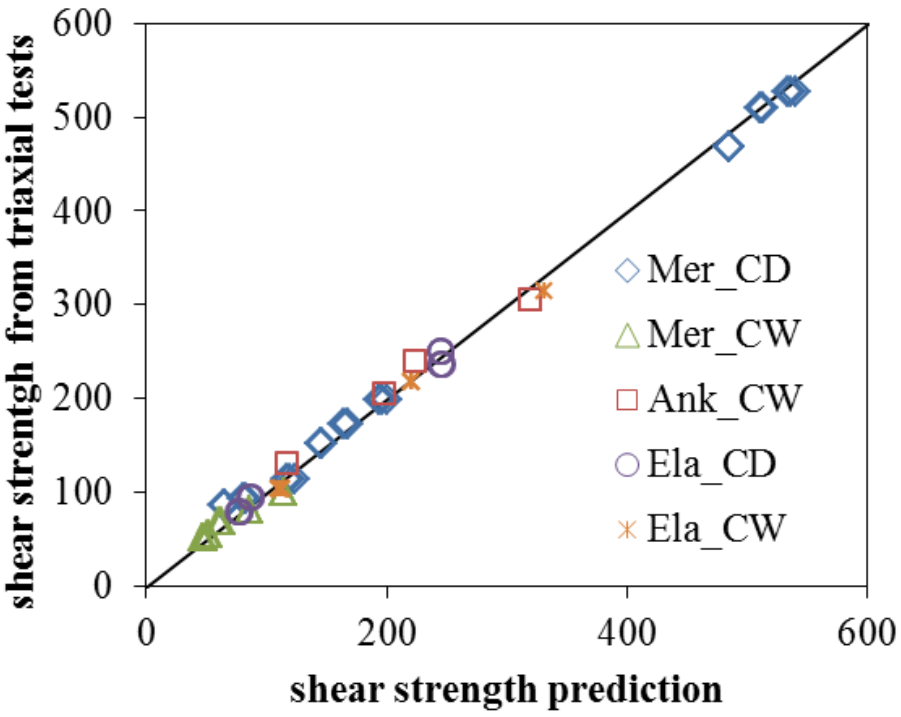

Figure 4.16 Prediction of shear strength using microstructural degree of saturation value that is provided by evaporation tests

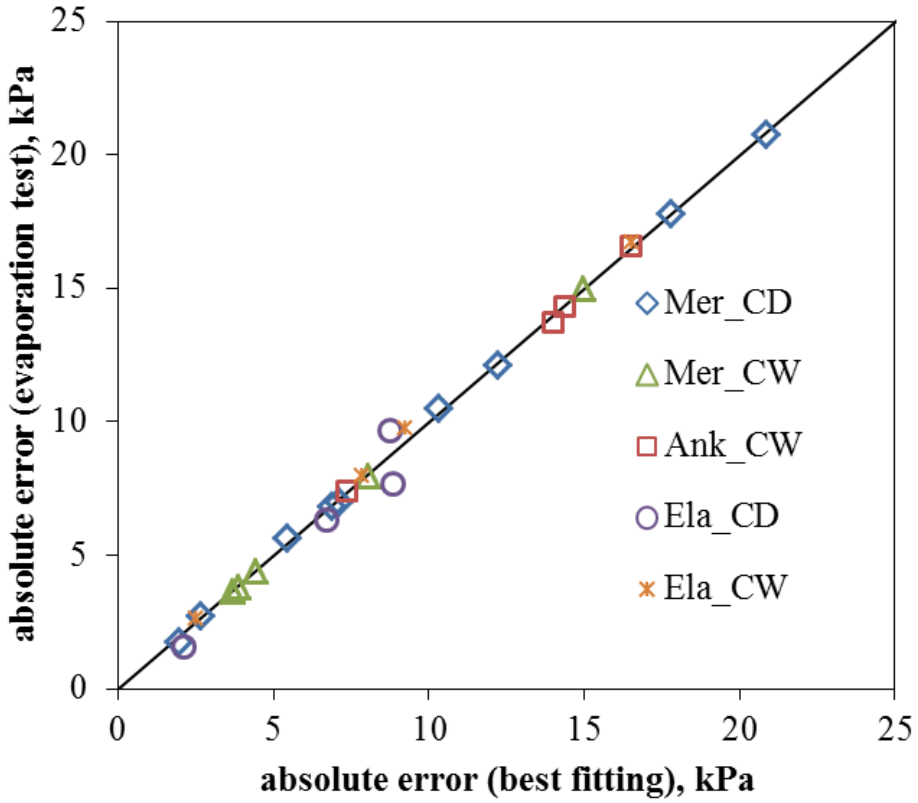

Figure 4.17 Comparison of absolute errors in terms of shear stress for ξ_m determined from both best fitting and evaporation test result.

4.3 Numerical Determination of Unsaturated Hydraulic Conductivity From Time-Series Outflow Data

Axis translation method is the most common technique of suction control during soil water retention curve measurements. During testing, water content and suction within the specimen vary after the application of a suction increment until hydraulic equilibrium is achieved. In this study, flow through specimen and ceramic inside a suction controlled oedometer is modelled as one-dimensional unsaturated seepage problem. The method proposed in this study can be applied any type of axis translation based test setup such as tempe cell or pressure plate. The transient variation of soil water mass is monitored to collect time-series water content data and it is used with the developed seepage model to estimate hydraulic

conductivity function. Thus, the experimental procedure for determining hydraulic conductivity of the soil specimen proposed in this study is embedded in the soil water retention curve measurements. The numerical seepage model can be implemented in a spreadsheet and it is used for determining the parameter of the selected water content type hydraulic conductivity function. The unknown parameter is found with least square fitting of predicted time-series data to experimental outflow curve. Therefore, the nonuniqueness in the combination of parameters obtained from an optimization run is avoided. The numerical model incorporates the volume change behaviour resulting from the suction variation which is a problematic feature especially for fine soils. The proposed simple method for the determination of hydraulic conductivity function is validated for different types of soils such as silt, sand and a highly plastic clay.

4.3.1.1 Materials

In addition to Mersin silt and Ankara clay whose properties were given in Sections 3.1, 3.4.5 and 3.4.6, quartz sand was also used in this part of the study. Index properties and hydraulic functions of quartz sand was given by Ahmadi-adli (2014). Soil water retention curve of quartz sand was measured using hanging column and pressure plate apparatus. Hydraulic conductivity function was determined using infiltration column method (ASTM D7664).

Table 4.4 Index properties of soils used in this study

	Quartz sand
Specific gravity	2.663
Liquid limit	-
Plasticity index	-
USCS classification	SP
Saturated conductivity (m/sec)	1.15×10^{-6}

Eyüpgiller and Ülker (2018) used HYPROP device to measure drying soil water retention curve and hydraulic conductivity function of Mersin silt specimen that was prepared at the same initial void ratio and initial water content.

The equation proposed by van Genuchten (1980) has been used to fit experimental data points to obtain complete retention curve branch (Fig. 4.18):

$$\theta = \theta_{res} + \left(\theta_{sat} - \theta_{res}\right) \Big/ \left(1 + \left(s/a\right)^{n}\right)^{m} \tag{4-9}$$

where s is suction and a, n, m are fitting parameters. θ_s and θ_r are respectively saturated and residual volumetric water contents. The estimated fitting parameters are given in Table 4.5.

Table 4.5 Fitting parameters for retention curves

Soil	θ_{sat}	θ_{res}	a	n	m
Mersin silt	0.429	0.08	42.8	1.09	0.65
Ankara clay	0.563	0.122	2892.9	0.69	0.98
Quartz sand	0.484	0	9.4	2.5	2.71

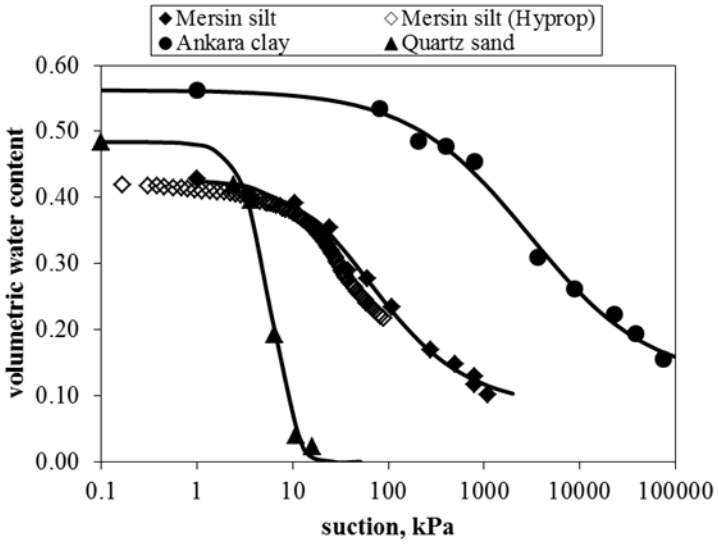

Figure 4.18 Soil water retention curves for soils used in this study (lines show van Genuchten (1980) fits to test data)

4.3.2 Numerical Model

Darcy law is used to express fluid flux through unsaturated soil:

$$q = -k(\theta)\nabla h \tag{4-10}$$

where $k(\theta)$ is hydraulic conductivity as a function of volumetric water content (θ), h is hydraulic potential. Hydraulic conductivity is not constant as in the case of saturated soil and becomes a function of suction or water content. The change of θ with time becomes equal to the gradient of flux based on conservation of mass principle:

$$\frac{\partial \theta}{\partial t} = -\nabla q \tag{4-11}$$

The combination of (4-10) and (4-11) is known as Richards Equation (1931) and the differential equation of seepage for one dimensional case is written in the following expression:

$$\frac{\partial \theta}{\partial t} = \frac{d}{dz}\left(k(\theta).\frac{\partial h}{\partial z} \right) \tag{4-12}$$

The flow through specimen placed in suction controlled oedometer apparatus is considered as one-dimensional unsaturated seepage problem. The specimen is divided into slice elements in the numerical configuration of the problem (Fig. 4.19). Evaporation/condensation is assumed to be insignificant in the timescale of an experiment, when compared to liquid phase flow through the HAE ceramic. As such, zero-flux boundary condition is applied at the top of the specimen. Suction at the interface between specimen and ceramic disc is prescribed as a variable bottom boundary condition. The head loss due to ceramic disc is considered in determining suction at the specimen-ceramic interface.

The flow between slices can be expressed in incremental form using first order approximation of (4-10):

$$Q_{i,j} = k_{i,j}\left(\frac{s_{i+1,j} - s_{i,j}}{\gamma_w \Delta z} + 1\right)A \qquad (4\text{-}13)$$

where indices i and j respectively refer to spatial (or slice elements) and temporal domain. For j^{th} time step, $q_{i,j}$ denotes the water flow between i^{th} and $i+1^{st}$ slices, $k_{i,j}$ is the average hydraulic conductivity between i^{th} and $i+1^{st}$ slices and $s_{i,j}$ denotes the value of suction at the middle of i^{th} slice. γ_w, Δz, A are respectively unit weight of water (9.8 kN/m^3), slice thickness and area of the specimen.

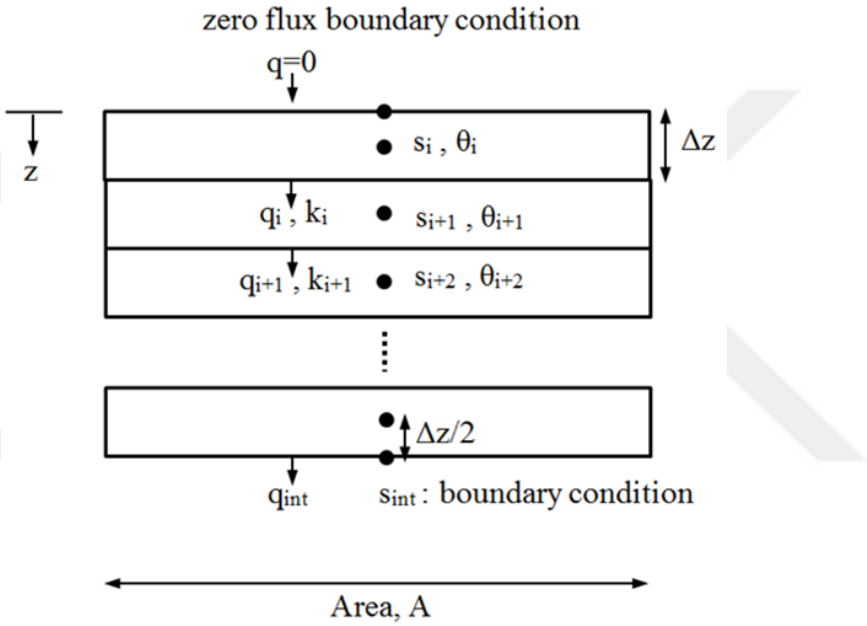

Figure 4.19 Numerical configuration of the problem

The volumetric water content of a slice element at t=j+1 can be expressed in the following incremental form using (4-11):

$$\theta_{i,j+1} = \theta_{i,j} + \left(q_{i-1,j} - q_{i,j}\right)\frac{\Delta t}{A\Delta z} \qquad (4\text{-}14)$$

(4-13) and (4-14) are used to solve one dimensional Richards equation with Euler method. The calculated θ values are linked with soil water retention curve to estimate suction for each slice. Thus, volumetric water content and suction at the middle of each slice are determined. The average hydraulic conductivity between successive slices is related with θ at the interface. The value of θ at the interface

($\theta_{i+1/2}$) is devised by a third order approximation of θ with calculated values of θ at the mid-height of each slice (Fig. 4-20). Second derivative of θ(z) becomes linear with depth and the following relation is used:

$$\theta''_{(i+1/2,j)} = \frac{\theta''_{(i,j)} + \theta''_{(i+1,j)}}{2} \tag{4-15}$$

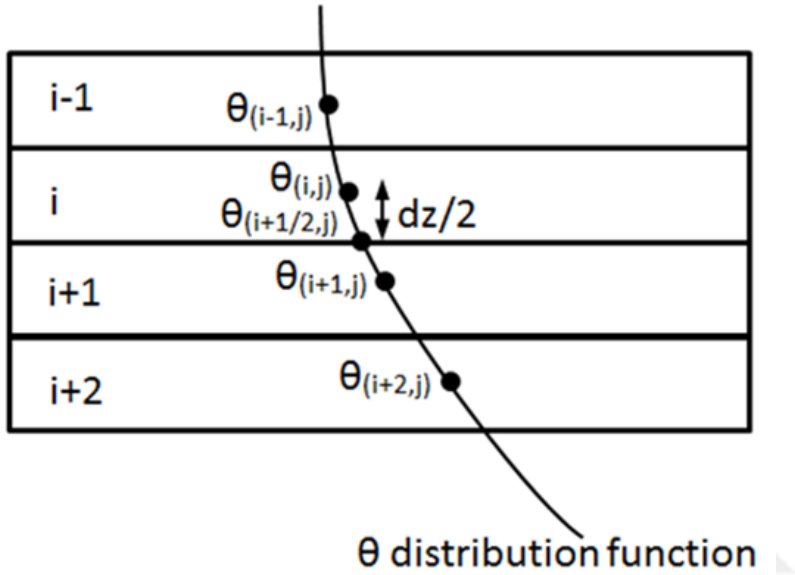

Figure 4.20 Schematic view of distribution function of volumetric water content and points used in the proposed relation (Kenanoğlu, 2017).

(4-16) and (4-17) can be respectively obtained after applying central finite difference approximation to (4-16):

$$\frac{\theta_{(i,j)} - 2\theta_{(i+1/2,j)} + \theta_{(i+1,j)}}{dz^2/4} = \frac{\theta_{(i-1,j)} - 2\theta_{(i,j)} + \theta_{(i+1,j)}}{2dz^2} + \frac{\theta_{(i,j)} - 2\theta_{(i+1,j)} + \theta_{(i+2,j)}}{2dz^2} \tag{4-16}$$

$$\theta_{i+1/2,j} = \frac{-\theta_{i-1,j} + 9\theta_{i,j} + 9\theta_{i+1,j} - \theta_{i+2,j}}{16} \tag{4-17}$$

θ_{i-1} is taken same as θ_i for the first interface and θ_{i+2} is taken same as θ_{i+1} for the last interface. The volumetric water content calculated from (4-17) is then used to estimate average hydraulic conductivity.

The hydraulic conductivity is expressed as a function of volumetric water content using two of many equations proposed in the literature. The first one is the following power equation (Averjanov, 1950):

$$k_{i,j} = k_{sat}\Theta^{\beta} = k_{sat}\left(\frac{\theta_{(i+1/2,j)} - \theta_r}{\theta_s - \theta_r}\right)^{\beta} \tag{4-18}$$

where, k_{sat} is saturated hydraulic conductivity, Θ is effective volumetric water content, θ_s and θ_r are respectively saturated and residual volumetric water contents. Mualem (1978) reported that power parameter β could vary between 2.5 to 24.5 based on literature data. The time-series outflow/inflow water mass data determined from the numerical model is matched with experimental outflow data through optimizing the power parameter, β. HCF is determined using this optimum value of β.

Alternatively, the van Genuchten-Mualem equation is used in this study (van Genuchten 1980) resulting in (4-20). In this case, power parameter κ is used for optimization of outflow data.

$$k_{i,j} = k_{sat}\left(\frac{\theta_{(i+1/2,j)} - \theta_r}{\theta_s - \theta_r}\right)^{0.5}\left[1-\left(1-\left(\frac{\theta_{(i+1/2,j)} - \theta_r}{\theta_s - \theta_r}\right)^{\frac{\kappa}{\kappa-1}}\right)^{\left(\frac{\kappa-1}{\kappa}\right)}\right]^2 \tag{4-19}$$

The suction boundary condition at the bottom of specimen is defined including head loss due to ceramic. Suction at the bottom of ceramic, that is s_{test} in Fig. 4-21, equals applied air pressure since water pressure is zero. Hydraulic head at the interface between the ceramic and specimen is less than that caused by s_{test} due to head loss within the ceramic. Therefore, suction at the bottom of the specimen, that is s_{int} in Fig. 4-21, is less than the applied suction. The saturated flow rate through ceramic (Q_{test}) is expressed by Darcy flow as:

$$Q_{test} = \left(\frac{-s_{test} + s_{int}}{\gamma_w H_c} - 1 \right) k_c A_c \qquad (4\text{-}20)$$

s_{int} is the unknown suction at the interface between ceramic and specimen, H_c is the height of the ceramic that is 7.38×10^{-3} m, kc is the hydraulic conductivity of ceramic that has been measured as 3.93×10^{-11} m/sec, A_c is the area of ceramic that is 0.001963 m^2. The hydraulic conductivity of ceramic was measured by flushing the plate at several pressure heads. Pressure is applied inside a water-filled oedometer ring to generate constant head difference between top and bottom of the ceramic. The steady state outflow from the cell is monitored to determine the volume of the flow. Hydraulic conductivity of ceramics is calculated using Darcy's law. Hydraulic conductivity of the ceramic has a major influence on the slope of the initial linear portion of time-series outflow data predicted from numerical model and its precise measurement is essential. It should be noted that hydraulic conductivity of the ceramic decreases in the long term over repeated soil water retention curve measurements. Therefore, the ceramic can be either resaturated prior to testing or ceramic hydraulic conductivity can be measured at the end of the test.

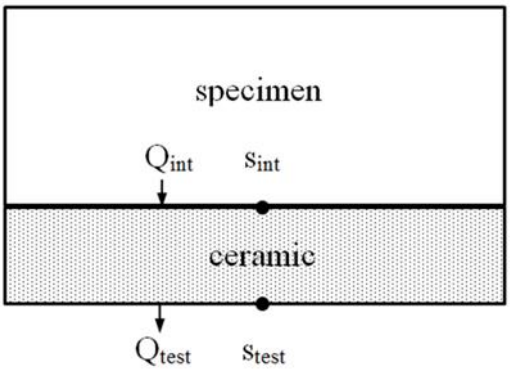

Figure 4.21 Boundary conditions for the flow through HAE ceramic

The flow from the bottom slice can be calculated using (4-13):

$$Q_{int} = \left(\frac{-s_{int} + s_{b,j}}{\gamma_w \, \Delta z/2} - 1 \right) k_{i,j} A_s \qquad (4\text{-}21)$$

Q_{int} is flow from bottom slice, $k_{i,j}$ hydraulic conductivity of bottom slice, $s_{b,j}$ is suction of the bottom slice, A_s is the area of specimen.

The flow into a saturated ceramic (Q_{int}) and the flow out of it (Q_{test}) have to be equal based on the conservation of mass principle. An expression for the unknown suction at the interface s_{int} can thus be obtained by equating (4-20) and (4-21):

$$s_{int} = \frac{\left(\frac{2s_{b,j}k_{b,j}A_s}{\gamma_w \Delta z} + \frac{s_{test}k_c A_c}{\gamma_w H_c} - k_{b,j}A_s + k_c A_c \right)}{\left(\frac{2k_{b,j}A_s}{\gamma_w \Delta z} + \frac{k_c A_c}{\gamma_w H_c} \right)} \tag{4-22}$$

The proposed numerical model is implemented in a spreadsheet. Specimen is divided into five slice elements in the model configuration. The time increment is adjusted to a value that is compatible with the slice thickness to avoid numerical error. Selecting a too large time increment could result in volumetric water content values higher than that of saturated state resulting in mathematical errors in the solution of nonlinear equations used in the model. The initial volumetric water content of the specimen defines the initial condition of numerical solution; therefore, it should be carefully measured prior to testing. The soil water retention curve function is used to estimate suctions within slices (4-9). Suction at the bottom boundary is determined in the next step using (4-21). Volumetric water contents at the slice interfaces ($\theta_{i+1/2}$) are calculated using (4-17). In the next step, hydraulic conductivities of slice elements can be determined using results of $\theta_{i+1/2}$ array and (4-18) or (4-19). In the final stage, flow between slice elements is calculated using (4-13). The outflow from the specimen is calculated using (4-21). Volumetric water contents are calculated using (4-144) to commence next time step calculations. Time-series water mass data calculated in (4-21) is compared with the experimental result to optimize the power parameter β of the HCF (4-18). Excel Solver add-in is used in optimization based on least square error in water mass. The spreadsheet calculations and corresponding equations are given in Table 4-6.

Table 4.6 Equations of spreadsheet calculations for model configuration of five slice elements

j	θ (i=1 to 5)	s (i=1 to 5)	s_{int}	θ_B (i=1 to 4)	k (i=1 to 4)	q (i=1 to 4)	q_{int}
$t_0 = 0$	θ_0 (initial condition)	(4-9)	(4-22)	(4-17)	(4-18 or 4-19)	(4-13)	(4-21)**
$t_0+\Delta t$ ⋮	(14 or 23)*	⋮	⋮	⋮	⋮	⋮	⋮

* $q_{i-1,j}$ is taken as zero for the first slice (i=1) due to zero flux boundary condition at the top.

**cumulative summation of this column gives total outflow.

4.3.2.1 Incorporation of Suction-induced Volume Change into Numerical Model

The proposed numerical model is extended to capture flow through soil specimens that are prone to suction induced volume change (e.g. Ankara clay specimens in this study). The drainage length or slice thickness Δz, flow area A and thus slice element volumes change with the volume change of specimen resulting from the suction increments during testing. Simple functions rather than rigorous constitutive model formulations are implemented with the aid of experimental measurements to incorporate volume change effects into numerical model.

At the end of each suction increment step during water retention curve extraction, the height and diameter of the test specimen is manually measured by means of calipers. Linear functions are fitted to the experimental data to describe the relationships between volumetric water content or suction with the height, diameter and volume. In this study, volumetric water content is preferred as an independent fitting variable. Although change in dimensions and volume being linearly related might seem counter-intuitive, for such small changes it is no different than volumetric strain being thrice the linear strain in isotropic conditions. Non-linear

relationship appears in the case of specimen's volume as a function of volumetric water content. Slice thickness and specimen area are then defined as functions in the relevant equations (i.e. 4-13,14,21,22) using relationships calibrated with the experimental measurements. The relationships obtained in the extraction of drying water retention curve of Ankara clay specimen are illustrated in Fig. 4.22.

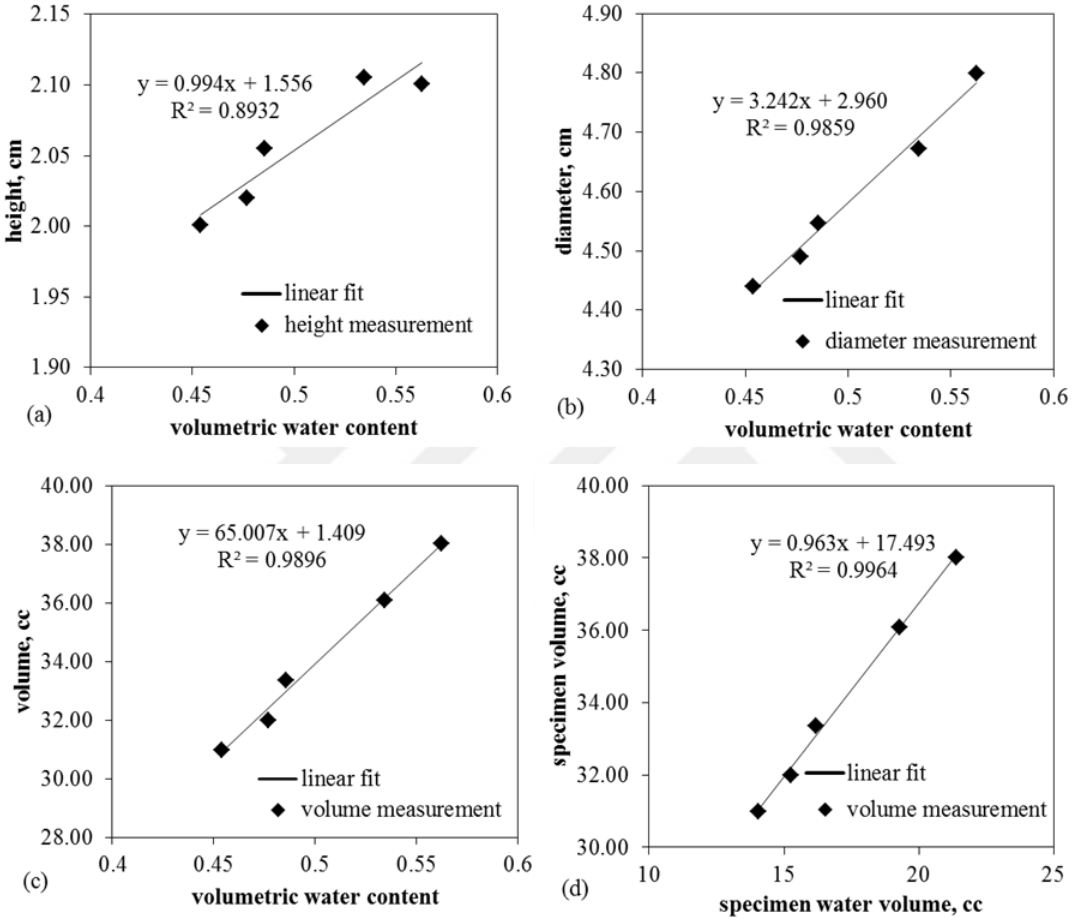

Figure 4.22 Volume-mass relation equations calibrated against experimental measurements that are taken during the extraction of soil water retention curve of Ankara clay specimen

These relationships appear to be mostly linear, so they are assumed as such in this study. Constant control volume condition in (4-14) is violated due to specimen's volume change and slightly different form of this equation should be used to calculate volumetric water contents:

$$\theta_{i,j+1} = \frac{\theta_{i,j} V_{i,j} + \left(Q_{i-1,j} - Q_{i,j}\right)\Delta t}{V_{i,j} + \lambda_w \left(Q_{i-1,j} - Q_{i,j}\right)\Delta t} \tag{4-23}$$

where V denotes the volume of slice element and can be obtained using relationship defined between volumetric water content and specimen volume (Fig. 4.22-c) and λ_w is a parameter that relates the specimen's water volume change with the specimen's total volume change. This parameter can be easily obtained as the slopes between data points on water volume versus total volume graph (Fig. 4.22-d). Volume of water within the specimen can be calculated from the outflow water mass measurements assuming water density is 1 gr/cm³. The value of λ_w becomes zero in case of constant volume condition and (4-23) is reduced to (4-14). Relationships between height and volume with volumetric water content are given for the whole specimen and slice thicknesses and volumes are obtained by dividing total height and total volume to number of slice elements.

4.3.3 Results

Simulations have been performed on experimental time-series data to see the performance of the numerical model. The hydraulic conductivity function of Mersin silt with initial void ratio of 0.72 was given by Eyüpgiller and Ülker (2018). Mersin silt specimens were prepared in 1 cm height and 5 cm diameter; therefore, slice thickness becomes 0.002 m for total of five elements. The time step size was taken as 3 seconds in the numerical model. The initial volumetric water content of saturated specimens was measured as 0.429. The hydraulic conductivity of ceramic was measured as 3.93×10^{-11} m/sec prior to testing. The experimental time-series outflow was measured during drying from initial suction of 0 kPa to 38 kPa, drying from initial suction of 0 kPa to 110 kPa and drying from initial suction of 0 kPa to 280 kPa. Power parameter β of (4-18) was optimized using time-series data from drying test of 0 kPa to 280 kPa (Fig. 4.23) and β was determined as 4.5. Drying tests 0 kPa to 110 kPa and 0 kPa to 38 kPa were simulated for validation (Fig.

4.23). The HCF corresponding to β as 4.5 was compared with experimental measurement in Fig. 4.24.

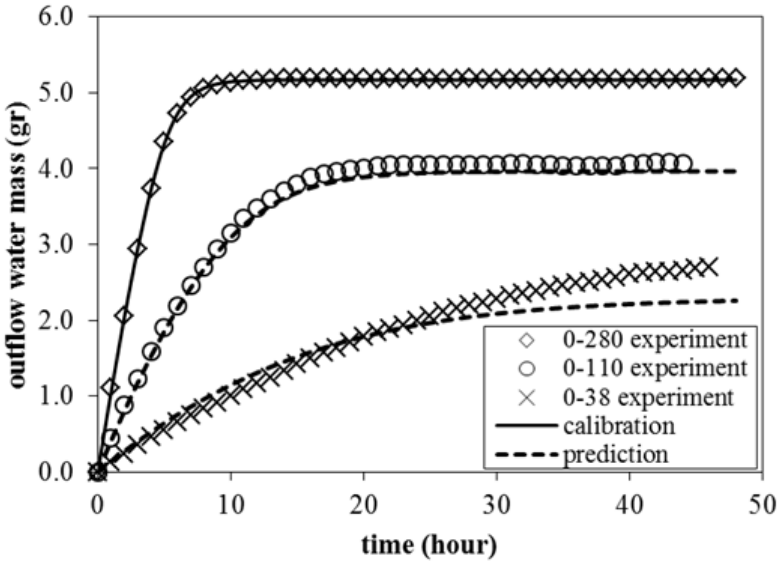

Figure 4.23 The water mass outflow variations for different suction increments during retention curve measurement of Mersin silt and model predictions

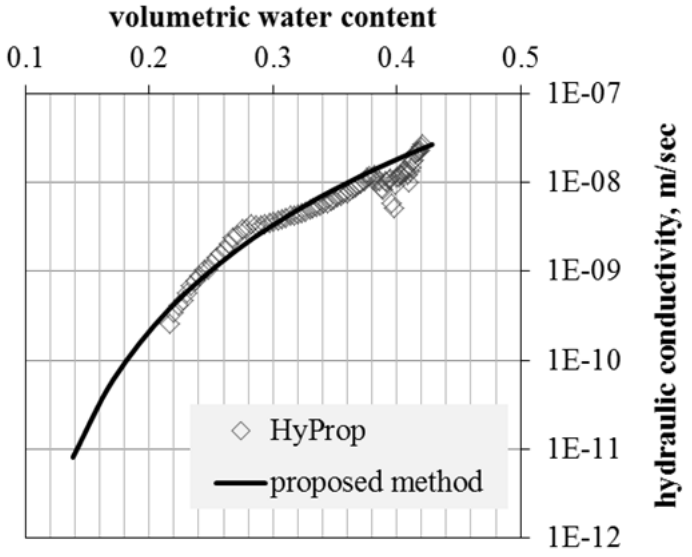

Figure 4.24 Calculated HCF of Mersin silt from proposed method and from Hyprop evaporation test (experimental data from Eyüpgiller and Ülker 2018)

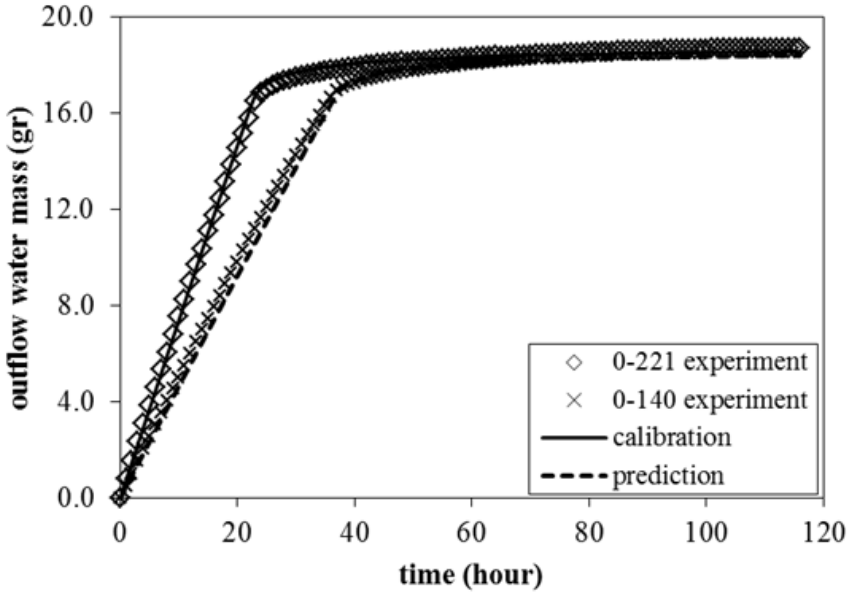

Figure 4.25 The water mass outflow variations for quartz sand and model results

Quartz sand sample was compacted at initial void ratio of 0.937 and initial gravimetric water content of 4% inside suction controlled oedometer ring. Specimen's height was 2 cm and its diameter is 5 cm. Specimen's volumetric water content was increased to 0.484 by slowly adding required amount of water using a burette. The hydraulic conductivity of ceramic was measured as 3.47×10^{-11} m/sec prior to testing. Experimental time-series outflow data was collected for drying from 0 kPa to 140 kPa suctions and drying from 0 kPa to 221 kPa suction (Fig. 4.25). In the numerical model, slice thickness is taken as 0.004 m and time step size is taken as 0.3 seconds. The power parameter of the HCF equation (4-18) was optimized to 3.0 using experimental data of 0 kPa to 221 kPa drying test. Experimental and estimated HCF for quartz sand is illustrated in Fig. 4.26, plotted together with infiltration column test (ASTM D7664) results by Ahmadi-adli (2016). As validation, results of another test of drying from 0 to 140 kPa suction was simulated using the HCF obtained from 0 to 221 kPa suction (Fig. 4.25).

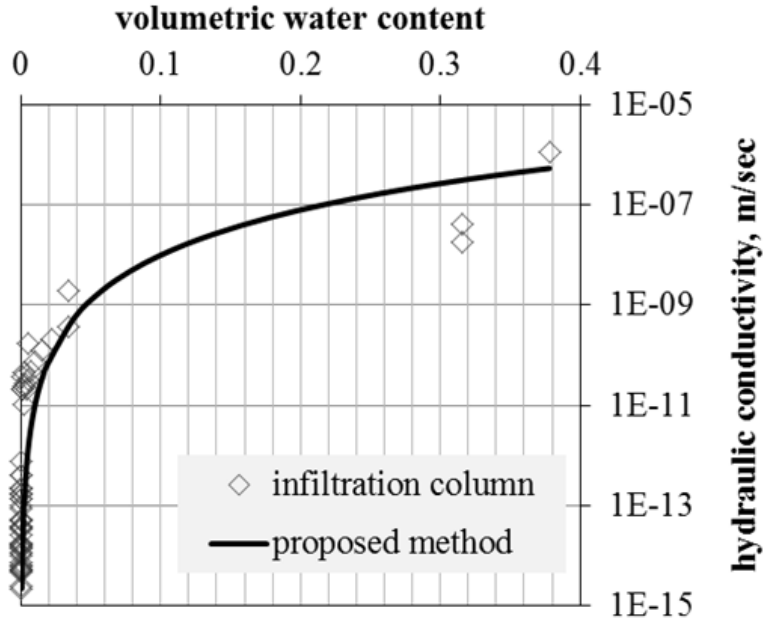

Figure 4.26 Calculated HCF of quartz sand from proposed method and from infiltration column test (experimental data from Ahmadi-adli 2016)

Ankara clay specimen at initial void ratio of 1.288 was used in the extraction of drying water retention curve. Initial gravimetric water content is 0.476 and initial volumetric water content is 0.563. Initial height and diameter of the specimen are respectively measured as 2.101 cm and 4.799 cm. The hydraulic conductivity of ceramic was measured as 2.06×10^{-11} m/sec prior to testing. The slurry sample is consolidated at the desired vertical stress inside a standard oedometer cell. Then, the consolidated specimen is removed from the standard oedometer setup and directly translated into the suction controlled oedometer test setup. The time step size is taken as 10 seconds and slice thickness, diameter and volume values are updated using equations given in Fig. 4.22-a. The hydraulic conductivity function given in (4-18) is found to be unsuitable to match the experimental outflow mass curve; therefore, van Genuchten-Mualem's (4-19) is preferred in the numerical model to simulate tests with Ankara clay. Outflow water mass was monitored during suction increments that are 0 kPa to 82 kPa, 82 kPa to 204 kPa, 204 kPa to 403 kPa and 403 kPa to 795 kPa. Experimental outflow data and simulation results

are given in Fig. 4.27. The parameter κ of (4-19) is optimized as 1.31 from the data of suction increment from 82 to 204 kPa. The prediction of 0 kPa to 82 kPa suction increment test does not conform to the experimental outflow data. This mismatch is probably caused by the equilibration duration that is not enough for the dissipation of negative pore water pressures developed within the specimen after removing from the standard oedometer. The water mass outflow curves for the retaining suction increments are used for validation (Fig. 4.27).

Unlike the two previous samples, the experimental data for the unsaturated hydraulic conductivity of Ankara clay is not available; therefore, it is not possible to compare the prediction with experimental measurement by a different method. Instead, Brooks and Corey (1964) equation is fitted to soil water retention curve test data to estimate the hydraulic conductivity function of Ankara clay specimen (using 4-24 and 4-25) showing that the difference for the prediction from the two-estimation method have the same order of magnitude (Fig. 4.28).

$$\theta = \theta_{res} + \left(\theta_{sat} - \theta_{res}\right)\left(\frac{s}{s_{aev}}\right)^{-\lambda} \tag{4-24}$$

$$k\left(\theta\right) = k_{sat}\left(\frac{\theta - \theta_{res}}{\theta_{sat} - \theta_{res}}\right)^{\frac{2+3\lambda}{\lambda}} \tag{4-25}$$

where s_{aev} is air-entry pressure and it is taken as 65 kPa, λ is pore size distribution index and it is optimized to 0.224; finally, θ_{sat} and θ_{res} are respectively taken as 0.563 and 0.122.

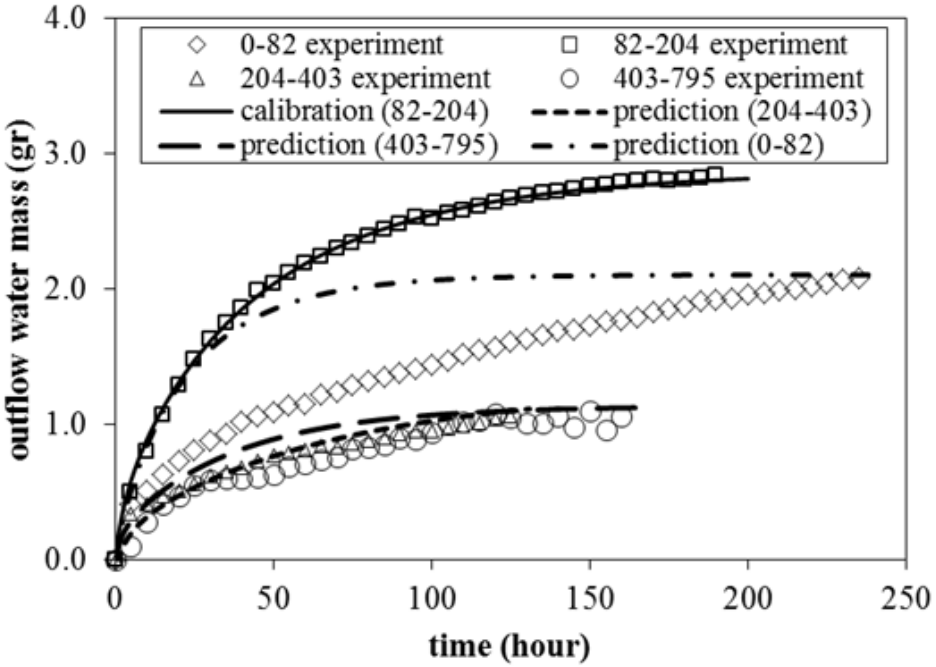

Figure 4.27 The water mass outflow variations for different suction increments during retention curve measurement of Ankara clay and model predictions

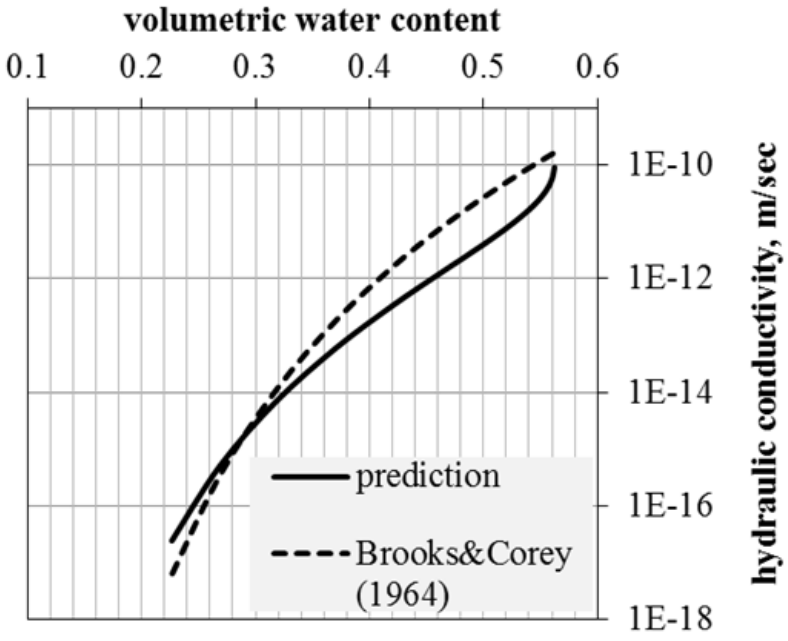

Figure 4.28 The comparison of the estimated hydraulic conductivity functions of Ankara clay from proposed method and Brooks and Corey (1964) method

Finally, the sensitivity of the predicted outflow water mass curve and so the hydraulic conductivity function to the number of slices is investigated. Sensitivity analyses are carried out for all the three types of soils. The slice thicknesses coarser and finer than that of corresponding to five slice elements are defined in the model with suitable time step increment resulting in convergent solution. The results of the sensitivity analyses are illustrated in Fig. 4.29. The results seem almost identical and using more than 3 slices does not have any meaningful effect on the performance of the predictions.

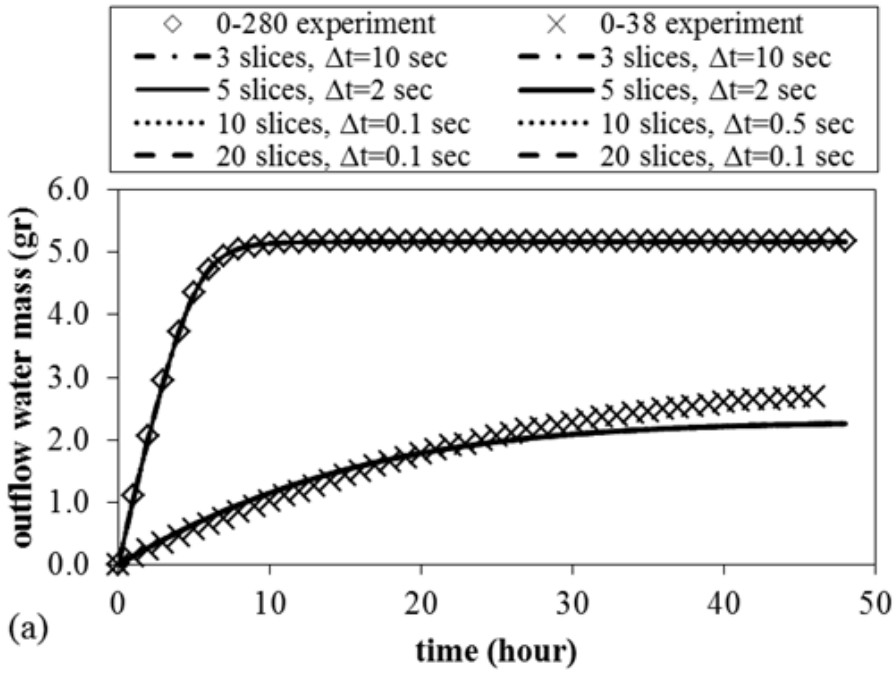

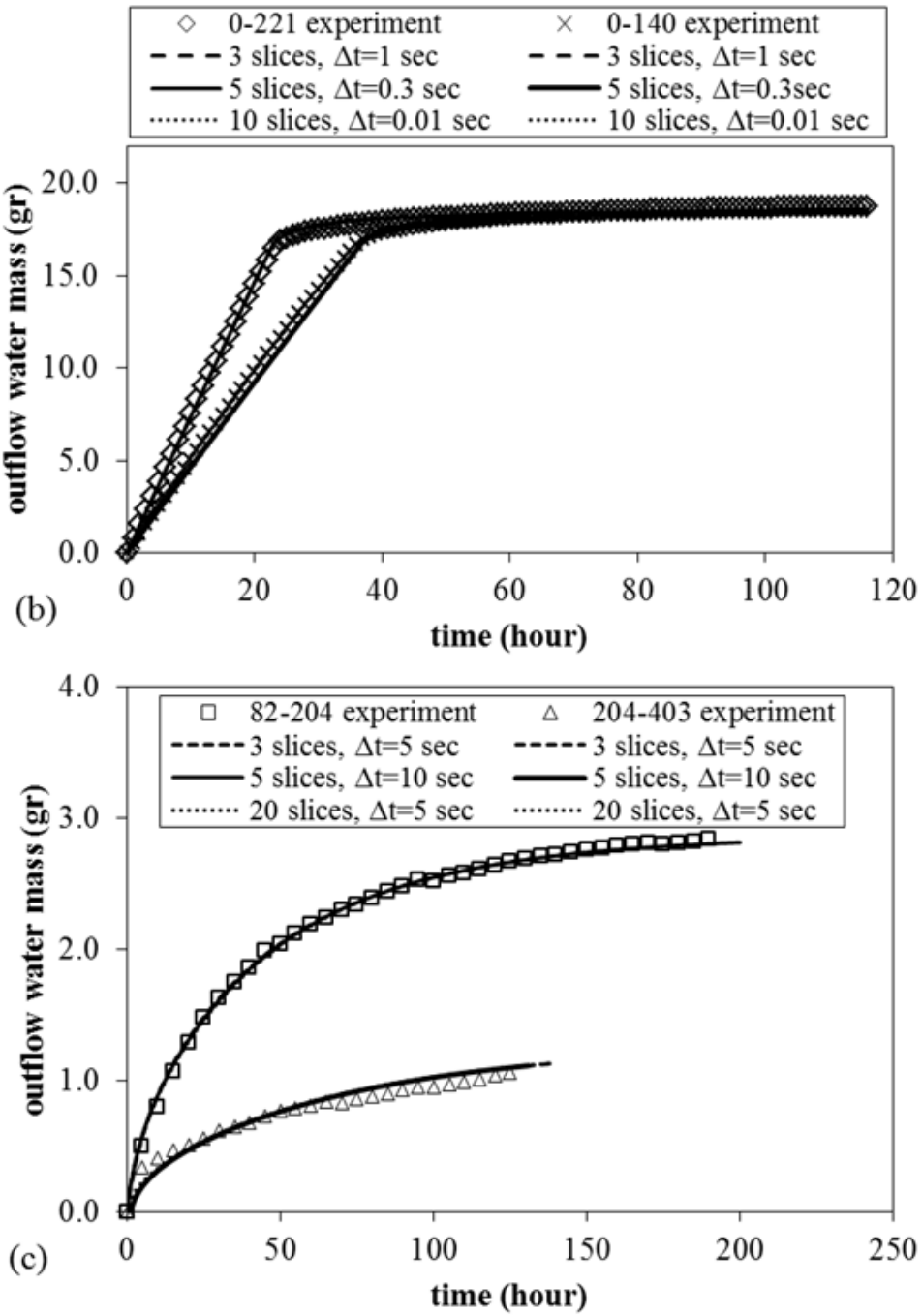

Figure 4.29 The effect of slice number on the performance of the prediction from numerical model (a) Mersin silt, (b) Quartz sand and (c) Ankara clay

4.4 Calibration of Barcelona Basic Model Parameters from Practical Test Procedures

Unsaturated soil testing requires advanced laboratory techniques, high cost equipment and most importantly very long test durations. These factors result in challenging problems for researchers and engineering practice. Developing simple laboratory protocols to calibrate parameters of constitutive models proposed in the literature or developing constitutive equations containing state variables suitable for simple calibration procedures can be beneficial in this regard.

The proposed laboratory work consists of simple oedometer and UU triaxial tests on unsaturated specimens at various water contents. Specimens' water content is adjusted through simple wetting and drying procedures explained in Section 4.1 as well as Kenanoğlu and Toker (2018a). Oedometer and UU triaxial tests are carried out on unsaturated specimens excluding soaking or back pressure saturation stages from standard test protocols. Ideal measurement or control of suction, loading rate, volume change are not a concern for these experiments. Although performing such a quick and simple laboratory campaign deprives delicate monitoring and/or control of certain state variables such as suction, degree of saturation, volume change etc., they can be used to calibrate the parameters of a constitutive model for unsaturated soils. The calibration process turns into an optimization of model parameters in order to fit a set of experimental results under rationale assumptions.

Barcelona Basic Model (see Section 2.3.3) is the best-known and most widely implemented constitutive model for unsaturated soils and it is preferred for this part of the study. The approach presented in this study can still be adapted to develop similar calibration procedures for other existing constitutive models for unsaturated soils. An Excel spreadsheet is prepared to easily implement the numerical framework of the model besides performing optimization analysis. The numerical implementation does not concern full application of BBM framework, instead, it only covers deviatoric formulation for given stress increments under constant

suction condition. Moreover, constant suction condition also omits the calculation of suction change induced elastic and plastic volumetric strain components.

4.4.1 Practical Test Procedures on Unsaturated Specimens

Unsaturated specimens of various water contents were tested on conventional triaxial and oedometer test equipment implementing several modifications in the standard test protocols. Unsaturated specimens of various water contents were obtained using methods proposed in Section 4.1. In summary, for increasing the water content of a low-plasticity specimen, a sprayer is used to moisten the specimen through its lateral surface. For increasing water content of high-plasticity specimen, rather different procedure is implemented to avoid undesirable volume change due to wetting. Specimen is wetted inside a rigid, perforated mold that restricts radial and vertical strains to prevent localized swelling of the specimen. For lowering the water content to a homogeneous value, leaving specimens to evaporate in open-air resulted in success, only if the specimen is turned up-side down halfway through the process. Specimens are sealed in nylon bags during the water content equilibration stage that follows either drying or wetting procedures. It becomes possible to bring specimens to moisture equilibrium at various water contents in less than one week for several scenarios.

Standard oedometer tests are carried out with unsaturated specimens without soaking. The oedometer cell was covered with nylon bags to eliminate evaporation from the specimen. Incremental loads were applied to specimens under K_0 condition. Each load increment is maintained until vertical displacement ceases.

In the UU triaxial tests, unsaturated specimen is tested omitting back pressure saturation stage. Air drainage was permitted during confining stress application and shearing stages by opening the drainage valve to atmosphere. Specimens were sheared under constant cell pressure at strain rate of 1%/min which is selected according to ASTM D2850-15. In both types of experiments, dry porous stones and

dry filter papers are used to restrict transfer of water mass between the specimen and underlying apparatus.

Modified area correction procedure is implemented to improve the UU triaxial test results which suffer from the lack of volume change data. This procedure is based on using the final dimensions of the specimen after shearing, to obtain more accurate values of cross-sectional area. The following (4-26) is used to calculate modified cross-sectional area of the for the specimen given axial strain:

$$A_c' = A_c \times \left(1 + \frac{D_r - 1}{\varepsilon_f} \times \varepsilon \right) \tag{4-26}$$

where A_c' is the modified corrected cross-sectional area, A_c is the cross-sectional area that is calculated by any selected theoretical equations (e.g. cylindrical or parabolic area correction methods), D_r is the ratio of the cross-sectional area which is calculated from theoretical equation at the end of shearing and the cross-sectional area which calculated by using the diameter that is measured at the middle height of specimen in the end of test, $\in_f$ is the axial strain value at the end of shearing and $\in$ is the any given axial strain. Using (4-26), the whole corrected cross-sectional area values for the given strains are scaled with respect to actual cross-sectional area at the end of shearing. An alternative procedure for the measurement of specimen's diameter based on image processing is given in Appendix A.

Oedometer test specimens were prepared by compacting Mersin silt sample at 0.102 initial water content to initial void ratio of 0.72 in single layer. For UU triaxial test specimens, Mersin silt sample at water content of 0.102 was compacted in ten layers to void ratio of 0.72 with undercompaction ratio of 0.06 (Ladd, 1978). Specimens' water contents are adjusted using methods proposed by Kenanoğlu and Toker (2018). The results of the practical tests are illustrated in Fig. 4.30 and 4.31. The results of the practical test carried out on Ankara clay specimens are given in Appendix C.

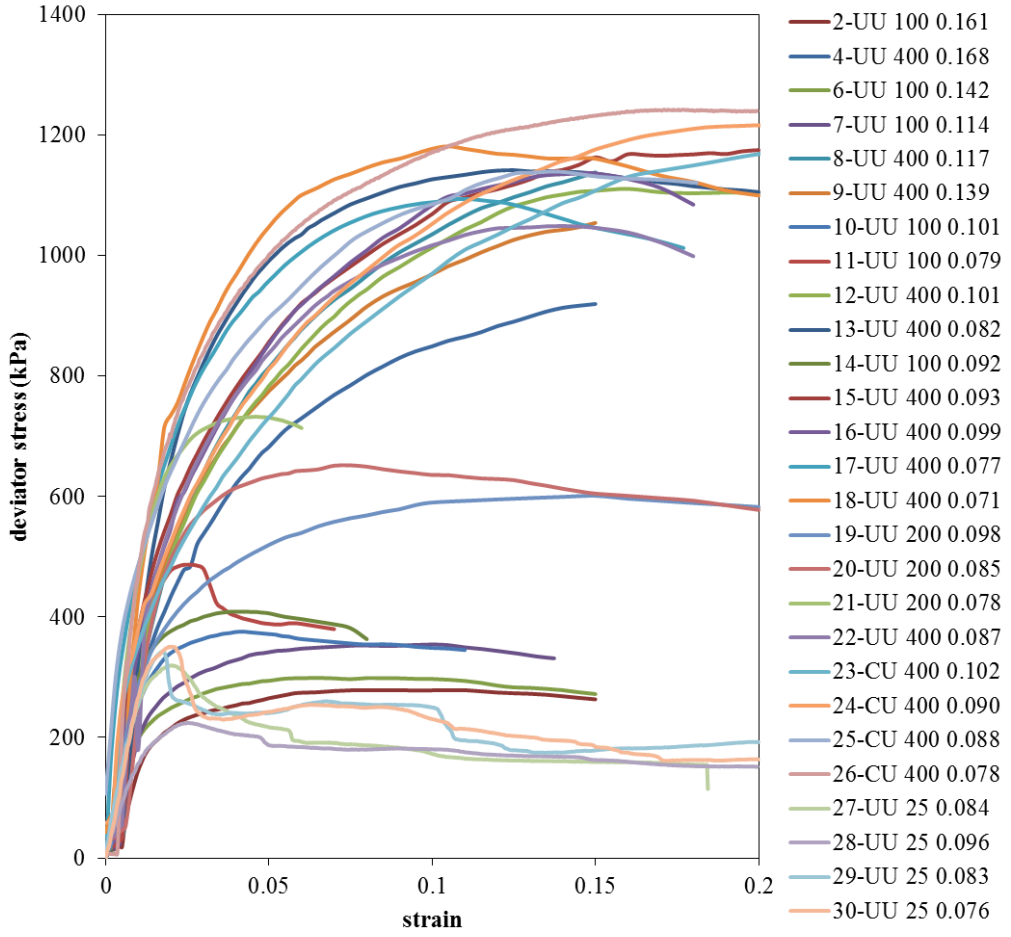

Figure 4.30 Results of UU tests carried out with unsaturated Mersin silt specimens at 25-100-200-400 kPa cell pressures (serie labels denote test cell pressure and gravimetric water contents)

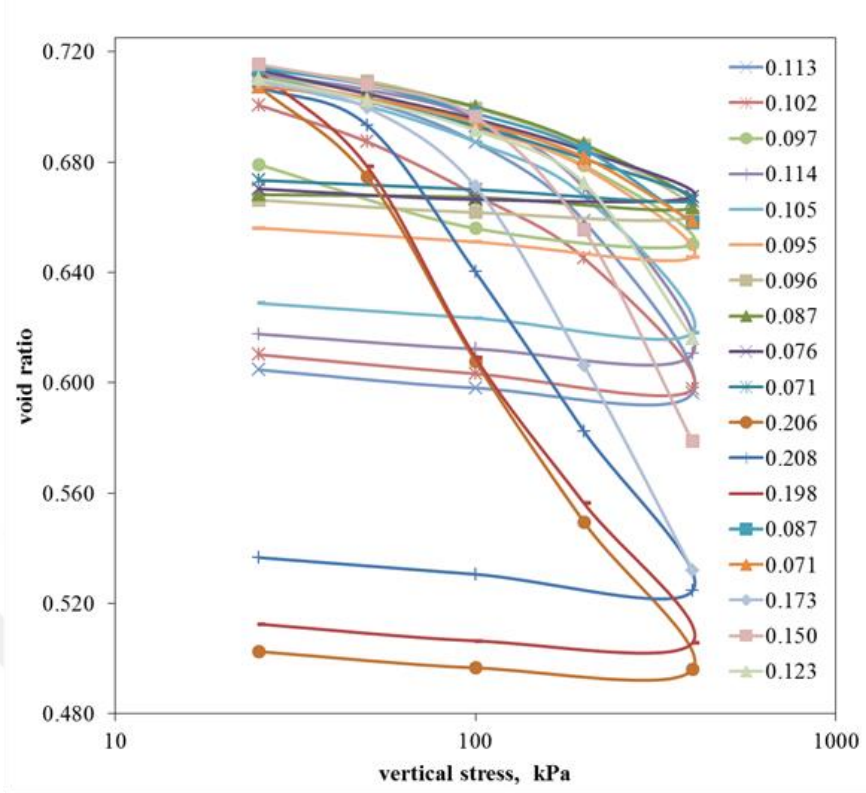

Figure 4.31 Oedometer tests with unsaturated Mersin silt specimens (series labels denote initial gravimetric water contents)

4.4.2 Assumptions in Modelling Practical Tests with BBM

The aforementioned practical test procedures can be considered as quick constant water content tests. This is most likely a problematic assumption when testing specimens at relatively higher water contents. However, the hydraulic conductivity of specimens at relatively lower water contents is expected to be quite low, which results in strict restriction of soil water expulsion from specimen. Therefore, testing of specimens only at relatively lower water contents is required for the test protocol.

The separation of relatively higher and relatively lower water contents is discerned from soil water retention curve, or an evaporation test, that is another practical test method which will be elaborated in the next paragraph. Soil water retention curve

measurement is required laboratory work item for the proposed parameter calibration protocol for estimating unsaturated specimen's suction from water content measurement. Soil water retention curve can also provide indication for relatively lower water contents. The soil water at residual saturation is held in the form of isolated pockets around soil particles. The interruption of hydraulic connectivity around residual saturation value results in immobility of soil water (Romero et al. 1999, Or et al. 2013) and specimen's hydraulic conductivity declines substantially near the residual state. The description "relatively lower water contents" can be ascribed to water contents near residual saturation. Residual state manifests itself as the second bend on a soil water retention curve at higher suctions. However, at the tail of soil water retention curve corresponding to the residual state, even very small water content changes result in drastic change of suction. Estimating suction from the soil water retention curve's tail portion is prone to significant error that can deviate the results of parameter optimization. Therefore, water contents slightly higher than residual saturation are preferred.

The more specific designation of relatively lower and higher water contents can be based on critical water content w_{cr} which is an experimental parameter determined from a simple evaporation test. In the evaporation test, a saturated specimen is placed on the mass balance and the decrease of specimen's mass due to evaporation under ambient conditions is monitored. The outcome is the rate of drying versus water content curve. The critical moisture content corresponds to the point that separates two distinct stages on the drying rate versus water content curve. Critical moisture content is deemed to be an intended indicator for mobile and immobile soil water fractions. The selection of initial water content of unsaturated specimens in the parameter calibration protocol is established on the basis of aforementioned interpretation: Unsaturated specimens at initial water contents from critical moisture content up to 4 percent higher than that value are used for oedometer and UU triaxial tests.

Evaporation tests were performed on a variety of soils including two different MH silts (Mersin silt and Elazığ silt), one poorly graded sand (quartz sand) soil and one

highly plastic clay (Ankara clay) soil. Critical moisture contents were determined as 0.055 for Mersin silt, 0.059 for Elazığ silt, 0.038 for quartz sand and 0.287 for Ankara clay. Soil water retention curves were extracted on these soils and shown in Fig. 4.32 together with selected portion for the range of unsaturated specimens' initial water contents. The prescribed range of water contents falls on the lower portion of the soil water retention curve. In Fig. 4.33, variation of unsaturated hydraulic conductivity within the w_{cr} and w_{cr}+0.04 interval is investigated. The suction ranges at the selected water content interval were estimated from the soil water retention curves and they were determined as 390 kPa to 2450 kPa for Mersin silt, 330 kPa to 1809 kPa for Elazığ silt, 654 kPa to 1038 kPa for Ankara clay and 8 kPa to 11 kPa for Quartz sand. At the highest value of water content, that is w_{cr}+0.04, the soils' hydraulic conductivities vary between 10^{-10} and 10^{-12} m/sec.

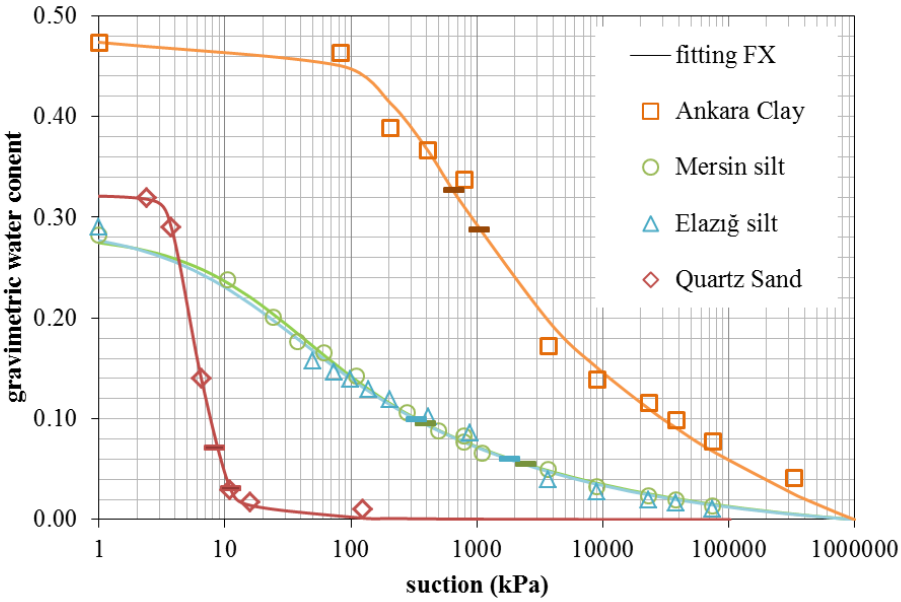

Figure 4.32 Soil water retention curves of soils used in this study. The dashes denote the w_{cr} and w_{cr}+0.04 interval. The equation proposed by Fredlund and Xing (1998) (FX) is used to fit experimental data

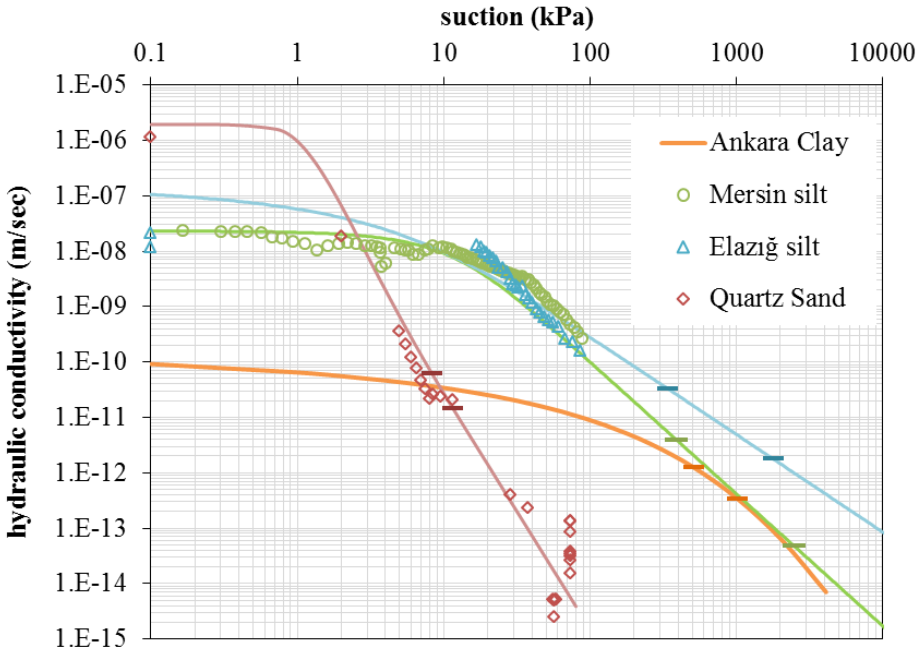

Figure 4.33 Hydraulic conductivity functions of soils used in this study. The dashes denote the w_{cr} and w_{cr}+0.04 interval (HYPROP results for Mersin and Elazığ silts provided by Eyüpgiller and Ülker, 2018)

Previous experimental studies on soil compaction curves have revealed that suction is essentially controlled by water content on the dry side of optimum rather than deformation (Romero, 1999; Dineen et al., 1999; Tombolato and Tarantino, 2005; Gonzalez and Colmeranes, 2006; Tarantino and De Col, 2008). This feature is attributed to the immobility of intra-aggregate soil water which is held in bonded on the particle surfaces. Chen et al. (2021) proposed a simple triaxial test method based on this behavioural feature. In their study, triaxial test specimens are equilibrated with various chemical salt solutions inside a sealed environment to impose a known initial high suction. Then, the specimens are triaxially sheared by preventing drainage to satisfy constant water content condition, thereby resulting in constant suction during triaxial shearing since suction is independent from the void ratio at high suctions. A similar approach is referred in this study and specimens' suction is presumed constant during practical tests.

4.4.3 Determination of BBM Parameters

The BBM parameters can be classified as a) parameters that define the initial conditions: v_0 is the initial specific volume, s_0 is the initial suction, p_0^* is the preconsolidation stress for saturated state b) parameters defining the LC yield surface: reference stress p_c, that is the mean stress corresponding to the intersection of virgin compression lines at different suctions, defines the LC yield surface, $\lambda(0)$ is slope of saturated virgin compression line, k is the slope of elastic compression line, β controls the distance between virgin compression lines, r restricts the virgin compression line's slope at highest suction c) parameters defining the shear strength: G is the shear modulus for elastic state, M is the slope of critical state failure envelope and k describes the contribution of suction to the cohesion.

The unknown model parameters are optimized for an objective function which is the least square fitting of model predictions to the experimental data gathered from UU and oedometer tests. Non-linear optimization with Generalized Reduced Gradient (GRG) method, that is a numerical method programmed into Microsoft Excel, is used to obtain best combination of parameters yielding the minimum of the objective function.

4.4.3.1 Preparation of Experimental Data for Optimization Analysis

The difference between the experimental data consisting of UU and oedometer tests and the model predictions is delineated in terms of normalized deviatoric stresses.The same weight of experimental data points to establish measured deviatoric stresses up to peak value are normalized by dividing them by cell pressure for UU tests. The deviatoric stress values further from the peak deviatoric stress are excluded from the comparison and are not used in the optimization. In the case of oedometer tests, experimental deviatoric stresses are normalized by dividing them by confining stresses which are equal to the applied vertical stresses multiplied by lateral earth pressure coefficient K_0, which is calculated by Jaky's

(1948) formula ($K_0 = 1 - \sin f'$) for K_0 estimation. The error between experimental data point and model prediction for UU test and oedometer test is calculated with (4-27a) and (4-27b), respectively:

$$\eta_{UU} = \frac{q_e - q_p}{\sigma_c} \tag{4-27a}$$

$$\eta_{oed} = \frac{\sigma_{v,e}(1-K_0) - q_p}{\sigma_{v,e}K_0} \tag{4-27b}$$

where h_{UU} is the relative error in between experimental data point from UU test, q_e is the experimental deviatoric stress value, σ_c is the cell pressure applied in the UU test, $\sigma_{v,e}$ is the experimental data point of vertical stress in the oedometer test and q_p is the deviatoric stress from the model prediction. For UU test, q_e is calculated for the same axial strain value corresponding to the model prediction. The model parameters vary during optimization analysis resulting in different outcomes for predicted axial strains. Michaelis-Menten equation is used to fit experimental data (4-28) and used in determining experimental deviatoric stress data points corresponding to predicted axial strain from the model.

$$q_e = \frac{q_M \varepsilon_a}{K + \varepsilon_a} \tag{4-28}$$

where q_M and K are the parameters determined from best fitting of Michaelis-Menten equation to the experimental data.

For the oedometer test, $\sigma_{v,e}$ is calculated for the same void ratio value corresponding to the model prediction. A bilinear function similar to the compression curves of the BBM is used to fit experimental data in order to determine experimental vertical stress data points corresponding to predicted void ratio values from the model.

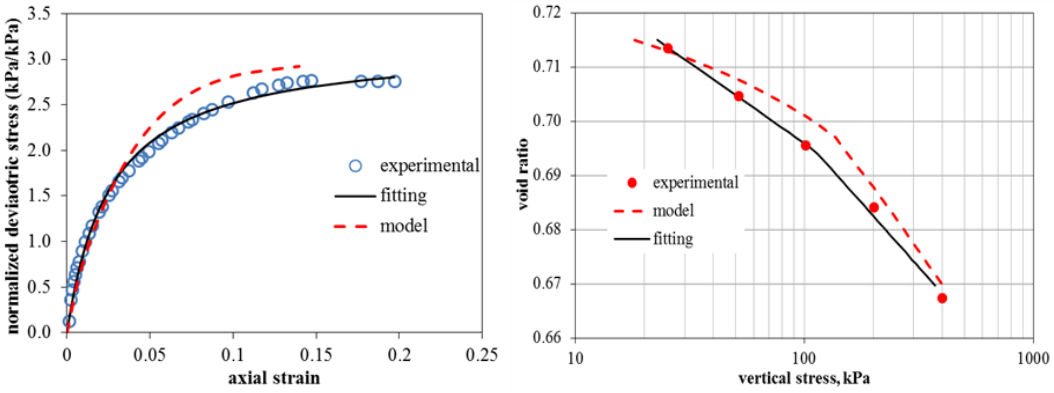

Figure 4.34 Fitting of experimental scattered data with continuous functions

4.4.3.2 Sequential Calibration of BBM Parameters

Nonlinear optimization with GRG method suffers from saddle points and solution does not guarantee true local minimum of the objective function depending on the initial values of the unknown parameters. Sequential calibration method is hereby proposed in order to avoid non-unique solution for best fitting combination of model parameters. Some of the parameters are determined based on their physical meaning using experimental data sets from practical unsaturated UU and oedometer tests together with conventional saturated triaxial and oedometer tests. However, the remaining parameters are optimized to end up being a set of parameters which best fit the overall experimental data. Step by step sequential calibration procedure is explained in the following:

1) Slope of elastic compression line `k` is estimated from the recompression or unloading lines of the oedometer tests. Estimated value is fixed for `k` prior to optimization of both triaxial and oedometer tests and excluded from the optimization. Following relationship converts recompression lines' slopes C_r on vertical stress axis to the mean stress axis:

$$\kappa = C_r \log\left(\frac{1+2K_0}{3}\right) \tag{4-29}$$

Another elastic state parameter is shear modulus G. Shear moduli are defined from experimental UU stress-strain curves for each test and excluded from the optimization using (4-40) such that $G=\sigma_{dev}/3/\varepsilon_{axial}$.

2) M is the slope of critical state line, and it can be directly determined from the saturated triaxial tests carried out at least at two different confining stresses. M is set to that value for unsaturated UU tests and excluded from the optimization.

3) $\lambda(0)$ is the slope of saturated virgin compression line on the mean stress axis, however different strategy is proposed to calibrate this parameter. Saturated triaxial shear behaviour is solely controlled by $\lambda(0)$, $\mathtt{k}$, M and p_0^* parameters. Deviatoric stress versus axial strain data from saturated triaxial tests at least two different confining pressures are best fitted only taking $\lambda(0)$ as independent variable. $\mathtt{k}$ and M are kept constant as the values determined in the previous steps. p_0^* value is the saturated preconsolidation mean stress and determined from the saturated isotropic compression curve. $\lambda(0)$ that best fits the saturated shear curves is fixed and excluded from the optimization analysis.

4) Shear strength of the soil is not fully mobilized in case of oedometer tests. $\lambda(0)$ and M parameters which are calibrated against saturated triaxial tests overestimate the saturated oedometric compression curve. Therefore, $\lambda(0)$ and M parameters that are specific to the saturated oedometer test are calibrated only using saturated oedometer test data similar to the saturated triaxial tests. p_0^* parameter in case of saturated oedometer test is directly determined as the preconsolidation stress on the converted saturated oedometric compression curve to the mean stress using Jaky's K_0 formula. $\lambda(0)$ and M that are best fit to the saturated oedometric compression curve are fixed for BBM model for oedometer test. M is constrained by its highest value as the value obtained in step 2 during best fitting of experimental data. Hence, different combination of $\lambda(0)$ and M are separately used for unsaturated UU triaxial tests and unsaturated oedometer tests during overall optimization of any remaining parameters.

5) k parameter describes the contribution of suction to the cohesion and UU triaxial test results are used to set its initial value. To do this, experimental apparent cohesion values are determined from UU triaxial shear tests based on the trigonometric interpretation on Mohr's circle:

$$c'' = \frac{\frac{\sigma_{d,e}}{2}(1-\sin\varphi) - \sigma_c \sin\varphi}{\cos\varphi} \tag{4-30}$$

where c'' is apparent cohesion, $\sigma_{d,e}$ is peak deviatoric stress for UU triaxial shear test, σ_c is confining stress or cell pressure and φ is friction angle. The contribution of suction to cohesion of soil is expressed as k parameter multiplied by suction (p_s=ks) in BBM. The relationship between suction contribution on cohesion and apparent cohesion is given in the following equation:

$$p_s = k \times s = \frac{c''}{\tan\varphi} \tag{4-31}$$

Using (4-31) experimental apparent cohesions are converted to p_s and corresponding suctions are estimated from soil water retention curve. Then a linear function is fitted on estimated suction versus p_s plot. The slope is set as the initial value for k in the optimization analysis.

6) The initial values for r and β are determined using oedometric compression curves. r parameter is related to the ratio of slope of virgin compression line at highest suction $C_{c,s\to\infty}$ to the slope of saturated virgin compression line $C_{c,sat}$. In the case of slope of virgin compression line at highest suction, the result from oedometer test at lowest gravimetric water content is used. The initial value for r is then obtained as in the following proportion:

$$r = \frac{C_{c,s\to\infty}}{C_{c,sat}} \tag{4-32}$$

Once r is determined, the initial value for β is determined by fitting (2-22) to all experimental slopes of oedometric compression curve, which are converted to

mean stress axis with similar procedure given in (4-29), taking β as independent variable together with pre-determined values of r and suctions estimated from soil water retention curve.

7) The initial values for preconsolidation stress corresponding to saturated state p_0^* for oedometer tests are revealed from the oedometric compression curves. The experimental preconsolidation stresses p_0 are determined from the saturated and unsaturated oedometric compression curves based on standard inspection procedure (i.e. intersecting bilinear portions and taking the stress corresponding to intersection as preconsolidation stress). p_0^* values are calculated from (2-21) keeping it as dependent on k, $\lambda(0)$ and p_c parameters which vary during optimization process. In case of unsaturated UU tests, the compression curves are missing and experimental preconsolidation stresses cannot be used to prescribe initial values for p_0^*. The initial value of p_0^* for each UU test is set as same as determined from isotropic compression curve of saturated triaxial test. Then p_0^* for unsaturated UU tests are taken as unknown and included as variable which is calibrated in the optimization process.

8) The reference stress p_c influences the stress point where the plastic deformations commence. Unrealistic shapes for predicted oedometric compression and triaxial shear curves emerge when p_c values are out of a certain range for the combination of parameters that are previously prescribed in the former calibration steps. Hence the initial value of p_c is prescribed by manual adjustment to any value which results in smooth shapes for oedometric compression and triaxial shear curves.

9) After setting the initial values for all parameters, optimization analysis (see Section 4.4.4) is carried out to minimize the objective function by defining r, β, k, p_c and p_0^* of UU tests parameters as variables and excluding k, $\lambda(0)$, M and p_0^* of oedometer tests.

4.4.4 Implementation of BBM into a Spreadsheet

Deviatoric stress state formulations of BBM in the stress incremental form are implemented into a spreadsheet presuming constant suction. There is no need to implement all features and capabilities of BBM in the coding process. SI yield surface components of BBM is not included in the spreadsheet formulations due to constant suction condition. Implementation of formulations only covers specified stress path for each practical test type in order to keep the coding process in its simplest form.

The stress path for practical UU triaxial test has a slope of 3 in p-q plane resulting in $\Delta p=\Delta q/3$ whereas K_0 stress path is chosen for practical oedometer test and the net mean stress increment Δp for a given deviatoric stress increment Δq is:

$$\Delta p = \Delta q \frac{1+2K_0}{3(1-K_0)} \tag{4-33}$$

The deviatoric stress increment Δq is specified to cover the range of experimental initial and final deviatoric stresses within 40 calculation steps in order to be able to simultaneously optimize BBM parameters for both oedometer and UU triaxial tests. The number of calculation steps can be increased, but the numerical exercises on the selected soil's test results in this study reveal that 40 calculation steps are suitable for modeling the oedometric compression and UU triaxial shear curves. In case of oedometer test, a constant Δq is calculated depending on soil's K_0 and initial and final vertical stresses since oedometer test is a stress-controlled test. However, UU triaxial test is a strain-controlled test and deviatoric stresses vary for each test. Δq for UU triaxial test is determined from the maximum deviatoric stress point where stress path with a slope of 3 intersects the critical state line in order to avoid computational errors in model predictions during optimization process in which model parameters are randomly altered.

$$q_M = \frac{3M\left(p_s + p\right)}{3-M} \tag{4-34}$$

where q_M is the deviatoric stress value intersecting the critical line, p is a constant value and equal to the cell pressure of the test. Δq is calculated by dividing q_M to number of calculation steps, hence deviatoric stress increment is recalculated for each optimization analysis iteration. This results in smooth transition within 40 calculation steps from zero deviatoric stress to the theoretical peak deviatoric stress value for any combination of model parameters.

Cumulative summation of Δq and Δp defines the stress path:

$$q^i = q^{i-1} + \Delta q \tag{4-35a}$$

$$p^i = p^{i-1} + \frac{\Delta q}{3} \tag{4-35b}$$

$$p^i = p^{i-1} + \Delta q \frac{1+2K_0}{3(1-K_0)} \tag{4-35c}$$

Superscript i denotes the calculation step number and initial values are defined for i=1. In case of UU triaxial test, q^0 is zero and p^0 is equated with the cell pressure in the test, and for oedometer test, q^0 is adjusted as it coincides with the vertical stress in the first step loading during oedometer test.

Initial value for preconsolidation stress p_0 is calculated from (2-21) and successive values are determined from (2-25) by taking yield surface function f=0:

$$p_0^{i=0} = p_c \left(\frac{p_0^{*i=0}}{p_c} \right)^{\frac{\lambda(0)-\kappa}{\lambda(s)-\kappa}} \tag{4-36a}$$

$$p_0^i = \frac{\left(q^i\right)^2}{M^2\left(p^i + ks\right)} + p^i \tag{4-36b}$$

If p_0^i is lower than the initial value of preconsolidation stress calculated in (4-36a) stress state is inside elastic region, otherwise plastic deformations occur.

The preconsolidation stress corresponding to the saturated state p_0^* is then calculated from (2-22):

$$p_0^{*i} = p_c \left(\frac{p_0^i}{p_c} \right)^{\frac{\lambda(s)-\kappa}{\lambda(0)-\kappa}} \tag{4-37}$$

The elastic and plastic strain increments are calculated in the following equations based on the updated hardening parameters:

$$d\varepsilon_{e,vp}^i = \frac{\kappa}{v^{i-1}} \frac{p^i - p^{i-1}}{p^i} \tag{4-38}$$

$d\varepsilon_{e,vp}^i$ is the elastic volumetric strain due to change in net mean stress, v^{i-1} is the specific volume in the preceding calculation step.

$$d\varepsilon_{p,vp}^i = \frac{\lambda(0)-\kappa}{v^{i-1}} \frac{p_0^{*i} - p_0^{*i-1}}{p_0^{*i}} \tag{4-39}$$

$d\varepsilon_{p,vp}^i$ is the plastic volumetric strain due to change in net mean stress. (4-39) is constrained with the condition of preconsolidation stress p_0^i being higher or equal than its initial value, otherwise $d\varepsilon_{p,vp}^i$ is taken as zero.

$$d\varepsilon_{e,q}^i = \frac{1}{3G}\left(q^i - q^{i-1}\right) \tag{4-40}$$

$d\varepsilon_{e,q}^i$ is the elastic shear strain due to change in deviatoric stress and it is taken as zero when p_0^i is higher or equal to its initial value.

$$d\varepsilon_{p,q}^i = d\varepsilon_{p,vp}^i \frac{2q^i\alpha}{M^2\left(2p^i + ks - p_0^i\right)} \tag{4-41}$$

$d\varepsilon_{p,q}^i$ is the plastic shear strain induced by change in deviatoric stress. $d\varepsilon_{p,q}^i$ is taken as zero when p_0^i is lower than its initial value.

The specific volume is calculated from the elastic and plastic strains:

$$v^i = v^{i-1} - v^{i-1}\left(d\varepsilon^i_{e,vp} + d\varepsilon^i_{p,vp} + d\varepsilon^i_{e,q} + d\varepsilon^i_{p,q}\right) \tag{4-42}$$

In case of UU triaxial shear test's model, axial strain increment $d\varepsilon^i_a$ is calculated from elastic and plastic strain increments and axial strain is the cumulative summation of axial strain increments:

$$d\varepsilon^i_a = \frac{\left(d\varepsilon^i_{e,vp} + d\varepsilon^i_{p,vp}\right)}{3} + d\varepsilon^i_{e,q} + d\varepsilon^i_{p,q} \tag{4-43}$$

In oedometer test's model, vertical stress σ^i_v is calculated from net mean stress and deviatoric stress:

$$\sigma^i_v = \frac{3p^i + 2q^i}{3} \tag{4-44}$$

Aforementioned coding process is repeated for each test used for the calibration of BBM parameters. Summation of square of the relative errors (4-27a and 4-27b) for all data points, each test has 40 data point and total number of relative errors is equal to number of practical tests multiplied by 40, results in the objective function. Optimization aims to minimize the objective function value through randomly adjusting prescribed BBM parameters.

Table 4.7 Illustration of spreadsheet calculations of UU triaxial shear test in BBM

i	q	p	p_0	p_0^*	$d_{e,vp}$	$d_{p,vp}$	$d_{e,q}$	$d_{p,q}$	v	$d_{e,a}$	h_{UU}
0	0	$\sigma_{c,test}$	4-36a	$p_0^{*}{}_{,opt}$					$v_{0,test}$		4-27a
1	4-35a	4-35b	4-36b	4-37	4-38	4-39	4-40	4-41	4-42	4-43	⋮
⋮	⋮	⋮	⋮	⋮	⋮	⋮	⋮	⋮	⋮	⋮	
40	4-34										

Table 4.8 Illustration of spreadsheet calculations oedometer test in BBM

i	q	p	p_0	p_0^*	$d_{e,vp}$	$d_{p,vp}$	$d_{e,q}$	$d_{p,q}$	v	σ_v	h_{oed}
0	$q_{0,test}$	4-35c	4-36a	$p_0^{*}{}_{,test}$					$v_{0,test}$	4-44	4-27b
1	4-35a	4-35c	4-36b	4-37	4-38	4-39	4-40	4-41	4-42	4-44	⋮
⋮	⋮	⋮	⋮	⋮	⋮	⋮	⋮	⋮	⋮	⋮	
40										$\sigma_{v,test}$	

4.4.5 Example of Sequential Calibration of BBM Parameters

Sequential calibration procedure of BBM parameters is demonstrated using experimental data from conventional oedometer and triaxial tests together with practical oedometer and UU tests on saturated and unsaturated Mersin silt specimens. Experimental data consists of 1 saturated oedometer test, 2 saturated CD triaxial tests which are performed at 100 kPa and 400 kPa confining stresses, 3 unsaturated oedometer tests on specimens at initial water contents of 0.076, 0.095, 0.105, 2 UU triaxial shear tests at 100 kPa confining stress with specimens having initial water contents of 0.101, 0.092 and 2 UU triaxial shear tests at 400 kPa confining stress with specimens having 0.102, 0.082. The preparation water content of 0.104 for both unsaturated oedometer and UU specimens are adjusted to prespecified initial water contents by exposing them to air drying according to Kenanoğlu and Toker (2018).

1) The first step is to determine the slope of elastic compression line k. The internal friction angle of Mersin silt specimen is determined as 35.5° from saturated CD triaxial tests. The coefficient of lateral earth pressure K_0 is estimated as 0.42 from Jaky's formula. The slope of oedometric recompression lines defined in vertical stress axis are determined and converted to mean stress axis based on (4-29) such as 0.0059, 0.0058, 0.0072. The average of 0.006 is set to value of k. Shear modulus G is set as 12000 kPa for all UU triaxial tests.

2) The value of critical state line M is determined from saturated CD triaxial tests as 1.44.

3) BBM model is fitted to saturated CD triaxial shear test results by only optimizing $\lambda(0)$ and prescribing k as 0.006, M as 1.44 and p_0^* as 127 kPa prior to optimization. The value of p_0^* is determined from the isotropic compression curve which is extracted during the consolidation stage of saturated CD triaxial test at 400 kPa confining stress. Other BBM parameters do not have any influence on the prediction of saturated shear curves hence they are excluded. $\lambda(0)$ is determined as 0.129 after simultaneously fitting BBM to two saturated triaxial shear tests (Fig. 4.35).

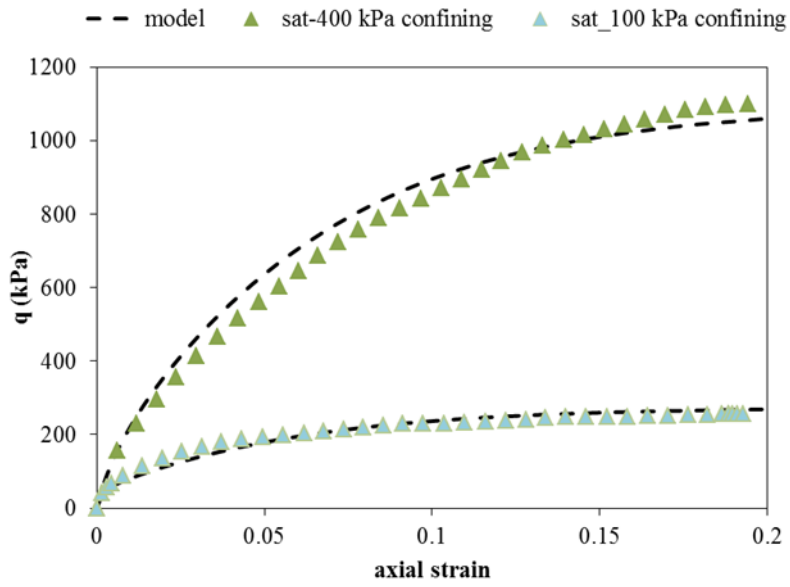

Figure 4.35 Fitting BBM to saturated triaxial tests at 100 kPa confining stress and 400 kPa confining stress for the calibration of $\lambda(0)$

4) Separate values of $\lambda(0)$ and M along K_0 stress path are determined only fitting BBM to saturated oedometer test. The upper limit for M is set as 1.44 prior to optimization. p_0^* is determined from the saturated oedometric compression curve itself. The preconsolidation vertical stress is determined as 44 kPa and the mean stress equivalent p_0^* is calculated as 27 kPa after multiplying with $(1+2K_0)/3$. k is

again taken as 0.006. After best fitting the saturated oedometric compression curve with BBM, $\lambda(0)$ and M are respectively optimized as 0.04 and 1.142 (Fig. 4.36).

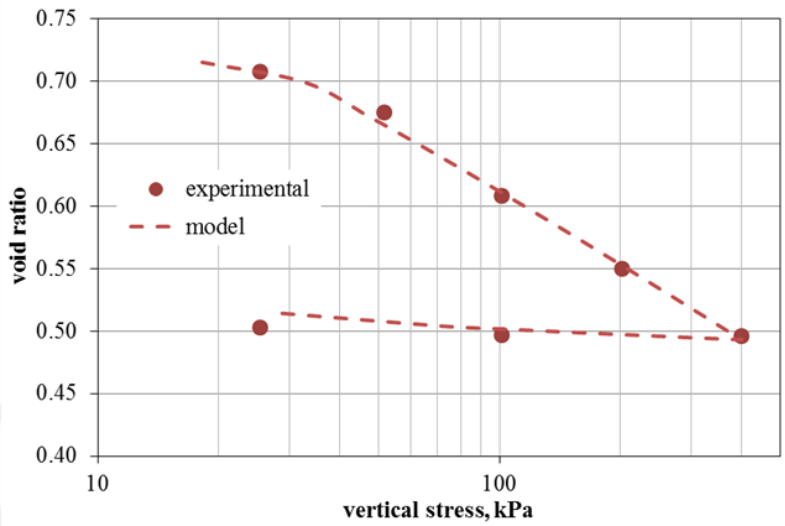

Figure 4.36 Fitting BBM to saturated oedometer test for the calibration of $\lambda(0)$ and M

5) Initial value for k parameter is determined from UU triaxial test results. Experimental apparent cohesions are calculated from (4-30) and converted to suction contribution to cohesion p_s using (4-31) (Table 4.7). Specimens' suctions are estimated from soil water retention curve.

Table 4.9 Determination of p_s from UU triaxial tests

Confining stress, σ_c (kPa)	Water content, w_c	Estimated suction, s (kPa)	Deviatoric stress, σ_d (kPa)	Apparent cohesion (kPa)	Cohesion increase (p_s=ks) (kPa)
100	0.101	320.6	375.8	25.5	35.7
100	0.092	421.8	408.8	34.0	47.6
400	0.101	317.8	1110.7	0.7	1.0
400	0.082	595.9	1141.6	8.7	12.1

Experimental p_s values are plotted against estimated suctions to fit linear function $y=mx$ resulting in initial value of k parameter as 0.053 (Fig. 4.37).

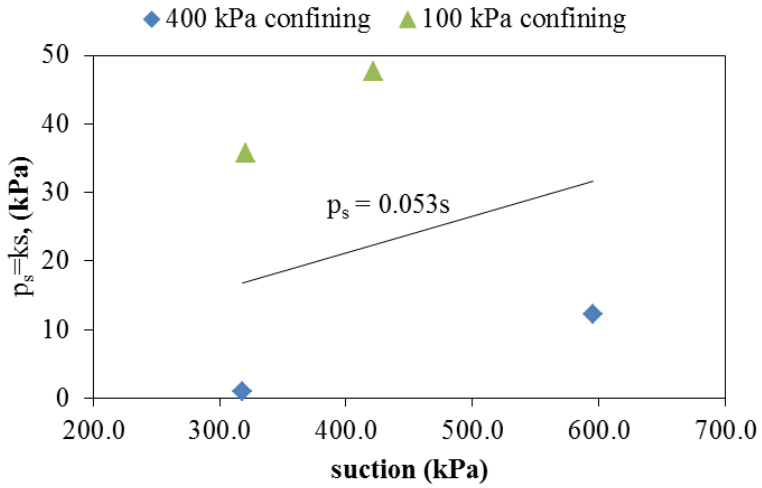

Figure 4.37 Determination of initial value for *k* parameter through fitting a linear function to UU triaxial test data

6) The initial value for *r* parameter is determined from proportion of oedometric compression line's slope for test at water content of 0.076, which is the lowest one among the oedometer tests, to that of saturated oedometeric curve. The ratio is 0.047/0.188=0.253 and taken as the initial value of *r*. (2-22) is fitted to all experimental slopes of oedometric compression curves C_c in order to determine the initial value of β parameter. In Table 4.10, C_c values are the slopes of oedometric compression lines plotted on the vertical stress axis, λ_s values are the conversion of C_c values after multiplying them with $\log((1+2K_0)/3)$ and $\lambda_{s,(2\text{-}22)}$ values give the result from (2-22) after best fitting. The initial value for β is determined as 0.0031 for the *r* parameter set constant as 0.253 (Fig. 4.38).

Table 4.10 Determination of initial values for *r* and β parameters

Estimated suction, s (kPa)	C_c	λ_s	$\lambda_{s,(4\text{-}31)}$
750.9	0.047	0.009	0.012
384.6	0.079	0.016	0.018
279.0	0.116	0.023	0.021
0.0	0.188	0.037	0.037

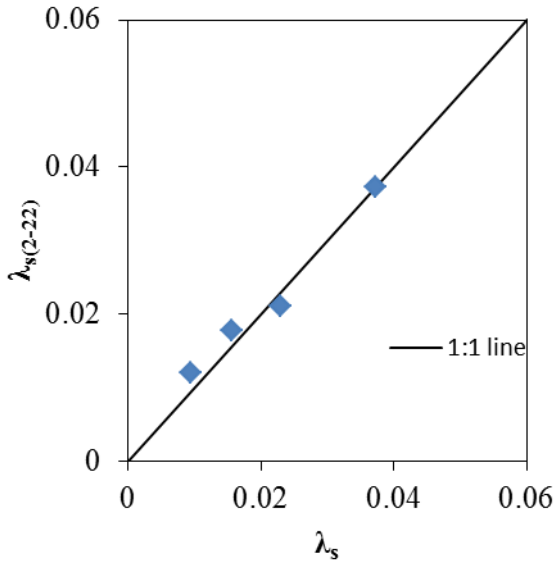

Figure 4.38 Comparison of experimental slopes of oedometric compression lines and predicted ones from (2-22) after best fitting of parameter β.

7) Preconsolidation stress p_0 for unsaturated oedometer tests are inferred from the experimental oedometric compression curves as 117 kPa for test at water content of 0.076, 111 kPa for test at water content of 0.095, 114 kPa for test at water content of 0.105. The preconsolidation stress corresponding to saturated state p_0^* is calculated from the predefined p_0 values using (2-21) in the model. Hence the initial guess of p_0^* vary depending on predefined p_0 values during parameter optimization analysis in case of oedometer tests. For the UU triaxial shear tests, the initials of p_0^* are prescribed equal to the value from the saturated as 127 kPa.

8) The initial value for reference stress p_c is manually adjusted to any value that results in smooth shape for UU triaxial shear curves when the all other parameters are set to their initial values. The initial value of p_c is adjusted to 35 kPa since lower values induce only elastic behaviour resulting in a linear stress-strain curve which only depends on the shear modulus G.

9) The initial values are prescribed as given in the aformentioned steps. r, β, p_c, k and initial p_0^* values for each UU triaxial test are varied during optimization

analysis and all other parameters such as G, k, M, $\lambda(0)$ and initial p_0^* values for oedometer tests are excluded. The set of parameters after optimization analysis together with their initial values are given in Table 4.11. The results of fitting BBM to practical test results after optimization analysis are given in Fig. 4.39 and 4.40.

Table 4.11 Optimized BBM parameters both for UU triaxial shear and oedoemeter tests together with their initial values prior to optimization. The best-fitted set of parameters on data from suction-controlled CD tests are also added in the last column.

parameters	***UU*** + ***Oedometer (oed) (initials)***	***UU*** + ***Oedometer (oed) (optimized)***	***CD*** ***(optimized)***
λ(0)	0.129 (0.04 for oed)	0.129 (0.04 for oed)	0.129
κ	0.006	0.006	0.006
r	0.253	0.307	0.471
β	0.0031	0.002	0.016
$\mathbf{p^c}$	35	40	42
k	0.053	0.104	0.208
M	1.44 (1.142 for oed)	1.44 (1.142 for oed)	1.44
$\mathbf{p^*_{0,test1}}$	127	179	-
$\mathbf{p^*_{0,test2}}$	127	146	-
$\mathbf{p^*_{0,test3}}$	127	155	-
$\mathbf{p^*_{0,test4}}$	127	160	-

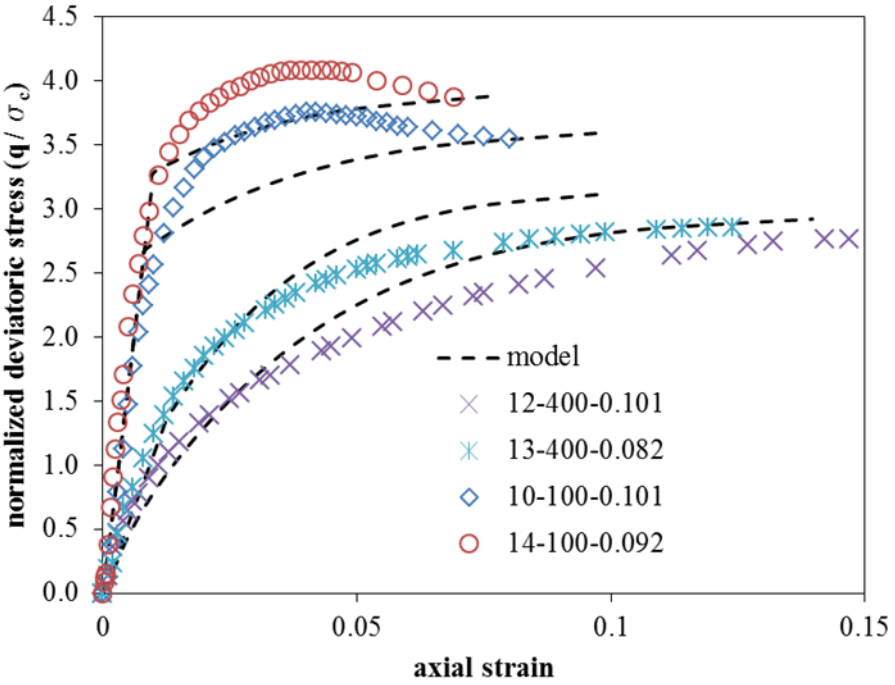

Figure 4.39 BBM predictions for UU triaxial shear tests after optimization analysis

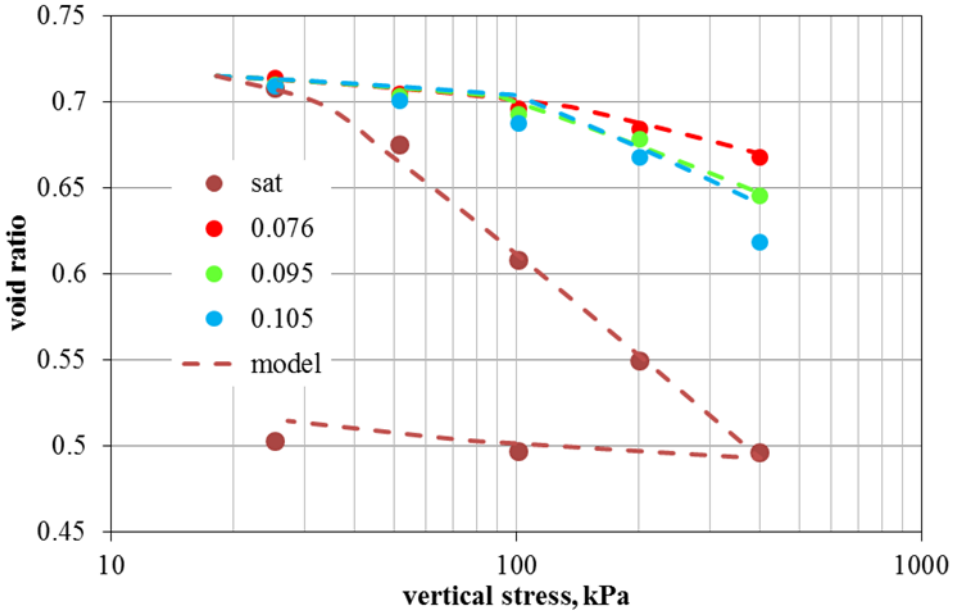

Figure 4.40 BBM predictions for oedometer tests after optimization analysis

The evaluation of proposed calibration method for BBM parameters is done by introducing suction controlled triaxial test results on the same soil specimens. Suction controlled triaxial test results were provided by Ahmadi-Naghadeh (2016). Experimental data (MCD02 –p100s100-, p and s respectively denote net confining stress and suction and their values in subsequent number, MCD03 -p400s100-, MCD05 –p100s200-, MCD06 –p400s200-, MCD08 –p100s400- and MCD09 –p400s400-) are compared with the predicted triaxial shear curves determined from calibrated BBM parameters. Suction controlled triaxial test results are fitted with BBM model and set of model parameters are given in Table 4.15. The set of parameters calibrated from practical UU and oedometer tests -the set of parameters given in column labeled as "UU (optimized)" in Table 4.15 is used for predicting suction controlled CD triaxial test data.

In Fig. 4.41, comparison of predicted triaxial shear curves from both set of parameters from best fitting of suction controlled CD test results and proposed calibration procedure on practical UU and oedometer test results is presented. The difference in k parameter affects the predicted peak deviatoric stresses, all predicted shear curves determined from set of parameters based on proposed practical calibration procedure underestimate the peak deviatoric stresses in suction controlled CD test results. But, proposed calibration method produces effective outcomes in predicting experimental behaviour monitored with advanced test techniques in unsaturated soil mechanics.

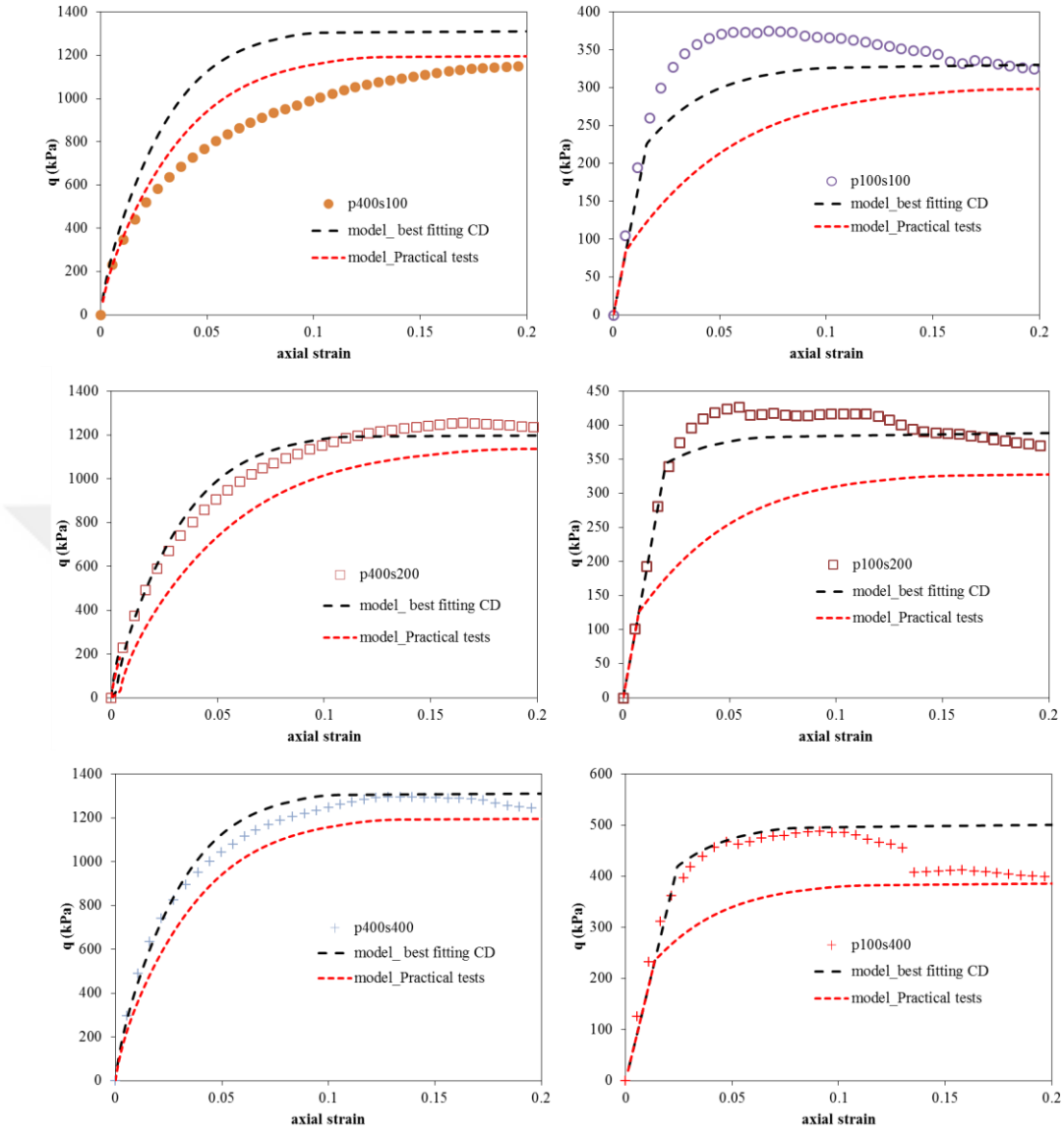

Figure 4.41 Comparison of predicted shear curves determined from set of parameters obtained through best fitting of BBM to suction controlled CD tests and shear curves determined from proposed calibration procedure on practical UU and oedometer test results

CHAPTER 5

CONCLUSION

In this research, simple and consistent methods in the implementation of unsaturated soil mechanics into engineering practice is investigated. Main components of this study can be categorized as: a) performing a large set of experiments on saturated and unsaturated soils b) theoretical study and c) developing practical test procedures and methods to extract unsaturated soil parameters.

A large set of tests were carried out on two low plastic silts and one highly plastic clay soils during the experimental campaign in this study. Isotropic and K_0 consolidated drained triaxial test were completed on saturated specimens of choosen soils. Constant suction and constant water content triaxial tests based on axis translation technique were completed to reveal unsaturated behaviour. Furthermore, the vapor equilibrium technique together with the double cell method were implemented to investigate the behaviour highly plastic clay under isotropic loading condition.

Novel test setups were developed for soil water retention curve extraction and testing of unsaturated specimens. The water retention behaviour of studied soils were determined in a wide range of suction implementing hanging column method, axis translation technique and vapor equilibrium method.

A complete framework of practical procedures was presented to obtain unsaturated soil properties.

5.1 Changing Specimens' Water Contents without Suction Control

In the section 4.1, practical and rapid methods for adjusting water content of triaxial test specimens were investigated and several procedures were proposed. Two different soils (CH and ML) were used during trials. The capillary soaking method did not yield useful results. The most important factor affecting duration for water content homogenization appears to be the flow distance. For low-plasticity specimens, changing water content through its lateral surface is shown to be a viable way to obtain homogeneous distribution of water content in a short period of time. Using a sprayer to moisten the specimen in the radial direc-tion resulted in acceptable homogeneity. High-plasticity specimens are successfully wetted inside a rigid, perforated mold that restricts radial and vertical strains to prevent localized swelling of the specimen. This process can be applied in multiple stages to reduce hysteresis effects.

For lowering the water content to a homogeneous value, leaving specimens to evaporate in open-air resulted in success, only if the specimen is turned up-side down halfway through the process.

Specimens are sealed in nylon bags during the water content equilibration stage that follows either drying or wetting procedures. It becomes possible to bring specimens to moisture equilibrium at various water contents in less than one week for several scenarios.

Such simplified procedures could be incorporated into conventional laboratory methodolgy, if unsaturated soil mechanics is to become more accessible for geotechnical engineering practice.

5.2 Evaluation of Shear Strength of Unsaturated Soils

Section 4.2 aims to provide a simple approach for the prediction of shear strength of unsaturated soils referring the previous works on different research fields. An

experimental parameter which can be easily calibrated through evaporation test is employed to estimate the shear strength of unsaturated soils. Simple evaporation tests are conducted to approximate the amount of soil water in the micropores. The experimental output is used for calibrating the parameter for shear strength equation proposed by Alonso et al. (2010). The validity of the assumption taking the critical moisture content as the microstructural state parameter is examined using constant suction and constant water content triaxial test results on selected soils. The shear strength of unsaturated specimens was predicted quite accurately.

5.3 Determination of HCF from Back Calculation of Outflow Data

In section 4.3, the hydraulic conductivity function of unsaturated soils can be back-calculated through numerical modelling of seepage during soil water retention curve measurement with axis translation technique considering the ceramic impedance. The time-series water mass change data during soil water retention curve extraction is collected and processed within the developed numerical model in order to estimate the hydraulic conductivity function. Numerical model can be easily implemented in a spreadsheet. The performance of the simple numerical model is validated using a wide range of soil types including poorly graded sand, non-plastic silt and highly plastic clay. The predictions are consistent with the available experimental data and it is considered that the proposed method could be used effectively for the estimation of hydraulic conductivity function of unsaturated soils. As a result, simple, cheap and yet accurate method in the estimation of unsaturated hydraulic conductivity is proposed.

5.4 Determination of BBM parameters

Simple and quick UU and oedometer tests are carried out on unsaturated soil specimens. The results covered in these tests together with the soil water retention curve measurements are processed in order to determine BBM parameters. A

reasonable prediction for BBM parameters is achieved from the proposed procedure.

5.5 Suggested Framework

This section summarizes the proposed practical methods as a laboratory protocol which could be preferred to determine unsaturated soil properties. The necessary tests are 1 saturated standart oedometer test, 2 saturated standart CD triaxial tests at low and high (e.g. 100 kPa and 400 kPa) confining pressures, 1 evaporation test, 3 practical oedometer tests on unsaturated specimens, 6 unsaturated practical UU tests at low and high confining pressures on unsaturated specimens, 1 soil water retention curve measurement. Saturated oedometer and CD triaxial tests, soil water retention curve measurements and evaporation test are commenced in the beginning of the proposed laboratory program. Once the critical moisture content is determined from the evaporation test as described in Section 4.2, practical unsaturated tests (see 4.4.1) are followed implementing water content adjusment procedures as given in Section 4.1. The techniques that are elaborated in Section 3.4 can be used to extract soil water retention curve. The HCF of the soil is determined during soil water retention curve measurements by implementing the proposed spreadsheet calculations presented in Section (4.3). Finally, all test results are processed as in Section 4.4 in order to predict BBM parameters. Depending on the type and the natural/initial water content of the undisturbed/compacted soil specimen, the total duration of the proposed laboratory program is constrained by the duration of whether saturated CD triaxial tests or soil water retention curve measurements. The proposed laboratory program is summarized in Fig. 5.1.

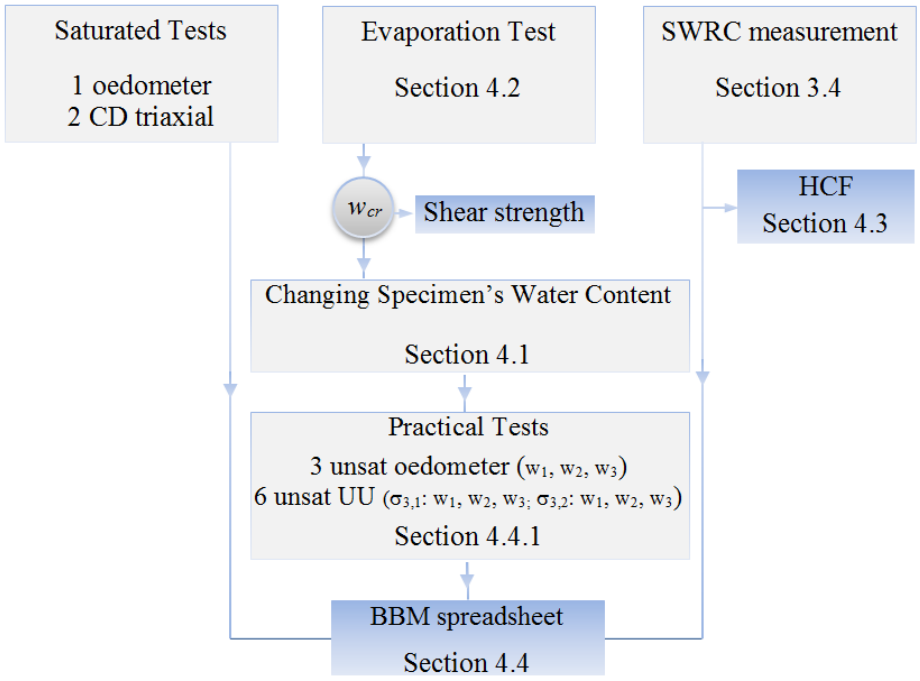

Figure 5.1 The proposed laboratory program for estimating unsaturated soil properties

5.6 Recommendations for Future Studies

- This work consists a large experimental campaign, however, the test results for Ankara clay should be enhanced after developing a new test setup. The experience gained in this study reveals that vapor equilibrium technique should be preferred to control suction and inner cell method can be implemented for volume change measurement; but, membrane properties should be suitable for the long term operations and higher confining stresses (i.e. a couple of MPa) must be applied on the test specimen in the new test setup.
- Several methods are developed in this study in order to propose practical procedures for the prediction of unsaturated soils' engineering parameters. In these studies, the soil water retention curve is always assumed as to be known. However, soil water retention curve extraction requires long testing durations, especially in case of wetting soil water retention curves.

Therefore, practical and accurate prediction methods for soil water retention curves might be developed based on the proposed approaches in this study.

- The approach proposed in the calibration of BBM parameters can be extended for other existing constitutive models.
- The performance of proposed practical procedures should be validated for new soils.
- The non-monotonic variation of degree of saturation during MCD10 test on Mersin silt should be investigated in a different test setup. After carrying out specific experimental study on this behaviour, new theories on soil water retention behaviour can be established.
- The volume change measurement method preferred in this work uses the method developed in Ahmadi-Naghadeh and Toker (2017). Their method provides accurate measurements for MH types soils used in this study. In the case of CH type Ankara clay, too slow loading rates were set during the trial tests in the axis translation based triaxial test setup. It is observed that the accuracy of the method becomes questionable for such slow loading rates. The method given in Ahmadi-Naghadeh and Toker (2017) can be extended considering the effect of loading rate on the viscoplastic behaviour of triaxial cell and tubings.

REFERENCES

Ahmadi-adli, M. 2014.Shallow Landslides Triggered by Rainfall in Unsaturated Soils. Doctor of philosophy dissertation in civil engineering, Middle East Technical University.

Ahmadi-Naghadeh, R. and Toker, N. K. 2017. Volume Change Measurement in Triaxial Tests by Monitoring Cell Fluid Volume Based on Viscoelastic Behavior of the Test Setup. Geotechnical Testing Journal, Vol. 40, No. 4, pp. 1–15, http://dx.doi.org/10.1520/GTJ20160093. ISSN 0149-6115

Ahmadi-Naghadeh, R., Toker, N. K. and Ahmadi-Adli, M. 2012. Water content variability of unsaturated soil specimens in conventional strength tests. 10th International Congress on Advances in Civil Engineering, 17-19 October 2012 Middle East Technical University, Ankara, Turkey

Ahmadi-Naghadeh, R.A. 2016. Hydro-mechanical behaviour of unsaturated isotropically reconstituted specimens from slurry and compacted specimens. Doctor of philosophy dissertation in civil engineering, Middle East Technical University.

Aitchson, G. D. 1965. Moisture Equilibria and Moisture Changes in Soils beneath Covered Areas. Butterworths.

Ajdari, M., Monghassem, M., and Reza Lari, H. 2016. A Modified Osmotic Diaphragmatic Oedometer for Investigating the Hydro-Mechanical Response of Unsaturated Soils. Geotechnical Testing Journal, Vol. 39, No. 6, pp. 906-921,

Alonso E.E., Gens A., Josa A. 1990. A constitutive model for partially saturated soils. Géotechnique; 40(3):405–30.

Alonso, E.E.,Pereira, J.M.,Vaunat, J. and Olivella, S. 2010. A microstructurally based effective stress for unsaturated soils. Géotechnique. 60. 913-925. 10.1680/geot.8.P.002.

Alonso, E.E., Pinyol N.M. & Gens, A. 2013. Compacted soil behaviour: initial state, structure and constitutive modelling. Geotechnique; 63(6):463–78.

Alonso, E.E. 2015. 7th Olek Zienkiewicz Summerschool on “Unsaturated Soil Mechanics: From Fundamentals to Applications”, May 25th- 29th 2015 Universitat Politecnica de Catalunya-Barcelona (Spain).

Arya, L. M. and Paris, J. F. 1981. Physicoempirical model to predict the SMC from particle size distribution and bulk density data. Soil Science Society of America Journal, Vol.45, pp.1023-1030.

ASTM D2216-10, Standard Test Methods for Laboratory Determination of Water (Moisture) Content of Soil

ASTM D2850-15, Standard Test Method for Unconsolidated-Undrained Triaxial Compression Test on Cohesive Soils

ASTM D4767, Standard Test Method for Consolidated Undrained Triaxial Compression Test for Cohesive Soils

ASTM D6836-02(2008)e2, Standard Test Methods for Determination of the Soil Water Chararcteristic Curve for Desorption Using a Hanging Column, Pressure Extractor, Chilled Mirror Hygrometer, and/or Centrifuge, ASTM International, West Conshohocken, PA, 2008

ASTM D7181, Standard Test Method for Consolidated Drained Triaxial Compression Test for Soils

ASTM D7664-10(2018)e1, Standard Test Methods for Measurement of Hydraulic Conductivity of Unsaturated Soils, ASTM International, West Conshohocken, PA, 2010

ASTM E104-02(2012), Standard Practice for Maintaining Constant Relative Humidity by Means of Aqueous Solutions

ASTM-D7263-(2021), Standard Test Methods for Laboratory Determination of Density and Unit Weight of Soil Specimens

Averjanov, S.F. 1950. About permeability of subsurface soils in case of complete saturation. English Collection,7,19-21.

Averjanov, S.F. 1950. About permeability of subsurface soils in case of complete saturation. English Collection,7,19-21.

Babu, G., Rao, R., and Peter, J. 2005. Evaluation of Shear Strength Functions Based on Soil Water Characteristic Curves. Journal of Testing and Evaluation, Vol. 33, No. 6, pp. 461-465,

Bao, C., Gong, B. and Zhan, L. 1998. Properties of unsaturated soils and slope stability of expansive soils, keynote lecture. Proc., 2nd Int. Conf. on Unsaturated Soils (UNSAT 98), Beijing, China, Vol.1, International Academic, 71-98.

Belhamri, A. 2003. Characterization of the First Falling Rate Period During Drying of a Porous Material, Drying Technology: An International Journal, 21:7, 1235-1252, DOI: 10.1081/DRT-120023178

Benson, C.H.,Gribb,M.M. 1997. Measuring unsaturated hydraulic conductivity in the laboratory and field. Unsaturated Soil Engineering Practise, Geotechnical Special Publication,vol.68,pp.113–168.

Bishop, A. W. 1959 . The principle of effective stress. Tek. Ukeblad, 106 39 , 859–863.

Bishop, A. W., and Gibson, R. E. 1963. The influence of the provisions for boundary drainage on strength and consolidation characteristics of soils measured in the triaxial apparatus, in Laboratory Shear Testing of Soils. ASTM STP No. 361,American Society for Testing and Materials, Philadelphia, PA, pp. 435–458.

Bishop, A. W., and Henkel, D. J. 1962. The Measurement of Soil Properties in the Triaxial Test , 2nd ed., Edward Arnold, London.

Bishop, A.W., and Donald, I.,B. 1961. The experimental study of partly saturated soil in the triaxial apparatus". Proc. 5th ICSMFE, Paris, 13-21.

Bishop, A.W.,and Henkel, D.J. 1964. The Measurement of Soil Properties in Triaxial Testing. Edward Arnold, London

Blatz, J.A., Cui, Y.J. And Oldecop, L. 2008. Vapour equilibrium and osmotic equilibrium technique for suction control. Geotech. Geol. Engng 26, No.6, 661-673.

Briggs, L.J. 1897. The mechanics of soil moisture. US Department of Agriculture, Division of Soils, Bulletin No.10.

Brooks, R., Corey, A. 1964. Hydraulic Properties of Porous Media. Hydrology Paper, 3, Colorado State University, CO, US.

Brooks, R., Corey, A. 1964. Hydraulic Properties of Porous Media. Hydrology Paper, 3, Colorado State University, CO, US.

Bruce, R., and Klute, A. 1956. The measurement of soil moisture diffusivity. Soil Science Society of America Proceedings, 20, 458-462.

Brutsaert, W. 1982. Evaporation into the atmosphere: Theory, history and applications. Kluwer Academic, Hingham, MA.

Buckingham, E. 1907. Studies on the Movement of Soil Moisture. US Department of Agriculture, Bureau of Soils No. 38.

Burdine, N.T. 1953. Relative permeability calculation from size distribution data. Transactions, American Institue of Miningi Metallurgical and Petroleum Engineers, 198, 71-78.

Burton, G., Pineda, J., Sheng, D. and Airey, D. 2015. Microstructural changes of an undisturbed, reconstituted and compacted high plasticity clay subjected to wetting and drying. Engineering Geology. 193. 10.1016/j.enggeo.2015.05.010.

Campbell, G. S. 1985. Soil Physics with Basic Transport Models for Soil–Plant Systems, Elsevier, New York.

Chen, B. Y., Gao, D. Sun and Li, J. 2021. Simple Testing Method for Measuring the Triaxial Stress-Strain Relations of Unsaturated Soils at High Suctions. Geotechnical Testing Journal 44, no. 2: 535–546. https://doi.org/10.1520/GTJ20190278

Childs, E.C., and Collis-George, N. 1950. The permeability of porous materials. Royal Society, London, Series A, 210, 392-405.

Chiu, T. F., Shackelford, C. D. 1998. Unsaturated hydraulic conducitivity of compacted sand-kaolin mixtures. J. Gecotech. Geoenviron. Eng., ASCE, Vol. 124, No. 2, pp. 160-170.

Corey, A.T. 1957. Measurement of water and air permeability in unsaturated soil. Proceedings Soil Science Society of America, 21(1), 7-10.

Crescimanno, G., and Iovino, M. 1995. Parameter estimation by inverse method based on one-step and multi-step outflow experiments. Geoderma, 68(4), 257-277.

Cui Y.J., Delage P. 1996. Yielding and plastic behaviour of an unsaturated compacted silt. Geotechnique; 46(2):291–311.

Cui, Y.J. and Delage, P. 1996. Yielding and plastic behaviour of an unsaturated compacted silt, Geotechnique, 46(2), 291-311.

Cui, Y.J., Yahia-Aissa, M. and Delage, P. 2002. A model for the volume change behaviour of heavily compacted swelling clays. Eng Geol 64(2-3):233-250.

Cuisinier, O. & Masrouri, F. 2005. Hydromechanical ehaviour of a compacted swelling soil over a wide suction range. Engineering Geology, Vol.81, pp.204-212.

Cuisinier, O. and Laloui, L. 2004. Fabric evolution during hydro-mechanical loading of compacted silt. International Journal for Numerical and Analytical Methods in Geomechanics. 28. 483 - 499. 10.1002/nag.348.

Çokça, E. 1991. Swelling potential of expansive soils with a critical appraisal of the identification of swelling of Ankara soils by methylene blue tests. Ph.D. - Doctoral Program, Middle East Technical University.

Daniel, D. 1983. Permeability tests for unsaturated soils. Geotech. Test. J., Vol. 6, No.2, pp. 81-86.

Delage, P., Howat, M.D. and Cui, Y.J. 1998. The relationship between suction and swelling properties in a heavily compacted unsaturated clay. Engineering Geology, 50, 31-48.

Delage, P., Lefebvre, G., 1984. Study of the structure of a sensitive Champlain clay and its evolution during consolidation. Can. Geotech. J 21, 21–35.

Delage, P., Romero, E. And Tarantino, A. 2008. Recent developments in the techniques of controlling and measuring suction in unsaturated soils. In: Unsaturated Soils: Advances in Geo-engineering, Toll, D.G. et al. (eds). Routledge, London, pp. 33-52. Proceedings of the First European Conference on Unsaturated Soils, E-UNSAT, Durham, UK.

Derdour, L., Desmorieux, H. and Andrieu, J. 1998. Determination and Interpretation of the Critical Mositure Content (C.M.C.) and the Internal Moisture Content Profile During the Constant Drying Rate Period. Drying Technology, 16:3-5, 813-824, DOI: 10.1080/0737393 808917437

Derdour, L., Desmorieux, H. and Andrieu, J. 2000. A Contribution to the Characteristic Drying Curve Concept: Application to the Drying of Plaster. Drying Technology, 18:1-2, 237-260, DOI: 10.1080/07373930008917702

Dineen, K., Colmenares, J. E., Ridley, A. M. and Burland, J. B. 1999. Suction and Volume Changes of a Bentonite-Enriched Sand. Proceedings of the Institution of Civil Engineers – Geotechnical Engineering 137, no. 4 (October): 197–201. https://doi. org/10.1680/gt.1999.370405

Dineen, K., Colmenares, J. E., Ridley, A. M. and Burland, J. B. 1999. Suction and Volume Changes of a Bentonite-Enriched Sand. Proceedings of the Institution of Civil Engineers – Geotechnical Engineering 137, no. 4 (October): 197–201. https://doi. org/10.1680/gt.1999.370405

D'onza, F., Gallipoli, D., Wheeler, S.J., Casini, F., Vaunat, J., Khalili, N., Laloui, L., Mancuso, C., Masin, D., Nuth, M., Pereira, J.M., Vassallo, R. 2011. Benchmarking different approaches to constitutive modelling of unsaturated soils. Geotechnique, 61(4):283-302.

Eching, S. O., and Hopmans, J. W. 1993. Optimization of hydraulic functions from transient outflow and soil water pressure data. Soil Science Society of America Journal, 57(5), 1167-1175.

Escario,V. and Juca, J.F.T. 1989. Shear strength and deformation of partly saturated soils. Proceedings of the 12th International Conference on Soil Mechanics and Foundation Engineering, Rio de Janeiro, Vol.1, pp.43-46.

Eyüpgiller, M.M., and Ülker, M.B.C. 2018. Siltlerde hidrolik iletkenlik-matrik emme ilişkisinin doygunluk derecesine bağlı belirlenmesi. 17th National Congress of Soil Mechanics and Geotechnical Engineering, İstanbul.

Fredlund, D. and Xing, A. 1994. Equations for the soil-water characteristic curve. Canadian Geotechnical Journal, 31(4), 521-532.

Fredlund, D. G. 1975. A Diffused Air Volume Indicator for Unsaturated Soils. Canadian Geotechnical Journal, 12(4), 533–539.

Fredlund, D. G. 2006. Unsaturated soil mechanics in engineering practice. ASCE Journal of Geotechnical and Geoenvironmental Engineering, Vol.132, No.3, pp.286-321.

Fredlund, D. G. and Morgenstern, N. R. 1977. Stress state variables for unsaturated soils. Journal of Geotechnical Division, ASCE, Vol.103, No GT5, pp.447-466.

Fredlund, D.G. and Rahardjo, H. 1993. Soil mechanics for unsaturated soils. John Wiley and Sons Inc. New York.

Fredlund, D.G., Rahardjo, H., and Fredlund, M.D. 2012. Unsaturated soil mechanics in engineering practice. New York: John Wiley and Sons Inc.

Fredlund, D.G., Xing, A., and Huang, S.Y. 1994. Predicting the permeability function for unsaturated soils using the soil water characteristic curve. Canadian Geotechnical Journal, Vol. 31, No. 4, 533-546.

Fredlund, M.D., Wilson, G.W. and Fredlund, D.G. 2002. Representation and estimation of the shrinkage curve. Proceedings of the Third International Conference on Unsaturated Soils, UNSAT 2002, Recife, Brazil, pp. 145-149.

Gallage, C. and Uchimura, T. 2015. Direct shear testing on unsaturated silty soils to investigate the effects of drying and wetting on shear strength parameters at low suction. J. Geotech. Geoenviron. Eng. 142(3):04015081.

Gallipoli D., Bruno A.W. 2017. A bounding surface compression model with a unified virgin line for saturated and unsaturated soils. Géotechnique, 67(8):703–12.

Gallipoli, D. 2000. Constitutive and numerical modelling of unsaturated soils. PhD thesis, University of Glasgow, UK.

Gallipoli, D. 2012. A hysteretic soil-water retention model accounting for cyclic variations of suction and void ratio. Geotechnique 63(2):155-164.

Gallipoli, D., Wheeler, S. and Karstunen, M. 2003. Modelling the variation of degree of saturation in a deformable unsaturated soil. Geotechnique 53(1):105-112.

Gardner, W. R., 1956. Calculation of Capillary Conductivity from Pressure Plate Outflow Data. Soil Sci. Soc. Am. J., Vol. 20, No. 3, pp. 317–320.

Geiser, F., Laloui, L, Vulliet, L. 1997. Constitutive modeling of unsaturated sandy silt, Computer Methods and Advances in Geomechanics. Yuan ed., Belkema, Rotterdam, ISBN 9054109041.

Geiser, F., Laloui, L. and Vulliet, L. 2000. Modelling the behaviour of unsaturated silt. In Tarantino, A. & Mancuso, C (Eds.) International Workshop on Unsaturated Soils, Trent, Italy.

Gens, A. 2010. Soil-environment interactions in geotechnical engineering. Geotechnique 60:1, 3-74.

Germaine, J.T. and Germaine, A.V. 2009. Geotechnical Laboratory Measurements for Engineers. John Wiley & Sons, Inc.

Goh, S.G., Rahardjo, H. and Leong, E.C. 2013. Shear strength of unsaturated soils under multiple drying-wetting cycles. J. Geotech. Geoenviron. Eng., 140(2):1-1.

Gonzalez, N. A. and Colmenares, J. E. 2006. Influence of matric suction on the volume change behaviour of a compacted clayey soil. Proceedings of the 4th International Conference on Unsaturated Soils, 2–6 April, Carefree, AZ, ASCE, pp. 825–836.

Gonzalez, N. A. and Colmenares, J. E. 2006. Influence of matric suction on the volume change behaviour of a compacted clayey soil. Proceedings of the 4th International Conference on Unsaturated Soils, 2–6 April, Carefree, AZ, ASCE, pp. 825–836.

Guan, G.,S., Rahardjo, H. and Leong, E.C. 2009. Shear strength equations for unsaturated soil under drying and wetting. J. Geotech. Geoenviron. Eng., 136(4):594-606.

Hamidi, A., Habibagahi, G., and Ajdari, M. 2013. A Modified Osmotic Direct Shear Apparatus for Testing Unsaturated Soils. Geotechnical Testing Journal, Vol. 36, No. 1, pp. 20-29,

Hamilton, J. M., Daniel, D. E., and Olson, R. E. 1981. Measurement of hydraulic conductivity of partially saturated soils. Permeability and Groundwater Contaminant Transport, ASTM STP 746 T. F. Zimmie and C. O. Riggs, Eds., ASTM, pp. 182-196.

Hilf, J.W. 1956. An investigation of pore-water pressure in compacted cohesive soils. (PhD), Tech. Memo. No. 654, U.S. Department of the Interior, Bureau of Reclamation, Denver, CO.

Hillel, Daniel 2003. Introduction to Environmental Soil Physics. Academic Press, Elsevier Science, USA.

Hu, R., Chen, Y.F., Liu, H.H. and Zhou, C.B., 2013. A water retention curve and unsaturated hydraulic conductivity model for deformable soils: consideration of the change in pore-size distribution. Geotechnique 63(16):1389-1405.

Huang, S., Fredlund, D., and Barbour, S. 2011. Measurement of the coefficient of permeability for a deformable unsaturated soil using a triaxial permeameter. Canadian Geotechnical Journal. 35. 426-432. 10.1139/cgj-35-3-426.

Huang, S., Fredlund, D., and Barbour, S. 2011. Measurement of the coefficient of permeability for a deformable unsaturated soil using a triaxial permeameter. Canadian Geotechnical Journal. 35. 426-432. 10.1139/cgj-35-3-426.

Jaky, J. 1948. Pressure in silos. Proc. 2nd Int. Conf: Soil Mech. and Fdn Engng 1, 103-107.

Jean-Louis Briaud 2013. Geotechnical Engineering: Saturated and Unsaturated Soils, John Wiley and Sons Inc., Hoboken, New Jersey.

Karube, D., Kato, S., Hamada, K. and Honda, M. 1996. The Relationship between the mechanical behavior and the state of pore water in soil. Journal of JSCE, Vol.535, pp.83-92.

Karube, D., Kato, S., Hamada, K. and Honda, M. 1996. The Relationship between the mechanical behavior and the state of pore water in soil. Journal of JSCE, Vol.535, pp.83-92.

Kassiff, G. and Ben Shalom, A. 1971. Experimental relationship between swell pressure and suction. Geotechnique, 21, 241-255.

Kawai, K., Karube, D. and Kato, S. 2000. The model of water retention curve considering effects of void ratio. In: Rahardjo, H., Toll, D.G., Leong, E.C. (Eds.), Unsaturated Soils for Asia, Balkema, Rotterdam, 329-334.

Kayadelen, C., Tekinsoy, M.A. and Taşkıran, T. 2007. Influence of matric suction on shear strength behaviour of a residual clayey soils. Environmental Geology, 53(4):891-901.

Kenanoğlu, M.B. 2017. Numerical Simulation of Infiltration and Evaporation for Unsaturated Infinite Soil Slopes. Master of Science, Middle East Technical University.

Kenanoğlu, M.B. and Toker, N.K. 2018a. Changing and equilibrating water content of test specimens without suction control. 7th International Conference on Unsaturated Soils (UNSAT-2018), Hong Kong.

Kenanoğlu M. B. and Toker N. K. 2018b. A formulation for scanning soil-water characteristic curves. Politeknik Dergisi, 21(4): 901-906.

Khalili, N. & Khabbaz, M. 1998. A unique relationship for χ for the determination of the shear strength of unsaturated soils. Geotechnique, 48(5):681-687.

Khalili, N. and Khabbaz, M. 1998. A unique relationship for χ for the determination of the shear strength of unsaturated soils. Geotechnique, 48(5):681-687.

Khalili, N., Geiser, F. and Blight, G.E. 2004. Effective stress in unsaturated soils:Review with new evidence. Int. J. Geomech., 4:115-126.

Khoshghalb, A. and Khalili, N. 2013. A meshfree method for fully coupled analysis of flow and deformation in unsaturated porous media. International Journal for Numerical and Analytical Methods in Geomechnics 37(7):716-743.

Khoury, C.N. and Miller, G.A. 2012. Influence of hhdraulic hysteresis on the shear strength of unsaturated soils and interfaces. Geotechnical Testing Journal, Vol.35, No.1, pp.135-149.

Klute, A., and Dirksen, C. 1986. 'Hydraulic conductivity and diffusivity: laboratory methods. Methods of Soil Analysis, Part 1. Physical and Mineralogical Methods, Soil Science Society of America, Monograph No. 9, Madison, WI, pp. 687–734.

Klute, A., and Dirksen, C. 1986. Hydraulic conductivity and diffusivity: laboratory methods: Methods of Soil Analysis, Part 1. Physical and Mineralogical Methods. Soil Science Society of America, Monograph No. 9, Madison, WI, pp. 687–734.

Knight, R., Tercier, P. and Goertz, D. 1996. A laboratory procedure for estimating irreducible water saturation from cuttings. The Log Analyst, 37(4): 18-24.

Kodikara, J. 2012. New framework for volumetric constitutive ehaviour of compacted unsaturated soils. Canadian Geotechnical journal, 49:1227-1243.

Kohler, R. and Hofstetter, G. 2008. A cap model for partially saturated soils. Int. J. Numer. Anal. Meth. Geomech., 32:981-1004.

Koliji, A., Vulliet, L. and Laloui, L. 2010. Structural characterization of unsaturated aggregated soil. Canadian Geotechnical Journal. 47. 297-311. 10.1139/T09-089.

Komornik, A., Livneh M. And Smucha S. 1980. Shear strength and swelling of clays under suction. Proc. 4th Int. Conf. On Expansive Soils, Denver, USA.

Kong, L. W. and Tan, L. R. 2000. A simple method of determining the soil-water characteristic curve indirectly. Proceedings of Asian Conference on Unsaturated Soils, Singapore, pp.341-345.

Kool, J. B., J. C. Parker, and M. Th. Van Genuchten. 1985. Determination of soil hydraulic properties from one-step outflow experiments by parameter estimation: I Theory and numerical studies. Soil Sci. Soc. Am. J. 49:1348-1354.

Koorevaar, P., Menelik, G., and Dirksen, C. 1983. Elements of Soil Physics, Elsevier, Amsterdam, The Netherlands.

Köksalan, A.O. 2013. Construction of a high-capacity tensiometer and its use in measurement of matric suction in unsaturated soils. Master of Science Thesis, Middle East Technical University.

Kumar, N. and Arakeri, J. 2018. Evaporation from confined porous media due to controlled IR heating from above.

Kunza, R.J. and Kirkham, D. 1962. Simplified accounting for membrane impedance in capillary conductivity determinations. Soil Sci. Soc. Am. Proc. 4th Int. Conf. On Expansive soils, Denver, USA.

Kunze, R. J., and Kirkham, D., 1962. Simplified accounting for membrane impedance in capillary conductivity measurements. Soil Science Society of America Proceedings, 26, 421–426.

Ladd, R. 1978. Preparing test specimens using undercompaction. Geotechnical Testing Journal, 1(1), 16-23.

Lee, I., Sung, S. and Cho, G. 2005. Effect of stress state on the unsaturated shear strength of a weathered granite. Canadian Geotechnical Journal, 42(2):624-631.

Lehmann, P., Assouline, S. and Or, D. 2008. Characteristic Lengths Affecting Evaporative Drying of Porous Media. Phys. Rev. E., 77.5, 056309.

Li, L. and Zhang, X. 2015. A new triaxial testing system for unsaturated soil characterization. Geotechnical Testing Journal, Vol.38, No.6, pp.823-839.

Li, X., Wen, H., Muhunthan, B. and Wang, J. 2015. Modelling and prediction of the effects of moisture on the unconfined compressive and tensile strength of soils. J. Geotech. Geoenviron. Eng., 141(7):04015028.

Li, Z., Derfouf, F.M., enchouk, A., Abou-Bekr, N., Taibi, S. and Fleureau, J. 2018. Volume change behaviour of two compacted clayey soils under hydraulic and mechanical loadings. J. Geotech. Geoenviron. Eng., 144(4):04018013.

Likos, W. J., and Lu, N. 2004. Hysteresis of capillary stress in unsaturated granular soil. J. Eng. Mech., 130(6), 646-655.

Likos, W.J., and Yao, J. 2014. Effects of constraints on van Genuchten parameters for modelling soil-water characteristic curves. J. Geotech. Geoenviron. Eng.,140(12):06014013.

Likos, W.J., Lu, N., Godt, J.W. 2013. Hysteresis and uncertainty in soil water-retention curve parameters. J. Geotech. Geoenviron. Eng., 140(4):04013050.

Lloret, A., Villar, M.V., Sanchez, M., Gens, A., Pintado, X. and Alonso, E.E. 2003. Mechanical behaviour of heavily compacted bentonite under high suction changes. Geotechnique 53(1):27-40.

Lockington, D.A. 1994. Falling rate evaporation and desorption estimates. Water Resour. Res. 30:1071–1074.

Lu, N. 2020. Unsaturated Soil Mechanics: Fundamental Challenges, Breakthroughs, and Opportunities. Journal of Geotechnical and Geoenvironmental Engineering. 146. 02520001. 10.1061/(ASCE)GT.1943-5606.0002233.

Lu, N., Kaya, M., Collins, B.D. and Godt, J. 2013. Hysteresis of unsaturated hydromechanical properties of a silty soil. J. Geotech. Geoenviron. Eng., 139(3):507-510.

Lu, N., Wayllace, A., Carrera, J. and Likos, W. J. 2006. Constant Flow Method for Concurrently Measuring Soil-Water Characteristic Curve and Hydraulic Conductivity Function. Geotechnical Testing Journal, Vol.29, No.3, pp.230-241.

Lu, N.,and Likos, W.J. 2006. Suction stress characteristic curve for unsaturated soil. J. Geotech. Geoenviron. Eng., 132(2), 131-142.

Lu, N.,Godt, J.W., and Wu, D. 2010. A closed-form for effective stress in variably saturated soil. Water Resources Research.

Lu,N. And Likos,W.J. 2004. Unsaturated Soil Mechanics, John Wiley and Sons Inc. Hoboken, New Jersey.

Ma,T., C. Wei, H. Wei, and W. Li. 2016. Hydraulic and mechanical behavior of unsaturated silt: Experimental and theoretical characterization. Int. J. Geomech. 16 (6): D4015007

Marcial, D., Delage, P., Ruiz, X. and Cui, Y. 2006. Ageing effects in a compacted bentonite: A microstructure approach. Geotechnique. 56. 291-304. 10.1680/geot.2006.56.5.291.

Masbashi, A. and Elkady, T. 2017. Prediction o unsaturated shear strength of expansive clays. Proceedings of Institute of Civil Engineering: Geotechnical Engineering, ICE Publishing, pp.1-10.

Masin, D. 2010. Predicting the dependency of a degree of saturation on void ratio and suction using effective stress principle for unsaturated soils. Int. J. Numer. Anal. Meth. Geomech., 34(1):73-90.

Matyas E.L. and Radhakrishna H.S. 1968. Volume change characteristics of partially saturated soils. Géotechnique, 18(4): 432–448.

Meerdink, J., Benson, C., and Khire, M. 1996. Unsaturated hydraulic conductivity of two compacted barrier soils. J. Gecotech. Geoenviron. Eng., ASCE, Vol. 122, No. 7, pp. 565-576.

Miao, L., Liu, S. and Lai, Y. 2002. Research of soil-water characteristics and shear strength features of Nanyang expansive soil. Engineering Geology (Amsterdam), Vol.65, pp.261-267.

Mitchell, J.K. 1993. Fundamentals of soil behaviour. John Wiley & Sons, Inc.

Mitchell, J.K. and Soga, K. 2005. Fundamentals of Soil Behavior. 3rd Edition, John Wiley & Sons, Hoboken.

Monroy, R. 2005. The influence of load and suction changes on the volumetric behaviour of compacted London clay. PhD thesis, University of London (Imperial College), London, UK.

Moyne C., Basilico C., Batsale J.C. and Degiovanni A. 1991. Physical Mechanisms During the Drying of a Porous Medium. In: Bear J., Buchlin JM. (eds) Modelling and Applications of Transport Phenomena in Porous Media. Theory and Applications of Transport in Porous Media, vol 5. Springer, Dordrecht. https://doi.org/10.1007/978-94-011-2632-8_5

Mualem, Y. 1978. Hydraulic conductivity of unsaturated porous media: Generalized macroscopic approach. Water Resour. Res., 14(2), 325–334.

Mualem, Y. 1978. Hydraulic conductivity of unsaturated porous media: Generalized macroscopic approach. Water Resources Research, 14(2), 325-334.

Mun, W., Coccia, C.J.R. and McCartney, J.S. 2017. Application of hysteretic trends in the preconsolidation stress of unsaturated soils. J.S. Geotech. Geol. Eng. 36: 193.

Murray, E.J. And Sivakumar V. 2010. Unsaturated Soils: A fundamental interpretation of soil behaviour. New York: John Wiley and Sons Inc.

Nasta, P., Huynh, S., Hopmans, J. W. 2011. Simplified Multistep Outflow Method to Estimate Unsaturated Hydraulic Function for Coarse Texted Soils. Soil Sci. Soc. Am. J., 75, 418-425.

Nelson, J.D. And Miller, D.J. 1992. Expansive Soils, Problems and Practice in Foundation and Pavement Engineering, John Wiley and Sons Inc., New York.

Ng C.W.W., Pang Y.W. 2000. Experimental investigations of the soil–water characteristics of a volcanic soil. Can .Geotech. J.; 37(6):1252–64.

Ng, C.W.W. and Chen, R. 2005. Advanced suction control techniques for testing unsaturated soils. Keynote lecture, 2nd Nat. Conf. On Unsat. Soils, Hangzhou, China, Zhejiang University Press, 144-167.

Ng, C.W.W. and Chiu, A.C.F. 2001. Behaviour of a loosely compacted unsaturated volcanic soil. J. Geotech. Geoenviron. Eng., 127(12):1027-1036.

Ng, C.W.W. and Chiu, A.C.F. 2003. Laboratory study of loose saturated and unsaturated decomposed granitic soil. J. Geotech. Geoenviron. Eng., 129(6):550-559.

Ng, C.W.W. and Menzies, B. 2007. Advanced Unsaturated Soil Mechanics and Engineering. London: Taylor and Francis Group.

Ng, C.W.W. and Zhou, R.Z.B. 2005. Effect of soil suction on dilatancy of an unsaturated soil. Proc. 16th Int. Conf. Soil Mech. And Geotech. Engrg. Osaka, Japan, 2, 559-562.

Ng, C.W.W., Cui, Y.J., Chen, R. and Delage, P. 2007. The axis-translation and osmotic techniques in shear testing of unsaturated soils:a comparison. Soils and Foundations, vol.47, no.4, 675-684.

Ng, C.W.W., Lai C.H., Chiu A.C.F. 2012. A modified triaxial apparatus for measuring the stress path-dependent water retention curve. Geotech. Testing J., ASTM; 35(3):490–5.

Nuth, M. and Laloui, L. 2008. Advances in modelling hysteretic water retention curve in deformable soils. Computational Geotechnics, 35(6):835-844.

Nyunt, T. T., Leong, E. C., and Rahardjo, H., 2011. Strength and Small-Strain Stiffness Characteristics of Unsaturated Sand. Geotechnical Testing Journal, Vol. 34, No. 5, pp. 551-561,

Oh, W.T. and Vanapalli, S. 2018. Undrained shear strength of unsaturated soils under zero or low confining pressures in the vadose zone. Vadose Zone J. 17:180024.

Oliveira, O.M. and Marinho, F.A.M. 2006. Study of equilibration time in the pressure plate. Proc. 4th Int. Conf. On Unsaturated Soils, Carefree, Arizona, Unsaturated Soils. Geotechnical Special Publication 147. G.A. Miller, C.E. Zapata, S.L. Houston and D.G. Fredlund (eds.). ASCE, 2:1864-1874.

Olsen, H., Willden, A., Kiusalaas, N., Nelson, K., and Poeter, E. 1994. Volume-Controlled Hydrologic Property Measurements in Triaxial Systems in Hydraulic Conductivity and Waste Contaminant Transport in Soil, ed. D. Daniel and S. Trautwein (West Conshohocken, PA: ASTM International), 482-504.

Olsen, H., Willden, A., Kiusalaas, N., Nelson, K., and Poeter, E. 1994. Volume-Controlled Hydrologic Property Measurements in Triaxial Systems. in Hydraulic Conductivity and Waste Contaminant Transport in Soil, ed. D. Daniel and S. Trautwein (West Conshohocken, PA: ASTM International), 482-504.

Omar, T. and Sadrekarimi 2015. Effect of triaxial specimen size on engineering design and analysis. A. Geo-Engineering 6: 5. doi:10.1186/s40703-015-0006-3

Or, D. and Shahraeeni, E. and Shokri, N. 2013. Advances in Soil Evaporation Physics—A Review. Vadose Zone Journal. 12. 10.2136/vzj2012.0163.

Or, D., Shahraeeni, E. and Shokri, N. 2013. Advances in Soil Evaporation Physics—A Review. Vadose Zone Journal. 12. 10.2136/vzj2012.0163.

Öberg, A. L. and Sällfors, G. 1995. A rational approach to the determination of the shear strength parameters of unsaturated soils. Proceedings of First International conference on Unsaturated Soils, Paris, Vol.1, pp.151-158.

Pasha, A., Khoshghalb, A., and Khalili, N. 2015. Pitfalls in Interpretation of Gravimetric Water Content–Based Soil-Water Characteristic Curve for Deformable Porous Media. Int. J.l of Geomechanics. 16. D4015004. 10.1061/(ASCE)GM.1943-5622.0000570.

Petrucci, R. H. 1989. General Chemistry: Principles and Modern Applications, Macmillan Publishing Co., New York

Power, K.C., and Vanapalli, K. 2010. Modified null pressure plate apparatus for measurement of matric suction. Geotechnical Testing Journal, Vol. 33, No.4 , pp. 335-341

Puigmartí, N. and Gens, A. and Alonso, E.E. 2013. Compacted soil behaviour: Initial state, structure and constitutive modelling. Géotechnique. 63. 463-478. 10.1680/geot.11.P.134.

Rahardjo, H. and Fredlund, D.G. 1996. Consolidation apparatus for testing unsaturated soils. Geotechnical Testing Journal, ASTM, Vol.19, No.4, pp.341-353.

Rahardjo, H. and Fredlund, D.G. 2003. Ko-volume change characteristics of an unsaturated soil with respect to various loading paths. Geotechnical Testing Journal, ASTM, Vol.26, No.1, pp.79-91.

Rampino,C., Mancuso, C. and Vinale, F. 1998. Behaviour of compacted silty sand during suction controlled tests. IN: Proceedings of 2nd International Conference on Unsaturated Soils, vol.1, p.108-113.

Rassam, D.W. and Williams, D.J. 1999. A relationship describing the shear strength of unsaturated soil. Canadian Geotechnical Journal, 36:363-368.

Richards, L. A. 1931. Capillary conduction of liquids through porous medium. Journal of Physics, 318-333.

Richards, L.A., and Weeks, L. 1953. Capillary conductivity values from moisture yield and tension measurements on soil columns. Soil Science Society of America Proceedings, 55, 206-209.

Rojas, E. 2008. Equivalent stress equation for unsaturated soils, I: Equivalent stress. Internationaş Journal of Geomechanics, 8(5):285-290.

Romero, E. 1999. Characterisation and thermo-hydromechanical behaviour of unsaturated Boom Clay: an experimental study. PhD Thesis, Universitad Politecnica de Cataluna.

Romero, E., Gens, A. and Lloret, A. 1999. Water permeability, water retention and microstructure of unsaturated Boom clay. Engng Geol. 54, No. 1–2, 117–127.

Romero, E., Gens, A. and Lloret, A. 1999. Water permeability, water retention and microstructure of unsaturated compacted Boom clay. Engineering Geology. 54. 117-127. 10.1016/S0013-7952(99)00067-8.

Salager, S., El Youssoufi, M. S. and Saix, C. 2010. Definition and experimental determination of a soil-water retention surface. Can. Geotech. J. 47, No. 6, 609–622.

Salager, S., Nuth, M., Ferrari, A. and Laloui, L., 2013. Investigation into water retention behaviour of deformable soils. Canadian Geotechnical Journal, 50(2):200-208.

Sattari, A. S., Toker, N.K. 2016. Obtaining soil-water characteristic curves by numerical modelling of drainage in particulate media. Computers and Geotechnics, 74, 196-210.

Schaap, M., and van Genuchten, M. 2006. A Modified Mualem–van Genuchten Formulation for Improved Description of the Hydraulic Conductivity Near Saturation. Vadose Zone Journal, 5. 27-34.

Schelle, H., Iden, S. C., Durner, W. 2011. Combined Transient Method for Determining Soil Hydraulic Properties in a Wide Pressure Head Range. Soil Sci. Soc. Am. J., 75, 1681-1693.

Scherer, G. W. 1990. Theory of drying, J. Am. Ceram. Soc., 73, 3 –14, doi:10.1111/j.1151-2916.1990.tb05082.x.

Shao, L.T., Wen, T.D., Guo, X.X., Sun, X. 2017. A method for directly measuring the hydraulic conductivity of unsaturated soil. Geotech. Test. J. 40(6), 20160197

Shao, L.T., Wen, T.D., Guo, X.X., Sun, X. 2017. A method for directly measuring the hydraulic conductivity of unsaturated soil. Geotechnical Testing Journal. 40(6), 20160197

Sheng, D. and Zhou, N. 2011. Coupling hydraulic with mechanical models for unsaturated soils. Canadian Geotechnical Journal, 48(5):826-840.

Sherwood, T. K. 1929. The Drying of Solids—II. Ind. Eng. Chem. 21, 976–980. DOI: 10.1021/ie50238a021.

Shokri, N. and Or, D. 2010. Liquid-phase continuity and solute concentration dynamics during evaporation from porous media: Pore-scale processes near vaporization surface. Physical review. E, Statistical, nonlinear, and soft matter physics. 81. 046308. 10.1103/PhysRevE.81.046308.

Shokri, N. and Or, D. 2011. What determines drying rates at the onset of diffusion controlled stage-2 evaporation from porous media?. Water Resources Research 47. 10.1029/2010WR010284.

Sivakumar, V., Sivakumar, R., Boyd,J. and MacKinnon, P. 2010b. Mechanical behaviour of unsaturated kaolin (with isotropic and anisotropic stress history). Part 2: performance under shear loading. Geotechnique, 60(8):595-609.

Sivakumar, V., Sivakumar, R., Brown, J., Murray, E.J. and MacKinnon, P. 2010a. Constitiutive modelling of unsaturated kaolin (with isotropic and anisotropic stress history). Part 1:Wetting and compression behaviour. Geotechnique Vol.60, pp.

Sridharan, A., Altschaeffl, A. G. and Diamond, S. 1971. Pore size distribution studies. J. Soil Mech. Found. Div. 97, No. SM5, 771-787.

Su, W., Cui, Y., Qin, P., Zhang, F., Ye, W., and Conil, N. (2018). Application of instantaneous profile method to determine the hydraulic conductivity of unsaturated natural stiff clay. Engineering Geology. 243. 10.1016/j.enggeo.2018.06.012.

Suits, L., Sheahan, T., Power, K., Vanapalli, S. (2010). Modified Null Pressure Plate Apparatus for Measurement of Matric Suction. Geotechnical Testing Journal - GEOTECH TESTING J. 33. 10.1520/GTJ102478.

Suleiman, A. and Ritchie, J. 2003. Modeling Soil Water Redistribution during Second-Stage Evaporation. Soil Science Society of America Journal - SSSAJ. 67. 10.2136/sssaj2003.0377.

Sun, D.A., Sheng, D. and Sloan, S.W. 2007. Elastoplastic modelling of hydraulic and stress-strain behaviour of unsaturated soil. Mechanics of Materials, 39(3):212-221.

Sun, D.A., Sheng, D., Xiang, L. and Sloan, S.W. 2008. Elastoplastic prediction of hydromechanical behaviour of unsaturated soils under undrained conditions. Computers abd Geotechnics, 35, 845-852.

Tang, A.M. and Cui, Y.J. 2005. Controlling suction by the vapour equilibrium technique at different temperatures and its application in determining the water retention properties of MX80 clay. Can Geotech J. 42:287-296.

Tang, G.X., Graham J., Wan, A.W.L. 1998. On yielding behaviour of an unsaturated sand-bentonite mixture. In Proceedings of the 2nd international conference on unsaturated soils, vol 1. Beijing, pp 149-154.

Tarantino, A. 2009. A water retention model for deformable soils. Geotechnique, 59(9):751-762.

Tarantino, A. and Col, E. 2008. Compaction behaviour of clay. Geotechnique. 58. 199-213. 10.1680/geot.2008.58.3.199.

Tekinsoy, M.A., Kayadelen, C., Keskin, M.S. and Soylemez, M. 2004. An equation for predicting shear strength envelope with respect to matric suction. Computers and Geotechnics, 31(7):589-593.

Terzaghi, K. 1943. Theoretical Soil Mechanics, John Wiley and Sons, Inc., New York.

Thiery, J., Rodts, S., Weitz, D. and Coussot, P. 2017. Drying regimes in homogeneous porous media from macro- to nanoscale. Physical Review Fluids. 2. 10.1103/PhysRevFluids.2.074201.

Thomson, W., 1871. Philosophical Magazine, 42, 448.

Thu, T., Rahardjo, H. and Leong, E. 2006. Shear strength and pore-water pressure characteristics during constant water content triaxial tests. Journal Geotechnical and Geoenvi-ronmental Engineering. 132(3): 411-419.

Thu, T.M., Rahardjo, H. and Leong, E.C. 2007. Elastoplastic model for unsaturated soil with the incorporation of soil-water characteristic curve. Canadian Geotechnical journal, Vol.44, pp.67-77.

Tiantian, M., Wei, C. and Yao, C. and Yi, P. 2020. Microstructural evolution of expansive clay during drying–wetting cycle. Acta Geotechnica. 15. 10.1007/s11440-020-00938-4.

Toker, N. K. 2007. Modeling the relation between suction, effective stress and shear strength in partially saturated granular media. PhD Thesis, Massachusetts Institute of Technology.

Toker, N. K., Germaine, J. T., Sjoblom, K. J. and Culligan, P. J. 2004. A new technique for rapid measurement of continuous SMC curves. Geotechnique, Vol.54, No.3, pp.179-186.

Toker, N.K. 2002. Improvements and Reliability of MIT Tensiometers and Studies on Soil Moisture Characteristic Curves. Master of Science Thesis, Massachusetts Institute of Technology.

Toker, N.K. 2007. Modelling the relation between suction, effective stress and shear strength in partially saturated granular media. Ph.D. Thesis, Massachusetts Institute of Technology.

Toker, N.K., Germaine, J.T. ve Culligan, P.J. 2014. Effective stress and shear strength of moist uniform spheres. Vadose Zone Journal, Vol.13, No.5, p.5-17.

Tombolato, S. and Tarantino, A. 2005. Coupling of hydraulic and mechanical behavior in unsaturated compacted clay. Geotechnique. 55. 307-317. 10.1680/geot.2005.55.4.307.

Toyota, H., Takada, S. and Susami, A. 2018. Mechanical properties off saturated and unsaturated cohesive soils with stress-induced anisotropy. Geotechnique, 68(10):883-892.

Tsiampousi, A., Zdravkovic, L. and Potts, D.M., 2013. A three-dimensional hysteretic soil-water retention curve. Geotechnique 63(2):155-164.

van Brakel, J. 1980. Mass transfer in convective drying. In Advances in Drying, ed. A. S. Mujumdar. Hemisphere, New York.

van Dam, J. C., Stricker, J. N. M., and Droogers, P. 1992. Inverse method for determining soil hydraulic functions from one-step outflow experiments. Soil science society of America journal, 56(4), 1042-1050.

van Genuchten, M.T. 1980. A closed-form equation for predicting the hydraulic conductivity of unsaturated soils. Soil Sci. Soc. Am. J. 44, 892-898.

Vanapalli, S.K., Fredlund, D.G., Pufahl, D.E. and Clifton, A.W. 1996. Model for the prediction of shear strength with respect to soil suction. Canadian Geotechnical Journal, 33(3), 379-392.

Vanapalli, S.K., Pufahl, D.E., Fredlund, D.G., 1999. The influence of soil structure and stress history on the soil-water characteristic of a compacted till. Geotechnique,49(2):143-159.

Vanapalli, S.K., Sillers, W.S., and Fredlund, M.D. 1998. The meaning and relevance of residual state to unsaturated soils. Proc., 51st Canadian Geotechnical Conf., Canadian Geotechnical Society, Richmond, BC, Canada.

Vanapalli, S.K.and Fredlund, D.G. 2000. Comparison of different procedures to predict unsaturated soil shear strength. In Advanced in Unsaturated Geotechnics. GSP 99. C.D. Shackelford, S.L. Houston and N.-Y Chang. American Society of Civil Engineers, Reston, Va. 195-209.

VandenBerge, D. R., Brandon, T. L., and Duncan, J. M. 2014. Triaxial Tests on Compacted Clays for Consolidated-Undrained Conditions. Geotechnical Testing Journal, Vol. 37, No. 4, pp. 705-716,

Vaunat, J., Cante, J., Ledesma, A. and Gens, A. 2000. A stress point algorithm for an elastoplastic model in unsaturated soils. International Journal of Plasticity 16(2): 121-141.

Wayllace, A., and Lu, N. 2012. A transient water release and imbibitions method for rapidly measuring wetting and drying soil water retention and hydraulic conductivity functions. J. ASTM Geotech Test., 35(1), 1–15.

Wheeler, S. J. 1996. Inclusion of specific water volume within an elastoplastic model for unsaturated soil. Canadian Geotechnical Journal, 33(1):42-57.

Wheeler, S. J., Sharma, R. S., Buisson, M.S.R. 2003. Coupling of hydraulic hysteresis and stress-strain behaviour in unsaturated soils. Geotechnique, 53-1, 41-54.

Wheeler, S.J., and Sivakumar V. 1995. An elasto-plastic critical framework for unsaturated soils. Geotechnique, Vol. 45, No. 1, 35-53.

Wheeler, S.J., Gallipoli D. and Karstunen M. 2002. Comments on use of the Barcelona Basic model for unsaturated soils. Int. J. Numer. Anal. Methods Geomechanics, 26: 1561-1571.

Wijaya, M., and E. C. Leong. 2017. Modelling the effect of density on the unimodal soil-water characteristic curve. Géotechnique 67 (7): 637–645.

Yuan, J., Liu, X., Romero, E., Delage, P. and Buzzi, O. 2020. Discussion on the separation of macropores and micropores in a compacted expansive clay. Géotechnique Letters. 10. 1-20. 10.1680/jgele.20.00056.

Zachmann, D. W., P. C. DuChateau, and A. Klute. 1982. Simultaneous approximation of water capacity and soil hydraulic conductivity by parameter identification. Soil Sci. 134: 157-163.

Zapata, E. C., Houston, N. W., Houston, L. S. and Walsh, D. K. 2000. Soil-water characteristic curve variability. Advances in Unsaturated Geotechnics, ASCE, Vol.99, pp.86-87.

Zhang, X., Liu, J. and Li, P. 2009. Determining the shapes of yield curves for unsaturated soils by modified state surface approach. J. Geotech. Geoenviron. Eng., 136(1):239-247.

Zhou, A.N., Sheng, D. and Li, J. 2014. Modelling water retention and volume change behaviours of unsaturated soils in non-isothermal conditions. Computational Geotechnics, 55:1-13.

Zhou, C. and Ng, C.W.W. 2014. A new and simple stress-dependent water retention model for unsaturated soil. Comput Geotech, 62:216-222.

Zhou, W. H., Yuen, K. V. and Tan, F. 2014. Estimation of soil–water characteristic curve and relative permeability for granular soils with different initial dry densities. Engng Geol. 179, 1–9.

Znidarcic, D., Illangasekare, T. and Manna, M. 1991. Laboratory testing and parameter estimation for two-phase flow problems. Geotechnical Special Publication 27, ASCE, pp.1089-1099.

Zou, W.L., Ye, Y.X., Han, Z. and Vanapalli, S.K. 2018. An insight into soilwater retention surface using soilwater space curves. UNSAT 2018: The 7th International Conference on Unsaturated Soils, Hong Kong.

APPENDICES

A. Diameter Measurement Technique and Area Correction for Unsaturated Soil Specimens

The main idea of the proposed procedure is based on counting pixels in the image of the specimen and to obtain diameter of the specimen by means of a calibration equation, which converts the number of pixels to the real dimension.

In order to obtain calibration equation, a calibration block, which consists cylindrical portions at different diameters, was used. The dimensions of the calibration block has been given in the Fig. A.1.

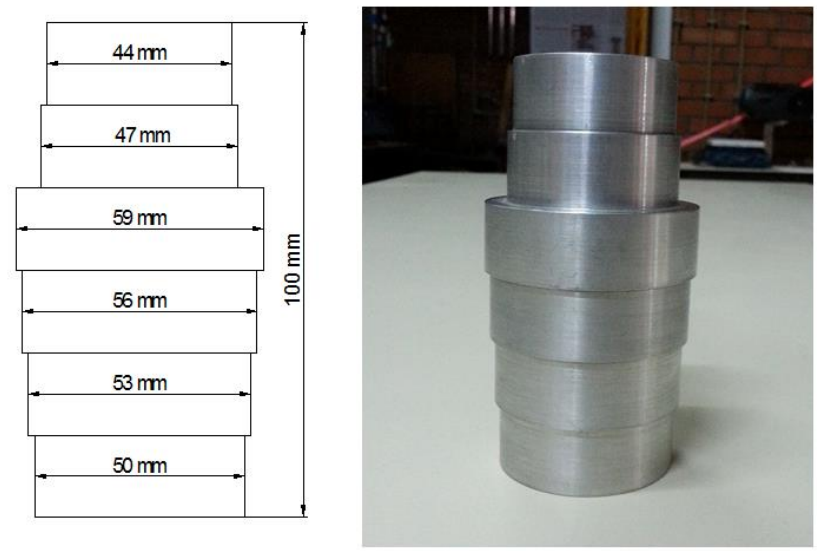

Figure A.1 The calibration mold and its dimensions.

The step-by-step procedure was given in the following part,

1. Place the calibration mold into the triaxial cell.

2. Fill the triaxial cell with water until the calibration mold is submerged and place the triaxial cell to the triaxial frame.

3. Take the picture of the calibration mold. This step is cruical and requires further description;

The picture quality is very important for counting the pixels in the picture; shadows and refractions cause poor contrast and it becomes very difficult to distinguish the transition between the calibration mold's color and the color of the background in the picture. A table lamp was placed behind the triaxial cell to improve the light and a colored plastic sheet was attached to the glass of the triaxial cell to prepare suitable background. The position of the table lamp (or other type source of light) effects the image quality and placing it behind the triaxial cell yields better quality pictures. The size of plastic sheet is important because covering too much surface on the triaxial cell with the plastic sheet can cause refractions on the calibration mold. In this study, a shiny calibration mold was used and different colors (yellow, red, blue) of plastic sheets as being background were tried to improve the contrast. It was observed yellow background yields better contrast in the picture. The other important factor that effects the quality of the picture is the camera used for taking picture. In this study, a 8.0-megapixel digital camera was used to take the pictures. The camera was placed on a tripod and its position was arranged to get the calibration mold at the center of the image.

4. After taking good quality picture, the number of pixels corresponding to each diameter on the calibration mold image was determined by cropping the image in the Microsoft Office Picture Manager programme. The picture is resized for each diameter by cropping, the changing dimensions of the picture is given in the programme.

5. It is difficult to locate the camera at the same position every time for future tests although the number of pixels is depend on the distance between the camera and the triaxial cell. In order to handle this problem, more pictures were taken at different distances, the number of pixels corresponding to each diameter was again determined. In order to obtain a calibration equation that is independent from the

distance between the camera and the triaxial cell following calculations are required;

a) Determine the number of pixels corresponding to each diameters of the calibration mold.

b) Determine the number of pixels corresponding to the width of the top cap and pedestal of the triaxial cell (these dimensions are 50 mm for most of triaxial setup). Then take the average of these two values (i.e. average of pixel number of pedestal and top cap). This step is necessary because the deviation of the position of the camera in the vertical alignment causes pixel number variation in vertical direction for the dimensions that are actually same (e.g. dimensions of top cap and pedestal). It is important to note that to use tripod for locating the camera prevents this problem.

c) Obtain the normalized version of the pixel number by dividing the pixel number corresponding to each diameter by the average value of the pixel number of the top cap and pedestal (see A-1).

$$normalized\ pixels = \frac{measured\ pixels}{average(pixels_{topcap}; pixels_{pedestal})} \qquad \text{(A-1)}$$

Where *measured pixels* is the pixel number of any diameter of the calibration mold.

d) Repeat the step 1 to 3 for each different distance. In this study, the distances in the range of 0.5 m to 1.0 m with the interval of 10 cm were choosen.

e)Plot the data points of the normalized pixels and the diameters of the calibration mold and obtain best-fit straigth line. The equation of the best-fit line is the calibration equation, which is independent from the distance between the triaxial cell and the camera. It is important to note that the calibration equation is unique for the triaxial cell of the testing setup which is calibrated and can not be used for any other triaxial testing system.

6. Once the calibration equation is determined, it can be used for all future tests. The calibration equations of both triaxial system used in this study were determined and have been shown in Fig. A.3.

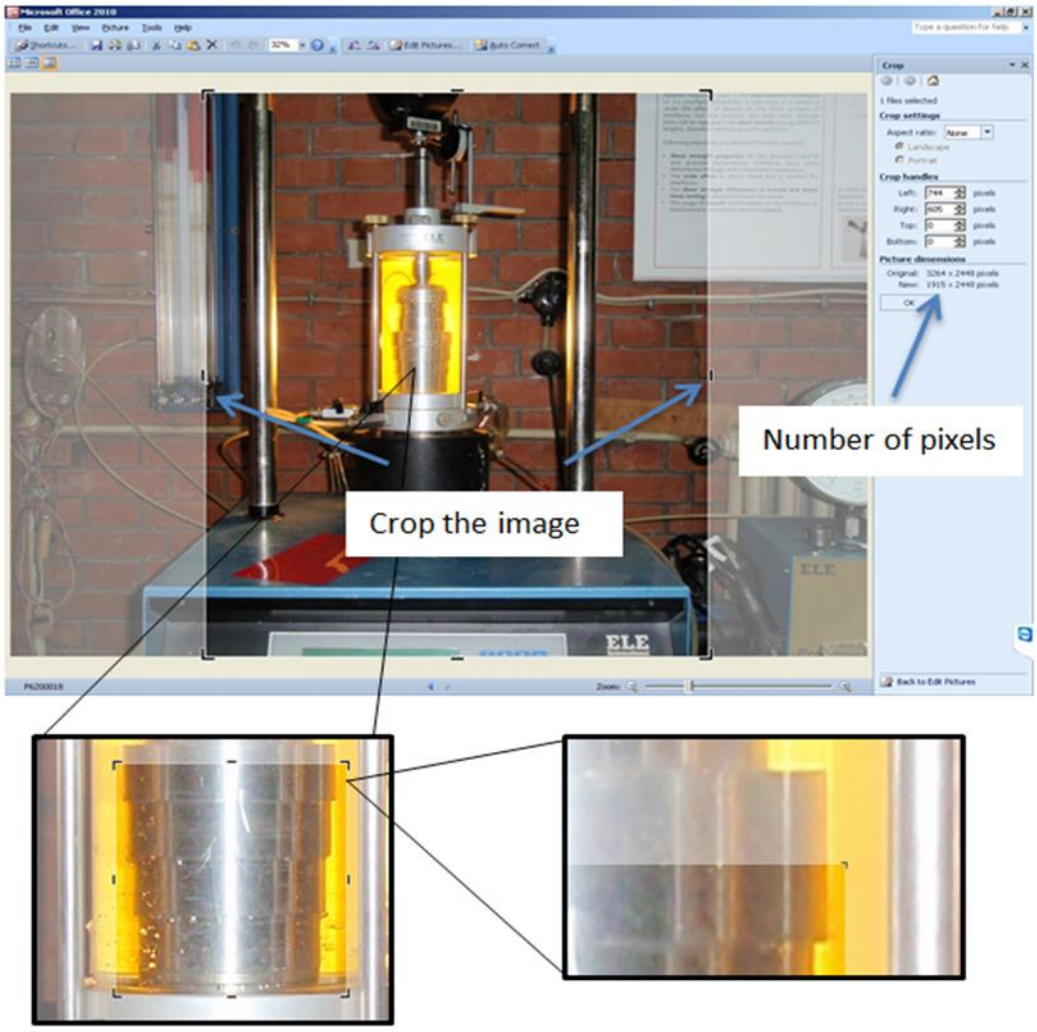

Figure A.2 The determination of number of pixels corresponding to diameter of the calibration mold. The image is narrowed by cropping until width of the image only include the diameters of calibration mold. The number of pixels corresponding to each diameter can be shown in the picture dimensions tab of the programme.

7. The other important step is to control the validity of the calibration equation. To do this;

a) The relative true errors for the real diameters and the calibrated values, which are the diameters calculated from the equation, are calculated for each data point (see A-2).

$$\varepsilon_t = \frac{D_{calibration\ mold} - D_{calibration\ equation}}{D_{calibration\ mold}} \times 100 \qquad \text{(A-2)}$$

where $D_{calibration,mold}$ (mm) is the actual diameters of the calibration mold, $D_{calibration,equation}$ (mm) is the diameters calculated from the calibration equation, $\in_t$ is the relative true error for the diameter measurement.

b) Find the largest relative true error. This is the maximum error in the diameter measurement.

c) The error in the diameter measurement causes error in the cross-sectional area calculation of the specimen, and this causes error in the calculation of deviator stress. The error in the deviator stress due to error in the diameter measurement can be calculated by using following (A-3) or this value can be taken as two times of the error in the diameter measurement for simplicity.

$$\varepsilon_{t,deviator} = \frac{\left(2 \times \varepsilon_{t,\max} / 100 + {\varepsilon_{t,\max}}^2 / 10000\right)}{\left(1 + 2 \times \varepsilon_{t,\max} / 100 + {\varepsilon_{t,\max}}^2 / 10000\right)} \times 100 \; or \; \varepsilon_{t,deviator} = 2 \times \varepsilon_{t,\max} \qquad \text{(A-3)}$$

Where $\in_t$ is the maximum error in diameter measurement and $\in_{t,deviator}$ is maximum error in deviator stress. According to ASTM D4767, the pressure devices should be capable of controlling the pressures to within ±2 kPa for pressures less than 200 kPa and to within ±%1 for the pressures greater than 200 kPa. Therefore, The maximum error in deviator stress should be less than ±2 kPa and if the value of $(200\,kPa) \times \varepsilon_{t,deviator} / 100$ is less than ±2 kPa, it is assumed that the calibration equation is accurate.

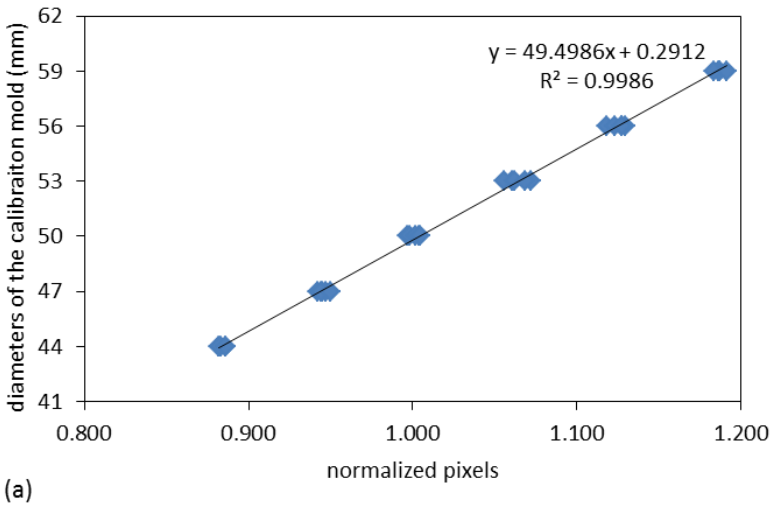

(a)

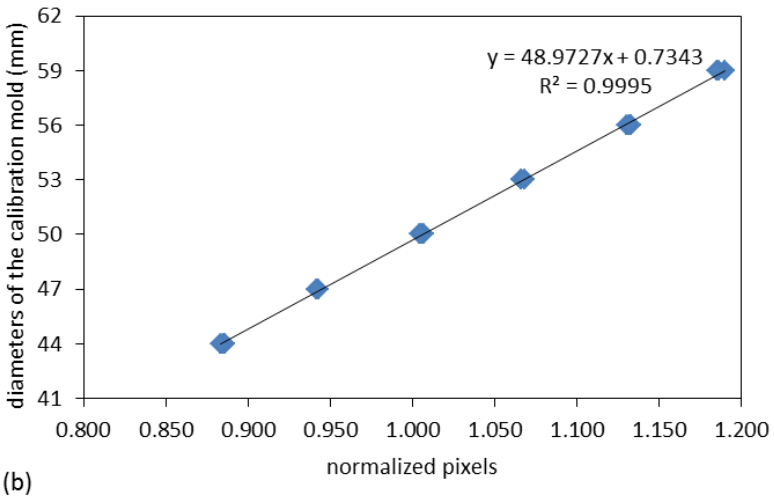

(b)

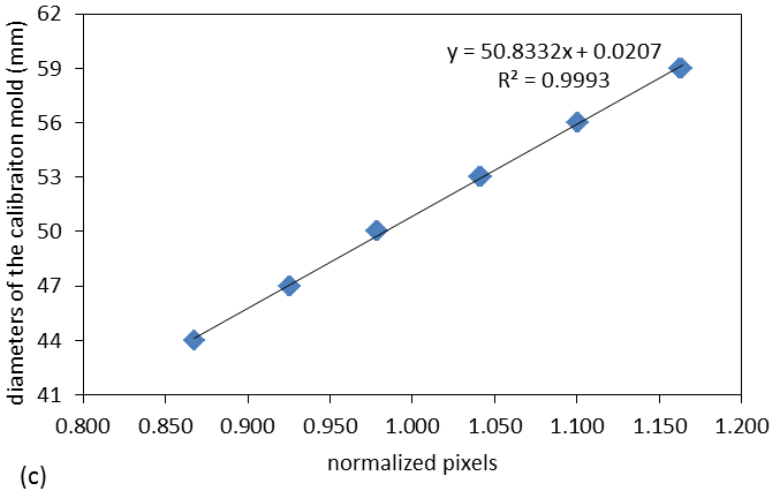

(c)

Figure A.3 The calibration equations, (a), an example of the calibration equation, which is unsatisfactory due to poor quality images, (b) the calibration equation of triaxial cell manufactured by ELE, (c) the calibration equation of triaxial cell manufactured by Geocomp.

8. The standard area correction calculation is carried out by using following equation (A-4) for specimens that deforms as right circular cylinder (ASTM D4767).

$$A_{corrected} = A_0 \frac{1-\varepsilon_v}{1-\varepsilon_a} \tag{A-4}$$

Where $A_{corrected}$ is the corrected area for the given axial strain, A_0 is the cross-sectional area just before the shearing stage, ϵ_v is the volumetric strain for the given axial load and ϵ_a is the axial strain for the given axial load. The parabolic area correction can also be used for specimens have bulging deformations by using following equation (A-5) (Toker, 2007).

$$D_{corrected} = \frac{D_0}{4}\left(\sqrt{30\times\left(\frac{1-\varepsilon_v}{1-\varepsilon_a}\right)-5}-1\right) \tag{A-5}$$

Where $D_{corrected}$ is the corrected diameter and D_0 is the diameter of the specimen just before shearing stage.

One of these corrections can be choosen depending on the observed deformations at the end shearing. In the calculations, the volumetric strain is taken as zero.

In this study, modified area correction procedure was used. This procedure is based on the fact that final dimensions of the specimen after shearing can be used to obtain more accurate values of cross-sectional area. The following equation (A-6) was used in this study to calculate modified cross-sectional area of the for the given axial strain:

$$A'_{corrected} = A_{corrected} \times \left(1+\left(\frac{D_{ratio}-1}{\varepsilon_{final}}\right)\times\varepsilon\right) \tag{A-6}$$

where $A'_{corrected}$ is the modified corrected cross-sectional area, $A_{corrected}$ is the cross-sectional area that is calculated by using (A-4) or (A-5), D_{ratio} is the ratio of the cross-sectional area which is calculated by using using (A-4) or (A-5) at the end of

shearing and the cross-sectional area which calculated by using the diameter that is measured at the end of shearing, $\in_{final}$ is the axial strain value at the end of shearing and $\in$ is the any given axial strain. By using (A-6), the whole corrected cross-sectional area values for the given strain are scaled with respect to actual cross-sectional area at the end of shearing. Then those are used for determining deviator stress.

As a result, accurate values of deviator stress can be determined without measuring volumetric strain of the test specimen, which is challenging for unsaturated specimen tests, by means described procedure. In this study, the diameters of the specimens at the end of shearing were measured by using proposed method and also by means of a caliper after dismantling the triaxial cell and the specimen. For measuring the diameter of the test specimen, blue plastic sheet was used as being background. Since the the color of membrane, which covers the triaxial test specimen, is yellow and blue color yields better contrast in the pictures. In order to take at least three diameter measurement (ASTM D4767) the triaxial cell was rotated and a picture was taken every 120° angle. It is important to note that the measurements by using caliper is only possible after dismantling the triaxial cell and the specimen and this means the cell pressure should be decreased to zero. The stress relief in the test specimen causes swelling of the specimen and this causes overestimation of the diameter of the specimen at the end of shearing.

B. A Formulation for Scanning Water Retention Curves (Further Improvement to Kenanoğlu and Toker, 2018b)

The closed form equations were proposed in Kenanoğlu and Toker (2018b) to model scanning water retention curves. These formualtions were enchanced in this study. An empirical equation for K was redevised, based on calibration against experimental data found in several sources from the literature. Consequently, only virgin wetting and virgin drying SWRCs and the point of regime reversal suffice to define the scanning curve.

The hysteretic nature of SWRC is captured assuming virgin drying and virgin wetting curves (which can be obtained from experiments or various fitting equations in the literature) bound all possible values following regime reversals. Two separate formulas (one for drying and another for wetting) were developed for modelling of scanning soil-water characteristic curves. Formulas were developed by interpolation of a power of volumetric water content ratios over ratios of logarithms of suction, devised from the observations on the shapes of graphs of experimental data.

$$\frac{a}{b} = \frac{c}{d}\left(\frac{e}{f}\right)^{K} \tag{B-1}$$

For each point on the scanning curve, the suction values on the virgin drying and virgin wetting SWRC correspond to preceding and current water content are determined. Unknown suction value for current water content should lie in between these suction values and following relations are devised. The proposed relations are given in the form such that subscript j refers to temporal variation. In the following Fig. B.1 variables of the developed relations are illustrated.

$$\log(\psi_j) = \log\left(\psi_j^w\right) + \frac{\log\left(\frac{\psi_{j-1}}{\psi_{j-1}^w}\right)}{\log\left(\frac{\psi_{j-1}^d}{\psi_{j-1}^w}\right)}\left(\frac{\theta_m - \theta_j}{\theta_m - \theta_{j-1}}\right)^K \log\left(\frac{\psi_j^d}{\psi_j^w}\right) \quad \text{(B-2)}$$

$$\log(\psi_j) = \log\left(\psi_j^d\right) - \frac{\log\left(\frac{\psi_{j-1}^d}{\psi_{j-1}}\right)}{\log\left(\frac{\psi_{j-1}^d}{\psi_{j-1}^w}\right)}\left(\frac{\theta_j - \theta_r}{\theta_{j-1} - \theta_r}\right)^K \log\left(\frac{\psi_j^d}{\psi_j^w}\right) \quad \text{(B-3)}$$

where, $\log(\psi_j)$ is the logarithm of unknown suction value at present, $\log(\psi^w_j)$ is the logarithm of corresponding value of suction on virgin wetting curve for θ_j, ψ_{j-1} is the value of suction at previous time step, ψ^w_{j-1} is the corresponding value of suction on virgin wetting curve for θ_{j-1}, ψ^d_{j-1} is corresponding value of suction on virgin drying curve for θ_{j-1}, θ_{max} is ultimate wetting saturated water content, θ_j is the water content at present condition, θ_{j-1} is the water content at previous condition, ψ^d_j is the corresponding value of suction on virgin drying curve for θ_j, ψ^w_j is the corresponding value of suction on virgin wetting curve for θ_j and K is the power-type parameter, which controls the flatness of the scanning curve. It should be noted that virgin drying and virgin wetting curves can be in the form of any retention curve equations such as Van Genuchten (1980).

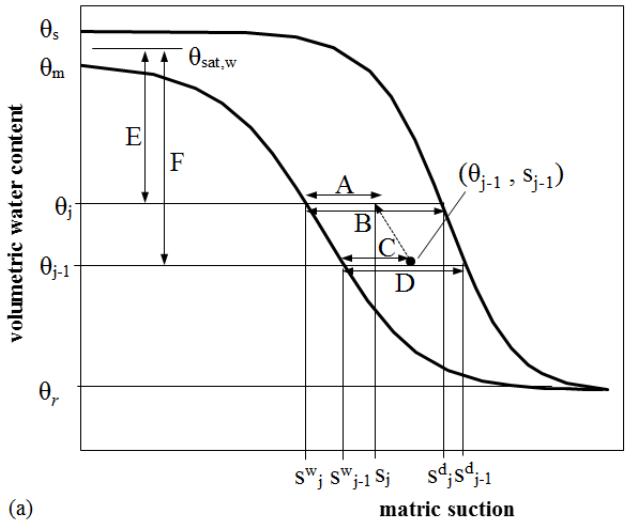

(a)

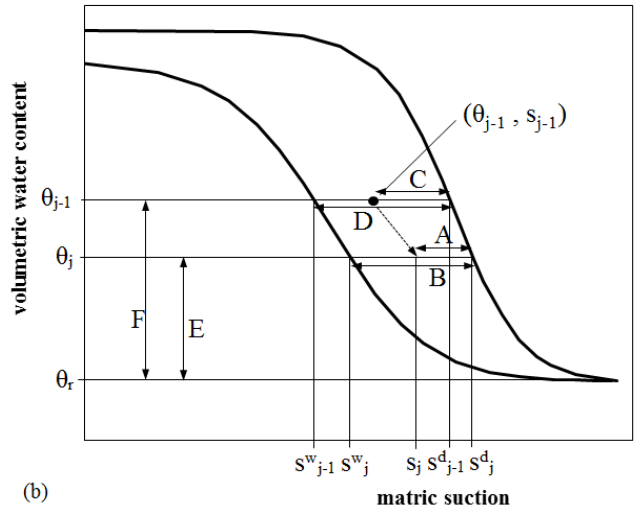

Figure B.1 Sketch of variables given in the general form of (B-1), a) wetting scanning curve, b) drying scanning curve.

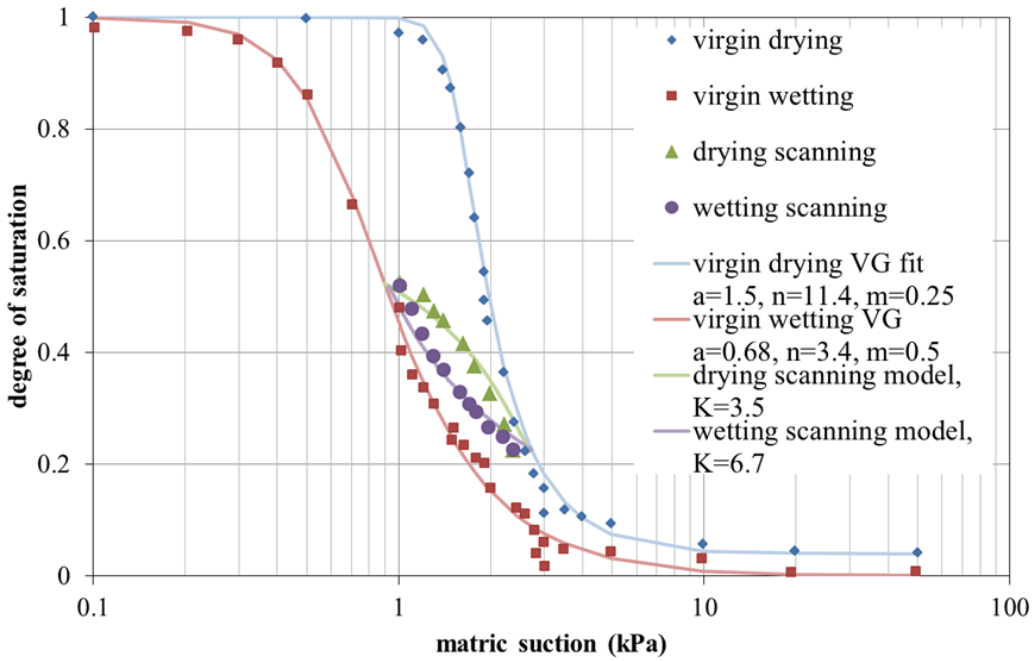

Figure B.2 The proposed hysteresis model for a scanning loop (experimental data fromLins et al., 2007), R^2 values for drying and wetting scanning curves are 0.890 and 0.917, respectively.

The power parameter, *K* in the relations appears to depend on various properties, such as regime (drying or wetting), soil type and regime reversal water content. An

empirical equation was proposed for power parameter using a variable termed as fractional water content. In the drying regime, fractional water content is the ratio of difference in present water content and residual water content to difference in saturated and residual water contents. In the wetting regime, it is the ratio of difference in saturated water content and present water content to difference in saturated and residual water contents. The collected literature data was processed and relationship between fractional water content and power parameter was investigated (Fig. B.3).

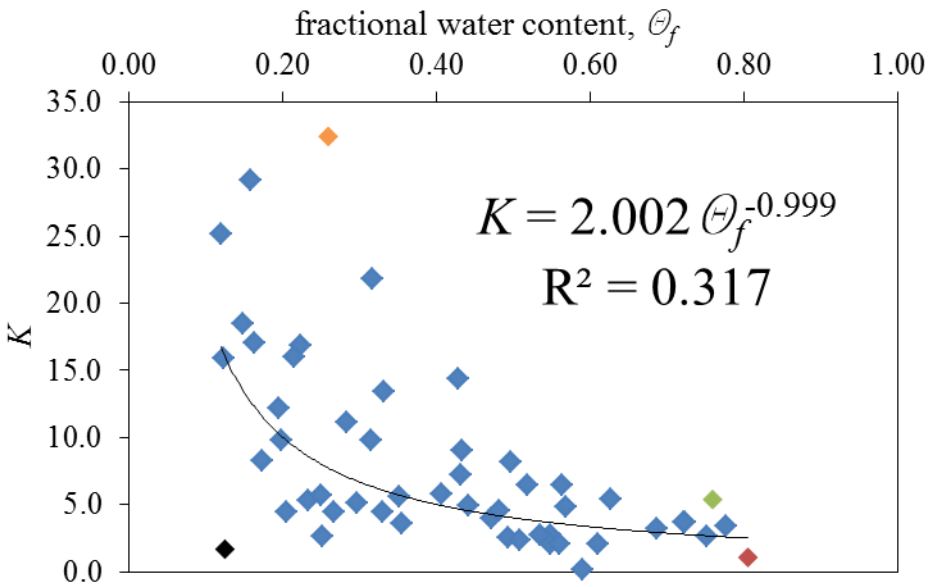

Figure B.3 Relationship between fractional water content and power parameter.

An empirical equation is proposed for quantifying the power parameter K using a variable termed as fractional water content (Θ_f). In the wetting regime, Θ_f is similar to widely used effective volumetric water content, Θ, except that Θ_m replaces the saturated water content (Θ_s). In the drying regime, Θ_f is equal to (1- Θ).

$$\Theta_f = \frac{\theta_{j-1} - \theta_r}{\theta_m - \theta_r} \tag{B-4}$$

$$\Theta_f = 1 - \Theta = \frac{\theta_s - \theta_{j-1}}{\theta_s - \theta_r} \tag{B-5}$$

Data collected from the literature are processed and the relationship between fractional water content values at the initial state and power parameter is investigated (Fig. B.3). Number of data is extended by processing successive experimental data points on scanning curve. A mathematical expression is fitted to experimental data given in Fig. B.3 using the least squares method leading to an empirical relationship that seems to be close to $2/\Theta_f$:

$$K = 2.002 \times \Theta_f^{-0.999} \approx 2/\Theta_f \qquad \text{(B-6)}$$

The low value for coefficient of correlation R^2 seems to poor correlation in experimental data; however, the sensitivity of scaning curve on higher values of power parameter is quite low. The scanning curves calculated with least square method and empirical equation was compared for inconsistent experimental data (Fig. B.4 to B.7).

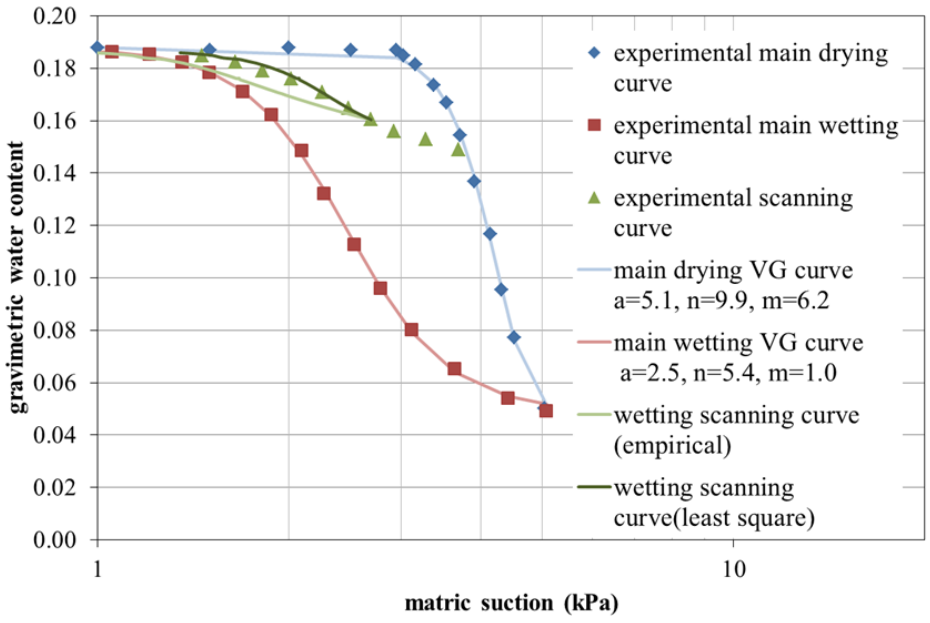

Figure B.4 Wetting scanning curve experimental data from Poulovassilis and Childs (1971) (red colored data point in Fig. B.3), (initial value of fractional water content is 0.8) comparison of scanning curves calculated from least square method and emprical relationship.

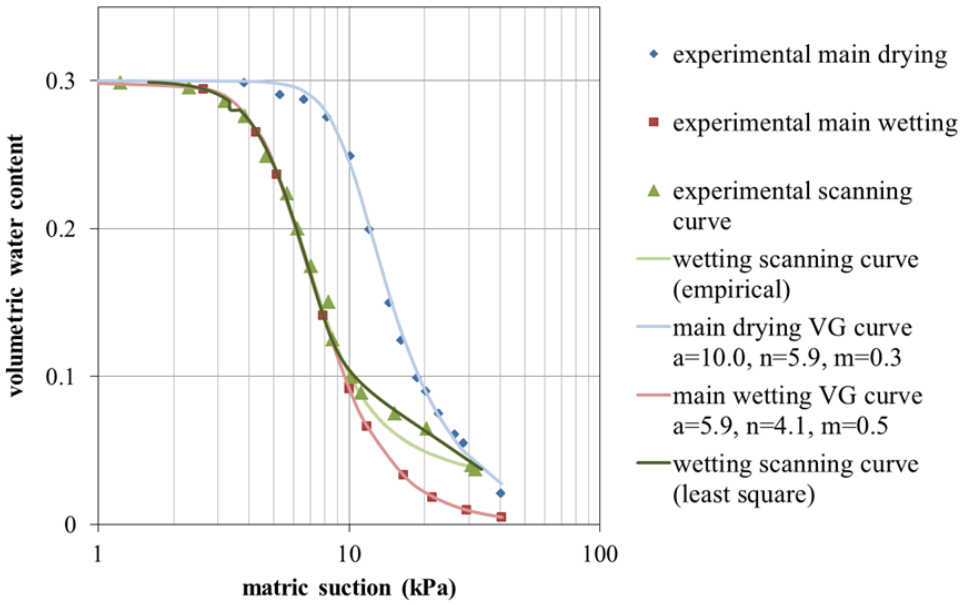

Figure B.5 Wetting scanning curve experimental data from Liakopoulos (1966) (black colored data point in Fig. B.3), (initial value of fractional water content is 0.12) comparison of scanning curves calculated from least square method and emprical relationship.

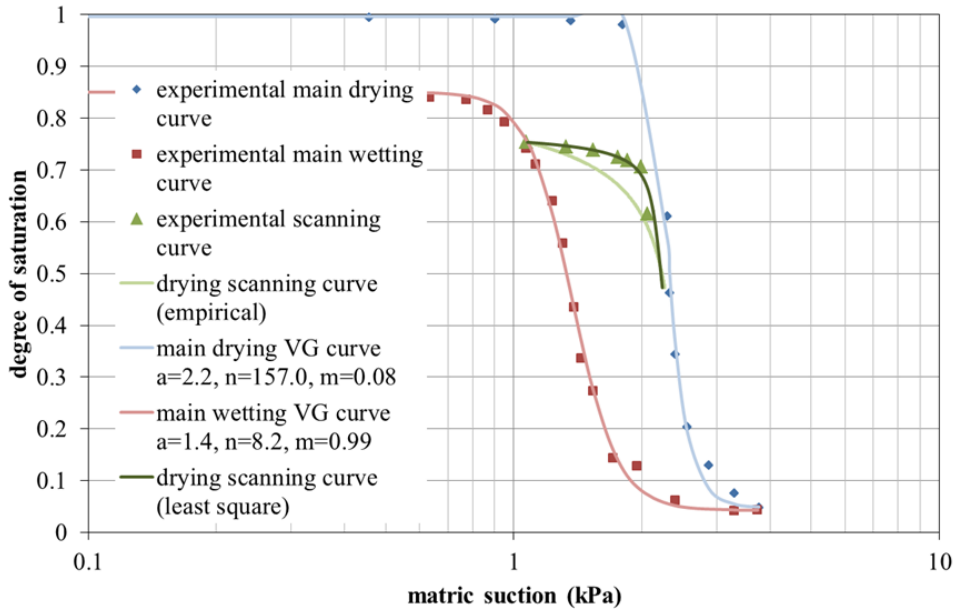

Figure B.6 Drying scanning curve experimental data from Mohamed and Sharma (2007) (orange colored data point in Fig. B.3), (initial value of fractional water content is 0.26) comparison of scanning curves calculated from least square method and emprical relationship.

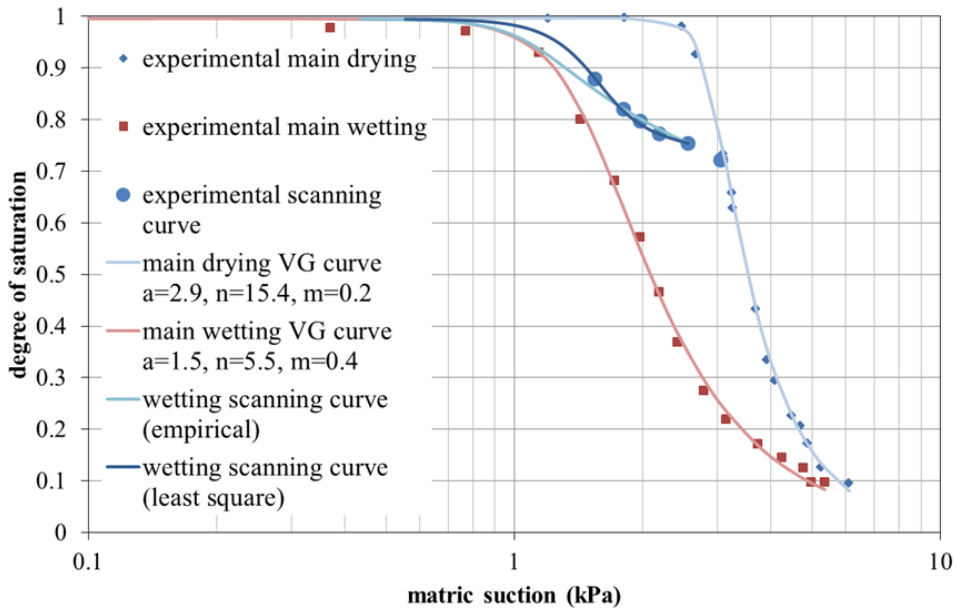

Figure B.7 Wetting scanning curve experimental data from Gillham et al., (1976) (green colored data point in Fig. B.3), (initial value of fractional water content is 0.76) comparison of scanning curves calculated from least square method and emprical relationship.

(B-2) and (B-3) take following form using empirical equation on the behalf of power parameter K, for wetting:

$$\log(\psi_j) = \log\left(\psi_j^w\right) + \frac{\log\left(\frac{\psi_{j-1}}{\psi_{j-1}^w}\right)}{\log\left(\frac{\psi_{j-1}^d}{\psi_{j-1}^w}\right)}\left(\frac{\theta_{sat,w}-\theta_j}{\theta_{sat,w}-\theta_{j-1}}\right)^{\frac{2\left(\theta_{sat,w}-\theta_{res}\right)}{\theta_{i,j-1}-\theta_{res}}}\log\left(\frac{\psi_j^d}{\psi_j^w}\right) \qquad \text{(B-7)}$$

and for drying:

$$\log(\psi_j) = \log\left(\psi_j^d\right) - \frac{\log\left(\frac{\psi_{j-1}^d}{\psi_{j-1}}\right)}{\log\left(\frac{\psi_{j-1}^d}{\psi_{j-1}^w}\right)}\left(\frac{\theta_j-\theta_{res}}{\theta_{j-1}-\theta_{res}}\right)^{\frac{2(\theta_{sat}-\theta_{res})}{\theta_{sat}-\theta_{i,j-1}}}\log\left(\frac{\psi_j^d}{\psi_j^w}\right) \qquad \text{(B-8)}$$

Proposed relations are presented in the form that can predict any suction increment from the given increment of water content which is then predicted from an iterative

solution of either (B-9) or (B-10). Following equations are used for the wetting and drying regimes, respectively:

$$\theta_j = \theta_r - (\theta_{j-1} - \theta_r)\left\{ \frac{\log\left[\left(a_d\left[\left(\frac{\theta_i-\theta_r}{\theta_s-\theta_r}\right)^{\frac{-1}{m_d}}-1\right]^{\frac{1}{n_d}}\right)\Big/ s_j\right]}{\frac{\log\left(\frac{s^d_{j-1}}{s_{j-1}}\right)}{\log\left(\frac{s^d_{j-1}}{s^w_{j-1}}\right)}\cdot\log\left[\frac{\left(a_d\left[\left(\frac{\theta_i-\theta_r}{\theta_s-\theta_r}\right)^{\frac{-1}{m_d}}-1\right]^{\frac{1}{n_d}}\right)}{\left(a_w\left[\left(\frac{\theta_i-\theta_r}{\theta_m-\theta_r}\right)^{\frac{-1}{m_w}}-1\right]^{\frac{1}{n_w}}\right)}\right]}\right\}^{\frac{\theta_s-\theta_{j-1}}{2\cdot(\theta_s-\theta_r)}} \quad \text{(B-9)}$$

and for drying regime:

$$\theta_j = \theta_s - (\theta_s - \theta_{j-1})\left\{ \frac{\log\left[s_j\Big/\left(a_w\left[\left(\frac{\theta_i-\theta_r}{\theta_m-\theta_r}\right)^{\frac{-1}{m_w}}-1\right]^{\frac{1}{n_w}}\right)\right]}{\frac{\log\left(\frac{s_{j-1}}{s^w_{j-1}}\right)}{\log\left(\frac{s^d_{j-1}}{s^w_{j-1}}\right)}\cdot\log\left[\frac{\left(a_d\left[\left(\frac{\theta_i-\theta_r}{\theta_s-\theta_r}\right)^{\frac{-1}{m_d}}-1\right]^{\frac{1}{n_d}}\right)}{\left(a_w\left[\left(\frac{\theta_i-\theta_r}{\theta_m-\theta_r}\right)^{\frac{-1}{m_w}}-1\right]^{\frac{1}{n_w}}\right)}\right]}\right\}^{\frac{\theta_{j-1}-\theta_r}{2\cdot(\theta_s-\theta_r)}} \quad \text{(B-10)}$$

C. Results of the Oedometer Tests on Unsaturated Ankara Clay Specimens

Quick oedometer tests were carried out on unsaturated Ankara clay specimens. Oedometer test specimens were prepared by consolidating Ankara clay slurry sample in standard oedometer test setup. The gravimetric water content of Ankara clay specimens were adjusted in the direction of both wetting and drying according to procedures described in section 4.1. The results of the practical tests are illustrated in Fig. C.1. The labels show the specimens' gravimetric water content at the of the tests, the final letters denote specimen's water content is varied in the direction of wetting for 'w', drying for 'd' and saturated for 'sat'.

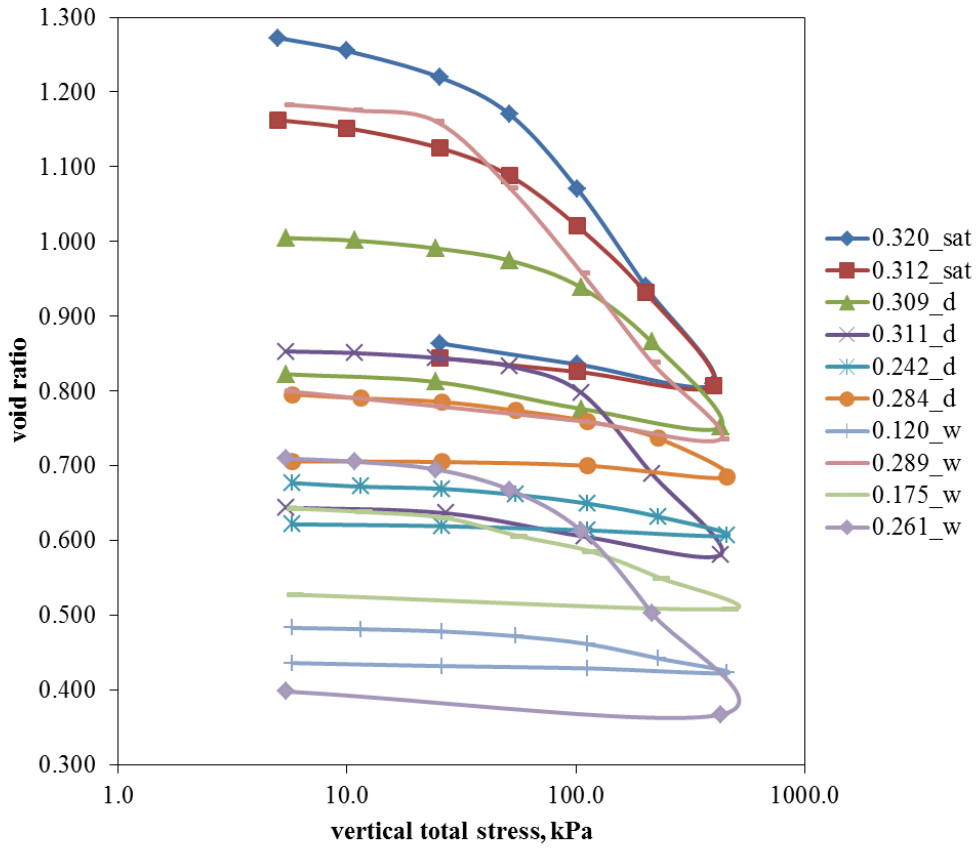

Figure C.1. Practical oedometer tests on unsaturated Ankara Clay specimens.

CURRICULUM VITAE

Surname, Name: Kenanoğlu, Melih Birhan

EDUCATION

Degree	Institution	Year of Graduation
MS	METU Civil Engineering	2017
BS	Gazi University Civil Engineering	2014
High School	Ankara Atatürk Anadolu High School	2010

FOREIGN LANGUAGES

Advanced English, Basic Italian

PUBLICATIONS

1. Kenanoğlu, M.B. and Toker, N.B., 2018. "Changing and equilibrating water content of triaxial test specimens without suction control" The 7th International Conference on Unsaturated Soils (UNSAT2018), 2018, Hong Kong.

2. Kenanoğlu, M. B. and Toker, N. B., 2018. "A formulation for scanning soil-water characteristic curves", Journal of Politechnic, DOI: 10.2339/politeknik.389619

3. Kenanoğlu, M. B., Ahmadi-adli, M, Toker, N.K. and Huvaj, N. 2019. "Effect of Unsaturated Soil Properties on the Intensity-Duration Threshold for Rainfall Triggered Landslides". Teknik Dergi, 30 (2) , 9009-9027 . DOI: 10.18400/tekderg.414884

Trekking, Digital Piano, Movies, Books